Full Time-Domain Electromagnetic Interference Measurements and Applications

Marco A. Azpúrua

UPC - BarcelonaTech (2018)

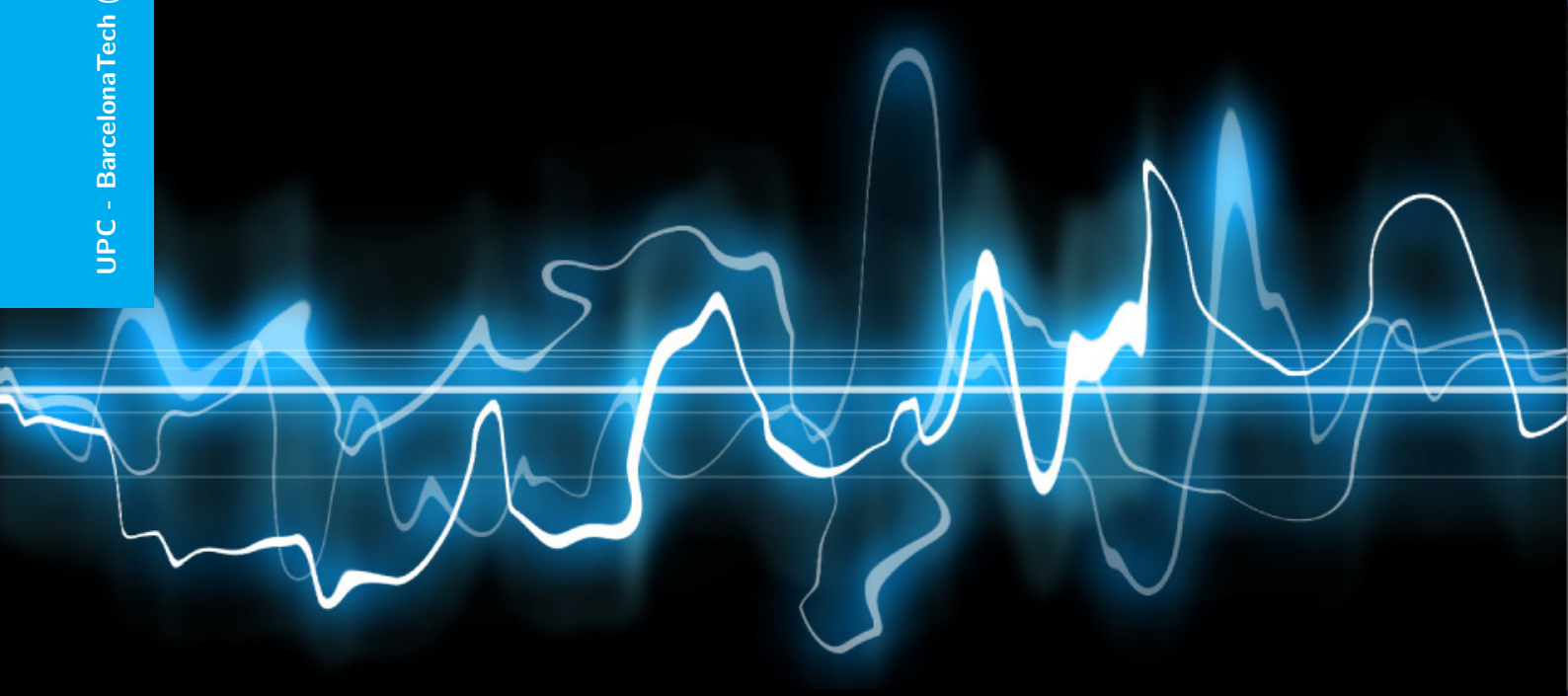

UNIVERSITAT POLITÈCNICA
DE CATALUNYA
BARCELONATECH

UNIVERSITAT POLITÈCNICA DE CATALUNYA BARCELONATECH

Full time-domain electromagnetic interference measurements and applications

by

Marco A. Azpúrua

ADVERTIMENT La consulta d'aquesta tesi queda condicionada a l'acceptació de les següents condicions d'ús: La difusió d'aquesta tesi per mitjà del repositori institucional UPCommons (http://upcommons.upc.edu/tesis) i el repositori cooperatiu TDX (http://www.tdx.cat/) ha estat autoritzada pels titulars dels drets de propietat intel·lectual **únicament per a usos privats** emmarcats en activitats d'investigació i docència. No s'autoritza la seva reproducció amb finalitats de lucre ni la seva difusió i posada a disposició des d'un lloc aliè al servei UPCommons o TDX. No s'autoritza la presentació del seu contingut en una finestra o marc aliè a UPCommons (*framing*). Aquesta reserva de drets afecta tant al resum de presentació de la tesi com als seus continguts. En la utilització o cita de parts de la tesi és obligat indicar el nom de la persona autora.

ADVERTENCIA La consulta de esta tesis queda condicionada a la aceptación de las siguientes condiciones de uso: La difusión de esta tesis por medio del repositorio institucional UPCommons (http://upcommons.upc.edu/tesis) y el repositorio cooperativo TDR (http://www.tdx.cat/?locale-attribute=es) ha sido autorizada por los titulares de los derechos de propiedad intelectual **únicamente para usos privados enmarcados** en actividades de investigación y docencia. No se autoriza su reproducción con finalidades de lucro ni su difusión y puesta a disposición desde un sitio ajeno al servicio UPCommons No se autoriza la presentación de su contenido en una ventana o marco ajeno a UPCommons (*framing)*. Esta reserva de derechos afecta tanto al resumen de presentación de la tesis como a sus contenidos. En la utilización o cita de partes de la tesis es obligado indicar el nombre de la persona autora.

WARNING On having consulted this thesis you're accepting the following use conditions: Spreading this thesis by the institutional repository UPCommons (http://upcommons.upc.edu/tesis) and the cooperative repository TDX (http://www.tdx.cat/?locale-attribute=en) has been authorized by the titular of the intellectual property rights **only for private uses** placed in investigation and teaching activities. Reproduction with lucrative aims is not authorized neither its spreading nor availability from a site foreign to the UPCommons service. Introducing its content in a window or frame foreign to the UPCommons service is not authorized (framing). These rights affect to the presentation summary of the thesis as well as to its contents. In the using or citation of parts of the thesis it's obliged to indicate the name of the author.

Full Time-Domain Electromagnetic Interference Measurements and Applications

by

Marco A. Azpúrua

Dissertation submitted as a *compendium of publications* in partial fulfillment of the requirements for the degree of

Doctor in Electronic Engineering

issued by the

Universitat Politècnica de Catalunya

April, 2018

Director:	**Ferran Silva Martínez, Ph.D.**
Co-director:	**Marc Pous Solá, Ph.D.**

UNIVERSITAT POLITÈCNICA DE CATALUNYA
BARCELONATECH

*Para **Anabella Natalie** y **Xileidys**...*

*Gracias a ti **hija**, por colmar de nobleza mis motivaciones y aspiraciones.*

*Gracias **Xileidys** por ser mi mujer, mi compañera de viaje.*
Eres un manantial de bondad y amor incondicional
en el cual siempre encontraré refugio.

PREFACE

My research in time-domain techniques for electromagnetic interference (EMI) measurements began in late 2013 when I enrolled in the Electronics Engineering program of the Universitat Politècnica de Catalunya (UPC). By that time, the UPC, through its Grup de Compatibilitat of Electromagnètica (GCEM), was a partner in the joint research project "Improved EMC Test Methods in Industrial Environments" (IND60 EMC) from the EURAMET's European Metrology Research Program (EMRP).

In this regard, the goal of the aforementioned project was to improve the existing electromagnetic compatibility (EMC) testing methods adapted for the industry as well as to develop alternative test methods in accordance with industrial needs. On the one hand, the IND60 EMC project tackled the challenges of on-site EMC testing by proposing a set of novel testing methods for large, complex, mounted and/or fixed systems and installation that cannot be assessed using the standardized methods. On the other hand, the IND60 EMC project also developed the metrology required for the newly introduced alternative EMC test methods.

Particularly, the role of GCEM–UPC in the IND60 project was centered on the development of improved conducted and radiated emissions measurements suitable for EMI testing in complex environments. In that context, complex environment means EMI measurements are carried without the (almost) noise free and reflection free conditions provided by the typical EMC test setup for either conducted or radiated emissions measurements. Moreover, the developed EMI testing methods should be superior in terms of performance, quality and, reliability, that is, faster to apply, more repetitive, easily reproducible, traceable and characterized by a lower uncertain in comparison with preceding practices.

Therefore, during the lifespan of the IND60 (2013- 2016), I worked hand-in-hand with my colleagues at GCEM–UPC for delivering suitable tools and the methods for in-situ EMI measurements. Our strategy was based on time-domain techniques and instrumentation because of the benefits they offer in comparison with the conventional frequency swept approach. Among those advantages, time-domain measurements allowed for a faster and full spectrum evaluation of the emissions that is suitable for transient EMI analysis. Likewise, the usefulness of multichannel, event-triggered EMI measurements was realized more and more as the research on time-domain EMI measurements progressed and propagated to all the other ongoing projects undergone at GCEM–UPC.

Consequently, since I started working on this thesis research, several projects have employed our time-domain EMI measurement systems enabling the growth and diversification of its applications. That is the case of the national research projects TEC2013-48414-C3-3-R and TEC2016-79214-C3-2-R entitled "Desarrollo de sondas y validación de resultados numéricos en el dominio del tiempo para efectos indirectos de descargas atmosféricas en UAV" (2014-2017) and "Evaluación numérica y experimental de efectos electromagnéticos ambientales en aviones no tripulados" (2016-2019), respectively, both funded by the Spanish's Ministry of Economy, Industry and Competitiveness.

In the same vein, the results of this Thesis are continually being deployed in ongoing research projects funded by the European Metrology Programme for Innovation and Research (EMPIR) such as the “Development of RF and microwave metrology capability” (15RPT01 RFMicrowave) and “Metrology for advanced energy-saving technology in next-generation electronics applications” (16ENG06 ADVENT) or the forthcoming “Electromagnetic Interference on Static Electricity Meters” (17NRM02 MeterEMI). That being said, the before mentioned research projects are just a small sample of the immediate future of time-domain EMI measurements and their applications.

At the present moment, the culmination of this Thesis is possible due to the notable degree of maturity achieved in the Full Time Domain EMI (Full TDEMI) measurement systems technology and on its diverse application domain. In the latest years, the usage of Full TDEMI measurement systems for testing the radiofrequency emissions of a variety of electronic products and systems spanning from the railway to the aeronautics industries has demonstrated its advantages in practice. In fact, nowadays, Full TDEMI measurements systems are an integral part of GCEM–UPC testing, consulting and training services to the industry.

Moreover, Full TDEMI measurement systems also became a software development project counting with tens of thousands of lines of code written along uncountable hours of dedication spent during the past years. Many practitioners have contributed by suggesting specific functionalities and features suitable for their needs. Similarly, industries have requested custom made software developments based in the Full TDEMI for automating their specific type of emissions test. Currently, the Full TDEMI measurement system software in its version 3.2 and it is stable.

However, this does not mean the work in Full TDEMI measurements and its applications is completed. In fact, there is plenty of ideas and possibilities concerning the continuation of both the research and the software development. I sincerely hope the future allow me to continue contributing to this field along with the excellent team I have found in GCEM–UPC.

For all the previous reasons, I am very thankful.

Marco A. Azpúrua
Barcelona, April 2018

ACKNOWLEDGEMENT

Muchas son las razones cuantificables por las cuales debo agradecer a las personas y a las instituciones que han hecho posible que esta Tesis haya sido culminada. Se podría estimar el coste económico del proyecto, los kilómetros recorridos, las horas de trabajo y enumerar los artículos publicados, las citaciones o incluso las líneas de código de programación que esta Tesis ha significado para, en retrospectiva, intentar reconocer los valiosos aportes que me han permitido llegar hasta este momento. Sin embargo, dejaré la objetividad aparcada temporalmente para ofrecer las próximas líneas a quienes con su solidaridad y consideración me han acompañado en esta última etapa de formación académica.

Comienzo entonces por agradecer a Ferran Silva, director de esta Tesis, porque fue él quien en definitiva me ofreció la oportunidad de incorporarme al GCEM-UPC con todo lo que esto ha implicado para mí y mi familia. A raíz de esta decisión se inició un proceso que nos ha llevado a residir en un nuevo país, donde hemos cambiado nuestro lugar de trabajo y en el que continuamos descubriendo y apreciando la cultura, la geografía y lengua de Cataluña. Ferran, es tuya la visión que dio origen a esta Tesis y sinceramente espero haber honrado las expectativas que ya hace más de cinco años se depositaron en aquel desconocido que finalmente terminó escribiendo estas palabras.

Asimismo, no podría dejar de mencionar al excelente equipo de GCEM liderado por Marc Pous y Marc Aragón quienes en todo momento han brindado un apoyo técnico y científico de alto valor agregado, caracterizado por un criterio eminentemente pragmático y fundamentado en la experiencia. A ambos les debo agradecer por sus recomendaciones, sus críticas y su tenacidad. Tampoco debo olvidar a Ricardo Jáuregui, que a pesar de no continuar en GCEM para el momento de mi incorporación, fue quien en un primer lugar recomendó mi nombre y dio su voto de confianza para favorecer mi aceptación como estudiante del programa de doctorado de UPC bajo la dirección de Ferran Silva.

Volviendo la memoria un poco más en el pasado, he de reconocer la importancia de personas sin las cuales tampoco podría estar en la situación en la que me encuentro actualmente. Se trata de mi primer mentor como joven investigador, Luis Rodríguez Quiroz, y de mis amigos Eduardo Páez y Ciro Tremola de la Fundación Instituto de Ingeniería en Caracas, Venezuela. Fue gracias a ellos que, por circunstancias insospechadas, acabé trabajando en el Laboratorio de Electromagnetismo Aplicado (LEA) en actividades de investigación y desarrollo relacionadas con la compatibilidad electromagnética y caracterización de antenas. Las memorables experiencias de aquellos 5 años que laboré en el LEA me permitieron construir un perfil profesional afín a los retos que debí abordar en los estudios doctorales. También fueron ellos quienes me otorgaron la primera referencia del trabajo realizado por GCEM a raíz de los cursos de formación que ellos habían realizado en el año 2008, es decir, aproximadamente hace 10 años.

Hasta el momento solo he mencionado a aquellos que han tenido una influencia directa en el inicio y consecución de esta Tesis. Sin embargo, muchas otras personas, entre las que se encuentran principalmente mis familiares y amigos, han ofrecido su ayuda desinteresada para que hoy día puedan escribirse estas palabras. Aunque no me sería posible nombrarles a todos aquí, me gustaría dedicar las próximas líneas a mis

suegros y a mis padres.

Agradezco a mis suegros Marlene Vivas y Cristo Antonio Parra quienes en todo momento se solidarizaron con esta causa, incluso cuando esto significó que debían apartarse físicamente de sus seres más queridos, entiéndase su hija y su nieta. Ellos fueron un gran apoyo logístico y económico para nosotros durante la todas las gestiones y trámites requeridos para poder establecernos con éxito en Barcelona. Toño, en donde quiera que te encuentres, me gustaría que supieras que espero que todo esto haya valido la pena y que siento mucho que estos últimos años de tu vida no haya sido posible que compartiésemos mas momentos en familia como tanto tu hubiese gustado. También me gustaría hacer una mención a mis padres Ana Margarita Auyanet González y Marco Aurelio Azpúrua Campos quienes, aunque no creo que entiendan muy bien a que me dedico, en todo momento me criaron en un ambiente que fue familiar con la universidad y la investigación científica y me alentaron a seguir mi vocación.

Por último, pero no por eso menos importante, debo agradecer a Xileidys Parra por todo su apoyo incondicional, amor y paciencia durante estos años. Si algo me ha resultado difícil durante este periodo, ha sido la mermada interacción social en todo lo concerniente las relaciones de amistad que van más allá de lo estrictamente profesional. Esto ha hecho que nuestro matrimonio se vea fortalecido ante el estrés que significó una reducción tan drástica de nuestro circuló de confianza.

En el ámbito institucional debo agradecer a la UPC, a la Generalitat de Catalunya y al Fondo Social Europeo quienes han otorgado los recursos para mí la contratación como investigador en formación y sin los cuales no habría sido posible asumir el trabajo que ha significado esta Tesis.

Marco A. Azpúrua
Barcelona, April 2018

ABSTRACT

This thesis comprises a compendium of contributions made by the author to the field of the radiofrequency measurements for electromagnetic interferences. In particular, this thesis presents a technology that has been called the "Full Time-Domain Electromagnetic Interference" (Full TDEMI) measurement systems and some of its most relevant applications.

Full TDEMI measurement systems are an implementation of an FFT-based measuring receiver that enables the usage of oscilloscopes for electromagnetic interference measurements. Full TDEMI measurement systems follow the virtual instrumentation approach for transforming general purpose oscilloscopes into a completely functional and compliant CISPR 16-1-1 measuring receiver.

On the one hand, this is feasible because of the specific signal processing techniques applied over the time-domain acquisitions using a dedicated software layer. On the other hand, Full TDEMI measurement systems have been exhaustively assessed for characterizing their performance using novel waveform oriented calibration procedures that bridge the gap between direct measurements in the time domain and the processed frequency domain magnitudes. As a result, the conformity of Full TDEMI test receivers is attested with respect to the requirements defined in the international standards for EMI measurements.

Moreover, Full TDEMI measurement systems have been proved to be advantageous over the conventional swept receivers for performing several challenging measurements typical of electromagnetic emissions assessments. For instance, time-domain captures enable full spectrum measurements required for a proper analysis of transient phenomena. Likewise, the number of channels available in most oscilloscopes enable multiple synchronous measurements that allow recording the interfering disturbances using a combination of transducers.

Some of the applications of the multichannel EMI measurement are the single stage evaluation of the conducted EMI of all the equipment under test (EUT) mains lines, the instantaneous measurement of the common-mode and the differential mode voltage noise, the concurrent conducted and radiated EMI measurements, and the parallelization of multi-antenna radiated emissions testing. Such alternative test methods, have improved significantly the EMC testing process in a variety of industries by reducing the amount of time and the efforts required for performing a complete system evaluation mainly due to the following reasons. First, time-domain EMI measurements deliver faster results because the interferences' spectrum is simultaneously estimated for all the standard weighting detectors required to determine compliance with the maximum emissions limits defined in the respective product standards. Second, the number of measurement iterations is reduced because of the multichannel possibilities and also because of an agile identification of the worst case emissions in EUT having different operating modes. Thirdly, Full TDEMI measurement system are a cost-effective and versatile alternative to the state-of-the-art real-time spectrum analysers for EMI measurements in the range of few gigahertz.

From the theoretical point-of-view, Full TDEMI measurement systems have extended the state-of-the-art

as in the case of a couple of contributions namely the expected maximum detector and the empirical interference decomposition.

The expected maximum detector is a statistical measure of the most probable level of the peak emissions that is based on a time-frequency modelling of the measured interferences using the extreme value theory. Using the variability information of the interference level at each frequency bin, the expected maximum detector can be used to estimate the equivalent max-hold value of a random interference. The expected maximum detector also provides a model quantifying the uncertainty of peak detector measurement of stochastic interferences.

The empirical interference decomposition (EID) is a modified implementation of the Hilbert–Huang transform with time-gating capabilities that allow a heuristic determination of characteristic oscillatory patterns without neither domain transformation nor a predefined set of basis function. The empirical interference decomposition has been used successfully for ambient noise cancellation purposes during proof-of-concept outdoors EMI measurements, obtaining more than 20 dB of attenuation of the usual broadcasting signals. The fundamentals of the ambient noise cancellation by means of EID is the identification, in the time and in the frequency domain, of intrinsic modes of emissions that are attributable to the EUT while subtracting the residual modes (ambient noise) from the measurement results. The aforementioned contributions are distributed in four journal papers. Complementary measurement results and applications of the Full TDEMI measurement systems have also been published in recognized conferences of the field.

From the reasons mentioned before, the developed Full TDEMI measurement technology has significant advantages for EMI testing, analysing and troubleshooting. It provides a complementary approach to the typical measurements entirely focused in the frequency domain and it exhibits a level of maturity that could allow it to be standardized in forthcoming years.

RESUMEN

Esta Tesis comprende un compendio de contribuciones hechas por el autor al campo de la tecnología de medición de radiofrecuencia para la compatibilidad electromagnética. En particular, esta Tesis presenta una tecnología de sistemas medición de interferencias electromagnéticas completamente basado en dominio del tiempo (Full TDEMI) y algunas de sus aplicaciones más relevantes.

Los sistemas de medición Full TDEMI son una implementación de un receptor de medida basado en FFT que permite el uso de osciloscopios para mediciones de interferencias electromagnéticas. Los sistemas de medición Full TDEMI siguen el enfoque de instrumentación virtual para transformar los osciloscopios de propósito general en un receptor de medida completamente funcional y conforme con la norma CISPR 16-1-1.

Por un lado, esto es factible debido a las técnicas específicas de procesamiento de señales aplicadas sobre las adquisiciones en el dominio del tiempo utilizando una capa de software dedicada. Por otro lado, los sistemas de medida Full TDEMI se han evaluado exhaustivamente para caracterizar su rendimiento utilizando procedimientos novedosos de calibración orientados a formas de onda que acortan la brecha entre las magnitudes medidas en el dominio del tiempo y las aquellas procesadas en el dominio de frecuencia. Como resultado, se certifica la conformidad de los sistemas completos de medición TDEMI con respecto a los requisitos definidos en los estándares internacionales para mediciones EMI.

Además, se ha demostrado que los sistemas de medición Full TDEMI ofrecen ventajas en comparación con los receptores de barrido convencionales para realizar varias medidas desafiantes típicas de las evaluaciones de emisiones electromagnéticas. Por ejemplo, las capturas de dominio de tiempo posibilitan mediciones de espectro completo que permiten un análisis adecuado de fenómenos transitorios. Del mismo modo, la cantidad de canales disponibles en la mayoría de los osciloscopios hace viables múltiples mediciones síncronas que para registrar las perturbaciones interferentes mediante una combinación de transductores.

Algunas de las aplicaciones de la medición EMI multicanal son la evaluación de etapa única de la EMI conducida de todas las líneas de alimentación de los equipos bajo prueba (EUT), la medición instantánea del voltaje del ruido en modo común y en modo diferencial, las mediciones concurrentes de la EMI conducida y radiada y la paralelización de los ensayos de emisiones radiadas con múltiples antenas. Tales métodos de prueba alternativos, han mejorado significativamente el proceso de prueba de EMC en una variedad de industrias al reducir la cantidad de tiempo y los esfuerzos necesarios para realizar una evaluación completa del sistema principalmente debido a las siguientes razones. En primer lugar, las mediciones de EMI en el dominio del tiempo arrojan resultados más rápidos porque el espectro de interferencias se estima simultáneamente para todos los detectores de ponderación estándar necesarios para determinar el cumplimiento de los límites máximos de emisiones definidos en las respectivas normas de producto. En segundo lugar, el número de iteraciones de medición se reduce debido a las posibilidades multicanal y también debido a una identificación ágil del peor caso de las emisiones de un EUT que tiene diferentes

modos de funcionamiento. En tercer lugar, el sistema Full TDEMI es una alternativa económica y versátil a los analizadores de espectro en tiempo real más avanzados en lo concerniente a mediciones EMI en el rango de pocos gigahertzios.

Desde el punto de vista teórico, los sistemas de medición Full TDEMI han extendido el estado del arte, como en el caso de un par de contribuciones denominadas el detector de máximo esperado y la descomposición empírica de interferencias.

El detector de máximo esperado es una medida estadística del nivel más probable de las emisiones pico que se basa en un modelado tiempo-frecuencia de las interferencias medidas utilizando la teoría del valor extremo. Usando la información de variabilidad del nivel de interferencia en cada componente de frecuencia, el detector de máximo esperado se puede usar para estimar el valor de retención máximo (max-hold) equivalente de una interferencia aleatoria. El detector de máximo esperado también proporciona un modelo que cuantifica la incertidumbre de la medición del detector de picos ante interferencias estocásticas.

La descomposición de interferencia empírica (EID) es una implementación modificada de la transformada de Hilbert-Huang con capacidades de sincronización de tiempo que permiten una determinación heurística de patrones oscilatorios característicos sin requerir transformación de dominio ni un conjunto predefinido de funciones base. La descomposición de la interferencia empírica se ha utilizado con éxito para la cancelación del ruido ambiental durante prueba de concepto de mediciones de EMI de al aire libre, obteniendo más de 20 dB de atenuación de las señales habituales de radiodifusión. El fundamento de la cancelación del ruido ambiental mediante EID es la identificación, en el tiempo y en el dominio de la frecuencia, de los modos de emisión intrínsecos que son atribuibles al EUT al restar los modos residuales (ruido ambiental) de los resultados de medición. Las contribuciones mencionadas se distribuyen en cuatro artículos de revista. Los resultados de medición complementarios y las aplicaciones de los sistemas de medición Full TDEMI también se han publicado en conferencias notables en el área.

Por los motivos antes mencionados, la tecnología Full TDEMI tiene ventajas significativas para los ensayos, el análisis y la resolución de problemas de EMI. Asimismo, proporciona un enfoque complementario a las mediciones típicas completamente enfocadas en el dominio de la frecuencia y exhibe un nivel de madurez que podría permitir su estandarización en los próximos años.

CONTENTS

LIST OF FIGURES

ACRONYMS

ADC	Analog to Digital Converter.
ANC	Ambient Noise Cancellation.
APD	Amplitude Probability Distribution.
AU	Auxiliary Unit.
BAN	Background Ambient Noise.
CISPR	Comité Especial Internacional de Perturbaciones Radioeléctricas.
CM	Common Mode.
DAC	Digital to Analog Converter.
DCS	Digital Communication Systems.
DM	Differential Mode.
DSP	Digital Signal Processing.
DVB-T	Digital Video Broadcasting – Terrestria.
EFT	Electrical Fast Transient.
EMC	Electromagnetic Compatibility.
EMD	Empirical Mode Decomposition.
EMI	Electromagnetic Interference.
EMPIR	European Metrology Programme for Innovation and Research.
EMRP	European Metrology Research Programme.
ESD	Electrostatic Discharge.
EU	European Union.
EUT	Equipment Under Test.
FFT	Fast Fourier Transform.
FPGA	Field-Programmable Gate Array.
FSV	Feature Selective Validation.
GCEM	Grup de Compatibilitat Electromagnètica.
GSM	Global System for Mobile communications.
GTEM	Gigahertz Transverse Electromagnetic (Cell).
IEC	International Electrotechnical Commission.
IF	Intermediate Frequency.
IMF	Intrinsic Mode Funtion.
JRP	Joint Research Project.
LISN	Line Impedance Stabilization Network.
LNA	Low Noise Amplifier.
OATS	Open Area Test Site.
OFDM	Orthogonal Frequency Division Multiplexing.
OSC	Oscilloscope.
PLL	Phase-Locked Loop.
RBW	Resolution Bandwidth.

RFID Radio Frequency IDentification.
SAC Semi Anechoic Chamber.
SFDR Spurious Free Dynamic Range.
SME Small and Medium sized Enterprises.
STFT Short Time Fourier Transform.
TDEMI Time Domain Electromagnetic Interference.
TEM Transverse Electromagnetic.
TETRA Terrestrial Trunked Radio.
UPC Universitat Politècnica de Catalunya.
UWB Ultra Wide Band.

COPYRIGHT

The papers comprised in this Thesis have been published or are accepted for publication in journals and conferences of The Institute of Electrical and Electronics Engineers, Incorporated (the "IEEE"). Therefore, the authors have transferred all rights under copyright that may exist in, according to the terms and conditions stated in the "*IEEE Copyright and Consent Form*" signed by the author's for each of the corresponding papers.

According to IEEE rules, *"The IEEE does not require individuals working on a thesis to obtain a formal reuse license"*. However, IEEE highlight the information in the following paragraph.

In reference to IEEE copyrighted material which is used with permission in this thesis, the IEEE does not endorse any of UPC's products or services. Internal or personal use of this material is permitted. If interested in reprinting/republishing IEEE copyrighted material for advertising or promotional purposes or for creating new collective works for resale or redistribution, please go to http://www.ieee.org/publications_standards/publications/rights/rights_link.html *to learn how to obtain a License from RightsLink.*

1

INTRODUCTION

Traditionally, the measurement of the radiofrequency emissions has been performed in the frequency domain by using measuring receivers having a superheterodyne architecture [1]. For standard electromagnetic interference (EMI) measurements, such approach usually involves very long measurement times, several iterations (e.g., mains lines, mast/turntable positions, antenna polarizations) and a number of attempts for detecting short-duration events responsible of the worst-case emissions while evaluating multiple modes of operation of the equipment under test (EUT).

In fact, the aforementioned drawbacks motivated the development of Fast Fourier Transform (FFT) based measuring receivers, as they are currently known in the latest version of the CISPR 16-1-1 standard [2]. All those FFT-based measuring receivers process the time-domain signal using mathematical transformations in order to estimate the interference's spectrum according to the different standard weighting detectors. The use of Fourier techniques in the field of electromagnetic compatibility (EMC) is very common nowadays and has grown rapidly during the last 20 years because of the accuracy and efficiency of FFT algorithms [3]. In that sense, the first paper proposing an FFT-based measuring receiver was published in 1989 by Bronaugh [4]. Between 1989 and 1993 those ideas were shaped by several designs proposed by different authors. Consequently, in 1994 the first proof-of-concept FFT-based measuring receivers were implemented by Schütte and Kärner [5].

Nonetheless, to the best of authors knowledge, the term "Time-Domain Electromagnetic Interference Measurement System" was first introduced in several papers by researchers from the Institute for High-Frequency Engineering of the "Technische Universität München" between 2002 and 2003 [5, 6]. In its origins, it was stated their TDEMI measurement system used an oscilloscope, and a PC for computing the spectrum of the interferences emulating based on acquisitions of tens of microseconds that took a couple of minutes to be processed.

The comparisons made between TDEMI measurement systems and conventional EMI test receivers were successful. However, even if it was theoretically possible to implement a measuring receiver based on an oscilloscope, it was not possible in practice due to the limited performance of both oscilloscopes and personal computers.

Likewise, the real-time spectrum analyzer architecture progressed rapidly and allowed for scalable frequency ranges while providing increasingly faster measurements thanks to the FFT processing at intermediate frequency [7]. Nowadays, real-time measuring receivers cope with CISPR 16-1-1 requirements, are the highest end receivers of all manufacturers and, are used for product certification worldwide [8].

However, in recent years, the research on alternative test methods for EMI measurements has brought back the idea of using oscilloscopes for EMI measurements, beyond the pre-certification purposes for which they have been commonly relegated. Those ideas have been continually developed since 2013 through intense research activities that have led to a number of papers published in recognized journals and conference proceedings in the field of the electromagnetic compatibility. This document is the framework that gather and relate those scientific contributions in the body of the Thesis.

In this regard, this Thesis comprises the research that gave rise to the "Full TDEMI measurement systems", a software defined implementation of a measuring receiver that allows for EMI testing using oscilloscopes while meeting all baseline requirements of CISPR 16-1-1 [9, 10]. Unlike other types of receivers, Full TDEMI measurement systems benefit of the oscilloscopes built-in capabilities such as the multiple synchronized channels and the triggering options for realizing enhanced testing methods. In the following sections, the rationale, the state of knowledge and the objectives of the Thesis will be presented before continuing to the description of the scientific contributions that define this Thesis structure.

1.1. RATIONALE

Nowadays, assuring the compliance of electrical and electronic devices with regards electromagnetic compatibility standards is a requirement worldwide [11]. On the one hand, EMC is a fundamental aspect for guaranteeing the performance, quality and in some cases, the safety of most electronic devices and systems [12, 13]. On the other hand, EMC standards also establish testing methods and requirements that electronic equipment shall comply with in order to ensure that, when used as intended, such equipment does not disturb radio and telecommunication, as well as other equipment.

However, due to the rapid development of new electronic products with emerging technologies and features, the ability to achieve and to improve electromagnetic compatibility is a major challenge in the development of electronic products. This is valid even in those cases where the technology of the products advances at a faster rate than their corresponding EMC testing standard.

Therefore, developing improved EMC test methods is a recognized need in order to provide time-saving, cost-effective and, especially, suitable techniques applicable in different scenarios such as the study of the impact of EMI on digital communication systems or the evaluation of EMI on industrial environments through *in-situ* measurements.

For example, the modern highly standardized industry has a growing and recurrent need for EMC pre-compliance and fully compliance certification tests. Throughout product development, most EMI measurements are performed in order to verify the frequency spectra of the disturbances meet the limits set in current product standards. Similarly, third-party EMC testing labs need to attend a variety of clients that are pressured to introduce their products into the market as soon as possible. In both cases, there is a

heavy load of tests that are costly and time consuming activities, to the point of becoming a troublesome imposition rather than a part of a product quality assurance policy.

This concerns designers and testing laboratories because they are urged for cost-effective and faster EMC measurement methods during the product development and the certification stages, respectively. Therefore, improving the measurement systems in order to conduct faster reliable measurements would reduce costs in the product development process and the time to market.

Additionally, developing and maintaining a fully compliant EMC testing facility (semi-anechoic chambers, TEM/GTEM cells, receivers, signal generators, power amplifiers, simulators of ESD/EFT/Surge, antennas, coupling/decoupling networks and line impedance stabilization networks among other equipment's and accessories, all of them with valid and traceable calibration) is a burden for the industry. The alternative of attending to an external third party EMC laboratory generally is expensive, time consuming and complicated, or even impossible, in the case of heavy, large or mounted equipment under test.

Consequently, there was, and still is, a need for novel test methodologies and procedures to assess the EMC compliance in order to fulfil the industry needs and expectations, as it was demonstrated in the European Joint Research Project (JRP) "EMRP JRP IND60 EMC Industry" [14]. This project focused on developing improved EMC test methods suitable for industrial environments. Hereafter, the Universitat Politècnica de Catalunya through its Grup de Compatibilitat of Electromagnètica, GCEM – UPC, played an important role that driven the development of full time domain measurement systems and the applications that belong to this Thesis.

In that sense, the time domain methods applied to the EMI measurement were selected as the potential solution strategy to many of the previously described problems. Time-domain measurements are not only useful to provide faster assessment of the conducted and radiated emissions, but also are required to evaluate transient disturbances that cause of electromagnetic incompatibilities and interferences. This is the case of digital communication systems for which the broadband impulsive noise unintentionally produced, i.e., by sparks or switching power supplies can become in-band interferences that affects the receivers, as happens in several contemporary applications such as Digital Video Broadcasting Terrestrial (DVB-T), Trans European Trunked RAdio (TETRA), Radio Frequency IDentification (RFID) and GSM-Railway system that are susceptible of degradation in their performance under the impact of transient broadband interfering noise [15, 16].

Thereupon, aware of the increasingly importance of attending the above-mentioned challenges, it was proposed to develop a toolset to enable general-purpose oscilloscopes not only for compliant EMI measurements but also for enabling enhanced/optimized multichannel test setups. The outcome of this research shall allow improved measurement capabilities while reducing the time and cost associated to the EMI assessments in complex environments. In other words, the Thesis research was addressed to provide validated and affordable instrumentation technology that drives to novel reliable methods for evaluation of the electromagnetic emissions through suitable time-domain techniques that are beyond the state-of-the-art.

1.2. AIM AND OBJECTIVES OF THE THESIS

The hypothesis of this Thesis is that time-domain measurement methods can be used for evaluating the electromagnetic emissions of electrical and electronic devices and that such techniques are adequate for addressing the interference assessment in complex scenarios. In that sense, appropriated signal acquisition and processing algorithms are required for enhancing the performance of general-purpose time-domain instruments, in particular oscilloscopes, for coping with the stringent characterization of transient, non-stationary and random disturbances. Thus, the Thesis research is intended to provide novel, comprehensive, affordable and practical means for analysing and troubleshooting EMI, in the frequency, time, time-frequency and statistical domains.

Accordingly, the following specific objectives were proposed. Each of them constitutes a milestone for achieving the main goal of this Thesis:

1. To develop a time-domain EMI measurement system comprising the signal processing techniques and algorithms that enable using general purpose time-domain instruments, in particular oscilloscopes, for measuring radiofrequency electromagnetic emissions.

2. To define alternative EMI measurement methods beyond current standardized practices that take advantage of time-domain instrumentation to enhance emissions test setups.

3. To process time-domain EMI measurement data for advanced applications such as the statistical modelling of the worst-case disturbance emissions levels (extreme values), transient and continuous wave noise decomposition and ambient noise cancellation.

4. To evaluate the performance of Full Time-Domain EMI measurement systems using automated and traceable calibration procedures designed according to the requirements defined in the CISPR 16-1-1 standard.

1.3. THESIS STRUCTURE

This document has been prepared as a compendium of four papers published in recognized journals in the field of electromagnetic compatibility, instrumentation and, measurement science. Those papers are fundamental for accomplishing the aim and the objectives of the Thesis. Likewise, several complementary articles are also included in this compendium as they allowed a more detailed description of relevant applications of Full TDEMI measurement systems. In that sense, after the introductory Chapter 1, this document is organized as follows.

- Chapter 2 describes the state of the knowledge that constitutes as the background of this Thesis. It includes a review of the preceding studies on time-domain EMI measurements, the fundamental theory of spectral estimation and the explanation of the different architectures of EMI measuring receivers.

- Chapter 3 comprises the papers that establishes the concepts regarding Full TDEMI measurement systems and its software-based architecture for processing EMI measurement data.

- Chapter 4 includes the articles related to alternative testing methods, practices and experiences enabled by the Full TDEMI measurement systems.

- Chapter 5 contains the publications dedicated to the exploitation of time-domain measurements for performing the estimation of worst-case emissions levels based upon the expected maximum detector developed according the statistical theory of extreme values.
- Chapter 6 comprehends the papers devoted to the decomposition of EMI in the time-domain and its application for ambient noise cancellation.
- Chapter 7 encompass the papers summarizing the results of the assessment of performance carried into representative implementations of Full TDEMI measurement systems.
- Finally, Chapter 8 presents the conclusions derived from the results of this Thesis and a discussion about the future of research, innovation and standardization activities related to time-domain EMI measurements and applications.

1.3.1. LIST OF FUNDAMENTAL PUBLICATIONS IN JOURNALS

Accordingly, the fundamental papers included in this compendium are listed below, organized in chronological order by date of publication.

- *Fundamental journal article 1.* The first paper is entitled "Improving Time-Domain EMI Measurements through Digital Signal Processing" [17]. It is reproduced in Chapter 3, section 3.1.
- *Fundamental journal article 2.* The second paper is entitled "On the Statistical Properties of the Peak Detection for Time-Domain EMI Measurements" [18]. It is reproduced in Chapter 5, section 5.1.
- *Fundamental journal article 3.* The third paper is entitled "Decomposition of Electromagnetic Interferences in the Time-Domain" [19]. It is reproduced in Chapter 6, section 6.1.
- *Fundamental journal article 4.* The last paper of the compendium is entitled "Waveform Approach for Assessing Conformity of CISPR 16-1-1 Measuring Receivers" [10]. It is entirely reproduced in Chapter 7, section 6.1.

1.3.2. APPLICATIONS DESCRIBED IN CONFERENCE PROCEEDINGS AND OTHER PUBLICATIONS

The papers listed below comprise the further applications of the Thesis fundamental ideas. Most of them correspond to proceedings in notable conferences in the field of electromagnetic compatibility that were presented during the years 2015 to 2018. Moreover, there is a mention to an additional journal paper. Those publications are spread in the corresponding chapters according to the type of application. Such complementary papers deliver the complete report of the activities developed as part of the research on Full TDEMI measurement systems. Such applications allowed a widespread dissemination of Full TDEMI measurement systems in a variety of industries, with emphasis in the emission measurements performed *in-situ*. Thereupon, their titles listed below in order of presentation.

- *Conference proceeding 1.* "A Measurement System for Radiated Transient Electromagnetic Interference based on General Purpose Instruments" [20]. It is reproduced in Chapter 3, section 3.2.
- *Complementary journal article 1.* "Measurement and Evaluation Techniques to Estimate the Degradation Produced by the Radiated Transients Interference to the GSM System" [21]. It is reproduced in Chapter 4, section 4.1.

- *Conference proceeding 2.* "On-board compact system for Full Time-Domain Electromagnetic Interference Measurements" [22]. It is reproduced in Chapter 4, section 4.2.
- *Conference proceeding 3.* "Benefits of Full Time-Domain EMI Measurements for Large Fixed Installations" [23]. It is reproduced in Chapter 4, section 4.3.
- *Conference proceeding 4.* "Full Time Domain EMI Measurement System applied to Railway Emissions according to IEC 62236-3-1/EN 50121-3-1 Standards" [24]. It is reproduced in Chapter 4, section 4.4.
- *Conference proceeding 5.* "Robust Extreme Value Estimation for Full Time-Domain EMI Measurements" [25]. It is reproduced in Chapter 5, section 5.2.
- *Conference proceeding 6.* "A Single Antenna Ambient Noise Cancellation method for In-Situ Radiated EMI Measurements in the Time-Domain" [26]. It is reproduced in Chapter 6, section 6.2.
- *Conference proceeding 7.* "APD outdoors Time-Domain Measurements for Impulsive Noise Characterization" [27]. It is reproduced in Chapter 6, section 6.3.
- *Conference proceeding 8.* "Fast and Automated Verification of Multi-channel Full Time-Domain EMI Measurement Systems" [9]. It is reproduced in Chapter 7, section 7.2.
- *Conference proceeding 9.* "Dynamic Performance Evaluation of Full Time Domain EMI Measurement Systems" [28]. It is reproduced in Chapter 7, section 7.3.

2

STATE OF KNOWLEDGE

The modern generation of measuring receivers has embraced FFT-based capabilities not only for speeding up emissions' testing but also to provide time-domain and time– frequency analysis features useful for evaluating and mitigating the impact of transient and stochastic disturbances [3]. Currently, real-time analyzers and oscilloscope-based implementations are two differentiated approaches for implementing FFT-based EMI measuring receivers. However, both architectures share a single origin and have evolved during the past 25 years, as it will be shown next.

2.1. OVERVIEW OF THE EVOLUTION OF FFT-BASED EMI MEASUREMENT SYSTEMS

As it has been mentioned before, to the best of author's knowledge the first reported paper proposing a FFT-based measuring receiver was published in 1989 by Bronaugh [4]. In the following years, Bronaugh basic proposal was further developed by different authors until, in 1994, the first FFT-based EMI measurement system was implemented [29–31].

However, it was until 2001 that one of the first fully functional FFT-based measuring receivers was introduced by Krug, et al. [5]. Two years later, Krug and Russer published severs papers presenting their progress in the development of a complete FFT-based measuring receiver in the 30 MHz - 1 GHz band that included several new features such as: correction factors for the antenna (factor), for the mismatch between the antenna and the amplifier, for the attenuation in the cables and for the frequency response of the low pass filter used for band limiting the measured signal [32]; calculation via FTT or Bartlett and Welch Periodogram [33]; and mathematical models for the emulation of the peak, average, root-median-squared (rms) detectors [5]. Afterward, they also presented a model for the quasi-peak detector [34]. They also proposed different pre-compliance measurement strategies to face different classes of interferences, that is, continuous narrowband signals, and continuous broadband signals, pulse modulated narrowband signals, random (statistically stationary and non-stationary) signals or deterministic signals (periodic, quasi-periodic, non-periodic) [35]. The FFT-based measuring receiver was validated on different scenarios showing a satisfactory agreement when compared against measurements taken with conventional super

heterodyne EMI receivers, while providing a measurement time is reduced by one order of magnitude [35].

Throughout the years 2004 and 2005 other research groups developed alternative mixed time-domain/frequency-domain measuring systems focused on specific applications. That is the case of York EMC services (YES) and the GCEM-UPC. In particular, YES developed a multi spectrum analyzer system to perform frequency domain measurements continuously over a given time, in the 9 Hz to 1 GHz band. This measurement system was specifically intended for performing the radiated emission testing of rolling-stocks. The system architecture consists of three spectrum analyzers that gather data continuously in the same frequency band. They are triggered one after the other, avoiding overlapping different capturing times in order to overcome the problem of downloading and measuring at once. This system was synchronized with a digital camera so it was possible to correlate train movement and position with the measurement results of the instantaneous spectrum of the radiated emissions. Other two additional spectrum analyzers configured in zero span mode where used to identify peaks caused by broadband signals [36].

On the other hand, the GCEM-UPC developed a mixed time-domain/frequency-domain measurement system conceived for evaluating the effect of non-periodic fast transients in a narrow measuring bandwidth (lower than 1 MHz) centred at a fixed frequency in the 9 kHz – 3 GHz range. This measurement system combined the intermediate frequency (IF) output of a test receiver with a digitizing card for measuring in the time domain. The architecture of the measurement system allowed taking advantage of the high sensitivity, the wide operating frequency and dynamic range of the receiver's front end. Besides, the required digitizer sampling frequency was only twice the intermediate frequency because the signal has been down-converted, which made possible to use analog-to-digital converters (ADC) featuring a resolution better than 10 bits. In order to synchronize the measurement system with the transient event/pulse, a trigger signal is provided by a 500 MHz digital oscilloscope that is also connected to the IF output of the EMI receiver [37].

Both aforementioned measurement systems were compared in a measurement campaign included in the COST action 286 "Electromagnetic Compatibility (EMC) in Diffused Communication Systems". Several improvement opportunities were identified for both systems, such as including continuous data logging combined with synchronous triggering in order to being able to obtain enough data for the extraction of statistic parameters using an affordable amount of memory. These additional features were needed in order to characterize impulse noise environments in which the noise sources can be either transient phenomena or diffused communication systems.

Furthermore, researchers from the Institute of High-Frequency Engineering of the Technical University of Munich continued improving their 30 MHz – 1 GHz FFT-based spectrum analyzers, focusing on achieving the CISPR 16-1 requirements. In 2005, they published several papers introducing a multi-resolution FFT-based spectrum analyzer which exhibits three channels with limiters, amplifiers, and analog-to-digital converters. Therefore, the amplitude range of the signal is subdivided into three intervals and in each interval the ADC is performed with an amplitude discretization proportional to the width of the amplitude interval [38]. They state the system had a lower Spurious-Free Dynamic Range (SFDR) than the conventional EMI receivers of the time. Additionally, the presented system fulfilled CISPR 16-1 requirements of SFDR for stationary signals, while for transient signals, the system had a SFDR that was below the requirements. This system also improved the noise floor by lowering it 5 dB on comparison with other super-heterodyne EMI receivers. They also reported measurements 50 times faster than those performed with conventional EMI receivers [39].

In the following years (2007-2008), Russer and Braun continued working on different applications for their FFT-based spectrum analyzer, as in the case of Automotive Testing for which they also obtained satisfactory results [40]. Due to the success obtained in different scenarios, they also proposed alternative test procedures and the first approximation to the uncertainty estimation in time-domain EMI measurements based upon contributions such as the variability observed in the spectrogram measured as the deviation from the mean spectrum [41]. Finally, they developed a real-time, Field Programmable Gate Array (FPGA) based, spectrum analyzer fully compliance with CISPR 16-1-1 requirements in the 30 MHz – 1 GHz band, that supported the standard weighting detectors modes (peak, average, rms, quasi-peak) [7], stating an approximated error of 1 dB, 0.2 dB and 0.4 dB when measuring with the peak, average and quasi-peak detectors in comparison with a conventional EMI receiver. For that purpose, they used 8 parallel 10-bit ADC at 250 MS/s. They also provided details on how estimating the measurement uncertainty in their measurement system in order to comply with CISPR specifications, concluding that the overlapping factor and the dwell time are the major parameters that must be adjusted in order to reduce the variability in pulse measurements [42].

By that time, an internal CISPR Joint Task Force formed by CISPR A/1 (EMC Instrumentation Specifications), CISPR A/2 (EMC Measurement Methods, Statistical Techniques and Uncertainty) and CISPR D/2 (Protection of On-Board Receivers) was formed to discuss and implement the changes required by the standards in order to contemplate the inclusion of FFT-based instrumentation in CISPR 16 [43]. Simultaneously, EMI/EMS hardware vendors started promoting and marketing new Real Time Spectrum Analyzers as commercial systems up to 1 GHz highlighting as their more important feature the time-saving capability when compared against the super heterodyne counterparts [44].

However, for FFT-based EMI receivers intended for measuring radiated emissions above 1 GHz, the more relevant references are found from 2011 onwards. Some FFT-based EMI receivers, such as those developed by Gauss Instruments (a spin-off company from the Institute for High-Frequency Engineering of the Technische Universität München) were designed to accomplish measurements at frequencies up to 18 GHz by means of a cascaded two-stage down converter, first from 1 GHz to 6 GHz and then from 6 GHz to 18 GHz [3]. As the frequency increases, the internal microwave circuits become more complex and sensible, requiring low noise components (PIN-diode switches, PLLs, LNA) [8]. Nonetheless, those new FFT-based EMI receivers exhibits an IF dynamic range of over 60 dB (more than 20 dB higher than required by CISPR 16-1-1) with respect to an IF bandwidth of 1 MHz, and noise floors as low as 6 dB [45].

Additionally, with the increasing computing power and larger amount of memory available for storage and signal processing, the inclusion of new features and measurement capabilities for real-time spectrum analyzers was finally feasible. For example, some FFT-based EMI receivers incorporate the Amplitude Probability Distribution (APD) feature that allows the characterization of broadband digital services using Orthogonal Frequency Division Multiplexing (i.e. Digital Video Broadcasting – Terrestrial) and Ultra Wide Band (UWB) signals [46]. Moreover, some of those real time analyzers were also capable of performing click rate analysis as required by CISPR 14 for discontinuous disturbances [47].

Recently, the problem of measuring intermittent disturbances has been investigated since it is fundamental to provide effective measurement methods to capture transient and potentially broadband disturbances that occur only when a specific event is triggered. For instance, this is a concerning issue for the automotive industry, expressly, when testing hybrid or electric vehicles [40]. GCEM-UPC developed a specific

time-domain system to address that problem and formally validated it under different scenarios using the Feature Selective Validation (FSV) method obtaining an overall excellent performance. The aforementioned system was used for conducted emission measurement (form 150 kHz to 30 MHz) of a sliding-step used for railway transport applications [48].

In the light if the above, it becomes clear that real-time spectrum analyzers have reached a level of technological deployment that made them a reliable alternative for emissions measurements, fully compliant with the EMC standards, time efficient and probably the highest-end commercialized test solution for a EMC testing laboratory. However, most commercially available real-time test receivers are a very costly piece of hardware that many small to mid-size laboratories cannot afford just for their internal pre-compliance testing or even for on-site measurements due to risk involved in transporting and employing such a delicate and expensive device outside the controlled environment of a laboratory.

Nonetheless, as has been exposed in the references cited before, general-purpose oscilloscopes and digitizers have also been used to implement measurement systems for specific type of electromagnetic disturbances and as an EMI debugging tool. For example, there are plenty of application notes with the recommended measurement techniques required to use general-purpose oscilloscopes as an EMI troubleshooting tool through near field scanning of PCB traces [49]. However, the above mentioned document also states the proposed measurement setup is not suitable to perform compliance measurements since it guarantees neither the resolution bandwidth nor the detector characteristics required by the CISPR.

As it was noted in this brief overview of the evolution of the FFT-based EMI measurements, most concepts are common to their different implementations. Consequently, those principles are the theoretical basis for the Full TDEMI measurement systems technology and their applications, and thus, they will be presented as follows.

2.2. PRINCIPLES OF FFT-BASED EMI MEASUREMENTS

A continuous-time signal function, $x(t)$, that represents the measured EMI is observed during a time period of length T_0. In order to computationally evaluate the frequency spectrum of $x(t)$, $X(f)$, the measured signal is sampled and digitized to obtain a time-discrete signal, $x[n]$, where n is integer and $x[n]$ is assumed as periodic with total number total number of samples, N, that is, $x[n+N] = x[n]$. Therefore,

$$x[n] = x(n\Delta t) \tag{2.1}$$

where $T_0 = N\Delta t$ and Δt is the sampling interval, that is, $\Delta t = 1/f_s$, f_s being the sampling frequency. It is understood that f_s at least fulfils the Nyquist-Shannon criteria.

Moreover, if the maximum measurable frequency is $f_{\max}$ it is recommended to use $f_s \geq 4f_{\max}$ in order to avoid undesired aliasing errors. Then, the discrete frequency spectrum $X[k]$ is related to the continuous frequency spectrum $X(f)$ by

$$X[k] = X(k\Delta f), \tag{2.2}$$

where k is integer and Δf is the spacing of the spectral lines. The quantities N, T_0, Δt, and Δf are related by

$$\Delta f = \frac{N}{T_0}. \tag{2.3}$$

The discrete Fourier transform (DFT) is given by

$$X[k] = \sum_{n=0}^{N-1} x[n] e^{-j\frac{2\pi nk}{N}}. \tag{2.4}$$

The spectral estimation is performed on the basis of the DFT under the assumption that the $x[n]$ is periodic in n with a period N. However, $x[n]$ is not really periodic since there is only a single continued measured signal sequence of length N.

Therefore, to reduce the scallop loss and the spectral leakage caused by its finite length, the time record $x[n]$ is multiplied by a window function $w[n]$ which exhibits a maximum value for $n = N/2$ and smoothly goes to zero for n approaching 0 or $N-1$, respectively [33, 39],

$$x_w[n] = x[n]w[n], \tag{2.5}$$

where $x_w[n]$ is the windowed signal in the discrete-time domain. Consequently, in the frequency domain this yields a convolution, which in the discrete domain is given by,

$$X_w[k] = X[k] * W[k] = \sum_{m=0}^{N-1} X[m]W[k-m]. \tag{2.6}$$

If windowing is used, it is necessary to compensate the corresponding energy loss caused by the window using the coherent gain scaling factor [50], G_C. The coherent gain, G_C, is given by,

$$G_C = \frac{1}{N}\sum_{n=0}^{N-1} w[n]. \tag{2.7}$$

Furthermore, calculating the spectrum for a specific (for instance at the 6 dB decay point) equivalent resolution bandwidth, RBW, requires a minimum number of samples in the time record, that is,

$$N_{\min} = f_s \frac{w_f}{RBW} \tag{2.8}$$

where w_f is the window factor of the windowing function used, i.e., Gaussian, Hann, or Kaiser–Bessel [17].

In addition, if $N > N_{\min}$, it is possible to define $M > 1$ overlapping windows, each of them of length equal to $N_{\min}$, in order to determine the frequency and phase content of the m-th local sections of an EMI signal as it changes over time. This process is called the Short-Time Fourier Transform (STFT) and it is given by,

$$X_m[k] = \sum_{n=0}^{N_{\min}-1} x[n]\, w\left[n - m\left(1-o_f\right)N_{\min}\right] e^{-j\frac{2\pi nk}{N_{min}}}, \tag{2.9}$$

where o_f is the overlap factor (generally between 0.5 and 0.95 depending on the type of windowing function) and $m = 0, 1, 2, \ldots (M-1)$ is the time shift index that controls the sliding of the overlapping window between successive time frames.

Besides, since EMI measurement (dwell) time is usually larger than the minimum, N_{min}/f_s, it is possible to apply non-parametric spectral estimation techniques based in the periodogram. This is convenient for improving the accuracy and the precision of the amplitude spectrum of stationary random signals by means of the reduction on the spectrum variance achieved through averaging on the frequency domain [3].

The periodogram method was first published by Bartlett [51]. In Bartlett's method the data is smoothed by averaging over the power computed for a number M of short-time signal segments. Later, Welch combined DFT methods with the use of window functions and developed a method for averaging short, modified periodograms [52].

As stated before, both periodogram methods, Bartlett- and Welch-, are based on the averaging of the spectra obtained by applying the STFT to the time-domain EMI signal. In the Bartlett method [32] the time domain sequence is subdivided into P non-overlapping segments, where each segment has length $N_{\min}$. For each segment the periodogram is computed and the Bartlett power spectral estimate is obtained by averaging the periodograms for the segments. Then, the frequency spectrum calculated by the Bartlett periodogram [5] is given by,

$$P_B[k] = \frac{1}{PN_{\min}} \sum_{p=0}^{P-1} \left| \sum_{n=0}^{N_{\min}-1} x[n+mN_{\min}] e^{-j\frac{2\pi nk}{N_{\min}}} \right|^2, \tag{2.10}$$

By this averaging of the spectrum the variance of the spectrum estimation is reduced by a factor M, however at the expense of a reduction of the frequency resolution by the same factor [3]. Welch [52] modified Bartlett's method by using windowed data segments overlapping in time. The windowing is applied to reduce the spectral leakage associated with finite observation intervals. The overlapping time windows yield a further reduction of the periodogram variance. The frequency spectrum calculated by the Welch periodogram [33] is given by

$$P_W[k] = \frac{1}{MN_{\min}W} \sum_{m=0}^{M-1} \left| \sum_{n=0}^{N_{\min}-1} x[n]\, w\left[n - m\left(1-o_f\right)N_{\min}\right] e^{-j\frac{2\pi k}{N_{\min}}} \right|^2, \tag{2.11}$$

where W is the discrete-time window gain, given by,

$$W = \frac{1}{N_{\min}} \sum_{n=0}^{N_{\min}-1} w^2[n]. \tag{2.12}$$

Considering that (2.9) provides the information of the time frequency distribution of $x(t)$, $X_m[k]$ can be used for calculating the single-sided amplitude spectrum, $S_A[k,m]$, corresponding to the different detector modes required for standard EMI measurements [7, 18, 34]. Accordingly,

$$S_A[k,m] = \begin{cases} \frac{1}{N_{min}G_C}|X_m[0]| & \text{for } k=0 \\ \frac{\sqrt{2}}{N_{min}G_C}|X_m[k]| & \text{for } 1 \le k < k_{Nyquist} \end{cases} \tag{2.13}$$

where the discrete Nyquist frequency, $k_{Nyquist}$, is given by

$$k_{Nyquist} = \begin{cases} N_{\min}/2 & \text{for even } N_{\min} \\ (N_{\min}+1)/2 & \text{for odd } N_{\min} \end{cases} \tag{2.14}$$

The equation (2.13) considers only the spectral amplitudes up to the Nyquist frequency. For the negative frequencies, that is, $k_{Nyquist} \le k < N_{\min}$, the respective spectral amplitudes are conjugate complex to the spectral amplitudes in positive side of the spectrum. Therefore, the single side spectrum corresponds to

twice the spectral amplitudes in the region $1 \leq k < k_{Nyquist}$ and then the whole expression is divided by $\sqrt{2}$ to account for the effective value.

Subsequently, in the particular case of the peak detector, $S_{peak}[k]$, it corresponds to,

$$S_{peak}[k] = \max\{|S_A[k,m]| \text{ for } m \in [0,\ M-1]\}. \tag{2.15}$$

Likewise, for the average, $S_{ave}[k]$, and the rms, $S_{rms}[k]$, detectors the corresponding expressions are,

$$S_{ave}[k] = \frac{1}{P}\sum_{m=0}^{M-1} S_A[k,m], \text{ and,} \tag{2.16}$$

$$S_{rms}[k] = \sqrt{\frac{1}{P}\sum_{m=0}^{M-1} {S_A}^2[k,m]}, \tag{2.17}$$

respectively.

Finally, regarding the quasi-peak detector, $S_{qp}[k]$, it is emulated by applying a weighting correction factor for each frequency bin that is a function of the equivalent pulse repetition frequency. In that sense, the equivalent pulse repetition frequency is calculated by inverting the pulse response curves defined in the CISPR 16-1-1 standard and using the measured $S_{peak}[k]/S_{ave}[k]$ and $S_{peak}[k]/S_{rms}[k]$ ratios [2]. The amplitude relationship between detectors must be respected, which means,

$$S_{peak}[k] \geq S_{qp}[k] \geq S_{rms}[k] \geq S_{ave}[k]. \tag{2.18}$$

2.3. ARCHITECTURES OF FFT-BASED EMI TEST RECEIVERS

Currently, real-time analyzers and oscilloscope-based implementations are two differentiated approaches for implementing FFT-based measuring receivers. In this section, both of them are briefly explained.

2.3.1. REAL-TIME ANALYZERS

A block diagram of the real-time EMI analyzer's architecture is shown in Figure 2.1. This type of measuring receiver uses the mixer and the local oscillator to convert the input signal to a constant intermediate frequency (IF), similarly as with the heterodyne architecture. At IF, the signal is sampled fulfilling the Nyquist criterion using analog-to-digital converters (ADCs) and filtered to avoid aliasing. The time and value-discrete IF signals are digitally downconverted to baseband and then processed for obtaining the signal spectrum.

There are two possibilities for preparing a frequency-domain display. The first one is using digital filters of certain resolution bandwidth for emulating the functioning of an analog spectrum analyzer. The second option is to calculate the spectrum of that frequency range using the FFT with the corresponding windowing for achieving the exact RBW setting. In both cases, it is still necessary to run through the frequency range that has been set on, which means that for spans larger than the IF bandwidth, several iterations of the acquisition are required [53, 54].

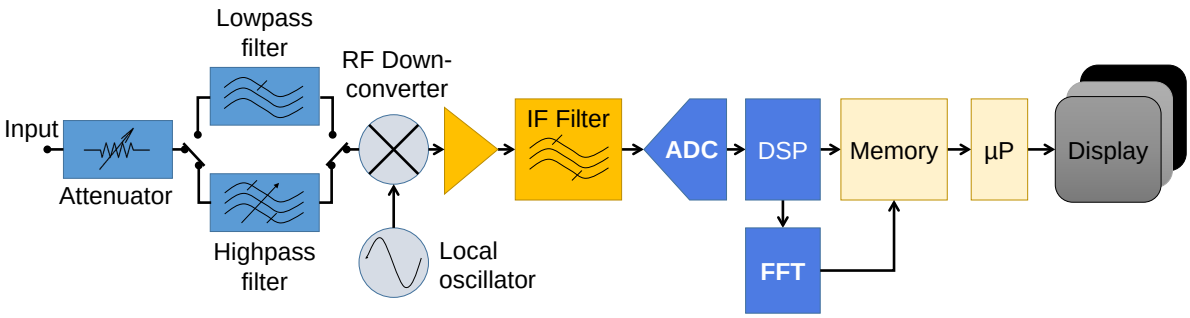

Figure 2.1: Block diagram of a real-time EMI analyzer.

2.3.2. FULL TIME-DOMAIN EMI MEASUREMENT SYSTEMS

Full TDEMI measurement systems are oscilloscope-based implementations of an EMI measuring receiver. They have been investigated in-depth across this Thesis and this subsection is only intended to provide a brief definition in the context of the different architectures of FFT-based EMI test receivers. In general terms, a Full TDEMI measurement system is described by the block diagram shown in Figure 2.2. For the measurement of radiated EMI, a broadband antenna shall be used, while for the measurement of conducted EMI corresponds either a current clamp or a line impedance stabilization network. The measured signal could be amplified or filtered for achieving better sensitivity. In the ADC, the full spectrum signal is digitized in real time and stored in as a time-discrete value-discrete signal.

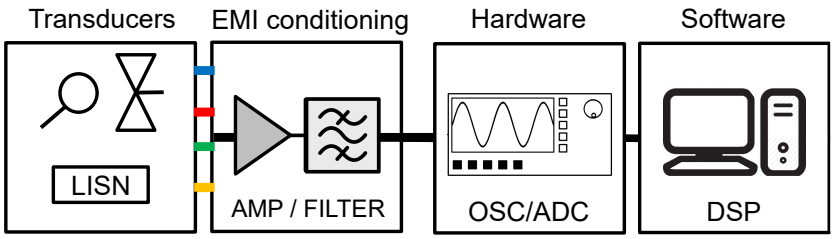

Figure 2.2: Block diagram of a Full Time-Domain EMI measurement system.

Full TDEMI measurement systems capture the whole spectrum of the EMI with every acquisition enabling multi-domain analysis. Besides, the triggering and multichannel capabilities found in most oscilloscopes provide additional tools for testing multi-functional mode equipment and for emissions testing parallelization. On the other hand, much higher sampling rates and a deeper memory are required than with real-time analyzers. This imposes bandwidth and dwell-time constraints based on the current oscilloscope technology.

2.4. ALTERNATIVE EMI TESTING METHODS ENABLED BY MULTICHANNEL MEASURING RECEIVERS

Multichannel test receivers allow for specific measurement methods that extend the standard procedure to an additional dimension in where several acquisitions are performed synchronously, that is, in parallel. For instance, the multi-line conducted emissions testing of single-phase or three-phase EUTs, the synchronous radiated and conducted EMI assessment, and the common-mode/differential-mode noise voltage measurement are direct application examples.

Nonetheless, before describing the alternative EMI testing methods enabled by multichannel test receivers, a brief overview of the conventional conducted and radiated emissions measurement procedure will be given for those readers that are not familiarized with the pertinent product, family or generic EMC standards.

2.4.1. STANDARD CONDUCTED EMISSIONS MEASUREMENTS

The conducted emission measured for verification of compliance with the regulatory limits must be measured with a line impedance stabilization network (LISN) inserted between the mains network and the EUT's ac power cord. A simplified test setup is shown in Figure 2.3. The EUT's is connected to the mains network through the LISN. The LISN has two objectives: a) to present a constant impedance to the product's power cord outlet over the frequency range of the conducted emission test b) to filter the radiofrequency disturbances found in the mains network that are not due to the EUT so that only the conducted emissions of the product are measured [55]. The LISN circuit and impendence requirements are specified in several standards including the CISPR 16-1-2, MIL-STD-461, FCC Part 15, ANSI C63.4. Finally, a test receiver or an spectrum analyzer is attached to the LISN RF output for measuring the conducted emissions, one line at the time.

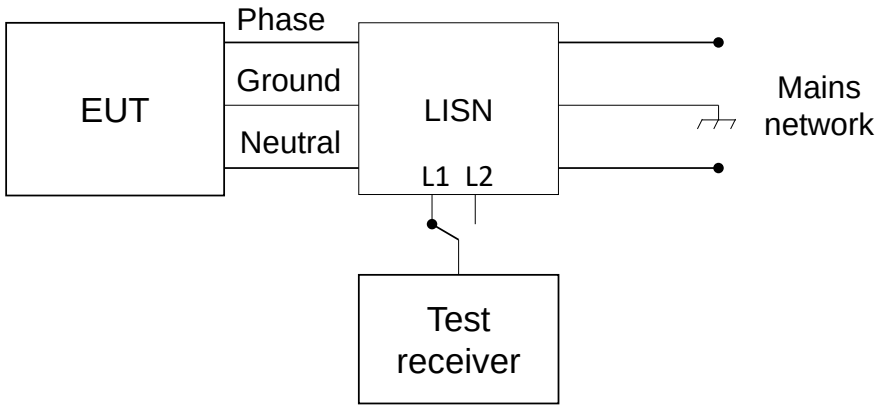

Figure 2.3: The test setup for standard conducted emissions testing.

2.4.2. STANDARD RADIATED EMISSIONS MEASUREMENTS

The basic test setup for measuring radiated emissions is shown in Figure 2.4. It requires an antenna for sensing the electric field placed at a certain height and distance, in the far field region, from the EUT. The measurement antenna is typically a broadband hybrid antenna in order to reduce the number of sub-bands included in the frequency range under assessment, thus avoiding the need of mounting and dismounting several antennas in each test iteration. The measurement distance, the antenna heights and the number of EUT's faces that must be evaluated are specified in standards for both tabletop and floor-standing types of equipment.

The radiated emissions measurements for assuring the compliance with regulatory limits must be carried

out either in an Open Area Test Site (OATS) or in an shielded semi-anechoic chamber (SAC). Nowadays, the usage of OATS is compromised by the ambient noise levels that are typically above the emissions limits. That's the fundamental reason why the almost noise free environment provided by the SAC is preferred for performing radiated emissions testing.

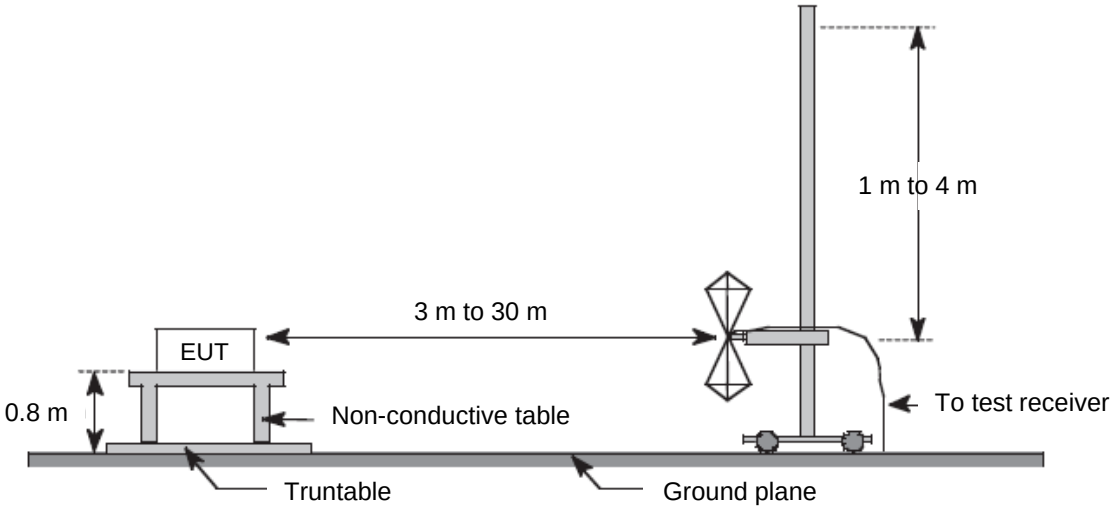

Figure 2.4: The test setup for standard radiated emissions testing [56].

2.4.3. MULTILINE CONDUCTED EMISSIONS

The conducted emissions of either single-phase (two lines) or three-phase (four lines) EUTs can be measured in a single shot by using a four-channel Full TDEMI measurement system and the appropriate transducer. In fact, in standard conducted EMI test setups the LISN already has the filter replicated for each of the EUT's lines and those lines are switched to the LISN's RF output according to the line that is being measured by the test receiver. This means the EMI spectrum corresponding to the different standard weighting detectors is provided for every line of the EUT mains that is included in the test. In general, the test setup for multi-line EMI measurements is shown in Figure 2.5.

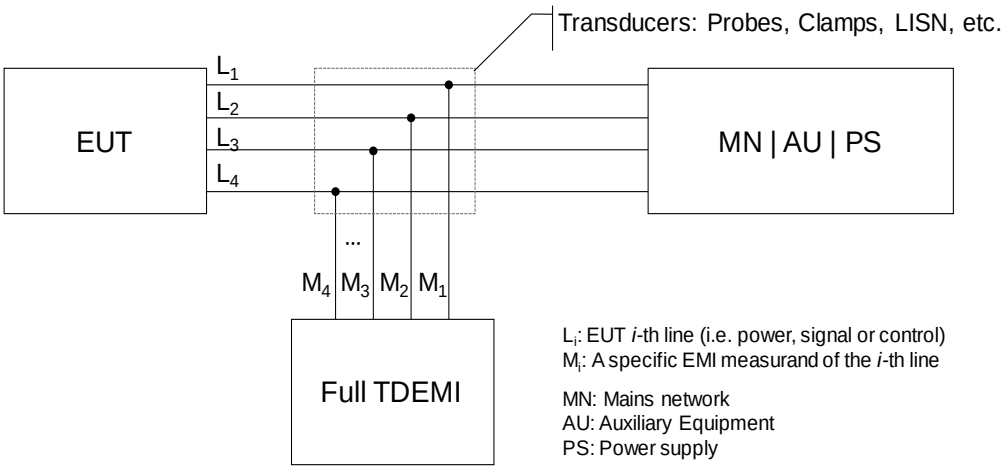

Figure 2.5: The test setup for multi-line conducted emissions testing.

2.4.4. COMMON MODE AND DIFFERENTIAL MODE NOISE MEASUREMENT

Isolating the common mode (CM) and differential mode (DM) components of the EMI is useful for deciding how to proceed when EMI mitigation is required to assure compliance. Identifying the predominant modes of noise propagation in the circuits helps to determine whether magnetic chokes, ferrites, EMI suppression filters or any other electronic design techniques are most effective for debug certain EMI problem, especially when it comes to ensuring compliance of power supplies. The measurement of the CM and DM noise was previously addressed using passive separation networks as the ones described in [57, 58].

However, multichannel Full TDEMI measurement systems can be used for measuring the common mode and the differential mode EMI voltages, using the test setup shown in Figure 2.6 because phase information is preserved.

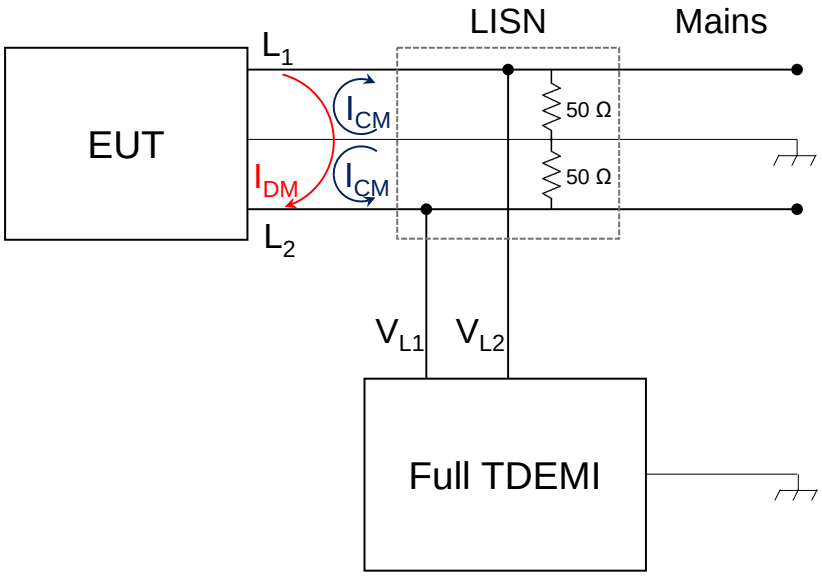

Figure 2.6: Common mode and differential mode EMI voltage measurement setup.

For conducted disturbance measurements performed using a LISN, the common mode voltage, V_{CM} is equal to half the sum of the phase side voltage, V_{L1}, and, the neutral side voltage, V_{L2}, of the LISN, that is,

$$V_{CM} = \frac{V_{L1} + V_{L2}}{2}. \tag{2.19}$$

Conversely, the differential mode voltage, V_{DM}, is equal to half the difference of the line voltages, to be exact,

$$V_{DM} = \frac{V_{L1} - V_{L2}}{2}. \tag{2.20}$$

Contrarily to what happens with a spectrum analyzer where the measurement consists only of the magnitude of the voltage, this is possible because both time-domain EMI measurements are synchronous, which means the phase information is available and that the measured interferences share a single phase references.

2.4.5. SYNCHRONOUS RADIATED AND CONDUCTED EMI ASSESSMENTS

In many situations, conducted and radiated EMI phenomena are interrelated. Unveiling the relationship between conducted and radiated disturbances is possible if the measurements are carried out simultaneously using the multichannel and triggering capabilities of oscilloscopes. In such cases, detecting and mitigating non-compliances caused by conducted emissions could help solving its radiated counterpart, and vice versa. shows a simplified diagram of the test setup for single-stage conducted and radiated EMI measurements.

In the single-stage EMI measurement setup shown in Figure 2.7, the measurement system could be configured to, for example, measure the conducted emissions on both mains lines using a multi-line LISN and the radiated emissions using two antennas, for measuring the electric field in horizontal and vertical polarizations. The advantages of such approach are the reduced testing time and the capability of correlating both radiated and conducted emissions.

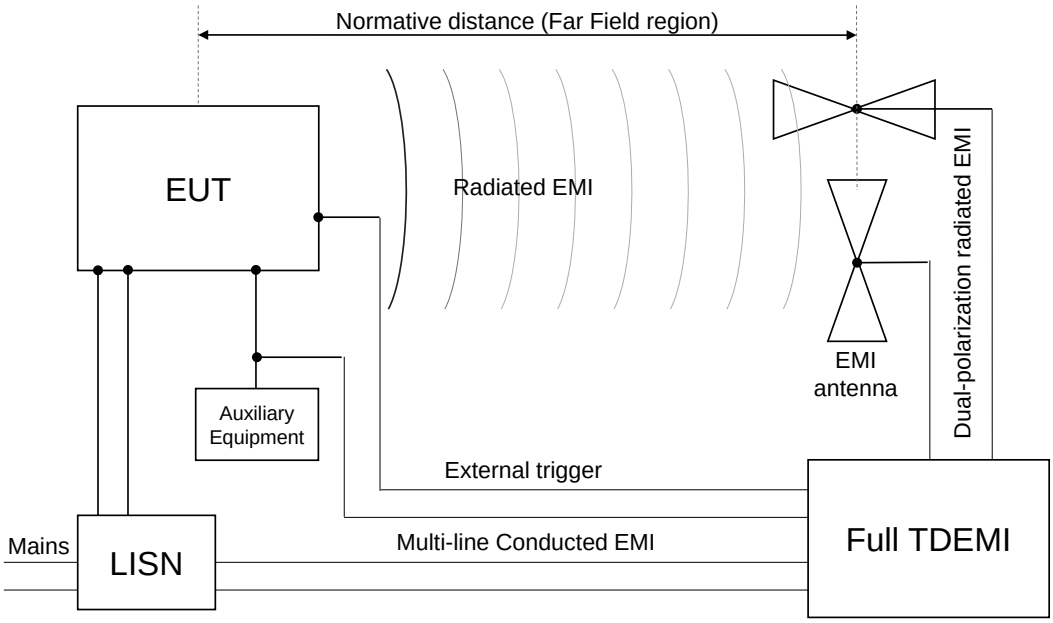

Figure 2.7: Test setup for single-stage conducted and radiated EMI measurements.

Moreover, measurements can be triggered by a critical event or using an external (control) signal. This is extremely valuable when troubleshooting a non-compliance due to unsteady broadband disturbances with both conducted and radiated impact.

2.4.6. CONCURRENT MULTI-BAND RADIATED EMI MEASUREMENTS

Certain EUTs requires evaluating the low frequency emissions of magnetic field (below 30 MHz) and also the electric field emissions (above 30 MHz) from the EUT, for instance, the rolling stocks of the railway sector as it is presented later in 4.4 [59]. In such scenarios, the concurrent multi-band EMI measurement test setup shown in Figure 2.8 could be used to reduce the number of test iterations required to complete the EUT assessment. In this example, a loop antenna is used to measure the H-field while the rest of the antennas (the biconical, the log-periodic and, the horn antennas) are used to measure the E-field emissions in different frequency ranges. Furthermore, for *in-situ* EMI measurements, another advantage of this kind of test setup

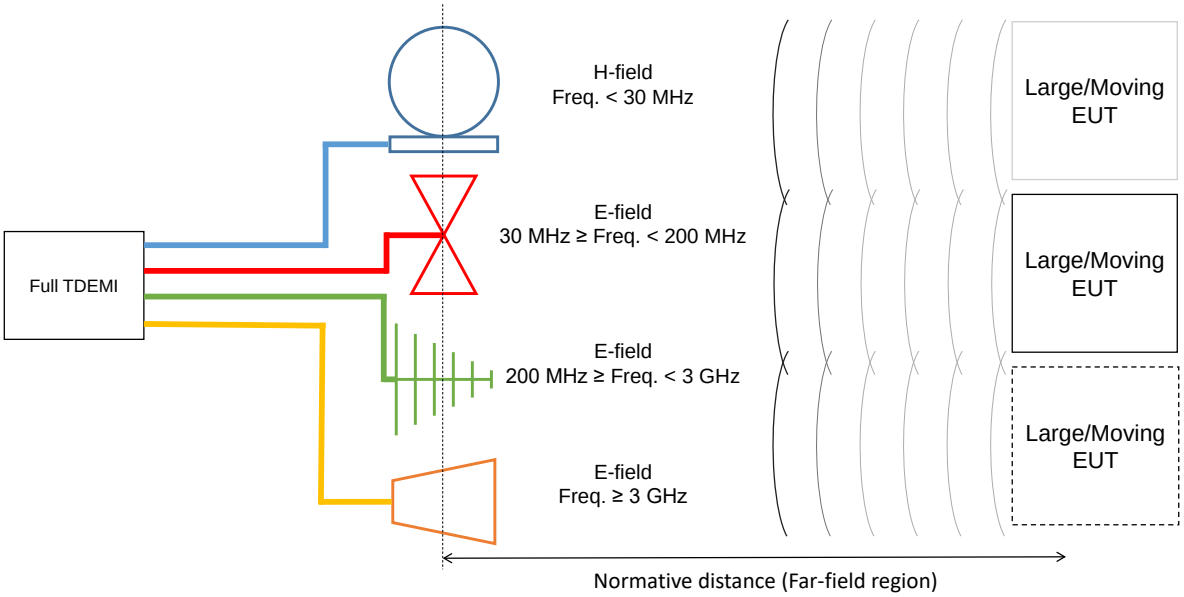

Figure 2.8: Test setup for concurrent multi-band radiated EMI measurements.

is that it avoids using hybrid antennas. Hybrid antennas cover a wider frequency range and are suitable for fixed EMC test facilities, but they could be cumbersome for *in-situ* emissions measurements because they are typically larger and heavier than the aforementioned antennas.

2.4.7. AMBIENT NOISE CANCELLATION

Nowadays, the populated radio-frequency (RF) spectrum poses limitations when performing radiated electromagnetic emissions tests on an Open Area Test Site (OATS) or during *in-situ* assessments [60]. Particularly, according to the standards CISPR 16-1-4 and CISPR 16-2-3, a satisfactory test site requires a "sufficiently" low ambient radio frequency noise in comparison to the expected emissions levels to be measured [61, 62]. In this respect, the accepted quality criterion is to provide at least a 6 dB margin between the ambient noise and the corresponding radiated emissions limit. Furthermore, an ambient noise level +20 dB below the measured emission level is recommended as an optimum condition[61].

Unfortunately, the ambient RF environment requirement can hardly be met in most test sites making it necessary to carry out EMI measurements inside shielded anechoic chambers. However, semi-anechoic chambers are expensive, they are not always available and they could not be suitable for certain types of EUTs due to size, weight or power constraints. Conversely, an OATS can be implemented with relative ease provided a sufficiently large obstruction-free area and an adequate, well-controlled ground plane [62].

Nonetheless, in order to enable accurate and repeatable EMI measurements in OATS, it is necessary to suppress the ambient RF noise up to the aforementioned tolerable threshold. Accordingly, ambient noise cancellation (ANC) is needed to improve the effective sensitivity and the EMI detection capabilities of the measurement receivers. In consequence, ANC techniques are aimed to provide alternative, yet reliable, EMI measurement methods for compliance radiated emissions assessment in unshielded test sites.

Previously, ANC techniques for EMI measurement applications have been reported. They are mainly

focused on employing alternative test methods and adaptive techniques, each one with its advantages and drawbacks. In the following, some of the most relevant ANC techniques are briefly described.

In that sense, the firstly developed methods of ANC for EMI measurement systems rely on adaptive filtering [63]. Those methods use simultaneous measurements performed with two identical antennas using a pair of high-speed digitizers as measuring instrument, one ADC is supposed to detect only background ambient noise (BAN) while the other one measures the combination of the EMI with the BAN. Figure 2.9 shows basic test setup for ANC using multichannel time-domain EMI measurements.

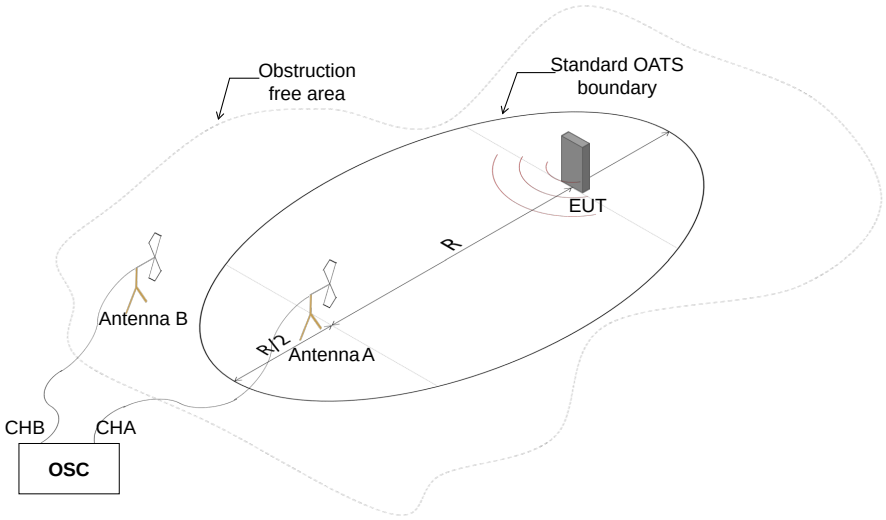

Figure 2.9: Basic test setup for ANC using multichannel time-domain EMI measurements.

Assuming that the EMI signal generated by the EUT is uncorrelated to the ambient electromagnetic noise, and provided that the ambient noise detected by the two separated antennas have a high correlation, an adaptive filter was used to suppress the unwanted noise. Some algorithms such as the Least-Mean-Square [64], the frequency domain Overlap-Save method [65], and affine projection algorithms [66] have been used to adjust the coefficients of finite impulse response filters. Attenuation of approximately 30 dB has been repetitively reported in the test scenarios. Figure 2.10 shows the block diagram of the ANC system proposed in the aforementioned studies.

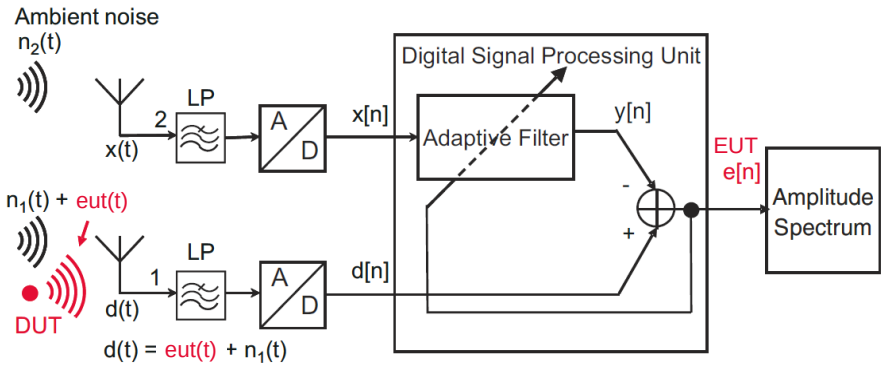

Figure 2.10: Block diagram of the ANC system [66].

Those adaptive filtering based methods of ANC have some shortcomings. On the one hand, they require

the emissions from EUT to be decoupled from only-noise reference channel, which is difficult to achieve in practice. On the other hand, their effectiveness is difficult to quantify when the ambient noise share the same frequency band as the EUT emissions and, the adaptive filtering could distort the desired signals.

More recently, an *in-situ* test method for radiated emission assessment that employs spatial spectrum estimation, adaptive beamforming, and spectrogram analysis was presented in [67] and further developed in [68]. Measurements were performed using a general purpose oscilloscope and a linear array of four omnidirectional antennas. The implementation of this so-called "virtual chamber" method is restricted either to detect a single interference source from a specific direction or to suppress interferences from three different directions of arrival. On the other hand, it would be troublesome to calibrate the antenna factor for an array whose radiation pattern adapts dynamically, thus adding significant uncertainty to the measurement results of electric field strength obtained with such a technique. Therefore, the results obtained with this approach are can hardly be used for standard EMI testing.

In the same vein, time-domain based signal decomposition techniques have been investigated with ANC applications as it is described in 6. Specifically, the empirical mode decomposition has been used for an ANC method that consist in finding an optimal combination of intrinsic mode functions that conforms the EMI after subtracting the residual components associated with BAN. Approximately, up to 30 dB noise suppression were obtained in the experiments [26].

3

FUNDAMENTAL OF FULL TIME-DOMAIN EMI MEASUREMENT SYSTEMS

The publications in subsections 3.1 and, 3.2 comprise the early stage results of this Thesis research. They are broad in scope and general in terms of their application domain. In the light of the Thesis objectives, their key contributions are:

Objective 1: The basic algorithm used for measuring transient EMI and its pulse repetition frequency is described. A general block diagram and a flow-chart for Full TDEMI measurements processing is defined. The influence of the pre and post processing techniques applied to the time-domain measurements is investigated and guidelines for their proper utilization for achieving, theoretically, improved EMI spectrum measurements.

Objective 2: Segmented memory acquisitions and their combination for evaluating transient and low repetition frequency impulsive noise in both time and frequency domains was presented.

Objective 3: The decomposition of interferences in continuous wave and transient components is proposed as a possibility. At the time, only early stage test with synthesized signals had been conducted.

Objective 4: Validations of the experiments were performed by comparing the Full TDEMI measurement results with the corresponding ones from a CISPR 16-1-1 compliant measuring receiver using the Feature Selective Validation (FSV) method.

3.1. FUNDAMENTAL JOURNAL ARTICLE 1

M. A. Azpúrua, M. Pous, S. Çakir, M. Çetintaş and F. Silva, "Improving time-domain EMI measurements through digital signal processing," in *IEEE Electromagnetic Compatibility Magazine*, vol. 4, no. 2, pp. 82-91, 2nd Quarter 2015. doi: 10.1109/MEMC.2015.7204056

Abstract-This article is intended to provide a set of recommended practices for improving of the Time-Domain EMI measurement systems by means of digital signal processing. We have focused on two major aspects: the optimal configuration settings of the direct measurement equipment and the deployment of algorithms to process the measurement result. In that sense, we believe that general purpose time-domain instruments, as oscilloscopes, can be successfully used as an

alternative hardware to measure EMI, since they provide accurate and reliable results, surpassing the conventional frequency-domain approach when transient disturbances are present.

3.2. CONFERENCE PROCEEDING 1

M. A. Azpúrua, M. Pous and F. Silva, "A measurement system for radiated transient electromagnetic interference based on general purpose instruments," *2015 IEEE International Symposium on Electromagnetic Compatibility (EMC)*, Dresden, 2015, pp. 1189-1194. doi: 10.1109/ISEMC.2015.7256338

Abstract-This paper presents a measurement system intended to be used to assets the radiated electromagnetic interference (EMI) in both time and frequency domains. In order to keep the measurement setup as accessible and practical as possible, the direct measurements are recorded with a general purpose digital oscilloscope and processed with a commonly available personal computer. The measurement system was validated for radiated emissions testing using well-known, controlled transient and continuous signals emulating typical interferences. The results are in satisfactory agreement with those provided by a conventional EMI receiver for different types of detectors. The proposed approach shows that, currently, it is possible to implement a timesaving, accurate and generally inexpensive time domain measurement system for radiated emissions that is capable to overcome the limitations of the superheterodyne EMI receivers regarding the measurement of discontinuous electromagnetic disturbances and also able to provide additional enhanced features to evaluate and troubleshoot EMI problems.

Improving Time-Domain EMI Measurements Through Digital Signal Processing

M. A. Azpúrua, Member, IEEE, M. Pous, S. Çakir, M. Çetinta, and F. Silva, Member, IEEE

Abstract—This article is intended to provide a set of recommended practices for improving of the Time-Domain EMI measurement systems by means of digital signal processing. We have focused on two major aspects: the optimal configuration settings of the direct measurement equipment and the deployment of algorithms to process the measurement result. In that sense, we believe that general purpose time-domain instruments, as oscilloscopes, can be successfully used as an alternative hardware to measure EMI, since they provide accurate and reliable results, surpassing the conventional frequency-domain approach when transient disturbances are present.

Index Terms—Digital Signal Processing, Electromagnetic compatibility, Electromagnetic interference, Electromagnetic measurements, Time-domain analysis.

I. Introduction

TIME domain Electromagnetic Interference (EMI) measurements have been previously proposed as an alternative and complementary technique for assessing the electromagnetic emissions, especially those arising from transient disturbances [1]. Therefore, even if the Time Domain EMI measurements are currently neglected by the standards, they are still very useful for pre-compliance evaluations and provide powerful insights of the measured EMI that cannot be achieved by conventional frequency domain receivers [2].

Particularly, the conventional EMI testing approach is not adequate for evaluating the impact of broadband impulsive noise disturbances that affect electronic devices and digital wireless communication systems receivers as in-band interferences [3]. This is because, the aforementioned methods were developed to protect continuous-wave analogue communication systems from interferences and, therefore, those standards and their associated measuring equipment are no longer appropriate in such situations. Likewise, even if the EMI under assessment is properly measurable using the conventional frequency domain framework, the corresponding measurement process tends to be exhaustive, costly and time-consuming [4].

Nowadays, those problems haven't been completely addressed by the FFT-based EMI test receivers designed for standard compliant measurements according the requirements of the International Special Committee on Radio Interference, since those equipment are focused on emulating the functioning, specifications and performance of the state-of-the-art super-heterodyne EMI receivers at the sacrifice of a comprehensive evaluation of the electromagnetic disturbance in the time domain [5].

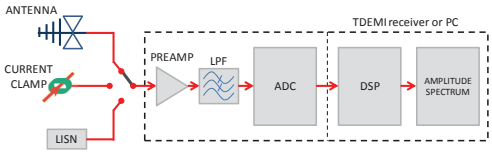

Fig. 1. Block diagram of a Time-Domain EMI measurement system.

Consequently, the large majority of the commercially available EMI receivers with the optional time domain scan functionality are very costly and sophisticated pieces of hardware that are neither affordable for small laboratories nor are suitable for in-situ measurements.

Recently, accurate and affordable Time Domain EMI measurement systems based upon general purpose instruments, as oscilloscopes, have been presented [2]. They are intended to evaluate both conducted and radiated EMI while developing the means for making the most of commonly available laboratory equipment. The aforementioned measuring systems typically rely on a personal computer to perform the required data processing to obtain the spectral estimation

In that sense, in this article we intend to describe and exemplify how digital signal processing (DSP) techniques can be used for improving the assessment of EMI by means of Time Domain measuring instruments. Therefore, in the following sections we will address a set of DSP techniques that covers acquisition modes, sampling schemes and spectral estimation methods which, when combined, provide a significant enhancement on dynamic range, noise impact and accuracy on the measured EMI.

II. Overview Of TDEMI Measurement Systems

In general terms, a Time Domain EMI (TDEMI) measurement system, for radiated and/or conducted disturbances, can be described by the block diagram shown in Figure 1 [6]. For the measurement of radiated electromagnetic interference a broad-band antenna shall be used, while for the measurement of conducted EMI it corresponds to either a current clamp or line impedance stabilization network. Sometimes the measured signal passes through a preamplifier and then it is low-pass filtered for band limiting proposes, so the signal fulfills the Nyquist condition for the maximum sampling rate supported by the TDEMI system. Then, in the analog-to-digital converter (ADC), the signal is digitized and then it is stored. Finally, the amplitude spectrum is computed via spectral estimation techniques.

©2015 IEEE Electromagnetic Compatibility Magazine – Volume 4 – Quarter 2

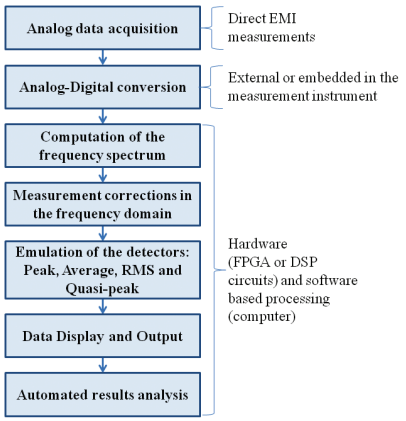

Fig. 2. General flow chart of the TDEMI measurement processing.

On the other hand, from the standpoint of the signal acquisition and processing stage, a TDEMI system is more naturally described by the flow chart shown in Figure 2.

In that sense, the data acquisition process for a TDEMI measurement system begins when the analog signal is sampled either directly by the measuring instrument (i.e., digital oscilloscope) or externally by means of ADC or digitizers. Then, the EMI data are transferred from the main memory to the device that will process it. For the commercial FFT-based EMI receivers this process is performed internally by the built-in processors and software [7]. However, a customized TDEMI measurement system may carry on the digital signal processing with the aid of specific software running on a personal computer. Then, the data are transferred to a personal computer via some communication port, such as the General Purpose Interface Bus (GPIB). Subsequently, the amplitude spectrum is digitally computed using the FFT (or some variant of), periodograms or other spectral estimation methods [8]. Later, the errors due to the frequency dependence of the antenna factor, the attenuation in the transmission line, the gain of the preamplifier, the frequency response of the anti-aliasing filter are corrected. Next, a mathematic emulation of the peak, RMS, average and quasi-peak detectors is made, either by applying a correction factor dependent on the pulse repetition frequency [8] or by means of the application of a digital infinite impulse response filter [9]. Additionally, other signal processing techniques can be used in order to reduce the impact of the noise but this has varied upon specific implementations. Finally, the results must be displayed and compared with the respective limit lines to provide a judgment about the test result regarding the EMI in the measured frequency band. For studying non-stationary signals, a spectrogram representation of EMI has also been used previously [10].

III. Improving TDEMI Measurements Through DSP

Let's start assuming we are interested in enhancing the measurement results from a TDEMI measurement system implemented using of a general purpose digital oscilloscope. As an initial condition, there are some basic limitations regarding hardware of the oscilloscope itself, such as the analog bandwidth, the maximum sampling rate and the maximum record length. However, provided the restrictions fixed by the equipment, there are several DSP techniques that will aid us taking the most of the available hardware.

Some of those DSP techniques are provided by the measuring instrument itself and therefore affect de direct measurement and must be configured by the user/software before the acquisition. Subsequently, we will refer to those processing features as Pre-acquisition DSP.

On the other hand, there is the subset of DSP techniques that are usually implemented via software after the time domain signal has been acquired by a personal computer. These Post-acquisition DSP techniques provide greater flexibility and can be continuously improved through software updates.

With that said, the proceeding sections present ten of the most straightforward and influential pre and post-acquisition DSP techniques, which are listed in Table I.

TABLE I

PRE AND POST ACQUISITION DIGITAL SIGNAL PROCESSING TECHNIQUES

Pre-acquisition DSP techniques	Post-acquisition DSP techniques
• Oscilloscope acquisition modes	• Filtering, windowing and equalization
• Sampling schemes	• EMI decomposition
• Segmented memory acquisition	• Transient pulse characterization
• Bandwidth limit & enhancement	• Spectral estimation & superposition
• Trigger options	• Detectors emulation

IV. Enhancements Through Pre-Acquisition DSP

As stated before, the pre-acquisition DSP (PreA-DSP) techniques are those included in the features of the measuring instruments and are applied before the datasets are sent to the personal computer. In most cases, the PA-DSP options are restrained by the options made available by the hardware manufacturer and, in the case of oscilloscopes, they are not primarily intended to perform EMI assessments. Nonetheless, they must be neither discarded or obviated whatsoever due to the enormous (positive or negative) impact they can have, as it will be presented next.

A. Oscilloscope acquisition modes

The first PreA-DSP technique to be introduced here refers to the selection of the appropriated acquisition mode of the oscilloscope. The Acquisition modes control how waveform points are produced

from sample points, and therefore this is extremely important for the proper EMI assessment. The Table II lists the most common acquisition modes and gives recommendations on their applicability for EMI measurements.

TABLE II

OSCILLOSCOPES' ACQUISITION MODES

Mode	Description	Applicability on EMI measurement
Sample	The oscilloscope creates a waveform point by saving one sample point during each waveform interval.	NOT GENERALLY RECOMMENDED. Highly sensitive to aliasing and white noise. Provides the poorest resolution.
Peak Detect	The oscilloscope saves the minimum and maximum value sample points taken during two waveform intervals and uses these samples as the two corresponding waveform points.	This mode is particularly useful for seeing narrow pulses spaced far apart in time. Creates a waveform with high frequency information. Recommended for a fast "WORST CASE" evaluation of EMI.
Envelope	The minimum and maximum waveform points from multiple acquisitions are combined to form a waveform that shows min/max accumulation over time.	The resulting waveform is the combination of several Peak Detect acquisitions. Since this mode removes the timing information from data, it is NOT SUITABLE for spectral estimation applications as required by EMI evaluation.
Average	The oscilloscope saves one sample point during each waveform interval and the waveform points from consecutive acquisitions are then averaged together to produce the final displayed waveform.	Reduces uncorrelated noise without loss of bandwidth and improved signal to noise ratio. Requires a repeating signal. Recommended for the evaluation of the CONTINUOUS WAVE average EMI levels.
Hi Res	Multiple samples taken within one waveform interval are averaged together to produce one waveform point. The result is a decrease in noise and an improvement in resolution for low-speed signals.	High-resolution acquisition on a noisy signal will tend to improve the dynamic range by increasing the effective vertical resolution. Recommended for the evaluation of the TRANSIENT PULSES EMI levels.

A direct consequence of the configuration of the appropriate acquisition modes comes from the improvement of the signal-to-noise ratio (SNR) of our TDEMI measurement system. It is well known that, if the measured signal (EMI) is sampled at the Nyquist rate, the theoretical SNR is given by,

$$SNR_{(\mathrm{dB})} = 6.02N_{bits} + 1.76\,, \qquad (1)$$

where N_{bits} is the numbers of (effective) bits of the ADC. As said before, Hi-Res mode can improve the effective vertical resolution, that is, a theoretical increase of $b_{hi\text{-}res}=0.5\log_2(N_{Hi\text{-}res})$ bits can be achieved, where $N_{Hi\text{-}res}$ is the number of samples averaged to produce a single waveform point.

For example, consider a general purpose oscilloscope Tektronix DPO7104C with an 8-bit ADC (6.7 effective bits) and a sample memory depth of 2 bytes, from which only 13 bits are useful due to the fact that 1 bit is reserved for the sign and other 2 bits are unreliable because of random round-off errors. Given that, the resolution could be increased up to +5 bits, which represents +30 dB of improvement in the SNR. However, for achieving such an improvement, it would require to oversample the measured signal thus each waveform point correspond to 1024 samples. This means decrease of the effective sampling frequency, limiting therefore the maximum measurable frequency of the EMI.

In practice, between 12 dB – 18 dB of SNR improvement are feasibly achievable for measurements of radiated and conducted EMI, respectively, when using a 20 GSamples/s oscilloscope and the Hi-Res mode.

On the other hand, the Average acquisition mode also improves the SNR by a factor of $\sqrt{N_{Ave}}$, through the reduction the variance of each waveform point where N_{Ave} is the number of waveform points from consecutive acquisitions that are averaged to produce the final waveform displayed. Hence, an improvement in the SNR of 5 dB is achievable for N_{Ave}=10 without losing bandwidth. On the other hand, reducing the uncorrelated noise by averaging might consume more computation time and memory of your oscilloscope and therefore we recommend using a moderate N_{Ave}, which shall lie approximately between 10 and 20, according to our experience. A disadvantage of Average mode is that trigger jitter degrades the timing information in the acquired data, and therefore it might not be recommendable for the measurement of sharp transient peaks and sparks that are commonly found to be an important cause of EMI.

B. Sampling schemes

Regarding the sampling scheme, we first need to be aware that most oscilloscopes provide two different types of sampling: the real-time sampling and the equivalent time sampling.

Real-time sampling acquires all samples from a signal in one cycle. The signal may be either a single or repetitive event. The sample rate must be high enough to allow the oscilloscope to acquire sufficient data to reconstruct the waveform. This sample scheme is recommended for transient measurements, and requires a higher sampling rate than the Nyquist frequency to reconstruct the waveform. This is because the assumption of a

©2015 IEEE Electromagnetic Compatibility Magazine – Volume 4 – Quarter 2

periodic signal is not always applicable. In practice, a common and effective interpolation uses the sin(x)/x function, and for those cases the oscilloscope should have a sample rate at least 2.5 times that of the highest frequency component within the signal. In the same way, if linear interpolation is used, then it is often accepted that the sample rate should be at least ten times the highest frequency signal component.

On the other hand, equivalent time sampling acquires a few samples from each triggered waveform, over many acquisition cycles. The advantage of equivalent-time sampling is that it allows the bandwidth to exceed the Nyquist criteria for repetitive signals. It is recommended for high repetition frequency continuous wave signals.

Either way, a sampling rate, fs, of at least 4 times the maximum measurable EMI is usually recommended for avoiding aliasing errors [8]. Additionally, oversampling the measured EMI contributes to improving the dynamic range as the theoretical SNR of the ADC driven by a harmonic input signal depends on fs, is given by [11],

$$SNR_{(\mathrm{dB})} = 6.02N_{bits} + 1.76 + 10\log_{10}\left(\frac{f_s}{2f_{\max}}\right). \quad (2)$$

In consequence, considering a radiated EMI measurement performed with an oscilloscope with 1 GHz bandwidth and a maximum sampling frequency of 20 GSamples/s, the SNR could be potentially increased by 10 dB as result of oversampling.

C. Segmented memory acquisition

Sampling at the highest possible rates has its drawbacks. All oscilloscopes have a limited amount of acquisition memory and their memory depth determines the amount of waveform time that can be captured at a particular sample rate. This could be a huge problem when trying to measure a high frequency transient EMI from a source with a very slow repetition frequency. Figure 3 shows an example of such situation.

That certainly justifies why, for TDEMI applications, is almost mandatory to be able to use some kind of segmented memory acquisition technique, in order to extend the scope's total acquisition time by dividing the scope's available acquisition memory into smaller memory segments. Segmented memory acquisition methods, such as Tektronix's FastFrameTM, enable the TDEMI measurement system to capture many successive single shot waveforms while taking advantages of the other previously explained PreA-DSP techniques.

For the aforementioned example, 10 pulses of 75 ns duration and with pulse repetition frequency of 112 kHz were measured at 5 GSamples/s and using the Hi-Res acquisition mode with a 20 Gsamples/s oscilloscope. The total equivalent time record would have been of approximately 90 µs, which corresponds to approximately to a record of 450 kSamples. However, by using the segmented memory acquisition there were only required 3.8 kSamples, that is, a memory reduction of about 120 times.

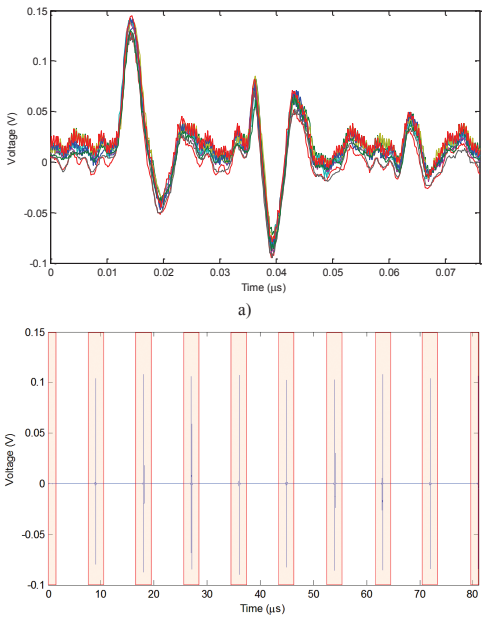

Fig 3. Transient EMI signal recorded through several single-shot measurements: a) superposed successive captures b) Reassembled time-domain signal (actual recorded frames are marked inside the red rectangles).

D. Bandwidth limit and enhancing

Most oscilloscopes have a circuit that limits their bandwidth. By limiting the bandwidth, it is possible to filter the undesired noise or interferences out of the band that is being assessed. For example, one would be interested in limiting the oscilloscope bandwidth to 1 GHz to perform in-situ measurements of the radiated emissions of certain equipment under test (EUT) in the 30 MHz to 1 GHz band, avoiding measuring undesired interferences from communication systems, WLAN networks and others allocated above 1 GHz.

Similarly, some scopes may provide an equalization filter which flattens the oscilloscope channel frequency response, improves phase linearity, and provides a better match between channels. It also decreases rise-time and improves the time domain step response. This option might only be available for the higher sampling frequencies. We suggest using the bandwidth enhancing features whenever possible.

E. Trigger options

The oscilloscope's trigger function synchronizes the horizontal sweep at the correct point of the signal. This is essential for clear EMI characterization. The trigger controls and modes allow the stabilization of a repetitive transient EMI waveform and capturing single-shot waveforms. Additionally, externally triggering an EMI measurement by synchronizing the oscilloscope with

changes in the operation state of the EUT is, sometimes, required to evaluate one-time events that occur on the transitions between functioning modes. Finally, it is important to state that TDEMI measurement systems are still very sensible to adjustments in the trigger level and mode, especially in cases where the EMI is formed by pulses of significantly different amplitude and repetition frequency.

V. Enhancements Through Post-Acquisition DSP

The post-acquisition DSP (PostA-DSP) techniques are a set of mathematical operations and transformations applied to the measurement data after it has been acquired by the personal computer. Those functions are programmed as software, depending on the particular features required by the measurement system, and their level of complexity and sophistication depend on our requirements and computational resources available.

An obvious example of what we have called PostA-DSP is the universally used Fast Fourier Transform (FFT) algorithm; however, the TDEMI measurement systems can take advantage from a wide range of techniques. Some of them will be covered next.

A. Filtering, windowing and equalization

Oscilloscopes, generally, are not able to reject undesired frequency components of the measured signal. Those noise components out of the frequency band under evaluation add jitter and unwanted variability to the TDEMI measurements. Adding an analog filter to the measurement chain is an option, but this may affect the system sensitivity and contributes to increasing the measurement uncertainty.

Conversely, digital filtering offers a straightforward alternative to face that problem. Therefore, for TDEMI measurements, it is a good practice to bandpass filter the measured signal using a finite impulse response (FIR) filter, designed to provide the corresponding bandwidth of interest. Hence, for example, we could reject noise components above or below 30 MHz for conducted and radiated EMI, respectively.

In fact, even if it seems that the filtering operation has no impact on measurement results displayed in the frequency domain, it helps the later algorithms of transient pulse characterization to perform better since the SNR is improved. Figure 4 shows how filtering reduces significantly the jitter and the amplitude variability between successive measurements of a transient EMI pulse using the segmented memory approach, thus making it easier to calculate pulse duration and repetition frequency.

On the other hand, even if the measurements and most signal processing have been performed in the time-domain, the final results comprise the spectral estimation of the assessed EMI, and the measured signal shall be, eventually, transformed to

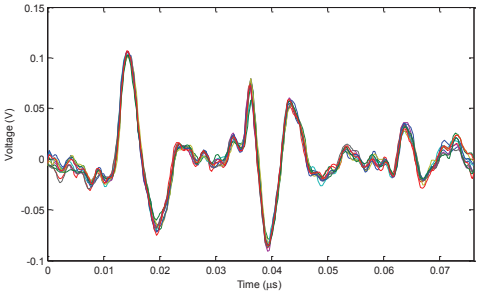

Fig 4. Filtered radiated transient EMI signal. Several records of single shots measurements are superposed.

the frequency domain for further evaluation. The spectral estimation techniques based on the FFT assume periodicity of the signal. However, the measured signal has finite record length, which may not exactly contain an integer number of periods, therefore, it is clear the aforementioned assumption may not be truly satisfied.

To prevent spectral leakage caused by periodic components, which do not fit an integer number of periods into the observation interval, a window function must be applied to the measured signal. Note that, since the windowed signal has less energy that the original, the coherent gain correction is required.

Nonetheless, different window functions offer distinct compromises between leakage suppression and spectral resolution. Hence, the window shape factor shall be considered to calculate the minimum record length necessary to achieve the required resolution bandwidth (RBW) [10]. Consequently, what's most important about the selection of the appropriate window function for our TDEMI system is to understand their advantages and weaknesses in terms of the type of measured signal, thus making the choice neither trivial nor irrelevant.

Also, since in most cases the record length of the measured EMI is larger than necessary to provide the desired frequency RBW of the spectral estimation, a good practice is to subdivide the time domain signal into smaller sets and window them individually. To mitigate the loss at the edges of the window function, the individual sets may overlap in time.

In this regard, CISPR 16-1-1 requires an overlap of more than 75 % to ensure that the level measurement uncertainty for the pulse amplitude remains less than ±1.5 dB [4]. Even if a 75% of overlapping is more than sufficient for most applications, the optimal overlapping proportion depends entirely on the selected window function. The accuracy of the results and computation time can be improved selecting the optimal overlapping factor (OOF).

Table III summarizes our recommendation and evaluation regarding the selection criteria of the window function for TDEMI measurement systems.

©2015 IEEE Electromagnetic Compatibility Magazine – Volume 4 – Quarter 2

TABLE III

WINDOWING FUNCTION COMPARISON AND RECOMMENDED APPLICABILITY

Type	BW (Bins) 3dB	BW (Bins) 6dB	Freq. Resolution	Spectral leakage	Amplitude accuracy	OOF (%)	Applicability
Rectangular	0.89	1.21	Best	Worst	Poor	0	Transient whose duration is shorter than the length of the window
Blackman-Harris (4-sample)	1.90	2.72	Poor	Very Good	Good	66.1	Random or periodic.
Hamming	1.30	1.82	Good	Fair	Fair	50	Random.
Hann	1.37	1.82	Good	Good	Fair	50	General Purpose and Transients whose duration is longer than the length of the window.
Kaiser-Bessel (β=16)	2.23	3.12	Good	Excellent	Excellent	80	Accurate random and periodic signals within a wide dynamic range.
Gauss (α=2. 5)	1.33	1.86	Good	Fair	Fair	50	General Purpose Random and continuous wave signals.
Flat-top	3.72	4.58	Poor	Good	Best	76	Pure Sinusoids - Accurate single-tone amplitude measurements such as those used for calibration purposes.

For EMI measurements, we recommend the Kaiser-Bessel window function, since it has a variable shape factor, β, which trades off side lobes for main lobe. By varying the shape factor, the Kaiser-Bessel function provides an excellent tradeoff between dynamic range, accuracy, and frequency resolution for TDEMI measurement systems.

Figure 5 shows the impulse and frequency response of some windows functions commonly used by TDEMI systems. Again, the Kaiser-Bessel function exhibits the best performance among the windows compared.

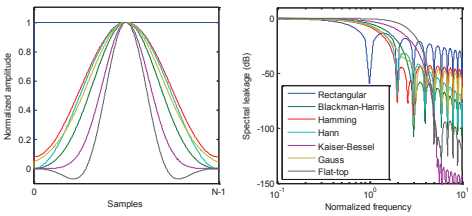

Fig 5. Impulse and frequency response of some windows functions commonly used by TDEMI systems.

Finally, the distortion introduced by the FIR and the impulse response of the oscilloscope shall be corrected. In the same manner, other correction and calibration factors such as cable attenuation and LISN/antenna factors can be compensated through PostA-DSP. For those purposes, equalization shall be performed. Equalization can be implemented in the time domain or in the frequency domain, being the later more straightforward.

B. EMI decomposition

An EMI can contain both continuous wave (CW) and transient components. Likewise, in most cases the EMI might be a mixed signal containing both periodic and random contributions. It is not an easy task, for not saying almost impossible, to discern clearly between CW/transient, stochastic/deterministic, sporadic/periodic when we measure a superposition of signals that are non-intentionally generated and do not follow a specific, previously known, pattern.

In this regard, several techniques and algorithms, previously used in the field of audio and biomedical signal processing, could be applied for EMI signal decomposition [12]. With the EMI signal decomposed it is possible to apply specific adaptive treatments to each signal mode depending on their characteristics, improving the measurement result.

It is not our intention to deepen the explanation of the implemented algorithms, since that would be out of the scope of this article. Nonetheless, Figure 6 shows a demonstrative simulated signal example on how a noisy EMI signal can be decomposed into CW/narrow-band and transient/broadband components in the using time-domain processing. In Figure 6, the plots in the left column correspond to the simulated signal in the time domain while the plots in the right column correspond to their spectral estimations. Similarly, the blue traces correspond to the total EMI signal while the rest are the three components decomposed by the algorithm.

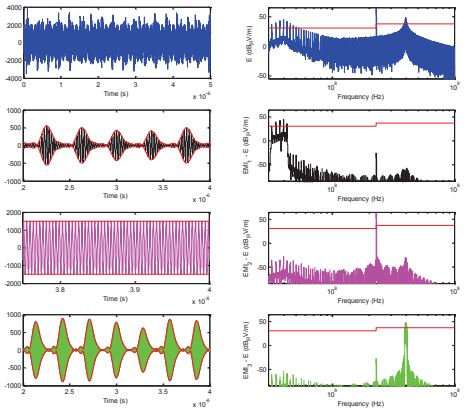

Fig 6. Example of EMI signal decomposition by means of PostA-DSP techniques applied in the time-domain.

C. Transient pulse characterization

One advantage of the EMI decomposition is that, once the transient components have been identified, it is practical to apply additional automated algorithms to characterize the pulsed interference.

The main characteristics of the transient EMI that need to be determined are the pulse duration and the pulse repetition frequency. Both are required to be able to configure optimally the measuring instrument. Depending on them, a TDEMI system could decide regarding the most convenient acquisition mode, sampling scheme, record length, among others.

Figure 7 displays a simulated example on the aforementioned situation. Based only in the original EMI "measurement" (blue trace) it would be very difficult to determine the pulse duration and the pulse repetition frequency. Although, after applying additional processing algorithms for feature extraction (red trace), it is easier for the system to estimate robustly, through statistical analysis of the data, the pulse duration and repetition frequency.

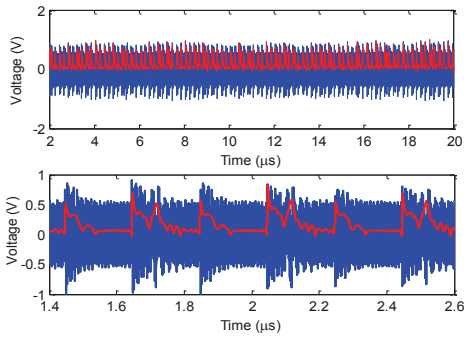

Fig 7. Example of feature extraction of a noisy EMI signal to estimate the transient pulse characteristics.

D. Spectral estimation and superposition

Intuitively speaking, the spectral density estimation is the mathematical transformation process used to analyze the frequency content of a signal. There are several methods for spectral estimation, but they are primarily classified into parametric and non-parametric.

The parametric approaches assume that the underlying stationary stochastic process has a certain structure which can be described using a small number of parameters. In these approaches, the task is to estimate the parameters of the model that describes the stochastic process. By contrast, non-parametric approaches explicitly estimate the covariance or the spectrum of the process without assuming that the process has any particular structure. For EMI measurement applications, the non-parametric methods are generally more suitable.

With that said, we recommend the use of the Welch's method of modified periodograms (windowed) for an averaged/smoother spectral estimation result. For identifying changes over time in the emissions spectrum, we suggest using the Short Time Fast Fourier Transform (STFFT) for evaluating local sections (windows) of a signal as it changes over time [13]. Spectrogram representations are possible, but their applicability is unclear for EMC testing purposes.

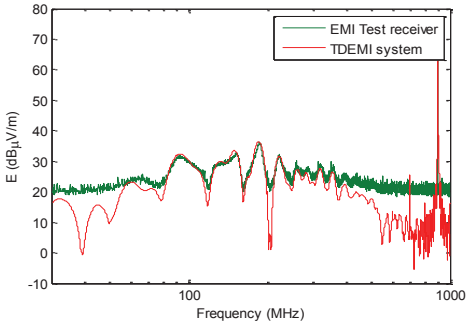

Fig 8. Example of spectral estimation between a conventional EMI test receiver and a customized TDEMI measurement system with DSP improved performance.

Furthermore, due to the linearity of Fourier transforms, it is possible to take advantage of the EMI signal decomposition to improve the spectral estimation a step beyond of what has been mentioned so far. Combining the optimal oscilloscope setup for each EMI component and the PostA-DSP techniques described in this article, the resulting spectral estimation is obtained through the superposition of the individual spectrums of each EMI component. The overall result provides an enhanced dynamic range and a lower noise floor for our TDEMI measure system.

Figure 8 shows an example of a radiated emission measurement carried on using an oscilloscope (Tektronix DPO7104) configured with the recommended criteria, compared with the results obtained by a conventional EMI Test receiver (R&S ESPI).

Through DSP, our TDEMI measurement system has achieved a lower noise floor than the conventional test receiver used for the verifications, and, therefore it makes possible to identify more spectral features of the measured EMI.

Additionally, by means of modifications on the STFFT algorithm, it is also possible to calculate the spectral content of the EMI with a variable/adaptive RBW depending on the requirement of the assessed band in terms of the corresponding frequency allocation, with only one acquisition of raw data. As an example, Figure 9 shows a synthetic multisine signal, whose spectrum has been estimated with a RBW starting in 100 kHz between 30 MHz and 100 MHz and increasing in +200 kHz for every additional 100 MHz of the measured bandwidth.

E. Detectors emulation

PostA-DSP has been extensively applied for attempting to emulate in the TDEMI measurement systems the performance of the detectors (MaxPeak, Average, Quasi-Peak, etc) used by the conventional EMI test receivers. The main goal is to achieve results directly comparable/compatible between both measurement systems.

One approach focuses on the application of correction factors that depend on the type of detector and on the pulse repetition

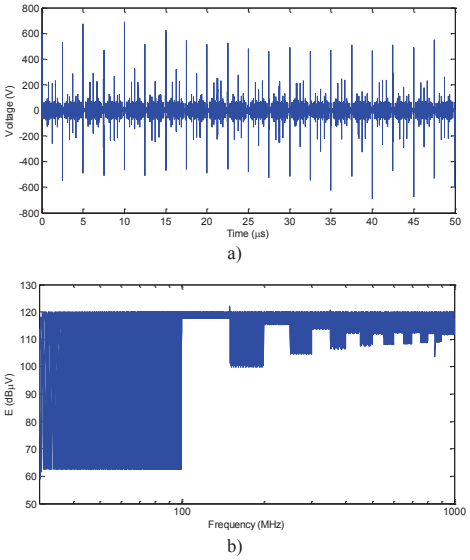

Fig 9. An example of a multisine signal measurement with a spectral estimation obtained for different RBW using a single time domain acquisition. a) Time domain signal b) Amplitude spectrum.

frequency [8]. Others have modeled the Quasi-Peak detector as an infinite impulse response filter [9].

Our TDEMI measurement system uses the STFFT to compute the estimated results for each detector based upon the variations of each frequency bin along all the observed time windows. Hence, for EMI signals with a low pulse repetition frequency, the TDEMI measurement system uses an approach that requires reassembling the time-domain signal measured through segmented memory acquisition techniques. Thus, our TDEMI measurement system is capable of achieving equivalent measurement times sufficient to properly emulate the detectors results.

VI. Conclusion

Current, time-domain general-purpose measurement instruments provide multiple of opportunities to develop custom made, accurate and reliable TDEMI systems. Digital signal processing is the key to unleash all the potential applications those instruments provide in terms of EMI assessment.

We have grouped the DSP techniques into pre-acquisition and post-acquisition in order to structure them and the examples of their applicability. However, the most important aspect in this regard is to understand what options and features are available in our instruments, such as oscilloscopes, and how we can boost them through the addition of PC-based processing, in order to benefit from them in terms of a better EMI assessment.

Even if nowadays the measurement systems as the ones treated in this paper are alternative measurement approaches neglected by the standards, we believe this situation could change in the future as their improvement continues, their cost is lowering and more EMC laboratories are embracing it.

ACKNOWLEDGMENT

This work was supported in part by EURAMET IND60EMC research project (the EMRP is jointly funded by the EMRP participating countries within EURAMET and the European Union) and by the Spanish "Ministerio de Economía y Competitividad", under project TEC2013-48414-C3-3-R.

REFERENCES

[1] S. Braun, "A novel time-domain EMI measurement system for measurement and evaluation of discontinuous disturbance according to CISPR 14 and CISPR 16," in Electromagnetic Compatibility, IEEE International Symposium on, 2011.
[2] G. Costa, M. Pous, A. Atienza and F. Silva, "Time-Domain Electromagnetic Interference Measurement System for intermitent disturbances," in Electromagnetic Compatibility (EMC EUROPE), International Symposium on, Gothenburg, 2014.
[3] M. Pous and F. Silva, "Prediction of the impact of transient disturbances in real-time digital wireless communication systems," Electromagnetic Compatibility Magazine, IEEE, vol. 3, no. 3, pp. 76-83, 2014.
[4] S. Braun, T. Donauer and P. Russer, "A Real-Time Time-Domain EMI Measurement System for Full-Compliance Measurements According to CISPR 16-1-1," Electromagnetic Compatibility, IEEE Transactions on, vol. 50, no. 2, pp. 259-267, May 2008.
[5] I. E. Commission, CISPR 16-1-1 ed3.0: Specification for radio disturbance and immunity measuring apparatus and methods - Part 1-1: Radio disturbance and immunity measuring apparatus - Measuring apparatus, IEC, 2010.
[6] P. Russer, "EMC measurements in the time-domain," in General Assembly and Scientific Symposium, 2011 XXXth URSI, 2011.
[7] Rohde & Schwarz, "Time-domain Techniques in EMI Measuring Receivers Technical and Standardization Requirements," February 2012.
[8] C. Keller and K. Feser, "Fast Emission Measurement in Time Domain," Electromagnetic Compatibility, IEEE Transactions on, vol. 49, no. 4, pp. 816-824, 2007.
[9] S. Braun, F. Krug and P. Russer, "A novel automatic digital quasi-peak detector for a time domain measurement system," Electromagnetic Compatibility, 2004 International Symposium on, vol. 3, pp. 919-924, 2004.
[10] C. Hoffmann and P. Russer, "A Time-Domain system for EMI measurements above 1 GHz with high sensitivity," in Microwave Conference (GeMIC), German, 2011.
[11] F. Krug and P. Russer, "The Time-domain Electromagnetic Interference Measurement System," Electromagnetic Compatibility, IEEE Transactions on, vol. 45, no. 2, pp. 330-338, May 2003.
[12] Z. Shan, J. Swary and S. Aviyente, "Underdetermined source separation of EEG signals in the time-frequency domain," in Acoustics, Speech and Signal Processing, 2008. ICASSP 2008. IEEE International Conference on, 2008.
[13] D. G. Manolakis, V. K. Ingle and S. M. Kogon, Statistical and Adaptive Signal Processing: Spectral Estimation, Signal Modeling, Adaptive Filtering, and Array Processing, Boston: Artech House, 2005.

Biographies

Marco A. Azpúrua (M'13) received the B.Sc. degree in telecommunications engineering, in 2008, and the M.Sc. degree in electrical engineering from the Universidad Central de Venezuela, Caracas, in 2013. He is currently working on his Ph.D. thesis at the Electromagnetic Compatibility Group (GCEM) of the Universitat Politècnica de Catalunya (UPC), Barcelona, Spain. Formerly, he

A Measurement System for Radiated Transient Electromagnetic Interference Based on General Purpose Instruments

Marco A. Azpúrua, Marc Pous and Ferran Silva
Grup de Compatibilitat Electromagnètica (GCEM), Departament d'Enginyeria Electrònica (DEE)
Universitat Politècnica de Catalunya (UPC)
Barcelona, Spain
Email: marco.azpurua@upc.edu

***Abstract*—This paper presents a measurement system intended to be used to assets the radiated electromagnetic interference (EMI) in both time and frequency domains. In order to keep the measurement setup as accessible and practical as possible, the direct measurements are recorded with a general purpose digital oscilloscope and processed with a commonly available personal computer. The measurement system was validated for radiated emissions testing using well-known, controlled transient and continuous signals emulating typical interferences. The results are in satisfactory agreement with those provided by a conventional EMI receiver for different types of detectors. The proposed approach shows that, currently, it is possible to implement a time-saving, accurate and generally inexpensive time domain measurement system for radiated emissions that is capable to overcome the limitations of the superheterodyne EMI receivers regarding the measurement of discontinuous electromagnetic disturbances and also able to provide additional enhanced features to evaluate and troubleshoot EMI problems.**

Keywords*—*Time domain measurements, electromagnetic interference, radiated emissions, spectral estimation, electromagnetic compatibility.

I. INTRODUCTION

Nowadays, an important cause of electromagnetic incompatibilities and interferences are broadband impulsive noise disturbances unintentionally produced, i.e., by sparks or switching power supplies that propagate as radiated signals affecting digital communication systems receivers as in-band interferences [1]. This is the case of several contemporary applications such as Digital Video Broadcasting Terrestrial (DVB-T), Trans European Trunked RAdio (TETRA), Radio Frequency IDentif cation (RFID) and GSM-Railway system that are susceptible of degradation in their performance under the impact of transient broadband interfering noise [2][3].

However, most of the standardized methods and measurement setups used for evaluating the radiated electromagnetic emissions were developed to protect analogue communication systems from interferences and, therefore, the aforementioned standards and their associated measuring equipment are not generally suitable to perform a proper assessment of the impact of radiated interference in such digital communication systems and applications [3]. Additionally, in general terms, the standard methods for evaluating the radiated electromagnetic emissions have evolved at a slower pace with respect to the communications technologies making them inadequate or insuff cient to ensure electromagnetic compatibility (EMC) in situations as those described previously [4].

Consequently and in view of the limitations of the superheterodyne EMI receivers, important advances have been achieved in order to implement Time Domain Electromagnetic Interference Measurement (TDEMI) systems fully compliant with CISPR 16-1-1 standard. Those CISPR compliant FFT-based EMI receivers tend to reduce the measurement time spent in the conducted and radiated emissions test by several orders of magnitude [1][5]. Nevertheless, in general terms, those TDEMI systems have been more focused on emulating the functioning, specif cations and performance of the *state-of-the-art* EMI receivers that operate in the frequency domain than in performing a more comprehensive evaluation of the electromagnetic disturbance in the time domain [6].

Perhaps, the approach taken so far in the TDEMI measurement systems propitiated their recognition as (FFT-based) test instruments for standard-compliant measurements according to the International Special Committee on Radio Interference (CISPR) requirements, specif cally by means of the publication of the Amendment 1 to the third edition of CISPR 16-1-1 [7]. Notwithstanding, the inclusion of the TDEMI measurement systems in the CISPR 16-1-1 standard neither attempt to address the study of electromagnetic disturbances in the time domain nor makes the test equipment less expensive. In fact, the large majority of the commercially available EMI receivers with the optional time domain scan functionality are a very sophisticated piece of hardware that is neither affordable for small laboratories nor is suitable for *in-situ* measurements [8].

Aware of the increasingly importance of evaluating the impact of transient, discontinuous and intermittent EMI while developing the means for making the maximum of commonly available laboratory equipment, this work is intended to introduce a low-cost time domain EMI measurement system for radiated emissions, that uses as general purpose digital oscilloscope to measure and acquire the signals that are later processed to obtain not only the estimated spectral content of the EMI, but also useful information on the time domain characteristics of the electromagnetic disturbance.

In the following sections, the aforementioned TDEMI system will be explained and the results from its experimental validation will be provided and compared with those obtained using a conventional frequency domain EMI receiver.

978-1-4799-6616-5/15/$31.00 ©2015 IEEE

II. OVERVIEW OF TDEMI MEASUREMENT SYSTEMS

In general terms, a TDEMI measurement system can be described by the block diagram shown in Figure 1[9]. Those TDEMI systems can be employed, in theory, for the measurement of either the radiated EMI or conducted EMI. For the measurement of radiated electromagnetic interference a broad-band antenna shall be used, while for the measurement of conducted EMI corresponds either a current clamp or line impedance stabilization network. Sometimes the measured signal passes through a preamplif er and then it is low-pass f ltered for band limiting proposes, so the signal fulf lls the Nyquist condition for the maximum sampling rate supported by the TDEMI system. Then, in the analog-to-digital converter (ADC), the signal is digitized and then it is stored. Finally, the amplitude spectrum is computed via a spectral estimation techniques.

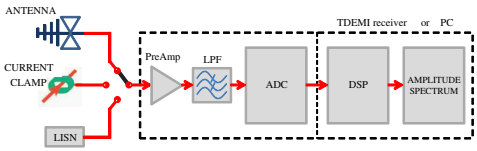

Fig. 1. Block diagram of a Time-Domain EMI measurement system.

On the other hand, from the standpoint of the signal acquisition and processing stage, a TDEMI system is more naturally described by the f ow chart shown in Figure 2.

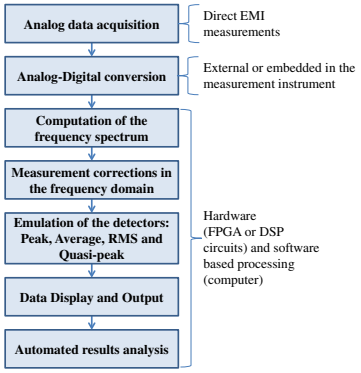

Fig. 2. General f ow chart of the TDEMI measurement processing.

In that sense, the data acquisition process for a TDEMI measurement system begins when the analog signal is sampled either directly by the measuring instrument (i.e., digital oscilloscope) or externally by means of ADC or digitizers. Then, the EMI data are transferred from the main memory to the device that will process it. For the commercial FFT-based EMI receivers this process is performed internally by the built-in processors and software [6]. However, a customized TDEMI measurement system may carry on the digital signal processing with the aid of specif c software running on a personal computer. Then, the data are transferred to a personal computer via some communication port, such as the General Purpose Interface Bus (GPIB). Subsequently, the amplitude spectrum is digitally computed using the FFT (or some variant of), periodograms or other spectral estimation methods [10]. Later, the errors due to the frequency dependence of the antenna factor, the attenuation in the transmission line, the gain of the preamplif er, the frequency response of the anti-aliasing f lter are corrected. Next, a mathematic emulation of the peak, RMS, average and quasi-peak detectors is made, either by applying a correction factor dependent on the pulse repetition frequency [11] or by means of the application of a digital inf nite impulse response f lter [12]. Additionally, other signal processing techniques can be used in order to reduce the impact of the noise but this has varied upon specif c implementations. Finally, the results must be displayed and compared with the respective limit lines to provide a judgment about the test result regarding the EMI in the measured frequency band. For studying non-stationary signals, a spectrogram representation of EMI has also been used previously[13].

III. GENERAL DESCRIPTION OF THE TDEMI MEASUREMENT SYSTEM

A. Hardware

Even if the measurement method is, by itself, neither restricted in terms of the maximum measurable frequency, dynamic range nor noise f oor, it is important to indicate the overall technical specif cation of the hardware in order to emphasize the use of general purpose instruments as a key aspect of our approach. In that sense, the developed TDEMI measurement system uses a general purpose digital oscilloscope and a personal computer for pre- and post-processing the results in both the time an the frequency domain. Specif cally, the make and model of the oscilloscope used is Tektronix DPO 7104, which has a 1 GHz bandwidth, a maximum sampling rate of 20 GSamples/s, and up to 8 bit (>11 bit with Hi-Res mode) ADC resolution (6.7 effective number of bits). Thus, the maximum frequency measurable by the oscilloscope is limited to 1 GHz by the hardware, making it unnecessary to apply an additional low-pass f lter as shown in Figure 1. The maximum theoretical dynamic range for a harmonic input signal with an amplitude equal to the ADC full-scale input is 110 dB (74 dB plus the processing gain and at full range signal), while typically the effective dynamic range is about 78 dB.

B. Sampling scheme

It is well-known that, according to the (uniform) sampling theorem, the minimum required sampling rate must be at least twice the upper frequency limit of the measured band in order to be able to reconstruct the sampled signal, that is 2 GSamples/s for a TDEMI system intended to measure up to 1 GHz. However, in order to avoid the aliasing inf uence, the generally recommended criteria is to select a sampling frequency, f_s, of approximately four times the upper frequency bound of the spectrum to be measured, that is, $4f_{max}$[14]. This particular TDEMI measurement system implementation selects, from a set of possible sampling frequencies conf gurable in the oscilloscope, the immediately sampling rate higher than

$4f_{max}$. For example, considering a measure between 30 MHz-1 GHz, f_s is set to 5 GSamples/s since $f_{max} = 1$ GHz. On the other hand, if measuring in the band 100 MHz-300 MHz, f_s is set to 1.25 GSamples/s. The main objective in adjusting f_s is to use the oscilloscope memory eff ciently so the capture time, $T_{capture}$, is suff cient to achieve the required frequency resolution, $\Delta f = 1/T_{capture}$.

C. Filtering and windowing

Before acquiring the measurements, the appropriated record length must be selected in order to provide the required Δf. In that sense, the minimum capture time, T_{min}, and the minimum record length, RL_{min}, are given by,

$$RL_{\min} = \text{round}\left(f_s T_{\min}\right) = \text{round}\left(f_s \frac{w_f}{\Delta f}\right), \qquad (1)$$

where, w_f is the window factor of the windowing function to be applied in order to reduce the scallop loss and the spectral leakage caused by the f nite length of the data.

After sampling and acquiring, the signal is digitally band-pass f ltered to remove frequency components outside the band of interest, primarily noise measured below the minimum frequency of interest. The time delay introduced by the convolution operation between the f lter's transfer function and the measured signal is then corrected.

The following step of the signal processing chain is windowing the data. The algorithm of this TDEMI measurement system use by default a Kaiser-Bessel window with the parameter $\beta = 16.7$ ($w_f \approx$2.23) since it offers a good compromise between amplitude accuracy and spectral leakage [15], which makes Kaiser-Bessel windows adequate to analyze both continuous and transient signals. However, the algorithm also offers the possibility of selecting other windowing functions such as the Gaussian, Hann, Hamming, Blackman or Flat-top that have been previously used in similar applications [14][16].

D. Basic measurement algorithm

As stated previously, our TDEMI measurement system is mainly intended to study transient, discontinuous and intermittent signals, still it must be able to handle continuous signals in order to provide a proper spectral estimation that includes narrow band and broadband signals, as required on the assessment of the radiated emissions.

Hence, the algorithm initially performs a preliminary measurement in order to identify transient, discontinuous and intermittent signals. This measurement must be conf gured for a capture time as long as possible, considering practical limitations such as memory restrictions. In our particular case, a record length, RL, of 10^6 samples is used by default. As a general rule, RL must be several times longer than RL_{min} in order to provide an accurate spectral estimation. For example, for f_{max}=1 GHz, Δf=120 kHz and w_f=2.23, $RL_{min} \approx 9.3 \times 10^4$ samples, which is more than 10 times smaller than the selected RL.

Then, by manually adjusting manually the trigger to an appropriate level it is ensured to record at least a complete sample of the pulsed signal. Next, the pulse envelope and duration, Δt_{pulse}, are automatically and robustly calculated by the algorithm. It is recommended to set the oscilloscope to acquire in averaging mode since it helps obtaining a more consistent calculation of Δt_{pulse}, since it improves the signal-to-noise ratio by reducing the uncorrelated noise. The number of pulses, n_{pulses}, occurred during $T_{capture}$ is also counted. After analysing the preliminary measurement, one of the following different scenarios must be selected by the algorithm:

- If no pulse was detected, $n_{pulses} = 0$, it is assumed that the measurement was triggered by a continuous signal, then the algorithm shall proceed with the spectral estimation using the preliminary measurement as input.
- If only one pulse was detected, $n_{pulses} = 1$, it means the pulse repetition frequency is lower than de inverse of the capture time. Then, RL is set so $T_{capture} \approx \Delta t_{pulse}$ and the oscilloscope is conf gured to acquire in the FastFrame™ mode. The number of frames must be selected according the internal memory limitations. The accuracy in the estimation of the average pulse repetition frequency, f_{pulse}, increases with the number of frames. Through our experiments, we have found empirically that recording at least 10 pulse frames is suff cient to estimate consistently f_{pulse}, but that number of frames is dependent on the time base of the oscilloscope and may vary in other implementations.
- If a few pulses were detected (i.e., $2 \leq n_{pulses} \leq 10$, in our case), f_{pulse} is estimated but it might not be a suff ciently accurate value. Therefore, in this scenario the oscilloscope is also conf gured to acquire in the FastFrame™ mode for a capture time corresponding to the estimated pulse duration. Again, the number of frames is selected according the internal memory limitations, applying the same criteria explained above.
- If several pulses were detected ($n_{pulses} > 10$, in our case), it means the preliminary measure contains at least a pulsed signal with a f_{pulse} properly estimable upon the initial measurement and then the algorithm shall proceed with the spectral estimation stage using the preliminary measurement as input.

E. Equivalent "reassembled-time" signal

If the algorithm decides to rerun the measures in FastFrame™ mode, it measures several records of the pulsed signal accompanied by an absolute time stamp of the triggered events which occur in sequence. The time stamps are processed in order to provide a relative time of occurrence of the pulses and also to calculate f_{pulse}. It has been observed that the high resolution acquisition mode provides the best performance when measuring the pulses in the FastFrame™ mode since it allows obtaining better details of the measured pulse waveform by increasing the ADC resolution through oversampling and then providing a better dynamic range. No additional changes are required regarding the oscilloscope settings.

The individual pulses measured during each frame are merged in a equivalent "reassembled-time" signal using the information provided by the time stamps. Therefore, it is possible that the equivalent capture time exceeds the maximum record length allowable in a single run measure, while the effective memory usage remains manageable since this approach leads to a enormous data reduction. The time between pulses in the

reassembled signal is, optionally, f lled with the background noise of the initially recorded signal for the time lapse posterior the pulse has fallen and after the occurrence of the following pulse.

F. Spectral estimation

The developed TDEMI measurement system provides a few different Spectral Density Estimations (SDE) for the radiated emissions. For this purpose, the SDE is carried out by means of the Short-Time Fourier Transform (STFT) and the Welch's periodrogram. Therefore, the signal is examined in overlapped time windows of T_{min} duration in order to assure, by default, a minimum frequency resolution comparable to the 120 kHz resolution bandwidth required by CISPR-16-1-1 for measurements in bands C and D. However, the algorithm is able to adjust the window length to provide an reasonably arbitrary resolution bandwidth. The default overlapping percentage between windows is set to 75%, being possible to increase it up to 90% (since a greater overlapping proportion would consume more memory without providing a signif cant improvement on accuracy) or decrease it down to 50% (when reducing the computation cost is needed) in order to adjust resolution in time domain.

The STFT is used to analyze the spectral content of local sections of a measured signal as it changes over time. The STFT provides a spectrogram matrix from which is possible to provide a worst case spectral estimation comparable with a measurement obtained with a max-peak detector. On the other hand, Welch's periodogram combines the STFT method with the averaging of each modif ed periodograms of the windowed time frames, providing a SDE comparable with a measurement obtained with an average detector. For a detailed explanation of spectral estimation techniques, please consult [17].

G. Correction and scaling of measurements

Since each component of the system (antenna, cables, preamplif er, oscilloscope) has a specif c impulse response, it would be required to correct the direct oscilloscope voltage measurements, $v(t)$, in order to obtain the corresponding electric f eld as it varies over time, $E(t)$. However, this would depend upon knowing or measuring the impulse response of all the elements of the measurement chain and then deconvolve it of the measured signal. This might be neither possible nor practical for most EMC measurements and, therefore, it result more convenient to apply corrections in the frequency domain.

Assuming that only the amplitude spectrum representation is required, our TDEMI measurement system applies the corresponding correction factors such as cable attenuation and signal path losses, antenna factors and the oscilloscope frequency response. Since the EMI spectrum is meant to be expressed in terms of decibels-microvolts per meter, the aforementioned correction factors are added, as usual, and the adequate scaling factors are incorporated for assuring consistency in the units.

H. Budget

In general terms, the oscilloscope is the most expensive equipment involved in the whole setup of the implemented TDEMI measurement system. For measurements up to 1 GHz, very affordable and versatile hardware options are available in the market including USB PC-based scopes which are relatively inexpensive (about €5,000) and very practical for in-situ measurements due to its size and weight. For measurements above 1 GHz, similar alternatives are also available for higher budgets being relatively common to found suitable oscilloscopes with a measuring bandwidth of 10 GHz and more for less than €20,000. In the near future, it's expected those prices will be reduced. Regarding the rest of the hardware, a quick survey have allowed us to estimate that an amount of €1,500 extra would be suff cient to procure the required accessories and personal computer. Nevertheless, in most cases, elements such as antennas, cables and preamplif ers are interchangeable items that are already available in an EMC lab, being unnecessary to include them in the overall cost of the TDEMI measurement system.

It is important to state that we have intentionally not mentioned references for the aforementioned prices because it is not our intention to advertise any vendor, however, this information can be easily verif ed by anyone who is interested.

I. Notes on the software implementation

All the signal processing algorithms applied after the PC acquisition stage are implemented in MATLAB® due its conveniently broad library of mathematical functions and its optimized approach for operations involving matrices and vectors. Statistics Toolbox and Signal Processing Toolbox functions are used throughout the code.

IV. Validation Methodology

The validation of the presented TDEMI measurement system was performed for radiated emissions testing by means of well-known controlled transient and continuous signals generated using a burst generator Schlöder SFT 1400, an arbitrary signal generator Agilent 81160A and a programmable synthesizer Hameg HM8134 as the source of the EMI. The EMI was radiated by an open cable and/or by antennas, respectively. The measurements were performed inside an anechoic chamber. Regarding the measuring antenna, a BiLog antenna Schaffner CBL6143 was used. The results were compared with those obtained from a conventional EMI test receiver model ESPI from Rohde&Schwarz. A general diagram of the measurement setup is shown in Figure 3.

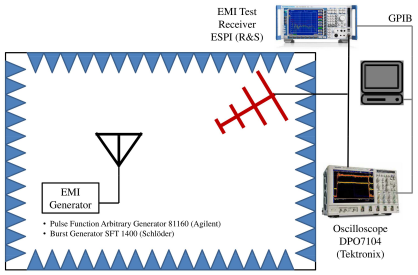

Fig. 3. Simplif ed experimental setup for the validation of the TDEMI measurement system.

Since for transient signals with a low pulse repetition frequency a single sweep measurement of the EMI test receiver is likely to provide an incorrect result for the spectral content of the disturbance, several sweeps of the EMI test receiver were required with the max hold enabled until the measurement was useful for comparison purposes. Finally, the Feature Selective Validation (FSV), a method widely known in the field of computational electromagnetics [18], was used for assessing a comparison between the measurement results obtained with the developed system with respect to measurements taken with the conventional EMI test receiver.

V. RESULTS

The following subsections present a pair of representative measurement results for which our TDEMI system has been validated. However, several other controlled validation stages has been performed previously in order to assure the correctness and consistency of our measurements procedures, algorithms, instruments and reference patterns.

A. Radiated burst

In this experiment, a radiated burst is measured as a representative case of a broadband EMI formed by single periodic pulses with $f_{pulse} \ll B_{imp}$ (impulse bandwidth). Particularly, our burst generator was set at 5 kHz with a 15 ms pulse duration and a burst period of 50 ms. Let us assume we are only interested in measuring the spectral components corresponding the aforementioned pulsed EMI. Since the standard burst (IEC 61000-4-4) has a rise time of 5 ns, it is *a priori* known that its radiated emissions are entirely expected in the 30 MHz - 300 MHz band, therefore $f_s = 1.25$ GHz is used. Antialiasing filtering was not required. The TDEMI and the corresponding ESPI test receiver were configured for measuring using coherent parameters: Δf = 120 kHz, Max Peak and Average detector. The ESPI Test receiver was configured to capture 8000 frequency points (maximum) with the max-hold feature active in order to capture the worst case emissions after several sweeps of 5 s duration each. The results corresponding to the EMI spectral estimation are shown in Figure 4 for both detectors and both measurement systems.

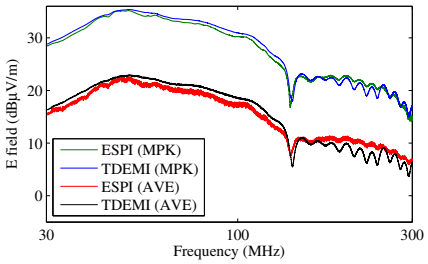

Fig. 4. Spectral estimation for a radiated burst pulse.

The difference between both measuring methods was of less than 0.4 dB at the frequency of maximum emission level. Then, applying the FSV, the overall results indicate that there is, in average for all the detectors, an "Excellent"-"Very Good" level of agreement between the traces regarding their amplitude ($ADM_{tot} = 0.114$), feature ($FDM_{tot} = 0.2724$) and global ($GDM_{tot} = 0.3177$) difference measures. However, the validation results might have been degraded by the noise in the traces.

B. Superposition of Broadband and Narrowband EMI

Our second experimental scenario deals with an EMI formed by a periodic transient pulse of f_{pulse}=100 kHz and a continuous tone at 900 MHz. Now, let's assume it is required measuring the whole spectrum covering form 30 MHz up to 1 GHz, thus setting f_s =5 GHz. Again, the TDEMI and the corresponding ESPI test receiver were configured for measuring using coherent parameters: Δf = 120 kHz, Max Peak and Average detector and the maximum number of samples corresponding in each case. The results corresponding to the EMI spectral estimation are shown in Figure 5 for both detectors and both measurement systems.

In Figure 5, the SDE provided by our TDEMI measurement system was performed using the reassembled signal constructed by superposing, in the time domain, the transient and continuous parts. The results indicate that our TDEMI measurement system provides results within ±1.5 dB when compared with a conventional EMI test receiver, provided that the signal level is above the noise floor of both measurement systems. Considering that, typically, the radiated emissions measurements have an expanded uncertainty higher that 3 dB, our system provides a comparable accuracy level.

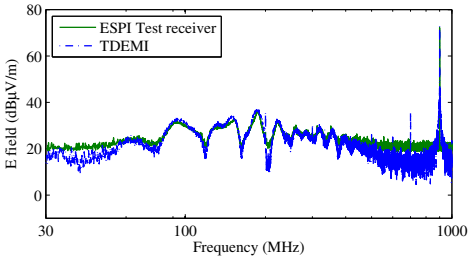

(a) Max-Peak detector

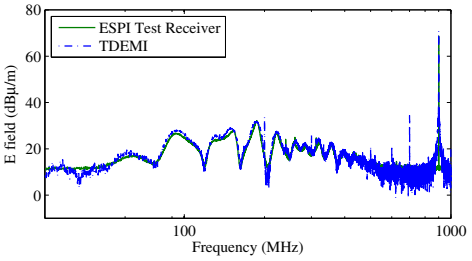

(b) Average detector

Fig. 5. EMI spectral estimation superposed broadband and narrowband EMI.

In this particular case, the standard FSV indicates that the overall level of agreement between the ESPI Test Receiver and our TDEMI measurement system results is, in average for all the detectors and methods, "Good"-"Fair" for their amplitude ($ADM_{tot} = 0.5463$), feature ($FDM_{tot} = 0.6882$) and global ($GDM_{tot} = 0.9832$) difference measures. However, careful must be take when comparing measurement results applying the standardized FSV because if such measurement include noisy frequency bands, as this particular case, the overall indicators provide misleading results and they should be accompanied by a proper uncertainty statement for the validation results [19].

VI. CONCLUSION

A TDEMI measurement system, that employs an alternative approach and different algorithms in comparison to previously published works that addresses this subject, has been presented. One of the principal advantages of our TDEMI system is that it can be continuously improved through signal processing implemented via software. Even if our general purpose equipment limits the measurement band up to 1 GHz, it would be completely feasible to enhance the current capabilities of the TDEMI measurement system by using an oscilloscope with a larger bandwidth.

As expected, the measuring and processing time required by our TDEMI measurement system is much lower than the required by conventional EMI test receivers, however, we believe this is not the most relevant improvement achieved. In our TDEMI measurement system the algorithms detect robustly the transient EMI pulses and adjust automatically the oscilloscope parameters and acquisition modes to capture only the pulse of interest with the optimal instrument conf guration, thus the measuring system manage more effectively aspects such as the dynamic range and the ambient noise. Implicitly, those features also reduces the amount of samples required for a proper SDE of the measured EMI, and therefore, it provides an improved capability for managing the required oscilloscope memory, even if this aspect was not discussed in detail in the main body of the paper.

On the other hand, one remarkable feature of our approach to the TDEMI measurement system implementation is that it was feasible to built it with a relatively small budget, starting approximately form €5,000; proving that radiated EMI assessment by means of time domain techniques is not only very accurate but also affordable for small in-company or university EMC laboratories which require a fast and cost effective alternative to evaluate accurately the performance of the radiated emissions of their products and prototypes.

The authors believe that TDEMI systems, as the one presented in this article, are an attractive alternative for performing *in-situ* measurements on industrial environments or under situations where the equipment under test can't be properly installed within a controlled measurement facility such a semianechoic chamber, since it would reduce signif cantly the cost of performing or contracting such measurements.

ACKNOWLEDGMENT

This work was supported in part by EURAMET IND60EMC research project (the EMRP is jointly funded by the EMRP participating countries within EURAMET and the European Union) and by the Spanish "Ministerio de Economía y Competitividad", under project TEC2013-48414-C3-3-R.

REFERENCES

[1] P. Torio and M. Sanchez, "Novel Procedure to Determine Statistical Functions of Impulsive Noise," *Electromagnetic Compatibility, IEEE Transactions on*, vol. 47, no. 3, pp. 559–568, Aug 2005.

[2] R. Adriano, N. Ben Slimen, V. Deniau, M. Berbineau, and P. Massy, "Prediction of the BER on the GSM-R communications provided by the EM transient disturbances in the railway environment," in *Electromagnetic Compatibility - EMC Europe, 2008 International Symposium on*, Sept 2008, pp. 1–5.

[3] M. Pous and F. Silva, "Full-Spectrum APD Measurement of Transient Interferences in Time Domain," *Electromagnetic Compatibility, IEEE Transactions on*, vol. PP, no. 99, pp. 1–9, 2014.

[4] ——, "Prediction of the Impact of Transient Disturbances in Real-Time Digital Wireless Communication Systems," *Electromagnetic Compatibility Magazine, IEEE*, vol. 3, no. 3, pp. 76–83, rd 2014.

[5] H. Westenberger, "Use of Time Domain methods for CISPR16 compliant EMI Measurements," in *Microwaves, Communications, Antennas and Electronics Systems, 2009. COMCAS 2009. IEEE International Conference on*, Nov 2009, pp. 1–4.

[6] P. Russer, "EMC measurements in the time-domain," in *General Assembly and Scientif c Symposium, 2011 XXXth URSI*, 2011, pp. 1–35.

[7] *Specif cation for radio disturbance and immunity measuring apparatus and methods - Part 1-1: Radio disturbance and immunity measuring apparatus - Measuring apparatus*, CISPR Std., july 2010.

[8] G. Costa, M. Pous, A. Atienza, and F. Silva, "Time-Domain Electromagnetic Interference Measurement System for intermittent disturbances," in *Electromagnetic Compatibility (EMC Europe), 2014 International Symposium on*, Sept 2014, pp. 833–837.

[9] S. Braun and P. Russer, "Requirements and Solutions for Emission Measurements in Time-Domain According to International EMC Standards," in *Electromagnetic Compatibility (APEMC), 2012 Asia-Pacif c Symposium on*, May 2012, pp. 209–212.

[10] F. Krug, D. Mueller, and P. Russer, "Signal Processing Strategies with the TDEMI Measurement System," *Instrumentation and Measurement, IEEE Transactions on*, vol. 53, no. 5, pp. 1402–1408, Oct 2004.

[11] F. Krug and P. Russer, "Quasi-peak Detector model for a Time-Domain Measurement System," *Electromagnetic Compatibility, IEEE Transactions on*, vol. 47, no. 2, pp. 320–326, May 2005.

[12] C. Keller and K. Feser, "Non-Linear Superposition Of Broadband Spectra For Fast Emission Measurements In Time Domain," in *Proceedings of 15th Zurich EMC Symposium*, 2003, pp. 505–510.

[13] C. Hoffmann and P. Russer, "A Time-Domain system for EMI measurements above 1 GHz with high sensitivity," in *Microwave Conference (GeMIC), 2011 German*, March 2011, pp. 1–4.

[14] C. Keller and K. Feser, "Fast Emission Measurement in Time Domain," *Electromagnetic Compatibility, IEEE Transactions on*, vol. 49, no. 4, pp. 816–824, Nov 2007.

[15] J. Solomon, O., "The Use of DFT windows in Signal-to-Noise ratio and Harmonic Distortion Computations," *Instrumentation and Measurement, IEEE Transactions on*, vol. 43, no. 2, pp. 194–199, Apr 1994.

[16] M. Keller, "Comparison of Time Domain Scans and Stepped Frequency Scans in EMI Test Receivers," *Rohde & Schwarz White Paper*, 12 2013.

[17] D. Manolakis and V. Ingle, *Statistical and Adaptive Signal Processing: Spectral Estimation, Signal Modeling, Adaptive Filtering, and Array*, ser. Communications and signal processing. McGraw-Hill, 2011.

[18] A. Duffy, A. Martin, A. Orlandi, G. Antonini, T. Benson, and M. S. Woolfson, "Feature Selective Xalidation (FSV) for Validation of Computational Electromagnetics (CEM). Part I-the FSV method," *Electromagnetic Compatibility, IEEE Transactions on*, vol. 48, no. 3, pp. 449–459, Aug 2006.

[19] M. Azpurua, E. Paez, J. Rojas-Mora, O. Ventosa, F. Silva, G. Zhang, A. Duffy, and R. Jauregui, "A Review on the Drawbacks and Enhancement Opportunities of the Feature Selective Validation," *Electromagnetic Compatibility, IEEE Transactions on*, vol. 56, no. 4, pp. 800–807, Aug 2014.

4

ALTERNATIVE FULL TIME DOMAIN EMISSIONS TESTING METHODS

The publications in subsections 4.1, 4.2, 4.3 and, 4.4 comprise the more practical facet of this Thesis research. This papers are diverse in terms of the spanning from communications, aeronautics, large industrial system and railway. In the light of the Thesis objectives, their key outputs are:

Objective 1: Optimizing Full TDEMI measurement systems for enabling the required measurements by using USB digitizers.

Objective 2: Firstly, through the time-domain measurements of the interferences at intermediate frequency, the impact of radiated transient interferences on the GSM system was determined using the APD detector and evaluated using limits defined in terms of the RxQual criteria. Secondly, a time-domain EMI measurement system was developed for measuring the radiated and conducted indirect effects of lightning strikes on-board of unmanned aerial vehicles, featuring multichannel and triggering capabilities that allowed for alternative measurement methods. Thirdly, multichannel Full TDEMI measurement systems were extensively used for assessing an automatic storage and retrieval system in-situ. Lastly, the applicability of multichannel Full TDEMI measurement systems for improving the emissions test procedures used in the railway sector was studied. Specifically, for evaluating the dynamic and static modes of the rolling-stock. From those experiences, several advantages of measuring interferences in the time-domain were reported.

Objective 4: Validations of the proof-of-concept experiments and *in-situ* test results were performed by comparing the Full TDEMI measurements with the corresponding ones from a CISPR 16-1-1 compliant measuring receiver.

4.1. COMPLEMENTARY JOURNAL ARTICLE 1

M. Pous, **M. A. Azpúrua** and F. Silva, "Measurement and Evaluation Techniques to Estimate the Degradation Produced by the Radiated Transients Interference to the GSM System," in *IEEE Transactions on Electromagnetic Compatibility*, vol. 57, no. 6, pp. 1382-1390, Dec. 2015. doi: 10.1109/TEMC.2015.2472983

Abstract-A common source of noise for digital communication systems is the radiated transient interference. As an example, it has been reported that the degradation is produced to the Global System for Mobile (GSM)-Railway signaling system when the impulsive noise is generated by

sparks caused by the discontinuity between the catenary and the pantograph. Concerning the measurement and evaluation procedures defined in the electromagnetic compatibility standards, they are not suitable for these types of transient disturbances. Therefore, new techniques must be developed to determine, with a high confidence level, the degradation that impulsive noise will produce in communication systems. In this paper, novel time-domain measurement procedures are carried out to acquire transient interferences generated by sparks properly. Moreover, two different evaluation methodologies, employing base-band simulation and amplitude probability distribution detector, are used to analyze the impact of the disturbance applied into a GSM system interference scenario. Finally, the results obtained with the developed methodologies are successfully compared with a reference measure where the GSM downlink channel quality is monitored by a mobile station test unit.

4.2. CONFERENCE PROCEEDING 2

M. A. Azpúrua, M. Pous and F. Silva, "On-board compact system for full time-domain electromagnetic interference measurements," *2016 ESA Workshop on Aerospace EMC (Aerospace EMC)*, Valencia, 2016, pp. 1-4. doi: 10.1109/AeroEMC.2016.7504579

Abstract-This paper presents a compact system for the measurement of electromagnetic interferences in the time domain. The measurement system is based on a USB oscilloscope, used as digitizer, and specific software for signal processing and spectral estimation. The measurement system is suitable for both conducted and radiated electromagnetic emissions up to 200 MHz. Its accuracy, precision and dynamic range are sufficient for the intended application. It is particularly suitable for measuring transient disturbances due to its triggering capabilities. Its relative low weight and cost makes it a valuable tool for investigating on-board the indirect effects of lightning strikes as disturbances coupled to cables and antennas inside launch vehicles, aircrafts, and unmanned aerial vehicles.

4.3. CONFERENCE PROCEEDING 3

M. Pous, **M. A. Azpúrua** and F. Silva, "Benefits of full time-domain EMI measurements for large fixed installation," *2016 International Symposium on Electromagnetic Compatibility - EMC EUROPE*, Wroclaw, 2016, pp. 514-519. doi: 10.1109/EMCEurope.2016.7739221

Abstract-It is difficult to properly evaluate the electromagnetic disturbances generated by large fixed installations because of, i.e., the background noise, unsteady emissions and transient interferences. Those challenging EMC issues have been recently studied in European research projects on improved test methods in industrial environments. In order to overcome traditional in-situ EMI measurement troubles, a novel time-domain methodology is proposed and used in a real fixed installation with large machinery. Firstly, a comparison between the developed measurement system, using an oscilloscope, and an EMI receiver is done in some test-cases for validation purposes. After verifying the accuracy of the measurements, we proceed with the measurement campaign applying the full time-domain methodology. The main benefits of employing the time-domain system are emphasised through the results. It was observed that the some remarkable advantages of the time-domain approach are: triggering by disturbance events, extremely reduce the capturing time, identify on real time the worst emissions modes of the EUT, avoid changes at the background noise and perform simultaneous multichannel synchronous measurements.

4.4. CONFERENCE PROCEEDING 4

M. Pous, **M. A. Azpúrua**, J. A. Oliva, M. Aragón, I. González and F. Silva, "Full Time Domain EMI measurement system applied to Railway emissions according to IEC 62236-3-1/EN 50121-3-1 standards,"

2018 International Symposium on Electromagnetic Compatibility - EMC EUROPE, Amsterdam, 2018, pp. 1-6. (Accepted paper)

Abstract-This paper studies the advantages of applying time domain based instrumentation to conduct electromagnetic interference emissions from rolling-stock. In IEC 62236-3-1 or EN 50121-3-1 standards, it is mandatory to measure the railway vehicle in static and in-motion conditions. When conventional frequency sweep instrumentation is employed, difficulties regarding ambient noise variation and the short-duration of worst-case emission modes take place. In Annex B of the standard, a test procedure is described to acquire the worst-case EMI, however, as it is explained at the paper the effective measured time at each frequency is only 0.08 ms in some frequency bands. Hence, multiple movements of the vehicle are needed increasing the uncertainty of the measured source and making difficult to distinguish vehicle EMI from background noise interference. To solve this problem, a Full TDEMI measurement system is proposed with the availability to increase the effective measured time, reduced the ambient noise variation, the usage of multiple antennas at the same time and the possibility to discard transient interference that should not be evaluated. At the end of the paper, measurements carried out with the time-domain system are shown demonstrating the effectivity of the methodology.

1382 IEEE TRANSACTIONS ON ELECTROMAGNETIC COMPATIBILITY, VOL. 57, NO. 6, DECEMBER 2015

Measurement and Evaluation Techniques to Estimate the Degradation Produced by the Radiated Transients Interference to the GSM System

Marc Pous, Marco A. Azpúrua, *Member, IEEE*, and Ferran Silva, *Member, IEEE*

***Abstract*—A common source of noise for digital communication systems is the radiated transient interference. As an example, it has been reported that the degradation is produced to the Global System for Mobile (GSM)-Railway signaling system when the impulsive noise is generated by sparks caused by the discontinuity between the catenary and the pantograph. Concerning the measurement and evaluation procedures defined in the electromagnetic compatibility standards, they are not suitable for these types of transient disturbances. Therefore, new techniques must be developed to determine, with a high confidence level, the degradation that impulsive noise will produce in communication systems. In this paper, novel time-domain measurement procedures are carried out to acquire transient interferences generated by sparks properly. Moreover, two different evaluation methodologies, employing base-band simulation and amplitude probability distribution detector, are used to analyze the impact of the disturbance applied into a GSM system interference scenario. Finally, the results obtained with the developed methodologies are successfully compared with a reference measure where the GSM downlink channel quality is monitored by a mobile station test unit.**

***Index Terms*—Amplitude probability distribution (APD), electromagnetic transients interferences, GSM, impulsive noise, time-domain measurements.**

I. Introduction

In the electromagnetic compatibility (EMC) research area, the measurement and evaluation of the degradation produced by radiated transient disturbances on digital communication systems (DCSs) is a technological challenge that has not been completely addressed. The impulsive noise, which is generated by switching devices or by sparks, is a broadband interference that covers the spectrum from dc to several hundreds of megahertz or some gigahertz. Additionally, this man-made noise is characterized by its short and random burst parameters, which makes it really difficult to measure it correctly. Radiated transient interferences are propagated as an electromagnetic wave, reaching DCSs antennas and causing distortion as well as system failures [1], [2]. For instance, previous research has found that the GSM-Railway signaling system is interfered by the impulse noise generated through the sparks produced by the discontinuity between the pantograph and the catenary [3], [4].

The EMC standards must prevent from interference situations where man-made noise produces failures of electronic products including the DCSs. However, electromagnetic transient interfering environments cannot be noticed beforehand if the measurements procedures described in the EMC standards are employed [5]. Radiated transient interferences are underestimated as most of EMC standards were developed to protect analog communication systems, which uses the signal-to-noise ratio as the main figure of merit. Moreover, in the standards, detectors such as the quasi-peak are still applied; nevertheless, it was developed to relate the human perception to the degradation of amplitude-modulated radio signals which are distant from the novel DCSs. Consequently, new measurement procedures must be considered to estimate, with a high level of confidence, the degradation produced to DCS [6], [7].

The main idea of the work presented in this paper is to demonstrate that it is possible to perform time-domain radiated emissions measurements of an interference environment and determine in advance the bit-error-rate (BER) produced in a DCS. To accomplish with this goal, time-domain measurements instead of frequency-sweep procedures defined in the EMC standards must be carried out obtaining the main parameters of the impulsive interferences. Furthermore, evaluation methodologies based on DCS baseband simulation and also the employment of statistical measurements are defined in this paper to deal with the radiated transient interferences.

Recently, statistical detectors have been introduced by CISPR, conversely, the usage of these detectors is not defined in any generic or product EMC standard. The amplitude probability distribution (APD) measurement offers the possibility to obtain the statistical parameters of the interferences, which is a really powerful tool to characterize the impulsive noise. Several studies have correlated APD measurements with the bit-error-probability (BEP) for coherent radio receivers [8], [9] and also novel time-domain APD measurement methodologies beyond EMC standards have been developed [10]. Furthermore, a method to define limits in the APD diagram in terms of the degradation produced to DCSs [11] has been published, thus providing the capability of evaluating the corresponding distortion produced by previously measured continuous interferences.

Manuscript received March 10, 2015; revised July 7, 2015; accepted August 8, 2015. Date of publication September 9, 2015; date of current version December 11, 2015. This work was supported in part by EURAMET IND60EMC Research Project (the EMRP is jointly funded by the EMRP participating countries within EURAMET and the European Union) and by the Ministerio de Economía y Competitividad, under Project TEC2013–48414-C3–3-R.

The authors are with the Electromagnetic Compatibility Group, Universitat Politècnica de Catalunya, Barcelona 08034, Spain (e-mail: marc.pous@upc.edu; marco.azpurua.a@ieee.org; ferran.silva@upc.edu).

Color versions of one or more of the figures in this paper are available online at http://ieeexplore.ieee.org.

Digital Object Identifier 10.1109/TEMC.2015.2472983

0018-9375 © 2015 IEEE. Personal use is permitted, but republication/redistribution requires IEEE permission.
See http://www.ieee.org/publications_standards/publications/rights/index.html for more information.

II. Proposed Methodologies

As stated earlier, measuring radiated transient interferences is exceptionally challenging due to their random and broadband intrinsic characteristics. With the aim of protecting sensible communication receivers, measurements beyond EMC standards must be meticulously defined and carried out.

The following sections present novel acquisition and evaluation procedures developed to overcome the limitations of the EMC standards, making it feasible to obtain the time domain and the statistical information of the impulsive noise. Furthermore, combining transient interference measurements with methodologies for analyzing digital communications, we must be able to predict the BEP suffered by any DCS. Alternatively, the statistical information provided by the APD measurement can be related directly with the degradation of the communication link.

A. IQ Capture and DCS Simulation Procedure

This methodology is based on the in-phase and quadrature (IQ) components acquisition of the radiated interference in the frequency band of the communication system. Afterward, a simulation of the DCS adding the interference previously measured is performed to determine the degradation produced by the impulsive noise.

Concerning the setup of the time-domain measurement, in the transient acquisition, the receiver antenna is connected to the electromagnetic interference (EMI) receiver, which is centered in the working frequency of the DCS. The analog input stage of the EMI receiver is used to filter the transient interference in the communication frequency band and down converts it to the intermediate frequency (IF). The IF output of the EMI receiver is connected to the input of the oscilloscope, which performs the tasks to detect transient events employing the trigger and also to store the IF transient interference described by the following equation:

$$x[n] = A_{\mathrm{IF}} \cdot \sin(2\pi f_{\mathrm{IF}}\,(n) + \varphi_{\mathrm{IF}}), \tag{1}$$

where $x[n]$ is the discrete input signal modulated in the f_{IF} frequency, where $n = k\Delta t$. As an example, the IF of the EMI receiver used in these measurements is 20.4 MHz. The IF signal is obtained, setting the most accurate resolution bandwidth (RBW) from the available ones in the EMI receiver. The RBW, which shall be selected by the user, must be larger than the bandwidth of the real time communication systems. Once the IF signal has been acquired, the measurement methodology is able to compute the IQ components of the interference employing the mathematical software. First, the data are bandpass filtered in the IF center frequency to avoid undesired spurious components. Second, the signal is demodulated obtaining the IQ components according to the following equations:

$$i[n] = x[n] \cdot \cos(2\pi f_{\mathrm{IF}}(n)) \tag{2}$$

$$q[n] = x[n] \cdot \sin\left(2\pi f_{\mathrm{IF}}\,(n)\right). \tag{3}$$

Afterward, $i[n]$ and $q[n]$ components of the interference are filtered with a low-pass finite impulse response filter equal to the RBW of the communication system. This is one of the main advantages that offer the measurement procedure, where the bandwidth can be equal to the bandwidth of the communication system. Therefore, the low-pass filter can be adjusted to obtain the portion of the interference that will be received by the DCS. The last stage of the postprocessing is to store the IQ data in a file; furthermore, in order to reduce the file size, the data are resampled with a lower sample rate. This sample reduction can be done because in the input of the postprocessing, we have the data modulated at 20.4 MHz, and at the end, the data are in baseband.

The second stage of the methodology is to employ the IQ baseband interference using it as the input for the base-band simulation of the communication system. The DCS simulation enables determining the BER of the communication system when the radiated transient interference is present in the environment. In order to estimate the performance of DCSs, computer-assisted techniques have been employed since the 70's [12]. The BER or BEP remains the most common figure of merit for a DCS. Computer simulations are often used to estimate the BEP in cases where the detection and/or decoding algorithms are too complex to admit useful mathematical expressions. If we consider that the transient interference channel also needs to be modeled, the bare mathematical approach becomes unmanageable due to the random characteristics in terms of amplitude, duration, frequency rate, and interval of the impulsive noise. The usual approach to overcome the none-model scenarios is to generate a sample of *N* bits to simulate the processing required to transmit and detect these bits. Then, the number of erroneous bit decisions in the output can be counted and the BER is commonly estimated using the following equation:

$$\mathrm{BER} = \frac{\text{Number of errors}}{N} \tag{4}$$

where *N* is the total number of bits transmitted.

As it has been explained, for a digital radio receiver, the BEP is used to evaluate the impact on the receiver performance when the disturbing noise is present in the channel. The BEP caused by a certain electromagnetic disturbance can be estimated and must be compared to the satisfactory requirements. These BEP requirements are strongly related with the service offered by the DCS and the quality of service defined in the standards. Examples of BEP typical requirements are 10^{-3} for speech communication and 10^{-6} for data transfer. Consequently, when the requirements are not fulfilled, a failure of the communication system is considered.

B. APD Calculation and DCS Evaluation

The second methodology, to determine if the radiated transient interferences generated by the sparks cause malfunction to the communication system, uses the APD diagram. The APD is defined as the amount of time that the measured envelope of an interfering signal exceeds a certain level [8]. Moreover, as it has been mentioned earlier, it is possible to establish limits in the APD diagram to analyze if certain interference will produce degradation on the DCS. Therefore, using the APD data obtained from the measurement and calculating the limits referred

to the technical specification, we will be able to estimate the degradation produced by impulsive noise sources.

The APD gives information about the envelope statistics from the IF filter output, which corresponds to the required information for performance evaluation in the radio receiver. Therefore, it is necessary to carry out an envelope detection using the interference filtered by the RBW in the IF frequency band if the RBW is equal to the DCS channel bandwidth. In this situation, the envelope detection is reached by means of the Hilbert Transform, which is used extensively for analysis and signal processing in passband communication systems. Otherwise, the envelope of the radiated transient interference can be obtained from the IQ components obtained in the postprocessing stage as

$$r[n] = \sqrt{i[n]^2 + q[n]^2}. \tag{5}$$

and the relation between $\mathrm{APD}_R(r)$ and the probability density function (pdf) of the envelope *R* is

$$\mathrm{APD}_R(r) = 1 - F_R(r) \tag{6}$$

and

$$f_R(r) = \frac{d}{dr} F_R(r) = -\frac{d}{dr}\mathrm{APD}_R(r) \tag{7}$$

where $F_R(r)$ is the cumulative distribution function (cdf) and $f_R(r)$ is the pdf. The cdf describes the probability that a value of the envelope variable *R* with a given pdf will be found to have a value less than or equal to *r*.

Finally, the APD is directly obtained from the cdf using the expressions shown above. The APD is plotted with the percentage of time, the ordinate is exceeded on the *y*-axis and the envelope values on the *x*-axis. These values are in accordance with the APD measurement function proposed by CISPR to make use of the correlation between the BEP and the APD. In the APD results presented in this paper, plot units of the envelope (*x*-axis) have been set to power units referenced to 1 milliwatt (dBm). However, they can be converted to voltage values or electric field applying the corresponding antenna factor.

Regarding the limits that must be introduced to the APD diagram, in general terms, those limits dots are related to the probability required by the system specifications and also to the amplitude of the received signal. Consequently, we will be able to compute and plot the APD limit points in the APD diagram following the equation described below when the shape of the APD diagram has a horizontal plateau [11]:

$$(u_{\mathrm{limit}}, P_{\mathrm{limit}}) \equiv \left(\frac{\beta A}{\sqrt{m}}, P_{\mathrm{req}}\right) \tag{8}$$

where *A* is the rms amplitude of the communication signal, P_{req} is the probability required by the communication system, *m* is the number of bits transmitted by one symbol, and β is defined as

$$\beta \equiv \frac{d_{\mathrm{min}}}{2}\frac{1}{\sqrt{E_b}} \tag{9}$$

where d_{min} is the minimum distance of the constellation diagram and E_b denotes the bit energy.

TABLE I
GSM-R SYSTEM SPECIFICATIONS

Parameter	Value
Downlink frequency band	921–925 MHz
Channel separation	200 kHz
Received power (P)	-100 dBm $\leq$ P ≤ -40 dBm
Bit rate	Up to 14.4 kbits/s
Modulation	GMSK (BT 0.3)

III. TEST SCENARIO

A. GSM System Interfered by Radiated Transients Produced by Sparks

In this paper, the GSM system will be interfered by radiated transients generated by sparks. The purpose of choosing this communication system is to reproduce a common interference scenario in the laboratory. The goal is to emulate when the GSM-R system is interfered by the arching effect caused by the discontinuity between the pantograph and the catenary [13]. The GSM-R antenna located at the roof of the rolling stock receives the signal coming far away from the base transceiver station (BTS) and also the close radiated transient interference. In the GSM-R system, the received power of the downlink channel is between -40 and -100 dBm, therefore, the electrical discharge produced by the air breakdown generates a transient interference strong enough to disturb the GSM-R downlink, which is located between 921 and 925 MHz. When the downlink is interfered, the communication link can be lost and the rolling stock goes toward a safe mode reducing the speed or stopping the train. In Table I, a summary of the GSM-R specifications is shown.

B. Laboratory GSM Interference Scenario

The interfering scenario that has been built in the test laboratory to interfere and measure the disturbance produced to the GSM system with the different methodologies is described as follows. For the sake of the experimental assessment, the aforementioned transient interference phenomenon was reproduced by following setup: first, the test has been performed in an anechoic chamber avoiding uncontrolled interferences. Inside the anechoic chamber, the Schlöder electrostatic discharge (ESD) simulator model SESD 200 in conformity with EN 61000-4-2 was used to generate the sparks to interfere the GSM system. The ESD gun emulates the sparks that are produced by the discontinuity between the pantograph and the catenary in the railway. In [14], the main parameters of the interference produced by the sparks of a real catenary were identified, establishing that the mean rise time is 0.4 ns and the duration is 5 ns, which are similar to the interference defined in IEC 61000-4-2. The sparks generated by the ESD gun in the laboratory produce an electromagnetic field that reaches a mobile station (MS) and also a GSM antenna, both are placed close to the spark generator at 50 cm.

Concerning the developed methodologies used to evaluate the performance of the GSM system when it is interfered by the sparks, the measurement system includes a GSM antenna, an

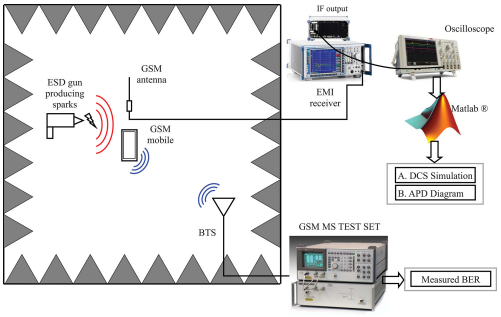

Fig. 1. Measurement setup of the GSM interfered system.

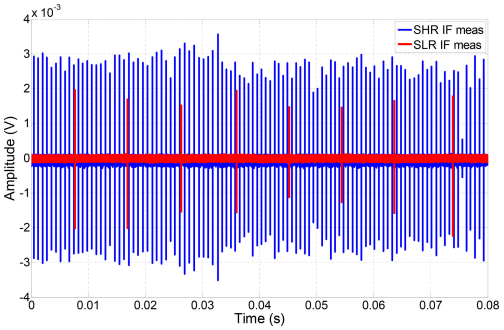

Fig. 2. Time-domain measurement of the IF signal when the SLR and SHR interferences are produced.

EMI receiver, and an oscilloscope. The GSM antenna is directly connected to the EMI receiver and the IF output is directly connected to the oscilloscope input. The IF data are captured in the time domain to afterward, by means of postprocessing employing MATLAB, to obtain the IQ components of the sparks interference in the frequency band of the GSM downlink channel. The GSM system is simulated employing Simulink, and the previous IQ measurement is added to the DCS simulation. The output of the simulation will allow us to estimate the BER of the communication system in the presence of the intentionally generated sparks produced by the ESD gun.

Alternatively, to obtain the results of the APD methodology, a different postprocessing is employed to reach the APD diagram employing the same time-domain measurements used earlier. In the next sections, a more detailed description is provided for each methodology. In Fig. 1, a schematic of the measurement and evaluation techniques described in this section is shown.

Regarding the sparks generated to interfere the GSM system, they were generated placing a metallic slice close to the air-discharge test electrode. The repetition frequency of the discharge pulses depends on the distance between the discharge electrodes and the metal where the discharge is produced. With the aim to study several cases of interference, the distance was varied to produce different repetition rate of the sparks. The first distance selected is the minimum distance required to trigger the spark. This distance will allow evaluating the case with the highest repetition rate. Moreover, a larger distance equal to 1 mm has also been selected to view the incidence of lower repetition rate interference over the degradation of the DCS. Regarding the amplitude set in the ESD gun, it has been set to $+12$ kV, however, as the dielectric breakdown voltage is lower due to the proximity between the electrode and the metal, this tension is not reached.

IV. Measurement of the Interferences

A detailed description of the instrumentation and the parameters configured to obtain the IQ components of the impulsive noise is explained in this section. Moreover, the time-domain results obtained for each of the radiated transient produced by the sparks are also shown.

As it has been mentioned earlier, two different radiated transient interferences have been generated to try to produce disturbances to the GSM downlink. The downlink is the problematic link in the GSM-R system because the signal level received from the BTS is extremely weak. When the electrode of the ESD generator is at minimum distance to the metal, sparks with higher repetition rate are produced; we have named this interference as sparks high rate (SHR) interference. Otherwise, when the metal is placed at a distance of 1 mm, sparks with lower repetition rate are generated, and the radiated transient has been named as sparks low rate (SLR) interference

For the time-domain acquisition, the GSM antenna is connected to the R&S ESPI3 EMI receiver. The EMI receiver is centered in the frequency band of the downlink GSM channel 20, which corresponds to 939 MHz. Regarding the RBW employed in the EMI receiver, it was set to 3 MHz for the SHR, while it was set to 10 MHz for the SLR. The RBW setting shall be adjusted in order to provide sufficient amplitude level to the IF signal for improving the transient pulse identification and the overall sensitivity. The reference level of the EMI receiver is also configured to maximize the dynamic range without saturating the instrument. The IF output signal is used as the input of the Tektronix DPO 7104 oscilloscope, which is sampling at 125 MSamples/s as the IF output of the EMI receiver is 20.4 MHz. The total record length set to carry out the measurements is 10^7 samples as it has been sufficient to measure all the main parameters of the transient interference. These 10 millions of samples correspond to a total acquisition time of 80 ms.

Fig. 2 shows the IF signal captured by the oscilloscope when the SHR and SLR interferences are produced. The total time observed is equal to 80 ms, where 104 pulses appear due to the high rate of the sparks produced by the breakdown of the air dielectric when the SHR interference is applied. Otherwise, when the SLR interference is measured, only eight pulses are acquired.

Once the IF measurement has been carried out, then, data are postprocessed to obtain the IQ components of each type of interference. Furthermore, in this stage, the interference

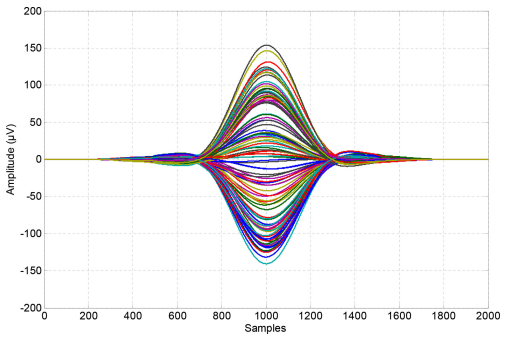

Fig. 3. In-phase component of the transient interference when the SHR interference is produced.

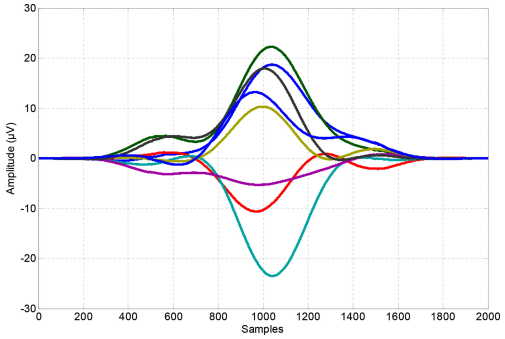

Fig. 4. In-phase component of the transient interference when the SLR interference is produced.

is bandpass filtered by the GSM frequency bandwidth in order to know the exact interference that would be received by the MS.

In Fig. 3, the in-phase component of the 104 transient pulses detected is represented after it has been filtered through 200-kHz bandwidth, and in Fig. 4, the in-phase component of the SLR interference is represented overlapping the transient pulses that occurs in 80 ms. The maximum value measured for the SHR interference is around 150 μV.

Regarding the SLR measurements, in comparison with the IQ components of the SHR interference, the amplitude has been reduced to 30 μV and the number of pulses generated by the sparks has been reduced to only eight pulses in 80 ms. Consequently, the repetition rate of the interference has been varied from a mean frequency of 1.3 kHz, when the SHR interference is generated to 100 Hz when the SLR interference is applied.

V. Evaluation of the Degradation Produced Over the GSM System

In this section, the results of both new procedures to determine the distortion produced by the two radiated transient interferences over the GSM system are compared with the mobile reference measurement.

TABLE II
GSM Technical Specification to Quantify the Signal Quality

Quality Band	Range of actual BER	Assumed value
RXQUAL_0	Less than 0.2%	0.14%
RXQUAL_1	0.2% to 0.4%	0.28%
RXQUAL_2	0.4% to 0.8%	0.57%
RXQUAL_3	0.8% to 1.6%	1.13%
RXQUAL_4	1.6% to 3.2%	2.26%
RXQUAL_5	3.2% to 6.4%	4.53%
RXQUAL_6	6.4% to 12.8%	9.05%
RXQUAL_7	Greater than 12.8%	18.1%

A. GSM Reference Equipment Measurement

First, a direct evaluation procedure is used as the reference to determine if the developed methodologies results are in accordance. As it has been mentioned earlier, the measurement carried out involves the following equipments: (a MS) and a BTS simulated by the Hewlett–Packard GSM MS Test unit model HP8922 M. The aim of the measurement is to evaluate the downlink of the GSM system which can be interfered by the sparks produced close to the MS.

The GSM technical specification ETSI GSM 05.08 establishes that the MS shall report the received signal quality. In this technical specification, it is specified how the received signal quality shall be measured by the MS in a manner that can be related to an equivalent average BER before channel decoding. The parameter that it is used to record the quality of the received signal is RXQUAL. The GSM technical specification defines eight levels of RXQUAL that must be mapped to the equivalent BER as detailed in Table II.

It is important to remark that the BER probabilities values used to define a quality band are the estimated error probabilities before channel decoding. After channel decoding, the RXQUAL probability values are also specified but are different from the values described in Table I. In our application, the RXQUAL value before the decoding is provided by the MS and it is shown at the screen of GSM MS Test unit. In addition to the RXQUAL reported by the MS, BER measurement can be also carried out using the GSM MS Test unit providing more accurate measurements than the RXQUAL.

Once the quality parameters to quantify the degradation of the GSM communication system have been defined, the procedure to measure the influence of the radiated transient is explained as follows. In order to carry out the measurements, the link between the MS and the GSM MS Test unit is created. The GSM communication channel designated has been chosen arbitrarily without any specific precondition; the channel selected is number 20 which corresponds to an uplink frequency of 894 MHz and the downlink frequency at 939 MHz. Regarding the output an input level set, the GSM MS Test unit has been configured providing the mobile a signal corresponding to an RXLevel equal to 25, which means that the signal level is between −86 and

−85 dBm. If a lower level of the receiver signal is selected, it will imply that it will be easier to disturb the communication; on the other hand, if the received signal level is higher, it will be more difficult to interfere the communication system. Therefore, the level of signal received has been selected in terms of a reliable situation, considering that usually the GSM-R communication system receives levels that vary from −40 to −100 dBm.

Regarding the measurement provided by the equipment, the MS reports the RXQUAL level and the GSM MS Test unit performs a BER measurement of 10 140 bits for each of the transient radiated interferences. When SHR interference is applied in the proximity of the MS, the RXQUAL reported by the MS is RXQUAL_4, meaning that the BER reported by the mobile is between 1.6% and 3.2%. Additionally, the measurement carried out by the GSM MS Test unit reports a BER of 2.07% when 10 140 bits are considered. When the interference with lower frequency is applied (SLR interference), the MS reports RXQUAL_0, which means that the BER is lower than 0.2%. In addition, when the BER measurement is performed by the GSM MS Test unit, the BER measured is 0.01% when 10 140 bits are considered.

From the results stated by the MS and the GSM MS Test unit, we observe that the influence of the radiated interferences generated by the sparks is worst when the interference with the highest spark rate is applied. When the interference with a mean rate of 100 Hz (SLR interference) is applied close to the MS, the degradation produced to the GSM system is negligible as the reported RXQUAL is zero. Otherwise, SHR interference produces a significant degradation to the quality of the GSM transmission, causing a BER around 2%. Consequently, the interference with a mean repetition rate of 1.3 kHz is capable to interfere meaningfully the GSM system.

B. Results Employing IQ Interference Capture and GSM Base-Band Simulation

The first developed methodology to evaluate the influence over the GSM system is based on the base-band simulation of the DCS, adding the IQ components previously measured.

Regarding the evaluation of the GSM system in the presence of the impulsive noise generated by the sparks, a simulation has been performed using Simulink. First, the baseband signal has to be modeled properly with the objective to reach accurate results. A GSM transmitter and a receiver are modeled according to the specifications defined in the GSM standards, also including the impulsive noise channel. Regarding the transmitter and receiver, they are divided into two main blocks; one block is responsible for generating the codification, while the other generates the modulation. In the coding block, the cyclic redundancy code is generated and also an interleaving of the bits is carried out. Afterward, in the modulation block, the Gaussian minimum shift keying (GMSK) modulation is produced as the GSM specification calls GMSK the physical layer modulation scheme. The main definition parameter of the GMSK modulation is the BT; where B is 3-dB bandwidth of the filter and T is the symbol duration. In the simulation, the bit rate selected is

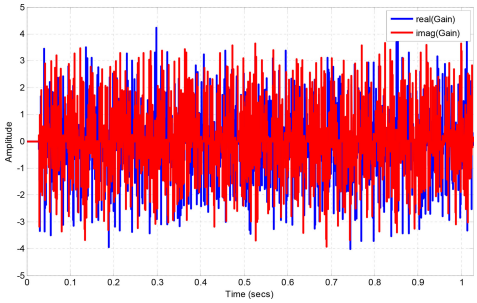

Fig. 5. IQ components of the SHR impulsive interference added to the base-band simulation after the amplitude normalization.

9.6 kbps and the BT parameter is assigned to 0.3. Concerning the bit-error measurement, the simulation permits us to obtain the BER before and after the coding is applied to the transmission. It is essential to consider that the results reported in the previous section by the GSM MS Test unit are provided before the decoding is produced; consequently, the BER computed before channel decoding will be the reference simulation data. In order to properly apply the interference in the simulated channel, the previously measured impulsive noise data must be normalized. A gain is included as the base band simulation is normalized to 1 V. Therefore, if we want to evaluate the GSM system considering the received level by the MS, the interference must be multiplied by the factor to normalize the −86 dBm signal to 1 V.

Regarding the simulated time, it has been fixed to 1 s in order to analyze a sufficient number of bits to achieve accurate results. During this period of time, the interference coming from the spark generator will be always present. Therefore, we are simulating the interference scenario where the transient interference longs at least 1 s. However, the measurements presented in Section IV were performed only for 80 ms (see Fig. 2); consequently, a concatenation of the 80-ms IQ measurements is done till the total time of 1 s is reached. This solution is the most optimized, because with the 80-ms measurement, the main characteristics of the transient interference have been measured properly. Additionally, it is not necessary to store a full second sampled at 125 MSamples/s which will have incurred in an unmanageable amount of data for the postprocessing.

Once the interference is added to the channel, the simulation can be run providing us the corresponding results when both interferences are taken into account. First, the high repetition spark interference case is simulated to analyze its influence over the GSM system. In Fig. 5, it is observed that the normalized IQ components are added to the channel when the SHR interference is applied and simulated. Regarding the BER produced by the interference, with the simulation, it is easy to estimate the errors produced as the transmitted bits are known. Consequently, when the SHR interference is present in the channel simulation, the BER obtained before decoding is 2.39%, which corresponds to a RXQUAL_4.

Concerning the distortion produced by the SLR interference, a reduction of the degradation produced to the communication

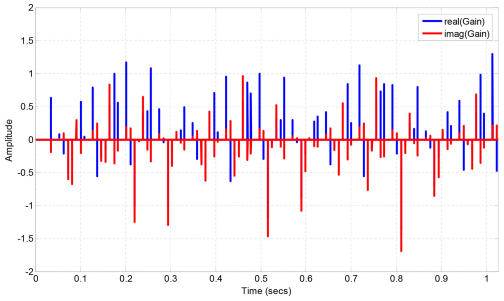

Fig. 6. IQ components of the SLR impulsive interference added to the base-band simulation after the amplitude normalization.

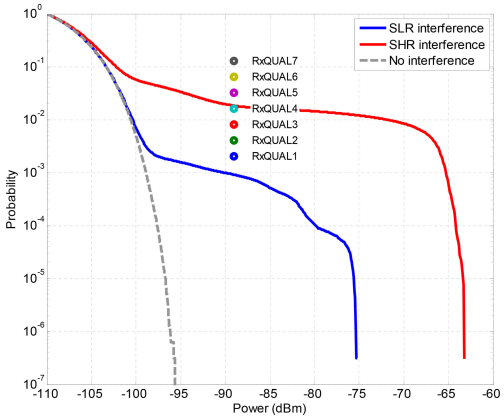

Fig. 7. APD diagram of the SHR and SLR interferences including the RXQUAL limits.

system in comparison with the SHR interference is expected. In Fig. 6, the IQ components of the SLR interferences added to the channel for the simulation are shown. If Fig. 6 is compared with Fig. 5, it is noticed that the distortion produced to the GSM system caused by the short-rate sparks interference will be reduced. Once the SLR interference simulation is carried out, the BER results before the decoding is 0.04%, which is related to a RXQUAL_0, meaning that the interference produced to the GSM system is negligible.

C. Results Employing the APD Diagram Including the GSM Specification Limits

The second developed methodology to determine the degradation produced by the SHR and SLR interference uses the APD diagram. As it has been mentioned, limit points can be established to the APD diagram to know the degradation produced to the GSM communication system.

The IQ components, measured in Section IV for both interferences, are employed as the input to compute the APD diagram. The statistical properties of the radiated transient interferences are obtained in the downlink 939-MHz channel of the GSM system and using the 200-kHz bandwidth. The results displayed for the rapid (SHR) and slow (SLR) interferences are shown in Fig. 7, as well as the computed case, when nonimpulsive interference is considered. Moreover, the limit points associated with each of the RXQUAL levels defined in the GSM specifications are also represented to rapidly identify the RXQUAL resulting level. The RXQUAL limit points which can be observed in Fig. 7 have been calculated according to (8). The level received by the mobile is -86 dBm, and the corresponding modulation scheme for the GSM system is a QPSK, which means that the bits transmitted per symbol is 2 ($m = 2$) and $\beta = 1$. Substituting the values in (8), the APD limits for each level of RXQUAL can be seen in Fig. 7. The resulting RXQUAL level will be determined considering the point below the line of the APD diagram. Additionally, if the APD diagram line is below all the limit points represented in the APD diagram, the RXQUAL value will be RXQUAL_0 which means a BER lower than 0.2%.

From the results shown in Fig. 7, the APD curve for each of the transient interferences represents the exceeding probability of the interference envelope amplitude. Therefore, it is easy to interpret the different slopes produced by each of the impulsive interferences. The SHR interference has higher amplitude and also higher probability than SLR interference, which means that in impulsive interferences such as the radiated transients, the repetition rate of the interference is also higher. Moreover, the limit points permit us to delimit that the SHR interference will produce a signal quality of RXQUAL_4 when the disturbance is present in the environment. On the other hand, from the APD diagram, it can also be concluded that the SLR interference will not cause any noticeable degradation to the GSM system, as the APD resulting curve is below all the RXQUAL levels. From the direct observation of the APD diagram, it can be established that the SHR produced a BER around 1.8%. Otherwise, when the slow repetition spark interference is generated, the error rate is around 0.09%.

The APD diagram has shown that the interference statistical information provided by the methodology is a useful and accurate tool to analyze the DCS performance rapidly and properly in the presence of radiated transient interferences. Considering the results shown in this section, the APD shows its powerful capabilities to be the best methodology to measure and analyze radiated transient interferences. Commonly, radiated transient interferences produce heavy-tailed distributions as it is observed in Fig. 7, this type of resulting distribution allows us to easily interpret the results from the APD diagram.

In addition, using the APD methodology with a single time-domain measurement, various GSM channels can be evaluated rapidly calculating the APD curve. As an example with the measurements performed in Section IV, where 3-MHz RBW was set in the EMI receiver, the APD diagram can be computed for either 15 GSM downlink channels. Otherwise, if a full-spectrum measurement is carried out employing time-domain methodologies developed [10], the APD diagram can be obtain in any channel of the GSM communication system.

TABLE III
COMPARISON OF THE MEASURED-SIMULATED DEGRADATION PRODUCED BY SHR AND SLR INTERFERENCES OVER THE GSM SYSTEM

Methodology	Interference	RXQUAL	BER
Measured signal quality by MS	SHR	4	2.07%
	SLR	0	0.01%
DCS simulation	SHR	4	2.39%
	SLR	0	0.04%
APD error estimation	SHR	4	1.8%
	SLR	0	0.09%

VI. METHODOLOGIES COMPARISON AND CONCLUSIONS

In this section, the results obtained following the different methodologies to evaluate the influence of both radiated transient interferences over the GSM downlink system are compared. The measurements reported by the GSM MS Test unit are the reference ones because an equipment transmitting information was placed under the radiated transient interferences. The measurement of the interferences and afterward performs the GSM simulation, and the APD diagram calculation are the methodologies developed to predict beforehand the degradation of the DCS. A summary chart of the results reached by the different methodologies is displayed in Table III.

Concerning the results obtained, first, it is essential to highlight the excellent agreement reached between all the different methodologies. When the impact of the SHR interferences is evaluated with the DCS simulation methodology and the APD error estimation, the RXQUAL_4 value anticipated is the same that is reported by the GSM MS Test unit. Additionally, if the BER differences are considered, the variation is around 0.3% compared with the reference value, which is a minimum difference if it is assumed that RXQUAL_4 level varies from 1.6% to 3.2%. Furthermore, if the results of the SLR interference are compared, each methodology concludes that a negligible interference effect is produced between the radiated transients and the downlink of the GSM system. All the methodologies associate the SLR interference to a received signal quality equal to RXQUAL_0, which incomes to an irrelevant interference scenario. Regarding the BER results related to the sparks generated around a repetition frequency of 100 Hz (SLR interference), all the results are below 0.1%.

The results show that the developed methodologies have provided estimations of the BER with excellent accuracy when results are compared with the reference obtained from direct BER measurements by the GSM MS Test unit. Even if the results presented here cover a particular scenario, extensive measurement campaigns have shown that this methodology is sufficiently general and coherent to be reliably used to estimate the degradation of any DCS produced by a previously measured radiated transient interference. Beforehand, the IQ capture and DCS simulation procedure must be suitable to evaluate any communication system interfered by the transient noise if the system is properly modeled. Otherwise, the APD methodology can be employed when the DCS under evaluation are digital coherent radio receivers. Finally, it is necessary to emphasize the APD diagram practical usability, which has been especially valuable due to its straightforward quantification and interpretation of the degradation produced in the GSM system due to transient interferences.

REFERENCES

[1] D. Middleton, "Statistical-physical models of electromagnetic interference," *IEEE Trans. Electromagn. Compat.*, vol. EMC-19, no. 3, pp. 106–127, Aug. 1977.

[2] M. Pous and F. Silva, "Prediction of the impact of transient disturbances in real-time digital wireless communication systems," *IEEE Electromagn. Compat. Mag.*, vol. 3, no. 3, pp. 76–83, 3rd Quarter 2014.

[3] S. Dudoyer, V. Deniau, R.R. Adriano, M. N. B. Slimen, J. Rioult, B. Meyniel, and M. Berbineau, "Study of the susceptibility of the GSM-R communications face to the electromagnetic interferences of the rail environment," *IEEE Trans. Electromagn. Compat.*, vol. 54, no. 3, pp. 667–676, Jun. 2012.

[4] V. Deniau, H. Fridhi, M. Heddebaut, J. Rioult, I. Adin, and J. Rodriguez, "Analysis and modelling of the EM interferences produced above a train associated to the contact between the catenary and the pantograph," in *Proc. Int. Symp. Electromagn. Compat.*, Sep. 2–6, 2013, pp. 721–726.

[5] A. Knobloch and H. Garbe, "Critical review of converting spectral data into prospective bit error rates," in *Proc. IEEE Int. Symp. Electromagn. Compat.*, 1Aug. 19–23, 2002, vol. 1, pp. 173–178.

[6] V. Deniau, S. Dudoyer, M. Heddebaut, A. Mariscotti, A. Marrese, N. Pasquino, "Test bench for the evaluation of GSM-R operation in the presence of electric arc interference," in *Proc. Elect. Syst. Aircraft, Railway Ship Propulsion*, Oct. 16–18, 2012, pp. 1–6.

[7] P. F. Stenumgaard, "On radiated emission limits for pulsed interference to protect modern digital wireless communication systems," *IEEE Trans. Electromagn. Compat.*, vol. 49, no. 4, pp. 931–936, Nov. 2007.

[8] K. Wiklundh, "Relation between the amplitude probability distribution of an interfering signal and its impact on digital radio receivers," *IEEE Trans. Electromagn. Compat.*, vol. 48, no. 3, pp. 537–544, Aug. 2006.

[9] Y. Matsumoto, "On the relation between the amplitude probability distribution of noise and bit error probability," *IEEE Trans. Electromagn. Compat.*, vol. 49, no. 4, pp. 940–941, Nov. 2007.

[10] M. Pous and F. Silva, "Full-spectrum APD measurement of transient interferences in time domain," *IEEE Trans. Electromagn. Compat.*, vol. 56, no. 6, pp. 1352–1360, Dec. 2014.

[11] Y. Matsumoto and K. Gotoh, "A method of defining emission limits including the gradient of an amplitude-probability-distribution curve," in *Proc. Int. Symp. Electromagn. Compat.*, Sep. 1–4, 2014, pp. 895–900.

[12] C. Jeruchim, "Techniques for estimating the bit error rate in the simulation of digital communication systems," *IEEE J. Sel. Areas Commun.*, vol. SAC-2, no. 1, pp. 153–170, Jan. 1984.

[13] FP7 European Project TREND: Test of rolling stock electromagnetic compatibility for cross-domain interoperability. (2014). [Online]. Available: www.trend-eu.org

[14] N. B. Slimen, V. Deniau, J. Rioult, S. Dudoyer, and S. Baranowski, "Statistical characterisation of the EM interferences acting on GSM-R antennas fixed above moving train," *Eur. Phys. J. Appl. Phys.*, vol. 48, p. 21202-1–21202-7, 2009.

Marc Pous was born in Barcelona, Spain, in 1983. He received the M.Sc. degree in telecommunications engineering and the Ph.D. degree from the Universitat Politècnica de Catalunya (UPC), Barcelona, Spain, in 2009 and 2015, respectively.

From 2003 to 2006, he was with the Electromagnetic Compatibility Department, LGAI Technological Centre. In 2006, he joined the Electromagnetic Compatibility Group, UPC, where he has been participating in international and national research projects related with automotive, aerospace, railway, and medical industries. His research is focused on the development of time-domain measurement techniques to capture interferences which are not properly measured following the harmonized electromagnetic compatibility standards. He studied radiated transient interferences and digital communication systems evaluation for the Ph.D. degree.

Marco A. Azpúrua (M'13) received the B.Sc. degree in telecommunications engineering and the M.Sc. degree in electrical engineering from the Universidad Central de Venezuela, Caracas, Venezuela, in 2008 and 2013, respectively. He is currently working toward the Ph.D. degree in the Electromagnetic Compatibility Group, Universitat Politècnica de Catalunya, Barcelona, Spain.

He was a Researcher in the Applied Electromagnetics Laboratory, Instituto de Ingeniería, Caracas. He is a member of the Venezuelan Standardization Committee for the Telecommunication Sector of CODELECTRA and FODENORCA and has participated in the adoption of the local standards of electromagnetic compatibility. His research interests include electromagnetic compatibility, antenna and microwave measurement technologies, and estimation of measurement uncertainty in complex systems and validation methods.

Ferran Silva (S'93–M'98) received the M.Sc. and Ph.D. degrees from the Universitat Politècnica de Catalunya (UPC), Barcelona, Spain, in 1989 and 1997, respectively.

He is currently an Associate Professor of electronics with the Department of Electronic Engineering, UPC. Since 2000, he has the Director of the Electromagnetic Compatibility Group, UPC, performing technology transfer activities to the industrial sector. His research interests include electromagnetic compatibility (EMC) in near field and time domain, including transients, with application to automotive, medical systems, and installations. He has contributed more than 90 papers to journals and conferences and contributed to the Wiley Encyclopedia of Biomedical Engineering. He has participated in 14 research projects related to EMC.

Dr. Silva is a member of the IEEE EMC Society and the Head of the Spanish chapter of this society; he is also member of the Spanish standardization committees SCTC77-210 and the CTN208 SCCISPR210A. He served as Chairman of the EMC Europe 2006 International Symposium. He belongs to the Board of Chairmen of EMC Europe.

ON-BOARD COMPACT SYSTEM FOR FULL TIME-DOMAIN ELECTROMAGNETIC INTERFERENCE MEASUREMENTS

M. A. Azpúrua [(1)], M. Pous [(1)], and F. Silva [(1)]

[(1)] *Grup de Compatibilitat Electromagnètica. Universitat Politècnica de Catalunya, Spain*

ABSTRACT

This paper presents a compact system for the measurement of electromagnetic interferences in the time domain. The measurement system is based on a USB oscilloscope, used as digitizer, and specific software for signal processing and spectral estimation. The measurement system is suitable for both conducted and radiated electromagnetic emissions up to 200 MHz. Its accuracy, precision and dynamic range are sufficient for the intended application. It is particularly suitable for measuring transient disturbances due to its triggering capabilities. Its relative low weight and cost makes it a valuable tool for investigating on-board the indirect effects of lightning strikes as disturbances coupled to cables and antennas inside launch vehicles, aircrafts, and unmanned aerial vehicles.

1. INTRODUCTION

Nowadays, the control systems of the aircrafts rely on electronics. Therefore, the electromagnetic compatibility has become essential for assuring the safety and reliability of manned and unmanned aerial vehicles. In that sense, previous research has identified three main types of electromagnetic disturbance that affect aircrafts: a) the man-made High-Intensity Radiated Fields (10 kHz - 40 GHz) [1], b) the non-nuclear electromagnetic pulse weapons (0-100 MHz) and c) the indirect effects of lightning strikes (0-50 MHz) [2].

In particular, some of the distinctive characteristics of lightings as sources of EMI are: a) the interaction of lightning with airborne vehicles is mainly caused by the aircraft or the launch vehicle itself, making it even more difficult to anticipate, b) given the impulsive and transient behaviour of lightning it has a broadband EMI signature that cannot be measured using the standard frequency sweep/stepped scan approach c), Lightning damage to airborne electronics is generally minimal, but it could be catastrophic for the launcher and payload electronic [3].

In order to improve the immunity of aircrafts to the aforementioned indirect effects of lightning strikes it is necessary to measure the interference coupled to cables and antennas placed inside the fuselage under real conditions. Hence, a compact and light weight measurement system for electromagnetic interference (EMI) capable of measuring properly transient disturbances is required.

Recently, specific implementations of Time-Domain EMI (TDEMI) measurement systems for conducted and radiated emissions measurements, with the emphasis in the evaluation of the impact of transient disturbances have been presented [4]. Those oscilloscope based TDEMI measurement systems do not require an intermediate frequency stage, therefore they will be further referred as Full-TDEMI measurement systems.

Currently, the improved capabilities of Full-TDEMI measurement systems and the advantages derived from measuring in the time-domain [5] make it feasible to implement a compact setup for on-board assessment of EMI with remarkable capabilities for performing: Mixed (Time/Frequency) domain analysis, signal decomposition [6], statistical evaluation of the EMI [7] and its impact on the degradation of communication systems [8], [9].

In that sense, this paper is intended to present an on-board compact system for electromagnetic interference measurements and experimental results that support suggested applications.

2. MEASUREMENT REQUIREMENTS

A specific EMI measurement system suitable for on-board measurements of the indirect effects of lightning strikes shall be able to:

- Measure simultaneously and synchronously electric and magnetic fields and induced currents and voltages.
- Provide a full spectrum measurement result, and not just monitoring selected frequencies.
- Comply with the usually restrictive volume and mass budget, therefore it shall be as compact and light weighted as possible.
- Be used to anticipate the degradation caused by the EMI in the on-board communication systems.

In this regard, time-domain measurement techniques seem to be the more straightforward alternative to satisfy the abovementioned requirements because:

- It takes advantage of the multichannel feature of oscilloscopes.
- It can be used to estimate the EMI spectrum in the whole measurement bandwidth using the Short-Time Fourier Transform and derived methods.
- USB oscilloscopes are relatively small, consume little power and are light-weighted.

Proc. '2016 ESA Workshop on Aerospace EMC',
Valencia, Spain, 23–25 May 2016 (ESA SP-738, May 2016)

- The measured EMI in the time-domain contains all the information required to predict accurately the degradation suffered by digital communication systems by means of the Amplitude Probability Distribution (APD) detector.

3. THE MEASUREMENT SYSTEM

The on-board compact system for Full-TDEMI measurements is based on a USB oscilloscope with the following main specifications: 4 channels, 200 MHz of analog bandwidth, 1 GS/s as the maximum sampling rate, a flexible resolution of 8 to 16 bits and a buffer memory of 512 MS. With regards to other relevant specifications, the size it is contained in the 190 x 170 x 40 mm volume, it consumes 1.5 A at 5 V of d.c. power and it weights approximately 0.5 kg.

This measurement system is able to measure simultaneously the indirect effect of a lightning strike in terms of the voltages, currents and/or electromagnetic fields depending on the type of probe/antenna used for monitoring. Its triggering capabilities allow to synchronize the acquisitions with the instant of occurrence of a certain event defined by the leading or the trailing edge of a pulsed EMI. Then the time-domain data is transferred to a computer that runs a specific software intended to perform the signal processing (windowing, filtering, equalization, decimation, spectral estimation, correction, and escalation) required to present the results in the frequency-domain according to the standards for emissions measurement.

4. EXPERIMENTAL SETUP

This experiment is intended to verify the suitability of the compact Full-TDEMI measurement system for the on-board assessment of the indirect effects of lightning strikes in aircrafts.

This experiment consisted in using the compact Full-TDEMI measurement system for measuring the voltage induced in a monopole antenna and in an unshielded cable placed over the same ground plane. The ground plane represents the fuselage of the aircraft.

The source of the disturbance was an arbitrary waveform generator Agilent 81160A. The coupled disturbance voltage was measured simultaneously in the 10 MHz – 200 MHz frequency range using two oscilloscope channels. Measurements were performed inside a fully anechoic room (FAR). The disturbance field was radiated using a Schaffner CBL6143 bilog antenna in horizontal polarization placed at a 1 m distance from the antenna. Fig. 1 shows the previously described test setup.

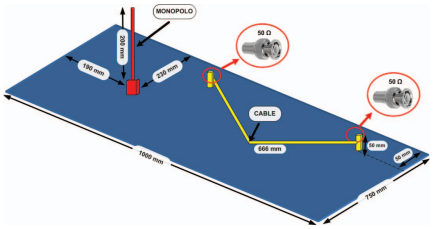

a) Diagram of the fuselage emulating setup.

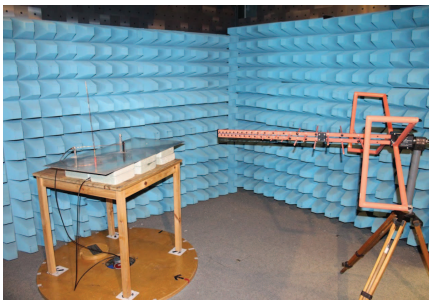

b) Test setup. Side view.

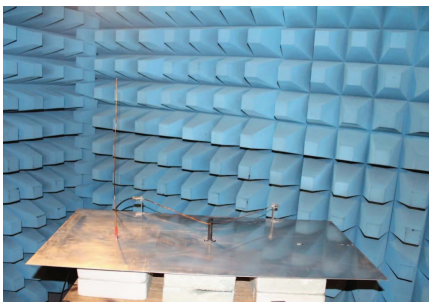

c) Test setup. Front view.

Figure 1. The experimental test setup.

Firstly, the accuracy of the compact Full-TDEMI measurement system was verified using a synthetized multi-tone test signal with 5 MHz tone spacing. This multi-tone test signal was applied into the radiating bilog antenna. Then the voltage coupled to the monopole and to the cable was measured using the compact full-TDEMI measurement system and an EMI test receiver. As shown in Fig. 2 and Fig. 3, both methods provide approximately the same results for the amplitude and the frequency of the tones. For the measurement of the amplitude of the prominent peaks, the difference between both measurement methods was ±1.28 dB in the worst case.

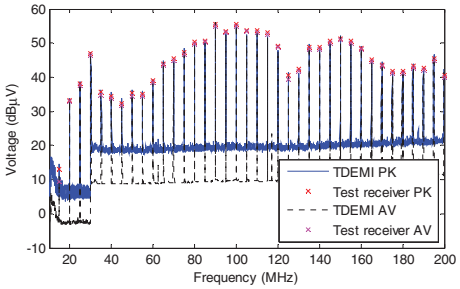

Figure 2. Voltage coupled to the antenna due to the indirect application of a radiated multi-tone test signal.

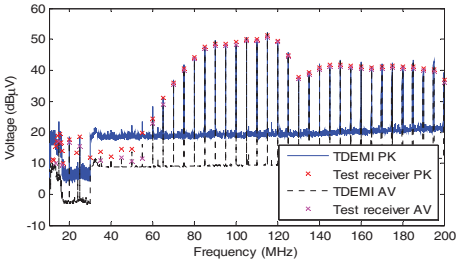

Figure 3. Voltage coupled to the cable due to the indirect application of a radiated multi-tone test signal.

In the next stage of this experiment, a surge pulse with the rise and fall times specified by the "RS105, radiated susceptibility, transient electromagnetic field MIL-STD-461E" standard was generated using the arbitrary waveform generator Agilent 81160A.Then, this surge pulse was applied to the input of the radiating antenna. The disturbance voltages induced in the monopole antenna and in the cable were measured using the compact Full-TDEMI measurement system and the results are shown in Fig. 4.

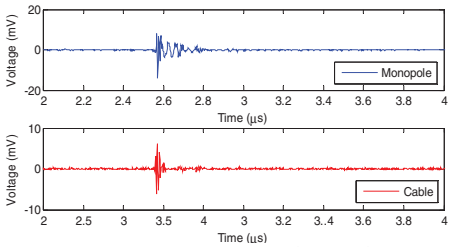

Figure 4. EMI measurement in the time-domain

This transient EMI is clearly a broadband disturbance that occupies almost the whole measured spectrum during its occurrence, as shown in Fig. 5. An EMI test receiver would have been unable to measure properly such disturbance since it is a one-time event.

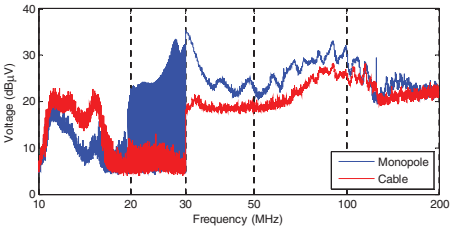

Figure 5. EMI measurement in the frequency-domain

From Figure 5 it is important to notice the change in the resolution bandwidth (RBW) used for presenting the results in the frequency domain. Below 30 MHz, a 9 kHz RBW was used (CISPR band B) while for the 30 MHZ – 200 MHz frequency band a 120 kHz RBW was used (CISPR band C). Since the direct measurement results are in the time-domain, practically any required RBW can be selected for the EMI spectral estimation by configuring the appropriate windowing parameters in the Short Time Fourier Transform.

5. DISCUSSION

This experiment was an approximation of a real scenario intended to exercise the implemented compact TDEMI measurement system to quantify disturbances induced as indirect effects of a lightning strike.

In that sense, the test method RS-105 from MIL-STD-461E was used to perform the described experiment as a proof of concept for the feasibility and convenience of using a Full-TDEMI for the on-board evaluation of lightning induced transient. However, other test methods and their waveforms, such as those described in the section 22 of the standard RTCA-DO-160G "Environmental Conditions and Test Procedures for Airborne Equipment" are also compatible with Full-TDEMI measurement systems.

6. CONCLUSION

The current USB oscilloscope technology complemented by specific measurement processing software allowed to implement a reliable and feasible Full Time Domain Electromagnetic Interference measurement system capable of being used for monitoring the electromagnetic fields on-board aerospace vehicles. The accuracy, the precision and the dynamic range of the on-board Full-TDEMI measurement system are sufficient for the required applications and have been verified for the measurement of both continuous wave and pulsed emissions. This compact TDEMI measurement technology is especially suitable for monitoring the indirect effects of a lightning strike on launch vehicles, aircrafts, and UAV because its acquisitions can be triggered by the transient disturbances coupled into cables and antennas inside the fuselage.

ACKNOWLEDGMENT

This work was supported by the Spanish "Ministerio de Economía y Competitividad," under project TEC2013-48414-C3-3-R.

REFERENCES

[1] G. A. Rasek, E. Pascual-Gil, A. Schroder, I. Junqua, R. Guidi, C. A. Kreller, H.-D. Bruns, and S. E. Loos, "HIRF Transfer Functions of a Fuselage Model: Measurements and Simulations," *IEEE Trans. Electromagn. Compat.*, vol. 56, no. 2, pp. 311–319, 2014.

[2] M. Aprà, M. D'Amore, K. Gigliotti, M. Sabrina Sarto, and V. Volpi, "Lightning Indirect Effects Certification of a Transport Aircraft by Numerical Simulation," *IEEE Trans. Electromagn. Compat.*, vol. 50, no. 3, pp. 513–523, 2008.

[3] M. A. Uman and V. A. Rakov, "The interaction of lightning with airborne vehicles," Progress in Aerospace Sciences, vol. 39, no. 1. pp. 61–81, 2003.

[4] M. A. Azpúrua, M. Pous, and F. Silva, "A Measurement System for Radiated Transient Electromagnetic Interference Based on General Purpose Instruments," *in Electromagnetic Compatibility (EMC EUROPE), International Symposium on*, 2015.

[5] M. A. Azpúrua, M. Pous, and F. Silva, "Improving Time-Domain EMI measurements through Digital Signal Processing," *Electromagn. Compat. Mag.*, vol. 4, no. 2, pp. 66–74, 2015.

[6] M. A. Azpúrua, M. Pous, and F. Silva, "Decomposition of Electromagnetic Interferences in the Time-Domain," *IEEE Trans. Electromagn. Compat.*, (early access), 2016.

[7] M. A. Azpurua, M. Pous, and F. Silva, "On the Statistical Properties of the Peak Detection for Time-Domain EMI Measurements," *Electromagnetic Compatibility, IEEE Transactions* on, vol. 57(6), pp. 1374 - 1381, 2015.

[8] M. Pous and F. Silva, "Full-Spectrum APD Measurement of Transient Interferences in Time Domain," *Electromagnetic Compatibility, IEEE Transactions on*, vol. 56, no. 6. pp. 1352–1360, 2014.

[9] M. Pous, M. A. Azpúrua, and F. Silva, "Measurement and Evaluation Techniques to Estimate the Degradation Produced by the Radiated Transients Interference to the GSM System," *Electromagnetic Compatibility, IEEE Transactions on*, vol. 57(6), pp. 1382 - 1390, 2015.

Proc. of the 2016 International Symposium on Electromagnetic Compatibility - EMC EUROPE 2016, Wroclaw, Poland, September 5-9, 2016

Benefits of Full Time-Domain EMI Measurements for Large Fixed Installation

Marc Pous[1], Marco Azpúrua[1] and Ferran Silva[1]
[1] Grup de Compatibilitat Electromagnètica (GCEM), Departament d'Enginyeria Electrònica (DEE)
Universitat Politècnica de Catalunya (UPC)
Barcelona, Spain
email: marc.pous@upc.edu

***Abstract*— It is difficult to properly evaluate the electromagnetic disturbances generated by large fixed installations because of, i.e., the background noise, unsteady emissions and transient interferences. Those challenging EMC issues have been recently studied in European research projects on improved test methods in industrial environments. In order to overcome traditional *in-situ* EMI measurement troubles, a novel time-domain methodology is proposed and used in a real fixed installation with large machinery. Firstly, a comparison between the developed measurement system, using an oscilloscope, and an EMI receiver is done in some test-cases for validation purposes. After verifying the accuracy of the measurements, we proceed with the measurement campaign applying the full time-domain methodology. The main benefits of employing the time-domain system are emphasised through the results. It was observed that the some remarkable advantages of the time-domain approach are: triggering by disturbance events, extremely reduce the capturing time, identify on real time the worst emissions modes of the EUT, avoid changes at the background noise and perform simultaneous multichannel synchronous measurements.**

Keywords—time-domain measurements; fixed installations; in-situ meaurements; conducted, radiated, background noise

I. INTRODUCTION

Within the framework of a European research project [1] novel measurement methodologies have been developed. The goal is to perform reliable *in-situ* electromagnetic interferences (EMI) measurements. It is well known that carrying out radiated and conducted EMI measurements is challenging in large fixed installations scenarios [2-4]. In comparison with the tests conducted in an electromagnetic compatibility (EMC) test laboratory, *in-situ* measurements have a common and meaningful problematic related to the inherent uncontrolled environment conditions.

In particular, the lack of a line stabilization impedance network (LISN) in *in-situ* conducted emissions assessments causes that the noise generated by other equipment connected to the same power network is not filtered from the EMI generated by the equipment under evaluation. Hence, uncontrolled and discontinuous interferences are present at the power supply measured cable increasing uncertainty of the results.

978-1-5090-1416-3/16/$31.00 ©2016 IEEE

The procedure to distinguish the emissions produced by the equipment under test (EUT) and the ambient noise described at CISPR 16-2-5 technical report consists, basically, into capturing the interferences when the EUT is switched off (or in standby) and then turning on the EUT and repeat the measurements. It is considered that the differences on the spectrum are due to the emissions of the EUT. However this procedure is obtaining the data at different moments and the results can be affected by the variations of the background noise. Nevertheless, these fluctuations can be caused by a discontinuous interference generated by other loads connected to the same power or communication network.

Another problem is that large machinery measured in fixed installations has many different functional modes producing numerous interferences. It shall be considered that a large fixed installation can have many engines, electronics, etc. that work following a long procedure for which it has been designed for. For instance, at the real installation presented in this paper, the noisiest engines were active only during few seconds within a long functioning cycle that last several minutes. Hence, if frequency sweep based or stepped scan based EMI measuring apparatus are employed, the required overall measurement time would be extremely long to measure properly all the frequency range. In addition to the time-constrain that we have mentioned, we must also add that if we use the detectors defined at the EMC standards such as the quasi-peak or the average detectors this trouble is even worst. For example, if we perform a conducted EMI measurement with the average detector from 150 kHz to 30 MHz for it can take around 10 minutes to complete a frequency sweep which is a waste of time if we consider that the worst interference is generated only during few seconds. Hence, if we employ conventional frequency sweep instrumentation, the emissions produced by the EUT will be constantly changing and the results obtained along the spectrum will correspond to different measured situations.

Fortunately, current capabilities of hardware and previously studies demonstrate that it is feasible and reliable to perform time-domain measurements instead of frequency sweeps to obtain the spectral information of the interference [5-7]. Therefore, in this paper a measurement system based on time-domain captures is employed to overcome these main difficulties that recurrently appear when *in-situ* measurements are carried out. Moreover, other benefits that time-domain

Proc. of the 2016 International Symposium on Electromagnetic Compatibility - EMC EUROPE 2016, Wroclaw, Poland, September 5-9, 2016

measurements offer will be highlighted and explained at the following sections.

II. METHODOLOGY

In this section the key aspects of the full-time-domain EMI measurement system and the main benefits of using it are explained.

A. Overview of the Full-Time domain measurement system

The full-time-domain (Full-TDEMI) EMI measurement system employed for the *in-situ* measurements have been developed and extensively used in recent years by GCEM-UPC [8-12]. This measurement system is based on a time-domain acquisition followed by a post-processing stage which allows obtaining equivalent results than conventional EMI test receiver.

Figure 1 shows a block diagram of the measurement system, indicating that the measurement can be done either with an antenna, a current clamp, a voltage probe, etc. The time-domain data is acquired by a general purpose oscilloscope and the post-processing is carried out with a standard laptop. The amplitude spectrum of the EMI is computed using the Short-Time Fourier Transform and non-parametric spectral estimation methods. More details can be found at [8-12].

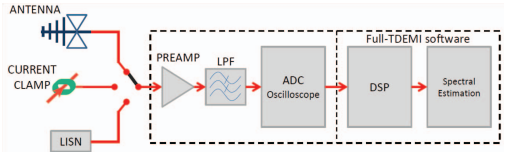

Fig. 1. Full TDEMI measurement system block diagram

Regarding the equipment and the software used to conduct the measurements at the fixed installation shown in this paper two different hardware have been used. To obtain the measurement for conducted emissions according to CISPR 16 standards, a Picoscope 5444B has been used for the acquisition stage. The conducted measurement system is limited to 200 MHz, the maximum sampling rate is 1 GSample/s and the total storage memory is 512 MSamples. Moreover, for conducted disturbances measurements, a multiline voltage probe has been constructed according to CISPR 16-2-1 specifications in order to measure the EMI at several lines of the EUT simultaneously. Fig. 2 shows an *in-situ* measurement using the multiline voltage probe which it is connected to the EUT and then to the oscilloscope.

Likewise, for radiated emission tests up to one gigahertz, an oscilloscope Tektronix model DPO5104B has been used. In this case the oscilloscope is connected to a biconical or to a log-periodic antenna depending on the frequency range.

B. Main benefits of the Full-TDEMI measuring system for in-situ measurements

- Reduction of the effective measurement time: Comparing Full-TDEMI measurements with traditional frequency sweep methodologies with regards to the effective measurement time; the time-domain based systems are able to obtain the full spectrum information in milliseconds instead of several minutes.

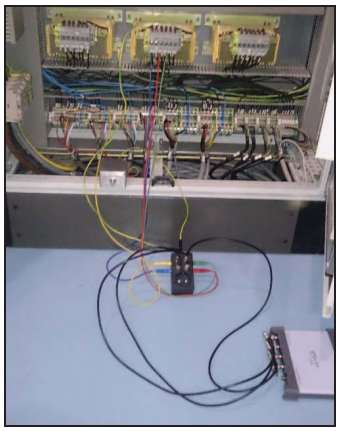

Fig. 2. In-situ example measurement for conducted emissions employing the time-domain methodology and the multi-channel in-situ voltage probe.

Therefore, capturing data at this speed reduce the possibility of changes in the EUT functional mode. As it has been mentioned at the introduction, in large installations the EUT could have many functional modes lasting only few seconds, and it is really challenging to measure the full spectrum mode in each functional mode. Additionally, reducing the capturing time to a practical instantaneous capture of some milliseconds, the uncertainty contribution due to the changes in the background noise during the observation time can be reduced. Escaping from continuous changes at the emissions produced by other equipment connected to the power supply or either intermittent transmitters. Finally, the reduction of the capturing time is an opportunity for the industry to perform more controls and measurements to the fixed installations due to the cost reduction.

- Full spectrum real-time measurements: Another advantage that time-domain methodologies offers to the end users is that it is possible to obtain both the spectral and time domain information in a real-time. This means that the user can view the entire spectrum and the time domain signal several times per second (depending on the hardware and software employed). This is an important advantage compared with the frequency sweep instrumentation as we have several benefits. Firstly, it is easy to identify the worst cases as the spectrum is refreshing constantly, moreover as we are using time-domain instrumentation, we have several trigger functionalities available. Therefore it is possible and simple to measure, for instance, transient events like the disturbances that appear when we are

Proc. of the 2016 International Symposium on Electromagnetic Compatibility - EMC EUROPE 2016, Wroclaw, Poland, September 5-9, 2016

switching ON or OFF. Moreover, it is important to mention that capturing transient phenomena employing frequency sweep instrumentation is near to impossible.

- Multichannel synchronous measurements: This feature is available because the instrumentation used for time domain acquisition has multiple input channels instead of the unique channel, as happens with EMI receivers. Therefore, for conducted emissions the multichannel Full-TDEMI allows to perform simultaneous measurements at the different lines of the power supply, which is particularly useful for *in-situ* measurements. The main benefits are the combined testing time reduction and also to avoid differences caused by influence of the background noise. These multichannel measurements can be performed with the aid of a multiline voltage probe, as shown in Fig. 2.

- Versatility of the measurement system: The Full-TDEMI system can be USB powered and it has sufficient autonomy to be used in conjunction with a standard laptop. Therefore, this is a grateful advantage for *in-situ* measurements where it is difficult to power the measuring equipment. Many times a long cable has to be placed in order to power the measurement instruments and other times the instruments are connected to the same mains from where EMI is being measured causing additional errors.

- Time-domain data available: Finally, it is important to highlight that having available the time domain data is a great advantage compared with the limited information provided by traditional EMC measurements using the EMI receiver. Previous research has demonstrated the time domain data of the EMI can be used to predict the bit-error-rate of digital communication systems [13].

III. RESULTS

Some of the results produced by measuring the real scenario of the large fixed installation are shown to illustrate the advantages of the time-domain measurement system. In the following sections you will find a description of the measured scenario, some validation results comparing the time-domain data with standard EMI receiver measurements and finally the results that highlight the main benefits of using the time-domain measurement system instead of the traditional frequency sweep instrumentation.

A. Measured scenario

A complex scenario was measured in accordance with the requirements of the customer. The large fixed installation is an automatic storage and retrieval system composed by various large machinery including engines, elevators, shuttles, etc. running a complex working cycle.

B. Validation

Several comparisons were made for conducted and radiated disturbance measurements to determine if the time-domain approach provided coherent results when compared with an EMI test receiver, which is taken as the standard reference. Following some comparison results of a conducted measurement test case are shown in Fig. 3.

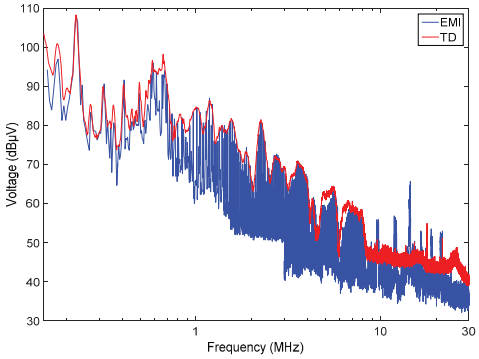

Fig. 3. Conducted EMI peak measurement comparision between time-domain methodology and a conventional EMI test receiver

From the Fig. 3, it is important to highlight that with the time-domain system a dynamic range up to 70 dB can be reached. This is important because dynamic range is one of the main concerns when oscilloscopes are employed instead of EMI receivers.

Regarding the comparison between the results obtained with the EMI receiver and the ones reached with the Full-TDEMI approach, there is and evident similarity between both results. Moreover, an objective validation method was applied to quantify the agreement of the measurement in terms of the EMI amplitude spectrum. The Feature Selective Validation (FSV) method, which is described into IEEE standard 1597.1 has been used with the limit-line consideration improvement [14] to compare the results. This limit-line criterion weights the influence of the points according to their relevance in terms of their proximity to a certain limit-line, which is an interesting capability from an EMC point of view. The limit line used for this purpose is the one defined for industrial environments (Class A limit). The results provided by the FSV method are shown below in Table I.

TABLE I. FSV VALIDATION RESULTS

Indicator	***Result***	
Amplitude Difference Measure (ADM)	0.193	Very Good agreement
Feature Difference Measure (FDM)	0.6	
Global Difference Measure (GDM)	0.66	

Hence, the conclusion of the comparison with the FSV is that the agreement is very good. This similarity is very good in terms of shape and excellent considering the amplitudes.

Also regarding the data displayed at Fig. 3, from 10 MHz till 30 MHz frequency band, differences can be appreciated between the EMI receiver and the TD system. These differences are attributable to the capturing time, which is

Proc. of the 2016 International Symposium on Electromagnetic Compatibility - EMC EUROPE 2016, Wroclaw, Poland, September 5-9, 2016

longer when the frequency sweep method is applied. The measuring time needed for the EMI receiver is around 5 minutes to obtain the peak measurement; consequently the noise produced by the other equipment connected to the power supply network is not stable. On the other hand, the instantaneous measurement of the full-TDEMI methodology allows more control in terms of the changes in the background noise.

According to the great similitude observed at the results shown and other measured cases, we decided to continue with the measurements using only the time-domain methodology due to the benefits commented at the previous sections.

C. *Time-domain results*

The fixed installation is measured using the methodology described in section II. Next, some representative results are used to illustrate the advantages.

The first set of measurements presented was obtained when conducted emissions measurements were carried out. As it has been discussed previously, the different functional modes of the large installation generate different type of interferences. In Fig. 4 and Fig. 5 the results in time domain and frequency domain shows as the huge differences that appear when the different components of the installation connected to the same power supply are working. The tools available at the software allow the user to see in real time the changes of the full spectrum making it easy to identify the cases with strongest emissions. From the comparison of the spectrum measured at two different functional modes, differences of more than 40 dB are observed in the EMI. In Fig. 4, the results are obtained when some rollers of the fixed installation start to move. Otherwise, Fig. 5 shows the results in time and frequency domain when an elevator was activated.

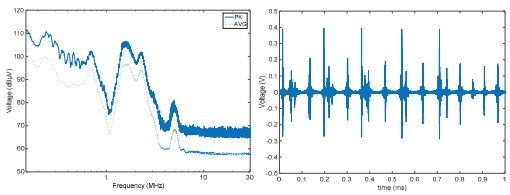

Fig. 4. Results in frequency domain with the peak and average detector and the time domain data when the rollers were measured.

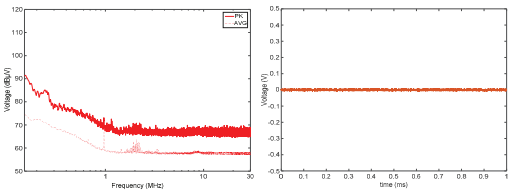

Fig. 5. Results in frequency domain with the peak and average detector and the time domain data when the elevator was measured.

It is really important to highlight that the movement of the rollers only last 5 s in the entire machinery cycle of several minutes. Therefore, if a traditional frequency sweep approach were used it would have been extremely unlikely to measure this worst case emissions. Probably, these worst case emissions have been omitted due to the short duration of the rollers cycle. Moreover, if an EMC expert has estimated beforehand that the worst test case should correspond to the elevator disturbances, a wrong assessment of the EMC would have been produced.

Then, in order to demonstrate other capabilities of the time-domain *in-situ* measurements, Fig. 6 shows the results obtained with the time-domain system in another location of the fixed installation. The results were obtained employing synchronous measurements from the three-phase EUT power supply. In Fig. 6, the results of the peak and average detector EMI measurements are presented. With an instantaneous measurement we were able to capture not only the highest emission level of the fixed installation, but also the average measurements. This is a step forward if we think in terms of ensuring that we are sure of getting the highest disturbances of the EUT and also in terms of time-reduction to have the full frequency range response of the three lines with both detectors. To illustrate this statement we have also conducted a measurement with a traditional EMI receiver.

In this case, only the peak detector was employed as it is the fastest alternative to sweep the spectrum. Compared with the time domain measurement, where the full peak and average spectrum are obtained for the three lines using only a 100 ms measurement, it was required to spend more than 20 minutes to obtain an almost equivalent results using the peak detector and measurement with the EMI receiver. Although frequency sweeps were repeated continuously over more than 20 minutes with the *maxhold* function, it was not sufficient to record the full spectrum interferences generated by the EUT. Due to the time restrictions it was not possible to perform the average measurement on this facility.

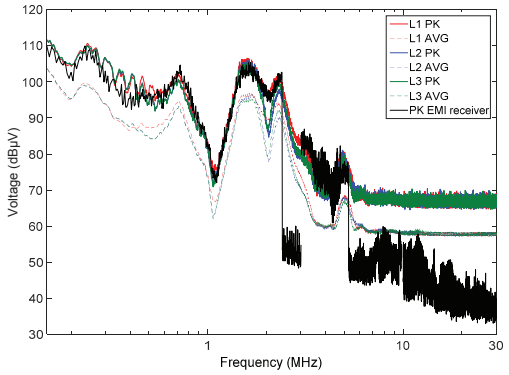

Fig. 6. Conducted peak and average EMI measurements for every line of the mains port of a three-phase EUT employing the full time-domain methodology and a peak measurement of one line using the EMI receiver.

From the results observed in Fig. 6, between 2 MHz and 3 MHz there is not significant data when the EMI receiver is used. In this frequency band, the emissions generated by the EUT are not captured as the frequency sweep is not synchronized with the occurrence of the interference in any of the multiple sweeps performed during the 20 minutes of measurement. In the rest of the EMI frequency spectrum the fitting of the TD method results and the EMI receiver are excellent in terms of amplitude and shape.

Next some results of the radiated emissions are also shown to demonstrate that measuring with the oscilloscope is also feasible for radiated emissions tests. As it has been mentioned before, ambient noise is one of the main concerns of *in-situ* measurements. From the results given by Fig. 7, the ambient noise of the FM radio broadcasting service and other transmitting signals close to 200 MHz are easily identified. However, broadband interferences are detectable around 50 MHz and they are clearly attributable to the EUT when it is switched on.

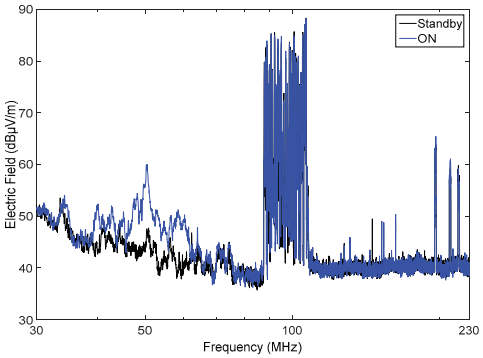

Fig. 7. Radiated peak measurements employing the full time-domain measurement system for an EUT when it was at standby and switched on.

In this case, the main advantage of using the time-domain methodology is that we are able to perform instantaneous measurements, avoiding changes at the background noise that introduce confusion to the EMC assessment. As we have the capability to analyse the full spectrum with instantaneous time domain captures we can identify the emissions produced by all the functional modes of the EUT and be immediately aware of the changes at the spectrum. Otherwise, using traditional slow frequency sweep instrumentation we can miss interferences that last few seconds and also misunderstand changes at the background noise confusing it with emissions of the EUT.

IV. Discussion and Conclusions

With the aim to improve the measurement of the disturbances at large fixed installations, the full time-domain methodology has been developed and validated with a measurement campaign. The results shown in this paper conclude that the main troubles of *in-situ* measurements can be partially solved by using a time-domain approach. Moreover, through the different comparisons done, it has been shown that it is also possible to obtain as good results in terms of accuracy as with an EMI receiver.

Regarding the main benefits observed, the time-domain methodology aids the test technician to overcome challenges such as the changes of background noise, evaluate accurately all the EUT functional modes (even the short lasting ones) and reduce significantly the effective measurement time. As has been shown along this paper, one key aspect is the multiple channel synchronous measurements capability, this allow us to carry out conducted disturbances measurements at three-phase power supply lines employing the multiline voltage probe. Furthermore, multiple channel synchronous measurements open many possibilities that are particularly interesting for *in-situ* measurements, including advance triggering capabilities and measurements post-processing for ambient noise cancellation. Finally, it is essential to highlight that with the time-domain measurements the spectrum data is available in terms of the amplitude and the phase. Therefore, it is possibly to use this data to predict if the noise generated by the EUT is degrading the performance of any digital communication system, since it has been shown that peak, quasi-peak or average measurements are not sufficient to estimate directly the degradation suffered by digital communication systems.

To conclude, in the near future time-domain EMI measurements are likely to become the standard approach for *in-situ* industrial assessments due to the benefits it offers in comparison with traditional frequency sweep instrumentation.

Acknowledgment

This work was supported in part by the EURAMET IND60 EMC research project (the EMRP is jointly funded by the EMRP participating countries within EURAMET and the European Union) and by the Spanish “Ministerio de Economía y Competitividad,” under project TEC2013- 48414-C3-3-R.

References

[1] EMPR JRP IND60 Improved EMC test methods in industrial environments. (http://www.emc-industry.com/)

[2] J. Catrysse, F. Vanhee, J. Knockaert, I. Hendrickx and V. Beauvois, "In situ testing of large machines: Alternative methods for conducted emission measurements," *Electromagnetic Compatibility, 2008. EMC 2008. IEEE International Symposium on*, Detroit, MI, 2008, pp. 1-6.

[3] A. Tacchini, "Radiated emission testing: In-situ measurements on large machines," *Electromagnetic Compatibility (APEMC), 2010 Asia-Pacific Symposium on,* Beijing, 2010, pp. 1610-1613.

[4] Z. H. Lu, J. B. Liu and P. G. Liu, "A Novel Method of Ambient Interferences Suppressing for In Situ Electromagnetic Radiated Emission Test," *in IEEE Transactions on Electromagnetic Compatibility,* vol. 54, no. 6, pp. 1205-1215, Dec. 2012.

[5] S. Braun, T. Donauer and P. Russer, "A Real-Time Time-Domain EMI Measurement System for Full-Compliance Measurements According to CISPR 16-1-1," *Electromagnetic Compatibility, IEEE Transactions on,* vol. 50, no. 2, pp. 259-267, May 2008

[6] C. Keller and K. Feser, "Fast Emission Measurement in Time Domain," *Electromagnetic Compatibility, IEEE Transactions on,* vol. 49, no. 4, pp. 816-824, 2007.

[7] F. Krug and P. Russer, "The Time-domain Electromagnetic Interference Measurement System," *Electromagnetic Compatibility, IEEE Transactions on,* vol. 45, no. 2, pp. 330-338, May 2003.

[8] M. A. Azpurua, M. Pous, S. Cakir, M. Cetinta and F. Silva, "Improving time-domain EMI measurements through digital signal processing," *in IEEE Electromagnetic Compatibility Magazine*, vol. 4, no. 2, pp. 82-91, 2nd Quarter 2015.

[9] M. A. Azpurua, M. Pous and F. Silva, "A measurement system for radiated transient electromagnetic interference based on general purpose instruments," *Electromagnetic Compatibility (EMC), 2015 IEEE International Symposium on,* Dresden, 2015, pp. 1189-1194.

[10] G. Costa, M. Pous, A. Atienza and F. Silva, "Time-Domain Electromagnetic Interference Measurement System for intermittent disturbances," *Electromagnetic Compatibility (EMC Europe), 2014 International Symposium on*, Gothenburg, 2014, pp. 833-837.

[11] M. A. Azpurua; M. Pous; F. Silva, "Decomposition of Electromagnetic Interferences in the Time-Domain," *in IEEE Transactions on Electromagnetic Compatibility* , vol.PP, no.99, pp.1-8

[12] M. A. Azpurua, M. Pous and F. Silva, "On the Statistical Properties of the Peak Detection for Time-Domain EMI Measurements," *in IEEE Transactions on Electromagnetic Compatibility*, vol. 57, no. 6, pp. 1374-1381, Dec. 2015.

[13] M. Pous, M. A. Azpurua and F. Silva, "Measurement and Evaluation Techniques to Estimate the Degradation Produced by the Radiated Transients Interference to the GSM System," *in IEEE Transactions on Electromagnetic Compatibility*, vol. 57, no. 6, pp. 1382-1390, Dec. 2015.

[14] R. Jauregui, M. Pous and F. Silva, "Use of reference limits in the Feature Selective Validation (FSV) method," *Electromagnetic Compatibility (EMC Europe), 2014 International Symposium on*, Gothenburg, 2014, pp. 1031-1036.

Full Time Domain EMI measurement system applied to Railway emissions according to IEC 62236-3-1/EN 50121-3-1 standards

Marc Pous, Marco A. Azpúrua, José A. Oliva, Marc Aragón, Iván González and Ferran Silva
Grup de Compatibilitat Electromagnètica
Universitat Politècnica de Catalunya
Barcelona, Spain
email: marc.pous@upc.edu

***Abstract*—This paper studies the advantages of applying time-domain based instrumentation to conduct electromagnetic interference emissions from rolling-stock. In IEC 62236-3-1 or EN 50121-3-1 standards, it is mandatory to measure the railway vehicle in static and in-motion conditions. When conventional frequency sweep instrumentation is employed, difficulties regarding ambient noise variation and the short-duration of worst-case emission modes take place. In Annex B of the standard, a test procedure is described to acquire the worst-case EMI, however, as it is explained at the paper the effective measured time at each frequency is only 0.08 ms in some frequency bands. Hence, multiple movements of the vehicle are needed increasing the uncertainty of the measured source and making difficult to distinguish vehicle EMI from background noise interference. To solve this problem, a Full TDEMI measurement system is proposed with the availability to increase the effective measured time, reduced the ambient noise variation, the usage of multiple antennas at the same time and the possibility to discard transient interference that should not be evaluated. At the end of the paper, measurements carried out with the time-domain system are shown demonstrating the effectivity of the methodology.**

Keywords—electromagnetic interference, measuring receiver, noise figure, time-domain measurements, railway

I. INTRODUCTION

The Electromagnetic Compatibility (EMC) assessment for Railway is carried out following the IEC 62236 / EN 50121 standard series [1], [2], which define the measurement procedure, the test site, the test conditions and the limits. The electromagnetic interference (EMI) emissions test for the complete vehicle is performed at an outdoors railway infrastructure, which implies important difficulties common with other *in-situ* measurements [3]-[4] due to the presence of non-stable background noise and varying interferences. Moreover, the rolling stock is evaluated in static conditions and in dynamic mode, circulating at low speed and accelerating and/or braking at the measurement point. This dynamic mode measurement is a challenge for the test technicians making sometimes unfeasible to acquire the worst emission mode and distinguish it from the Background Noise (BGN). Furthermore, according to the standards, transient interference produced by events like the discontinuity between the pantograph and the catenary should be ignored. This is an undesired phenomenon that usually appears when railway EMI assessment is performed [5], [6], [7].

These problems are emphasized by the use of traditional EMI receivers based on a Superheterodyne architecture. The frequency-sweep instrumentation measures the EMI spectrum-components at different observation time, doing hard to decide which measurement is caused by the rolling-stock, changes in the background noise or transient interferences. This limitation is even more critic if we consider the short-duration events like braking or acceleration that should be measured by the dynamic measurement. With the aim to overcome the problematics of the dynamic measurement, Annex B of EN 50121-3-1 explains the test procedure for in-motion measurements, defining the sweep time at different small frequency bands (Table I). Each sub-band is divided with the intention to reduce the sweep time and to be capable of catching the worst emission mode.

TABLE I. FREQUENCY SWEEP CONFIGURATION ACCORDING TO EN 50121-3-1 ANNEX B.

Band	**Test guide according to EN 50121-3-1 Annex B for dynamic measurements**			
	Subrange (Hz)	***Span (Hz)***	***RBW (kHz)***	***Sweep time (ms)***
B	150 k -1.15 M	1 M	9/10	37
	1-11 M	10 M	9/10	370
	10-20 M	10 M	9/10	370
	20-30 M	10 M	9/10	370
C/D	30-230 M	200 M	100/120	42
	200-500 M	300 M	100/120	63
	500-1000 M	500 M	100/120	100

If we study Table I, the peak measurement is obtained at a rate of 37 ms to 100 ms, depending on the frequency sub-band. Nevertheless, this is the time elapsed to complete the full

sweep with the peak detector, meaning that we are only measuring one frequency point each 100 ms. Hence, the effective measurement time can be obtained by dividing the sweep-time of the sub-band by the number of points of the frequency sweep. To provide some data, in Table II the effective time is computed considering two different situations. The first one is when we are conducting a full dynamic measurement, since the train is coming, passing through the measurement point and leaving, this measurement usually lasts 30 s. Otherwise, for highlighting the inconvenience of using traditional superheterodyne receivers, another situation has been contemplated in Table II. This is the short-duration event column, where the observation time lasts around one second. This short-duration event is a plausible scenario as the maximum emissions generated by acceleration or deceleration could appear in less than a second.

TABLE II. EFFECTIVE MEASUREMENT TIME AT EACH FREQUENCY-POINT

			Effective time measured (ms)		
Subrange (Hz)	Measured points	time at each frequency (ms)	Full dynamic measurement 30 s	Short-Event duration 1s	time measured (%)
150 k - 1.15 M	250	0.148	120	4	0.4
1-11 M	2500	0.148	12	0.4	0.04
10-20 M	2500	0.148	12	0.4	0.04
20-30 M	2500	0.148	12	0.4	0.04
30-230 M	5000	0.0084	6	0.2	0.02
200-500 M	7500	0.0084	4	0.13	0.013
500-1000 M	12500	0.008	2.4	0.08	0.0008

Considering Table II data, we are only measuring between 0.4 % and 0.008 % of the time depending on the sub-band evaluated. Elsewhere, if we consider a short-duration event of 1 s, this implies that we are only measuring 80 µs between 500 MHz and 1 GHz, which apparently seems improbable to ensure to catch the maximum emission. Therefore, usually, several movements of the vehicle are needed to acquire the worst emission mode, however, it causes a more complex assessment with more variability on the outdoors measurements. We should consider that between each time that the rolling stock circulates in front of the measurement point, several minutes could occur. Meaning that at the end several hours of measurement are elapsed and uncontrollable changes at the background noise appear, making sometimes difficult or impossible to associate the interference measured with the vehicle or with the changes at the BGN. Even more, as it has been mentioned before, we had to include the appearance of transient interference, which should be avoided from the evaluation.

Although the presence of Annex B at the standard, the problem is still present and the test technicians reported us their difficulties to identify the EMI produced by the rolling stock. Therefore, novel methodologies not based on traditional frequency-sweep instrumentation should be applied to improve the EMC evaluation. Fortunately, during the recent years, new software developments and the improvement of hardware capabilities make feasible to employ Real Time or Full TDEMI measurement systems. The time-domain systems based on Fast Fourier Transform (FFT) allows reducing the observation time increasing the effective measured time [8]-[11]. Additionally, the Full TDEMI system has been successfully employed at *in-situ* measurements providing other advantages like the multi-channel synchronous measurements or the possibility to trigger the measurements with the time-domain data.

In the next section, the Full TDEMI methodology is explained identifying the main advantages to be applied at the EN 50121-3-1 standard. Moreover, results obtained from a rolling stock evaluation using the novel methodology are presented in section III.

II. METHODOLOGY

A. Full TDEMI Measurement system overview

Full TDEMI measurement systems have been developed according to CISPR 16-1-1 and it is employed for conventional and *in-situ* emissions tests [11]-[13]. The system is based on acquiring the time-domain data of the EMI using oscilloscopes and thereafter compute the spectrum with the detectors defined at CISPR 16-1-1 standard. A basic schematic of the measurement system is shown in Fig. 1.

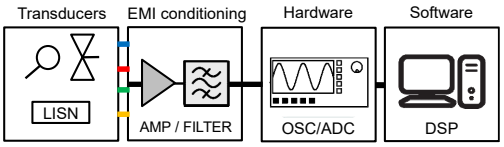

Fig. 1. Overview of the Full TDEMI measurement system

The transducers of the Full TDEMI measurement system are connected to one or several channels, as oscilloscopes have the capability to measure synchronously multiple inputs. For the railway application, the transducers are the antennas to measure the Magnetic Field (H-field) or the Electric Field (E-Field), nevertheless, other transducers like Line Impedance Stabilization Networks are suitable to be used.

Regarding the oscilloscope, it limits the measurement bandwidth; consequently, it needs to ensure that the Voltage Standing Wave Ratio (VSWR) is less than 2 within all the measurable frequency range. Otherwise, the memory of the scope and the sample rate are the other key-points of the hardware. To fulfill CISPR 16-1-1 requirements, generally, it is necessary to oversample the time-domain signal five times the maximum measured frequency and to use the memory needed to compute the weighting detectors. The scopes used to obtain the results presented at the next section are a 5444B Picoscope® (OSC1) for measurements at A and B bands and a DPO 5104B Tektronix® (OSC2) employed at C and D bands. The OSC1 is sampling at 250 MSamples/s and the OSC2 at 5 GSamples/s.

Finally, all the post-processing tasks are done with a laptop, where the software is conducting windowing, resolution enhancing, resampling, spectral estimation (using the Short-Time FFT and the Welch's method) and the detector emulation.

B. *Effective time improvement using Full TDEMI systems*

As it has been stated in the introduction section, the effective measured time is extremely low when frequency sweep instrumentation is used. With the Full time-domain methodology, we can improve the dwell time at each frequency as we are obtaining the full spectrum at every acquisition. Hence, the final effective time, using the Full TDEMI, is the time set at the scope multiplied by the number of acquisitions. Clearly, we have some idle time between different trigger events due to deep memory acquisitions transfer data to the Personal Computer (PC).

A study has been completed analyzing the optimum time scale and data-transfer time to maximize the total evaluated time. Considering that the detector employed for dynamic measurement is the peak one, short-time captures are allowed to compute the spectrum. In tables III and IV, it is presented the effective time measured by Full TDEMI system, compared with the frequency sweep, highlighting the gain, which is referred to the total time measured by the Full TDEMI instrumentation divided by the total time at each frequency by the frequency sweep instrumentation. In table III, the Full TDEMI is optimized to measure an entire dynamic movement that usually lasts 30 seconds and in table IV the system is adjusted to acquire a worst-case event that lasts one second.

TABLE III. EFFECTIVE MEASUREMENT TIME CONSIDERING A DYNAMIC MEASUREMENT THAT LASTS 30 S

Frequency band according to CISPR16-1-1	Frequency sweep		OSC 2			OSC 1		
	(ms) [a]	%	(ms)	%	Gain [b]	(ms)	%	Gain [b]
A	48	0,160	5400	18	112,5	1140	3,8	23,75
	24	0,080			225			47,5
B	120	0,400	540	1,8	4,5			9,5
	12	0,040			45			95
	12	0,040			45			95
	12	0,040			45			95
C	6	0,020	207,9	0,69	34,65			
D	4	0,013	41,58	0,14	10,40			
	2,4	0,008			17,33			

[a] *Measured time at each frequency for sweep (see Table II)*

[b] *Gain is referred to the total time measured by the Full TDEMI instrumentation divided by the total time at each frequency for the sweep method*

In Table III it is observed that a gain between 4.5 and 95 times on the equivalent measured time is obtained with the Full TDEMI system. In B-Band, we increase the measured time at each frequency by 95 times with OSC1 and 45 times with OSC2. Therefore, with a single dynamic measurement, we measure the same effective-time as moving the vehicle 95 times with the frequency sweep method. Moreover, in C-Band the improvement is close to 35 times and in D-Band it is between 10 and 17 times. For instance, in D-Band we increase the effective time from 2.4 ms to a 41.58 ms, when the 30 s measurement is analysed.

Alternatively, if the objective is to evaluate a short-duration braking or accelerating event, it is recommended to increase the acquisition time set at the scope, being able to rise the percentage of the effective time. In Table IV, the observation time has been reduced from 30 s to 1 s, but at the same time, we are capable to enlarge the effective-time as the data-transfer to the PC is not a penalty.

TABLE IV. EFFECTIVE MEASUREMENT TIME CONSIDERING A SHORT-DURATION EVENT THAT LASTS 1 S

Frequency band according to CISPR16-1-1	Frequency sweep		OSC 2			OSC 1		
	(ms) [a]	%	(ms)	%	Gain [b]	(ms)	%	Gain [b]
A	1,60	0,160	1000	100	625	1000	100	625
	0,80	0,080			1250			1250
B	4,00	0,400	100	10	25			250
	0,40	0,040			250			2500
	0,40	0,040			250			2500
	0,40	0,040			250			2500
C	0,20	0,020	50	5	250			
D	0,13	0,013	10	1	75			
	0,08	0,008			125			

[a] *Measured time at each frequency for sweep (see Table II)*

[b] *Gain is referred to the total time measured by the Full TDEMI instrumentation divided by the total time at each frequency for the sweep method*

In this occasion, when we are employing OSC2 in B-Band, we are capable to observe the 100% of the short-event. Making feasible not to miss the worst-case emission. At this frequency band, we improve from observing only 0.4 ms to 1000 ms with OSC1 and 100 ms with OSC2, meaning a gain up to 2500 times. Otherwise, the gain in C and D bands are between 75 and 250. Therefore, the Full TDEMI system is a remarkable step-forward in terms of effective time measured at each frequency, compared with the sweep times defined in Annex B of EN 50121-3-1. Furthermore, other advantages take place when the Full TDEMI system is used, some of them related to the increase of the effective time measured.

C. *Advantages of using Full TDEMI systems instead of frequency sweep receivers*

Applying Full TDEMI measurement system to measure rolling stocks implies different advantages as a consequence of increasing the measurement effective-time and the use of multiple synchronous channels.

- *Simultaneous Multi-antenna measurements*. The employment of scopes instead of spectrum analyzers or EMI receivers allows us to conduct multiple-channel synchronous measurements. Therefore, multi-antenna set-up is used in parallel to measure H-Field and E-Field, reducing the number of vehicle movements needed. Moreover, the simultaneous measurement ensures to obtain the radiated emissions for the same functional mode at all the frequency bands, making possible to acquire the worst-case at all the frequency ranges with a single movement of the rolling stock.

- *Availability to discard transient interference*. Another great advantage is to eliminate from the useful data broadband transient interference produced by transients like pantograph discontinuities. This type of impulsive noise is difficult to identify at the spectrum domain. However, in time-domain, transient interference is characterized by huge amplitude and a short-duration. Therefore, the transient interference is clearly observed in the time domain and can be discarded without a doubt. An example of a discarded measured is shown in Fig. 2, where we can identify easily the transient interference. This short-time domain acquisition shall be discarded for the final analysis, as it is described in standards.

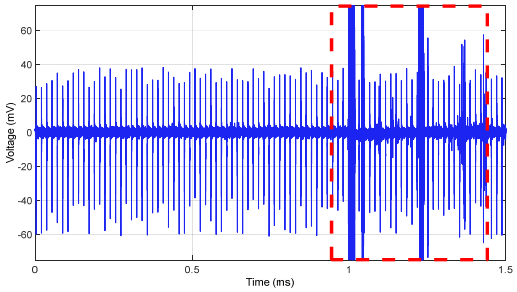

Fig. 2. Example of transient interference in time-domain, which should be avoided for the EMC assessment. The transient interference is identified by the red rectangle

- *Reduction of the background noise variation*. Another main advantage, as a consequence of the reduction of the overall elapsed time, is the reduction of the ambient noise variability. The short-time full spectrum captures enable to use fewer vehicle-movements and to discard transient interferences, hence, the effect of the BGN is moderated. On the other hand, the measurement of the BGN made before and after the EMI measurement of the vehicle is more accurate as we are measuring more effective-time to characterize it. Hence, the common trouble of measuring an uncharacterized ambient interference during the measurement of the EUT is less probable.

- *Triggering capabilities*. As we are using an oscilloscope, all the triggering capabilities can be used to synchronize the Full TDEMI measurement with a particular event.

III. RESULTS

In this section, the time-domain system is applied to measure the emissions from a railway vehicle according to EN 50121-3-1. The motivation of the measurements is to put into practice the developed methodology and evaluate the main theoretical advantages. Ensuring at the same time that the novel employment of the oscilloscopes is appropriate for the application. We measured an urban vehicle at a railway infrastructure allowing us to carry out static and dynamic measurements. Due to a non-disclosure agreement, it is not possible to provide more data of the measured vehicle, however, a simplified schematic of the measurement set-up is shown in Fig. 3.

Fig. 3 shows the test configuration of the Full TDEMI measurement system. It is important to highlight that simultaneous measurements were conducted with an ETS-Lindgren 6502 loop antenna to measure the H-Field at the B-Band, a PMM BC-01 biconical antenna for E-Field at the C-Band and a PMM LP-02 log-periodic antenna for the D-Band. Regarding the hardware used, OSC1 was connected to the loop antenna and OSC2 simultaneously to the biconical and log-periodic. For the post-processing, one laptop is linked to the OSC1 via USB and another to OSC2 using an Ethernet TCP/IP connection.

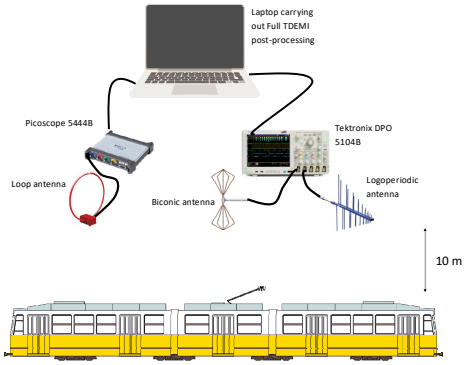

Fig. 3. Measurement schematic of the railway vehicle applying the Full TDEMI measurement system with multiple antennas

Some of the results obtained are presented to highlight the main advantages and to demonstrate that although oscilloscopes were used, we had a great dynamic range of 70 dB and enough sensibility to refer the data to the limits. Firstly, in Fig. 4, we present the results for the static mode with the log-periodic antenna. The aim of showing these data is to accentuate the similarity between the background noise measurement (the ambient noise) and the static emissions of the vehicle. Clearly, non-contribution from the railway vehicle is observed at this frequency range with the quasi-peak (QP) detector. Otherwise, when outdoor measurements are conducted with frequency sweep receivers differences appear and is difficult to distinguish between BGN changes and EUT emissions. On the contrary, by using the Full TDEMI system, we increase the effective measured time, reducing the observation period and making the BGN more stable.

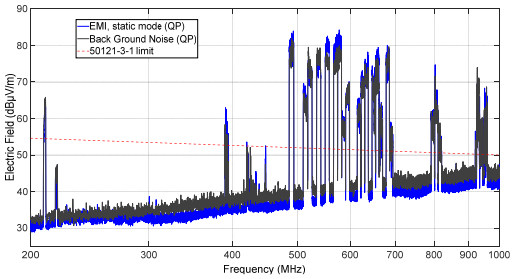

Fig. 4. E-Field results obtained for the static measurement. In blue trace the measurement of the EUT and in black the ambient noise measurement.

Regarding the dynamic mode, we perform the measurement reducing the number of vehicle-movements needed, by acquiring simultaneously the H-Field and the E-Field. As in the static mode, we still have the advantage of reducing the observation period, which implies a steadier ambient noise. Moreover, for the dynamic mode, it is mandatory to measure the EM emissions due to braking or accelerating. Therefore, we have the advantages of increasing the effective measured time, discarding transients and ensuring to evaluate the worst-

emission case. In Fig. 5 and Fig. 6 dynamic results of the B-Band and the C-Band are displayed.

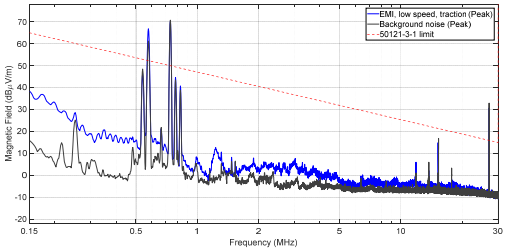

Fig. 5. H-Field results obtained for the dynamic measurement. In blue trace the measurement of the EUT and in black the ambient noise measurement

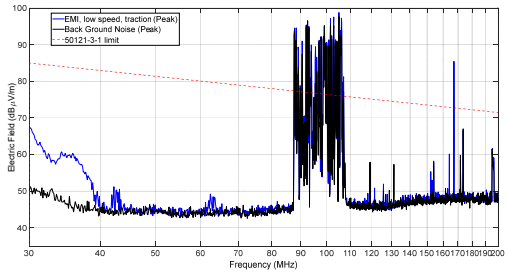

Fig. 6. E-Field results obtained for the dynamic measurement. In blue trace the measurement of the EUT and in black the ambient noise measurement

The emissions results of the vehicle in-motion show disturbances at the lower frequencies, which are properly measured with the Full TDEMI. In fact, we carried out up to 10 movements of the train, however, non-changes were observed at the spectrum between the first measurement and the other nine. Implying that with a unique movement of the rolling-stock it is sufficient to measure the worst-case emission at all the frequency range. This is a great advantage compared with the difficulties that appear when conventional receivers are employed, making essential to move the train several times to complete the spectrum emissions. Furthermore, the background noise is also changing and it makes near to impossible to differentiate between the vehicle emissions and the ambient noise. Hence, it is a significant improvement to use the time-domain approach as it makes necessary to measure just once the vehicle in motion to perform the evaluation.

IV. CONCLUSIONS

The applicability of the Full TDEMI system to conduct properly EN 50121-3-1 EMI measurements has been demonstrated theoretically and practically through in-situ measurements. Overcoming the main difficulties due to the background noise and the mandatory dynamic mode. The main advantages of the Full TDEMI are the increasing of the effective measured time at each frequency, which can rise up to 2500 times, the availability of employing multiple antennas synchronously and the possibility to discard transient interference that should not be evaluated.

Therefore, authors consider time-domain methodologies should be included in Annexes of the railway standards. Novel time-domain based systems are in compliance with CISPR 16-1-1, henceforward, a specific guide should be included to maximize the performance and explain the main benefits of the system, as it is done in Annex B for frequency sweep instrumentation. Furthermore, the Full TDEMI systems offer us the possibility to measure properly the worst-case scenario using instrumentation with a moderate cost, where the most expensive hardware is the 1 GHz oscilloscope.

ACKNOWLEDGMENT

This work was supported in part by the EURAMET 15RPT01 research project (the EMPIR is jointly funded by the EMPIR participating countries within EURAMET and the European Union), by the Spanish “Ministerio de Economía, Industria y Competitividad,” under project TEC2016-79214-C3-2-R (AEI/FEDER, UE), by the “Secretaria d’Universitats i Recerca del Departament d’Economia i Coneixement de la Generalitat de Catalunya” and the European Social Fund and The author(s) would like to acknowledge the contribution of the COST Action IC1407 ‘ACCREDIT’.

REFERENCES

[1] IEC *62236-3-1 Railway applications - Electromagnetic compatibility - Part 3-1: Rolling stock - Train and complete vehicle.* IEC

[2] CENELEC - *EN 50121-3-1: Railway applications - Electromagnetic compatibility - Part 3-1: Rolling stock - Train and complete vehicle*. CENELEC

[3] J. Catrysse, F. Vanhee, J. Knockaert, I. Hendrickx and V. Beauvois, "In situ testing of large machines: Alternative methods for conducted emission measurements," *Electromagnetic Compatibility, 2008. EMC2008. IEEE International Symposium on,* Detroit, MI, 2008, pp. 1-6

[4] M. Pous, M. Azpúrua and F. Silva, "Benefits of full time-domain EMI measurements for large fixed installation," *2016 International Symposium on Electromagnetic Compatibility - EMC EUROPE*, Wroclaw, 2016, pp. 514-519.

[5] G. Romero, E. P. Simon, V. Deniau, C. Gransart and M. Kousri, "Evaluation of an IEEE 802.11n communication system in presence of transient electromagnetic interferences from the pantograph-catenary contact," *2017 XXXIInd General Assembly and Scientific Symposium of the International Union of Radio Science (URSI GASS)*, Montreal, QC, 2017, pp. 1-4.

[6] S. Dudoyer, V. Deniau, S. Ambellouis, M. Heddebaut and A. Mariscotti, "Classification of Transient EM Noises Depending on their Effect on the Quality of GSM-R Reception," *in IEEE Transactions on Electromagnetic Compatibility*, vol. 55, no. 5, pp. 867-874, Oct. 2013.

[7] M. Pous, M. A. Azpúrua, and F. Silva, “Radiated transient interferences measurement procedure to evaluate digital communication systems,” in *2015 IEEE International Symposium on Electromagnetic Compatibility (EMC)*, 2015, pp. 456–461.

[8] S. Braun, T. Donauer, and P. Russer, “A real-time time-domain EMI measurement system for full-compliance measurements according to CISPR 16-1-1,” *IEEE Trans. Electromagn. Compat.*, vol. 50, no. 2, pp. 259–267, 2008.

[9] C. Hoffmann and P. Russer, “A real-time low-noise ultrabroadband time-domain EMI measurement system up to 18 GHz,” *IEEE Trans. Electromagn. Compat.*, vol. 53, no. 4, pp. 882–890, 2011.

[10] F. Krug and P. Russer, “The time-domain electromagnetic interference measurement system,” *IEEE Trans. Electromagn. Compat.*, vol. 45, no. 2, pp. 330–338, 2003.

[11] M. A. Azpúrua, M. Pous, and F. Silva, "A measurement system for radiated transient electromagnetic interference based on general purpose instruments," in *IEEE International Symposium on Electromagnetic Compatibility (EMC)*, 2015, vol. 2015–*Septm*.

[12] M. A. Azpúrua, M. Pous, S. Çakir, M. Çetinta, and F. Silva, "Improving time-domain EMI measurements through digital signal processing," *IEEE Electromagn. Compat. Mag.*, vol. 4, no. 2, pp. 82–90, 2015.

[13] M. A. Azpúrua, M. Pous, J. A. Oliva, and F. Silva, "Fast and automated verification of multi-channel full time-domain EMI measurement system," in *2017 IEEE International Instrumentation and Measurement Technology Conference (I2MTC)*, 2017, pp. 1–6

5

STATISTICAL EMI ANALYSIS AND THE EXPECTED MAXIMUM DETECTOR

The publications in subsections 5.1 and, 5.2 comprise the contributions made to the statistical processing of time-domain EMI measurements in the line of the third objective of this Thesis. Their highlights are described below.

Objective 3: The worst-case disturbance emissions levels (extreme values) were analytically modeled to find the properties of the peak detector measurements. Then, a more robust model for predicting the expected maximum emissions levels was proposed based on the non-parametric kernel-fitting of the EMI distribution and bootstrapping techniques. The later approach provided better estimates for non-Gaussian conditions than the former analytical approximation.

5.1. FUNDAMENTAL JOURNAL ARTICLE 2

M. A. Azpúrua, M. Pous and F. Silva, "On the Statistical Properties of the Peak Detection for Time-Domain EMI Measurements," in *IEEE Transactions on Electromagnetic Compatibility*, vol. 57, no. 6, pp. 1374-1381, Dec. 2015. doi: 10.1109/TEMC.2015.2456983

Abstract-This paper presents a discussion on the inherent characteristics of the measurements performed with time-domain electromagnetic interference measurement systems in regards of the detection of the maximum emissions levels. In that sense, some relevant statistical properties of the frequency components of the maximum emissions levels in the amplitude spectrum are investigated using the extreme value theory to provide a model based on the Gumbel probability distribution and estimates for its parameters, expected value, variance, and Cramer-Rao bounds. The results suggest that using the expected maximum value of the emissions levels instead of the just the observed maximum value improves the measurement repeatability and also reduces the uncertainty in the results. This paper presents an additional insight measure that enhances our understanding of the statistical behaviour of the measured EMI and of the time-domain measurement process itself.

5.2. CONFERENCE PROCEEDING 5

M. A. Azpúrua, J. A. Oliva, M. Pous and F. Silva, "Robust extreme value estimation for full time-domain EMI measurements," *2017 International Symposium on Electromagnetic Compatibility - EMC EUROPE*, Angers, 2017, pp. 1-6. doi: 10.1109/EMCEurope.2017.8094729

Abstract-A robust approach for estimating the expected maximum levels of radiofrequency, time-varying, electromagnetic emissions is proposed. The expected maximum peak value is intended to provide a statistical approximation for the worst case emissions scenario that accounts for the variability of the measured interference. The estimates are obtained through Monte Carlo resampling from a non-parametric distribution fitted by means of kernel density estimation applied to the time-frequency representation of the assessed interference. As a key advantage, calculating the expected maximum peak value does not require increasing the dwell time or holding the maximum value over successive sweeps. Results indicate the methodology is better suited than previous approaches for calculating the expected maximum peak value because it does not depend on normality assumptions difficult to guarantee in practice. The proposed technique is an example of how full time-domain EMI measurements can be exploited for obtaining further insights.

On the Statistical Properties of the Peak Detection for Time-Domain EMI Measurements

Marco A. Azpúrua, *Member, IEEE*, Marc Pous, and Ferran Silva, *Member, IEEE*

***Abstract*—This paper presents a discussion on the inherent characteristics of the measurements performed with time-domain electromagnetic interference measurement systems in regards of the detection of the maximum emissions levels. In that sense, some relevant statistical properties of the frequency components of the maximum emissions levels in the amplitude spectrum are investigated using the extreme value theory to provide a model based on the Gumbel probability distribution and estimates for its parameters, expected value, variance, and Cramer–Rao bounds. The results suggest that using the expected maximum value of the emissions levels instead of the just the observed maximum value improves the measurement repeatability and also reduces the uncertainty in the results. This paper presents an additional insight measure that enhances our understanding of the statistical behavior of the measured EMI and of the time-domain measurement process itself.**

***Index Terms*—Electromagnetic compatibility, electromagnetic interference (EMI), electromagnetic measurements, statistical signal processing, time-domain analysis.**

I. Introduction

THE electromagnetic interference (EMI) measurement receivers covered in CISPR 16-1-1 and ANSI C63.2 documents [1], [2] include the peak, quasi-peak, average, and rms-average detector modes. Those detectors are circuits intended to provide weighted lectures of the amplitude of the EMI depending on the pulse repetition frequency [3].

The peak detector has a peak-value holding capability. In general terms, the peak detector is an analog maximum-hold circuit realization. In frequency sweep EMI receivers, the signal applied at the input of the peak detector circuit has been previously lowered to intermediate frequency, filtered, and rectified. The peak detector holds the maximum of the measured voltage for a long time indicating the peak value measured over the dwell time of the interference signal.

Therefore, an EMI test receiver in the peak detector mode measures the maximum value of impulsive perturbations for each spectral component included in the assessed band, one frequency step at a time. However, the dwell time shall be adjusted considering the EMI pulse repetition rate. Hence, EMI measurement with frequency-sweep-based instruments is a time-consuming task.

On the other hand, in entirely time-domain EMI (TDEMI) measurement systems, there are neither analog detector circuits nor analog signal processing; measurements can be adjusted to be triggered by pulsed interferences and one single acquisition in the time domain is used to perform spectral estimation providing most result through postprocessing. Consequently, mathematical emulation of the detectors is often applied to weigh the amplitude spectrum in order to obtain spectral estimations directly comparable to results from frequency-domain sweeping receivers.

The aforementioned emulation of the standard weighting detectors is a significantly complex task because the charge/discharge time constants and the meter time constant are implemented by means of multistage parallel digital filter functions that require a large amount of memory [4]. Even if this method provides very accurate results, its mathematical complexity makes it difficult to perform a rigorous uncertainty assessment on the measurement results.

As an alternative and less computationally intensive method, some TDEMI measurement systems have used the detector emulation by means of additive weighting factors, which depend only upon the EMI pulse repetition frequency [5]. However, in this particular case, the accuracy is compromised because it is really difficult to provide a single correction factor when the EMI is formed by a superposition of pulses with different repetition rate and continuous-wave signals.

In any case, the current approach taken to emulate the peak detector of a conventional EMI test receiver is very simple and straightforward: the highest value of the video voltage observed during the measurement time is recorded and displayed. Nevertheless, this very intuitive approach has a fundamental flaw from the statistical point of view, because it provides a biased estimator that has least robust statistics because it is maximally sensitive to outliers. Therefore, the aforementioned current implementations of detector emulation in TDEMI measurement systems have potential drawbacks in terms of accuracy, robustness, and uncertainty assessment, representing an obstacle to achieve measurement traceability in TDEMI measurement systems.

Conversely, the extreme value theory has been used in the field of reverberation chambers to model the electric field distribution near the wall cavity, providing meaningful results for modeling the maximum E-field [6]. In that sense, this paper provides an insight on the measurement process carried out by TDEMI measurement systems and then develops a compressive approach to evaluate the expected value, the variance, and Cramer–Rao bound (CRB) for the estimation of the maximum

Manuscript received March 12, 2015; revised June 4, 2015; accepted July 12, 2015. Date of publication July 28, 2015; date of current version December 11, 2015. This work was supported in part by the EURAMET IND60EMC research project (the EMRP is jointly funded by the EMRP participating countries within EURAMET and the European Union) and by the Spanish "Ministerio de Economía y Competitividad," under Project TEC2013–48414-C3–3-R.

The authors are with the Group of Electromagnetic Compatibility, Department of Electronic Engineering, Universitat Politècnica de Catalunya—BarcelonaTech, Barcelona 08034, Spain (e-mail: marco.azpurua@upc.edu; marc.pous@upc.edu; ferran.silva@upc.edu).

Color versions of one or more of the figures in this paper are available online at http://ieeexplore.ieee.org.

Digital Object Identifier 10.1109/TEMC.2015.2456983

0018-9375 © 2015 IEEE. Personal use is permitted, but republication/redistribution requires IEEE permission.
See http://www.ieee.org/publications_standards/publications/rights/index.html for more information.

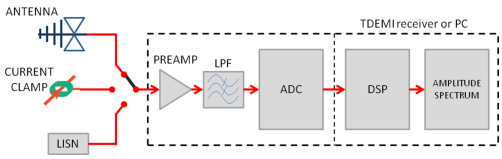

Fig. 1. Block diagram of a TDEMI measurement system.

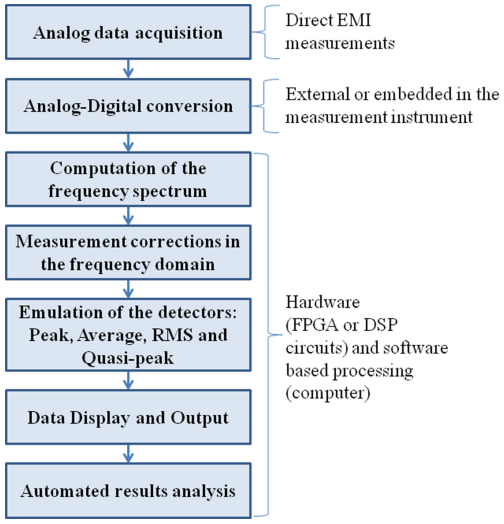

Fig. 2. General flowchart of the TDEMI measurement processing.

emissions levels based on statistical inference techniques and on the extreme value theory.

II. Overview of TDEMI Measurement Systems

In general terms, a TDEMI measurement system, for radiated and/or conducted disturbances, is described by the block diagram shown in Fig. 1 [3]. For the measurement of radiated EMI, a broadband antenna shall be used, while for the measurement of conducted EMI corresponds either a current clamp or a line impedance stabilization network. Sometimes the measured signal is amplified, and then it is low-pass filtered for band-limiting purposes, so the signal fulfills Nyquist condition for the maximum sampling rate supported by the TDEMI system. Then, in the analog-to-digital converter (ADC), the signal is digitized and stored. Finally, the amplitude spectrum is computed via spectral estimation techniques.

On the other hand, from the standpoint of the signal acquisition and processing stage, a TDEMI system is more naturally described by the flowchart shown in Fig. 2.

In that sense, the data acquisition process for a TDEMI measurement system begins when the analog signal is sampled either directly by the measuring instrument (i.e., digital oscilloscope) or externally by means of ADC or digitizers. Then, the EMI data are transferred from the main memory to the device that will process it. For the commercial fast Fourier transform (FFT)-based EMI receivers, this process is performed internally by the built-in processors and softwares [4]. However, a customized TDEMI measurement system may carry on the digital signal processing with the aid of specific software running on a personal computer. Then, the data are transferred to a personal computer via some communication port. Subsequently, the amplitude spectrum is digitally computed using the FFT (or some variant of), periodograms, or other spectral estimation methods [5]. Later, the errors due to the frequency dependence of the antenna factor, the attenuation in the transmission line, the gain of the preamplifier, the frequency response of the antialiasing filter are corrected. Next, a mathematic emulation of the peak, RMS, average, and quasi-peak detectors is made, either by applying a correction factor dependent on the pulse repetition frequency [5] or by means of the application of a digital infinite impulse response filter [7]. Additionally, other signal processing techniques can be used in order to reduce the impact of the noise but this has varied upon specific implementations. Finally, the results must be displayed and compared with the respective limit lines to provide a judgment about the test result regarding the EMI in the measured frequency band. For studying nonstationary signals, a spectrogram representation of EMI has also been used previously [8].

III. Fundamentals of Digital Signal Processing for Peak Detection in a TDEMI Measurement System

A continuous-time signal function $x(t)$ that represents the EMI directly measured by a TDEMI system is observed during a time period of length T_0. In order to computationally evaluate the frequency spectrum of $x(t)$, $X(f)$ the measured signal is sampled and digitized to obtain a time-discrete signal $x\,[n]$, where n is integer and $x[n]$ is assumed to be periodic with total number of samples$N$, which means $x[n+N] = x[n]$. Therefore

$$x[n] = x(n\Delta t) \tag{1}$$

where $T_0 = N\Delta t$ and Δt is the sampling interval, i.e., $\Delta t = 1/f_s$, f_s being the sampling frequency. Conversely, the discrete frequency spectrum $X[k]$ is related to the continuous frequency spectrum $X(f)$ by

$$X[k] = X(k\Delta f) \tag{2}$$

where k is an integer and Δf is the spacing of the spectral lines. The quantities$N$, T_0, Δt, and Δf are related by

$$\Delta f = \frac{N}{T_0}. \tag{3}$$

The discrete Fourier transform (DFT) is given by

$$X[k] = \sum_{n=0}^{N-1} x[n] e^{j\frac{2\pi n k}{N}}. \tag{4}$$

The spectral estimation is performed on the basis of the DFT under the assumption that $x\,[n]$ is periodic in n with a period

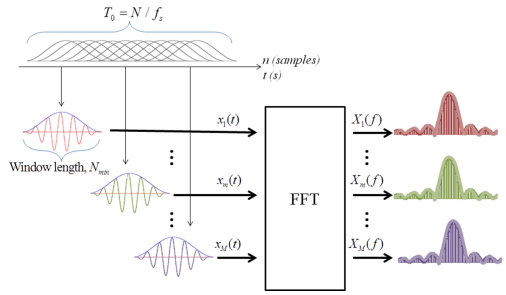

Fig. 3. Spectral estimation process by means of the STFT.

N. However, $x\,[n]$ is not really periodic since there is only a continued measured signal sequence of length N.

To reduce the scallop loss and the spectral leakage caused by the finite length, the time record $x\,[n]$ is multiplied by a window function $w\,[n]$ [9], [10]. If windowing is used, it is necessary to compensate the corresponding energy loss caused by the window using the coherent gain scaling factor [11].

On the other hand, to obtain a spectral estimation with Δf equivalent to the required resolution bandwidth, the minimum record length $N_{\min}$ shall be

$$N_{\min} = f_s \frac{w_f}{\Delta f} \tag{5}$$

where w_f is the window factor of the windowing function used, i.e., Gaussian, Hann, or Kaiser–Bessel [12].

Then, if $N > N_{\min}$, it is possible to define M overlapping windows of $N_{\min}$ length in order to determine the frequency and phase content of the *m*th local sections of an EMI signal as it changes over time. This process is called the short-time Fourier Transform (STFT) and it is given by

$$X_m[k] = \sum_{n=0}^{N_{\min}-1} x[n]w[n - m(1-o_f)N_{\min}]e^{-j2\pi n \frac{k}{N_{\min}}} \tag{6}$$

where o_f is the overlap factor (generally between 0.5 and 0.8 depending on the type of windowing function) and $m = 1, 2, \ldots, M$ is the time shift index that controls the translation of the overlapping window between successive time frames. Fig. 3 shows a simplified diagram on the spectral estimation process performed by the STFT.

Therefore, the STFT provides a matrix with the values of each spectral component of the measured EMI as it changes over time

$$X_m[k] = \begin{bmatrix} X_1[0] & X_1[1] & \cdots & X_1[k_{\max}] \\ X_2[0] & X_2[1] & \cdots & X_2[k_{\max}] \\ \vdots & \vdots & \ddots & \vdots \\ X_M[0] & X_M[1] & \cdots & X_M[k_{\max}] \end{bmatrix}. \tag{7}$$

Consequently, in a TDEMI measurement system, the maximum amplitude peak value of the spectral estimation $\tilde{X}_{\text{peak}}$ is the vector containing the maximum signal magnitude observed in each frequency bin for all the windowed time frames given by

$$\tilde{X}^T_{\text{peak}}[k] = \begin{bmatrix} \max\{|X_1[0]| & |X_2[0]| & \cdots & |X_M[0]|\} \\ \max\{|X_1[1]| & |X_2[1]| & \ldots & |X_M[1]|\} \\ \vdots & \vdots & \ddots & \vdots \\ \max\{|X_1[k_{\max}]| & |X_2[k_{\max}]| & \ldots & |X_M[k_{\max}]|\} \end{bmatrix}. \tag{8}$$

IV. Statistical Properties of the Maximum Peak Spectral Estimation

Let us start assuming that the measured EMI signal is a random variable and that the recorded time length is a representative sample of the interference under assessment. Likewise, we assume that each measured waveform point captured in the time domain is independent of each other.

Our first assumption is valid because of the stochasticity of the process that generates interferences and also due to the sources of variability introduced by the measurement process itself. Regarding the second assumption, it shall be satisfied because the confidence of the results depends upon it and, it is verified through the repeatability of the results.

Then, from the measured sample, the STFT creates M windowed time frames that are, by themselves, a group of subsamples from which the EMI spectral content will be estimated M times, one spectral estimation from each subsample. Since each windowed time frame is different from the others, their spectral content is also different and the variability of each frequency bin can be analyzed in terms of random variables.

With that said, it is clear that $\tilde{X}_{\text{peak}}\,[k]$ is an estimator of the extreme value taken by the distribution of each *k*th component of the amplitude spectrum $X_{\text{peak}}[k]$. In the following sections, the statistical properties of such estimators will be investigated.

A. Probability Distribution

Let us suppose that $G(X)$ is the distribution of X_{peak}

$$G\,(X) = P\,(X_{\text{peak}} \leq X) \tag{9}$$

that is equivalent to the event

$$G\,(X) = P\,(X_1 \leq X, \ldots, X_M \leq X) \tag{10}$$

and since it has been assumed independency between the outcomes of the spectral estimation obtained from each individual subsample, and also, considering that each individual subsample is identically distributed as $F(X)$ since they belong to the same population, then,

$$G\,(X) = \prod_{m=1}^{M} P\,(X_m \leq X) = [F(X)]^M\,. \tag{11}$$

Finally, the probability density function (PDF) of $\tilde{X}_{\text{peak}}$ is given by

$$X_{\text{peak}} \sim \frac{d}{dX} G(X) = M\left[F(X)\right]^{M-1} f(X) \tag{12}$$

where $f(X)$ is the PDF of X. This means that the PDF of the maximum of each spectral component depends directly on the sample size and on the distribution function of the spectral component.

Nonetheless, the distribution function of each spectral component is generally unknown. However, according to the extreme values theory, the Fisher–Tippett–Gnedenko theorem provides an asymptotic result for the distribution of the largest extreme value of the sample, regardless of the parent population, provided a sufficiently large sample size [13].

Hence, (11) is asymptotically approximated to the Gumbel distribution, which is given by

$$G(X;\alpha,\beta) \approx e^{-e^{\frac{X-\alpha}{\beta}}} \tag{13}$$

where α and β are the location (mode) and scale parameters, respectively, of the Gumbel distribution [13]. Thus, differentiating (12) with respect to *X*, the PDF of $\tilde{X}_{\text{peak}}$is

$$\tilde{X}_{\text{peak}} \sim \frac{d}{dX} G(X;\alpha,\beta) = \frac{1}{\beta}\left(e^{-\left(\frac{X-\alpha}{\beta}\right)}\right)\left(e^{-e^{-\left(\frac{X-\alpha}{\beta}\right)}}\right). \tag{14}$$

The approximation provided by (14) is a particular case of the generalized extreme value distribution. The appropriateness of the Gumbel distribution for modeling extreme values has been demonstrated when the parent distribution has an unbounded tail that decreases at least as fast as an exponential function, and has finite moments, as does the Gaussian distribution [14].

For EMI measurement applications, the aforementioned condition is reasonably satisfied because the combination of the multiple sources of variability that influence the measurement result causes the distribution function of the spectral estimation to converge approximately into a normal distribution, according to the central limit theorem [6], [15].

B. Parameter Estimation

As stated before, the Gumbel distribution has two parameters, α and β. These parameters are generally unknown and must be estimated from the information provided by the sample. Several techniques, such as maximum likelihood estimation or method of moments, have been used to provide mathematical expressions of the corresponding estimators [16]. However, these approaches require a sample of maximum values, i.e., a set of maximum values taken from several different samples generated by the same process.

In this particular case, only one sample of *M* different spectral estimations for each frequency component is available from a single measurement of EMI in the time domain.

Nevertheless, for the particular case, where the spectral estimations are normally distributed with mean μ and variance σ^2, $X \sim N(\mu,\sigma)$, the parameters of the Gumbel distribution can

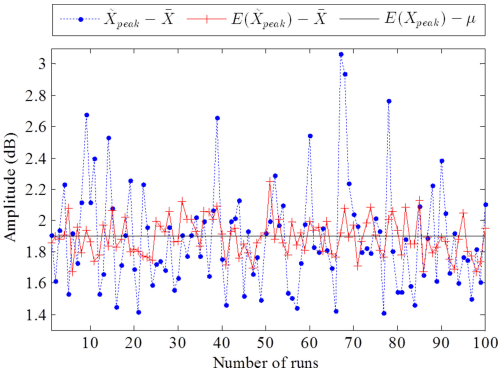

Fig. 4. Comparison between the estimated maximum emission levels and their corresponding expected value for 100 successive MC trials, $M = 100$, and $\sigma = 0.75$ dB.

be expressed as

$$\alpha = {\Phi_{\mu,\sigma}}^{-1}\left(1-\frac{1}{M}\right) \tag{15}$$

$$\beta = {\Phi_{\mu,\sigma}}^{-1}\left(1-\frac{1}{eM}\right) - {\Phi_{\mu,\sigma}}^{-1}\left(1-\frac{1}{M}\right) \tag{16}$$

where $\Phi^{-1}(p)$ is the normal inverse cumulative distribution function of X applied to the probability value p.

In consequence, the parameters of the Gumbel distribution are estimated using the sample average $\bar{X}$ and standard deviation s as the best estimates of μ and σ, respectively,

$$\hat{\alpha} = {\Phi_{\bar{X},s}}^{-1}\left(1-\frac{1}{M}\right) \tag{17}$$

$$\hat{\beta} = {\Phi_{\bar{X},s}}^{-1}\left(1-\frac{1}{eM}\right) - {\Phi_{\bar{X},s}}^{-1}\left(1-\frac{1}{M}\right). \tag{18}$$

C. Expected Value

Since $\tilde{X}_{\text{peak}}$ is modeled as a random variable distributed as (14), the expected value of the maximum peak measurement for a TDEMI measurement system is given by [13]

$$E\left(\tilde{X}_{\text{peak}}\right) = \hat{\alpha} + \gamma\hat{\beta} \tag{19}$$

where γ is the Euler–Mascheroni constant ($\gamma \approx 0.5772$).

Then, substituting (17) and (18) into (19), the mean of $\tilde{X}_{\text{peak}}$ can be rewritten as

$$E\left(\tilde{X}_{\text{peak}}\right) = (1-\gamma)\,\Phi_{\bar{X},s}\left(1-\frac{1}{M}\right) + \gamma\Phi_{\bar{X},s}\left(1-\frac{1}{eM}\right). \tag{20}$$

As a result from (20), it is clear that $E(\tilde{X}_{\text{peak}}) - X_{\text{peak}} \neq 0$ and, therefore, $\tilde{X}_{\text{peak}}$ is a biased, but consistent, estimator.

In order to exemplify the importance of $E(\tilde{X}_{\text{peak}})$, Fig. 4 shows the results of a Monte Carlo (MC) simulation that represent the results from 100 successive $\tilde{X}_{\text{peak}}$ measurements, for

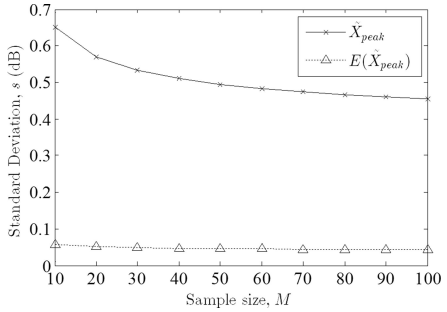

Fig. 5. Standard deviation of $\tilde{X}_{\text{peak}}$ and $E(\tilde{X}_{\text{peak}})$ as a function of the sample size.

any single spectral component of EMI, obtained for $M = 100$ and $\sigma = 0.75$ dB.

Under the simulation conditions, the results of the max peak emissions ($\tilde{X}_{\text{peak}}$) have a variability range of approximately 2 dB. However, its expected value $E(\tilde{X}_{\text{peak}})$ has a range of 0.77 dB. Possibly, the most important aspect that must be noticed is that in about 50% of the cases, the measurements of maximum emissions might be underestimated by chance and $E(\tilde{X}_{\text{peak}})$ is able to provide more robust results.

D. Variance

The variance of a $\tilde{X}_{\text{peak}}$ depends on β and is given by [13]

$$\text{Var}\left(\tilde{X}_{\text{peak}}\right) = \frac{\pi^2}{6}\hat{\beta}^2. \tag{21}$$

Thus, according to (18) and (22), $\text{Var}(\tilde{X}_{\text{peak}})$ is estimated as

$$\text{Var}\left(\tilde{X}_{\text{peak}}\right) = \frac{\pi^2}{6}\left(\Phi_{\bar{X},s}{}^{-1}\left(1-\frac{1}{eM}\right) - \Phi_{\bar{X},s}{}^{-1}\left(1-\frac{1}{M}\right)\right)^2. \tag{22}$$

From (23), it is important to notice that $\text{Var}(\tilde{X}_{\text{peak}})$ decreases as $M \to \infty$. However, M is a finite quantity and it shall be expected variability in the results provided by the maximum peak reading, as is evident in Fig. 4. In this regard, Fig. 4 verifies that $\text{Var}(E(\tilde{X}_{\text{peak}})) < \text{Var}(\tilde{X}_{\text{peak}})$.

Fig. 5 shows the standard deviation of both $\tilde{X}_{\text{peak}}$ and $E(\tilde{X}_{\text{peak}})$ as a function of M for $\sigma = 1$ dB. The standard deviation of $E(\tilde{X}_{\text{peak}})$ was calculated numerically using 10^5 MC iterations, due to the complexity of the corresponding analytical expression.

In both cases, the standard deviation slowly decreases with M, but the standard deviation of $E(\tilde{X}_{\text{peak}})$ is always in the order of magnitude lower than the standard deviation of $\tilde{X}_{\text{peak}}$ and is less sensitive to changes in M.

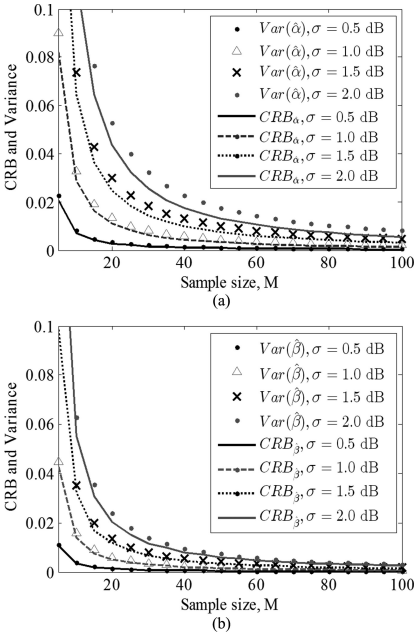

Fig. 6. CRB and variance of the estimators of the parameters for the Gumbel distribution as a function of the sample size M and the standard deviation of the process that generates the samples, σ. (a) Location parameter, α. (b) Scale parameter, β.

E. Cramer–Rao bound

Since for EMI measurement applications the parameters α and β are unknown, the estimated parameters $\hat{\alpha}$ and $\hat{\beta}$ are also random variables. However, their efficiency can be compared with the CRB in order to establish if their use is appropriated. In this particular case, the CBR will be interpreted as a lower bound on the variance of estimators of the deterministic parameters of a PDF.

The authors of [17] have demonstrated that the CRB of the Gumbel distribution parameters are independent of the location parameter, and are approximately given by

$$\text{CRB}_{\hat{\alpha}} = \frac{6\beta^2}{\pi^2 M}\left(1+\frac{\pi^2}{6}+\gamma^2-2\gamma\right) \approx 1.109\frac{\beta^2}{M} \tag{23}$$

$$\text{CRB}_{\hat{\beta}} = \frac{6\beta^2}{\pi^2 M} \approx 0.608\frac{\beta^2}{M}. \tag{24}$$

Additionally, through MC simulation, it has been proven that the estimators bias have small effects on the CRB mostly when M is large [17].

Fig. 6 shows the calculated CRB using (23) and (24) compared with the variance of the estimator of $\hat{\alpha}$ and $\hat{\beta}$ calculated by means of MC simulation for 10^5 iterations in each combination of M and σ. Since the variance of the estimators is very similar

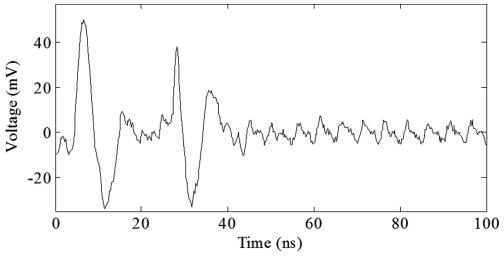

Fig. 7. Waveform of the measured transient EMI.

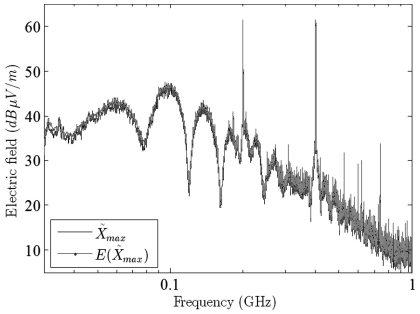

Fig. 8. Measurement results for the maximum and the expected maximum emission levels obtained using a TDEMI system.

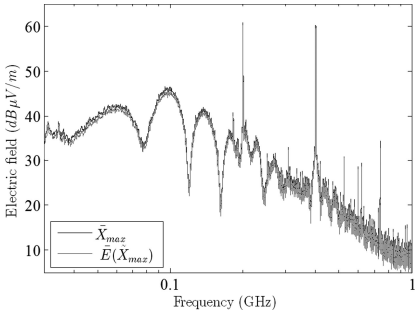

Fig. 9. Average of the measurement results for the maximum $\bar{X}_{\mathrm{peak}}$ and the expected maximum $\bar{E}(\bar{X}_{\mathrm{peak}})$ emission levels obtained using a TDEMI system.

to the CRB, it is possible to conclude that (17) and (18) are efficient and provide reliable estimators for the calculation of the expected maximum value.

V. On the Use of the Expected Maximum Value in TDEMI Measurement Systems

In this section, an application example of radiated EMI measurement will be presented. Our TDEMI measurement system has been implemented using a general purpose oscilloscope Tektronix DPO 7104. The aforementioned oscilloscope has the following main technical specifications: 8-bit ADC resolution (6.7 effective bits), 1 GHz of analog bandwidth, 20 GSamples/s of the maximum sampling rate, and 125 MSamples of the maximum record length. A detailed explanation on the features of this TDEMI measurement system is found in [18]. In the same manner, an explicit description of the signal processing techniques applied to the measured signal is given in [12]. Measurements were performed using a standard setup for radiated emissions assessment inside a full anechoic chamber.

The measured EMI was an intentionally generated transient disturbance provided by a pulse function arbitrary generator Agilent 81160A. The transited EMI is superposed with two narrow band tones at 200 and 400 MHz. Additive white Gaussian noise was intentionally added to the EMI. The pulse repetition frequency of the disturbance is 110 kHz and the pulse duration is approximately 40 ns. The sampling frequency was set to 5 GSamples/s. The resolution bandwidth was configured at 120 kHz, and according to (5), the required minimum record length is $N_{\min} \approx 93000$ samples given a window function with $w_f = 2.23$.

The synthesized disturbance was intended to provide narrowband and broadband interferences in order to exercise the measurement system in a complex and representative scenario. The consistency of the results for other different measured EMI waveforms has been verified. In that sense, Fig. 7 shows a 100-ns time frame of the measured signal where the transient EMI waveform is displayed. The total recorded time was approximately 200 μs which correspond to $M = 50$ for an overlapping factor of 80%.

Using the general procedure explained in Section III and, particularly equation (8), the maximum emissions levels $\tilde{X}_{\mathrm{peak}}$ were measured from 30 MHz to 1 GHz. Likewise, applying (20), the corresponding expected value for the maximum emissions levels $E(\tilde{X}_{\mathrm{peak}})$ was also estimated in the same frequency band. Both results are shown in Fig. 8.

As expected, the results are coherent with the theory and the values of $\tilde{X}_{\mathrm{peak}}$ and $E(\tilde{X}_{\mathrm{peak}})$ have a very similar behavior in the frequency domain. For each frequency, $E(\tilde{X}_{\mathrm{peak}})$ underestimates or overestimates the observed $\tilde{X}_{\mathrm{peak}}$, similarly as shown in Fig. 4. Differences between $\tilde{X}_{\mathrm{peak}}$ and $E(\tilde{X}_{\mathrm{peak}})$ are within 2 dB in this particular case.

However, in order to effectively verify the impact of using $E(\tilde{X}_{\mathrm{peak}})$ instead of just $\tilde{X}_{\mathrm{peak}}$, it was required to perform several measurements and evaluate the ranges of variation and the average results for each quantity. In that sense, the measurement was repeated ten successive times using the same setup and settings.

Fig. 9 shows the average of the measurement results for the maximum $\bar{X}_{\mathrm{peak}}$ and the expected maximum $\bar{E}(\tilde{X}_{\mathrm{peak}})$. As expected, both averaged traces are even more similar and they will tend to converge if more independent measurement repetitions are performed and included in the average. However, since $E(\tilde{X}_{\mathrm{peak}})$ is less variable than $\tilde{X}_{\mathrm{peak}}$, it would be reasonable to assume that it provides smaller ranges of values, being therefore a more repeatable measure.

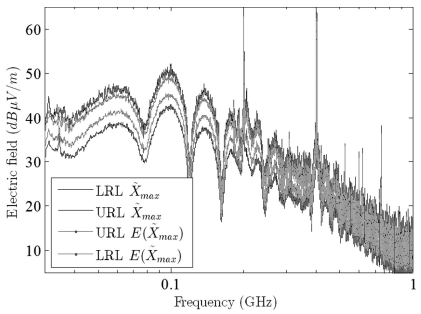

Fig. 10. URL and LRL of the observables $\tilde{X}_{\mathrm{peak}}$ and $E(\tilde{X}_{\mathrm{peak}})$.

Subsequently, Fig. 10 shows that the interval of $\tilde{X}_{\mathrm{peak}}$ includes the $E(\tilde{X}_{\mathrm{peak}})$ interval between its upper range limit (URL) and lower range limit (LRL), verifying the abovementioned observation about the ranges of the estimates.

For the presented example, the range of $\tilde{X}_{\mathrm{peak}}$ can be as high as approximately 8 dB while the range of $\bar{E}(\tilde{X}_{\mathrm{peak}})$ is below 4 dB. The fluctuation ranges are smaller when measuring a continuous wave EMI since their spectral components are less variable between the different independent windowed time frames. This particular fact was also verified by the resulting ranges observed at 200 and 400 MHz for which the difference was about 1.2 dB.

VI. Discussion

Leaving aside the outstanding time-saving capabilities of TDEMI measurement systems, one of their most important limitations is that the equivalent measurement time cannot be as long as the one achieved by the conventional super-heterodyne EMI test receivers, simply because of memory restrictions for storing the digitized signal. Therefore, from the statistical point of view, the sample size (EMI observation time) is smaller in TDEMI measurement systems.

However, this is not necessarily a weakness of the TDEMI systems, provided an adequate understanding of the measurement results and their proper statistical processing. In fact, TDEMI measurement systems give us interesting insights of the results through the exploration of the statistical properties of the measured EMI. This would not be easily achieved using the conventional frequency domain approach.

In that sense, TDEMI measurement systems shall continue improving through alternative measurement approaches. Hence, one of the aspects that still require our attention is the final processing stage of the results, in particular, the emulation of detectors and the development of meaningful measurable quantities for characterizing the EMI.

Particularly, the measurement of the maximum emissions levels of EMI is very important, even more when assessing transient disturbances, since those maximum emissions levels correspond to the specific time frames containing the highest disturbance energy. Therefore, in this paper, we investigated some statistical properties of the peak detection for TDEMI measurement systems.

Using the extreme value theory, the maximum emissions levels were modeled as random variables with the Gumbel distribution. Having a statistical model for the maximum emissions levels allowed us to identify interesting properties involving the PDF of the results. Also, it has been proposed to use the expected maximum emissions to represent the worst-case emissions, since this would improve measurement's repeatability and uncertainty. But $E(\tilde{X}_{\mathrm{peak}})$ is not observable, since it is calculated by means of a statistical model, and it is not equivalent to any measure obtainable with a conventional frequency-domain receiver. This might be seen as a drawback, but we consider it as an opportunity to further research for advancements in our understanding of the EMI measurement systems and process.

Consequently, an aspect that could be cumbersome and challenging for the use of $E(\tilde{X}_{\mathrm{peak}})$ instead of $\tilde{X}_{\mathrm{peak}}$ would be providing a test verdict in its terms, since an adequate interpretation of the expected maximum value is not as easily and intuitively understood at first hand.

Furthermore, one could argue that $E(\tilde{X}_{\mathrm{peak}})$ is not as different from any other results provided by a TDEMI measurement system as it would be natural to think at a first glance. All results provided by a TDEMI measurement system are not observables; they are estimates obtained as output of algorithms and transformations applied to the measured EMI in the time domain, which is the real observable.

VII. Conclusion

The results showed that, using the extreme values theory, the maximum emissions levels can be modeled as random variables with the Gumbel distribution, and the expressions to evaluate its parameters, expected value, variance, and CRBs were provided.

The expected maximum emissions $E(\tilde{X}_{\mathrm{peak}})$ complement the observed maximum emissions levels $\tilde{X}_{\mathrm{peak}}$ as a metric to represent the worst-case emissions. This provides a better measurement repeatability because $E(\tilde{X}_{\mathrm{peak}})$ has less variance than $\tilde{X}_{\mathrm{peak}}$. Additionally, the proposed model indicates the measurement variability, and therefore, the uncertainty can be reduced for TDEMI measurement systems by selecting an adequate record length and overlap factor since the number of windowed frames is a variable of influence on the parameters of the Gumbel distribution. This has been verified using the MC simulation and explained through a measurement scenario. On the other hand, since $E(\tilde{X}_{\mathrm{peak}})$ is not observable, it is cumbersome to use it for assessing compliance.

References

[1] *Specification for Radio Disturbance and Immunity Measuring Apparatus and Methods—Part 1-1: Radio Disturbance and Immunity Measuring Apparatus—Measuring Apparatus*, IEC CISPR, 16-1-1 ed. 3.0, 2010.

[2] *American National Standard for Electromagnetic Noise and Field Strength Instrumentation, 10 Hz to 40 GHz Specifications*, ANSI Standard C63.2–2009, 2009.

[3] P. Russer, "EMC measurements in the time-domain," in *Proc. 30th URSI General Assembly and Sci. Symp.*, 2011, pp. 1–35.

[4] *Time-domain Techniques in Receivers: Technical and Standardization Requirements*, Rohde & Schwarz, Munich, Germany, 2012.

[5] C. Keller and K. Feser, "Fast emission measurement in time domain," *IEEE Trans. Electromagn. Compat.*, vol. 49, no. 4, pp. 816–824, Nov. 2007.

[6] G. Gradoni and L. R. Arnaut, "Generalized extreme-value distributions of power near a boundary inside electromagnetic reverberation chambers," *IEEE Trans. Electromagn. Compat.*, vol. 52, no. 3, pp. 506–515, May 2010.

[7] F. Krug and P. Russer, "Quasi-peak detector model for a time-domain measurement system," *IEEE Trans. Electromagn. Compat.*, vol. 47, no. 2, pp. 320–326, May 2005.

[8] C. Hoffmann and P. Russer, "A time-domain system for EMI measurements above 1 GHZ with high sensitivity," in *Proc. German Microw. Conf.*, 2011, pp. 1–4.

[9] F. Krug and P. Russer, "Signal processing methods for time domain EMI measurements," in *Proc. IEEE Int. Symp. Electromagn. Compat.*, 2003, vol. 2, pp. 1289–1292.

[10] S. Braun and P. Russer, "A low-noise multiresolution high-dynamic ultra-broad-band time-domain EMI measurement system," *IEEE Trans. Microw. Theory Tech.*, vol. 53, no. 11, pp. 3354–3363, Nov. 2005.

[11] S. L. Marple, *Digital Spectral Analysis with Applications*. New York, NY, USA: Dover, 2014.

[12] M. A. Azpúrua, M. Pous, S. Çakir, M. Çetintaş, and F. Silva, "Improving time-domain EMI measurements through digital signal processing," *IEEE Electromagn. Compat. Mag.*, vol. 4, no. 2, pp. 66–74, 2015.

[13] S. Coles, *An Introduction to Statistical Modeling of Extreme Values*. London, U.K.: Springer, 2013.

[14] E. J. Gumbel, *Statistics of Extremes*. New York, NY, USA: Dover, 2012.

[15] *NIST/SEMATECH e-Handbook of Statistical Methods*, U.S. Dept. Commerce, Nat. Inst. Standards Technol., Gaithersburg, MD, USA, 2012.

[16] H. N. Phien, "A review of methods of parameter estimation for the extreme value type-1 distribution," *J. Hydrol.*, vol. 90, no. 3–4, pp. 251–268, Apr. 1987.

[17] G. Corsini, F. Gini, M. V. Greco, and L. Verrazzani, "Cramer-Rao bounds and estimation of the parameters of the Gumbel distribution," *IEEE Trans. Aerosp. Electron. Syst.*, vol. 31, no. 3, pp. 1202–1204, Jul. 1995.

[18] M. A. Azpúrua, M. Pous, and F. Silva, "A measurement system for radiated transient electromagnetic interference based on general purpose instruments," in *Proc. Int. Symp. Electromagn. Compat.*, 2015.

Marco A. Azpúrua (M'13) received the B.Sc. degree in telecommunications engineering and the M.Sc. degree in electrical engineering from the Universidad Central de Venezuela, Caracas, Venezuela, in 2008 and 2013, respectively. He is currently working toward the Ph.D. degree at the Electromagnetic Compatibility Group, Universitat Politècnica de Catalunya, Barcelona, Spain.

Formerly, he was a Researcher in the Applied Electromagnetics Laboratory, Instituto de Ingeniería (FII), Caracas, Venezuela. His research interests include electromagnetic compatibility (EMC), antenna and microwave measurement technologies, and estimation of measurement uncertainty in complex systems and validation methods.

Mr. Azpúrua is a Member of the Venezuelan Standardization Committee for the telecommunication sector of CODELECTRA and FODENORCA and has participated in the adoption of the local standards of EMC.

Marc Pous was born in Barcelona, in 1983. He received the M.Sc. degree in telecommunications engineering and Ph.D. degree on the topic "Radiated transient interferences and digital communication systems evaluation" from the Universitat Politècnica de Catalunya (UPC), Barcelona, Spain, in 2009 and 2015, respectively.

From 2003 to 2006, he was with the LGAI Technological Centre, Electromagnetic Compatibility Department. In 2006, he joined Electromagnetic Compatibility Group, UPC, where he has been participating in international and national research projects related with automotive, aerospace, railway, and medical industries. His research is focused on the development of time-domain measurement techniques to capture interferences which are not properly measured following the harmonized electromagnetic compatibility standards.

Ferran Silva (S'93–M'98) received the M.Sc. and Ph.D. degrees from the Universitat Politècnica de Catalunya (UPC), Barcelona, Spain, in 1989 and 1997, respectively.

He is currently an Associate Professor of electronics with the Department of Electronic Engineering, UPC. Since 2000, he has been the Director of the Electromagnetic Compatibility Group, UPC, performing technology transfer activities to the industrial sector. His research interests include electromagnetic compatibility (EMC) in near field and time domain, including transients, with application to automotive, medical systems, and installations. He has made more than 90 publications in journals and conferences and contributed to the Wiley Encyclopedia of Biomedical Engineering. He has participated in 14 research projects related to EMC.

Dr. Silva is a member of the IEEE EMC Society and the Head of the Spanish chapter of this society; he is also member of the Spanish standardization committees SCTC77–210 and the CTN208 SCCISPR210A. He served as the Chairman of the EMC Europe 2006 International Symposium, since then, he is the Chairmen of Board of EMC Europe.

Proc. of the 2017 International Symposium on Electromagnetic Compatibility - EMC EUROPE 2017, Angers, France, September 4-8, 2017

Robust Extreme Value Estimation for Full Time-Domain EMI measurements

Marco A. Azpúrua, José A. Oliva, Marc Pous, Ferran Silva
Grup de Compatibilitat Electromagnètica (GCEM), Departament d'Enginyeria Electrònica (DEE)
Universitat Politècnica de Catalunya (UPC)
Barcelona, Spain
email: marco.azpurua@upc.edu

***Abstract*—A robust approach for estimating the expected maximum levels of radiofrequency, time-varying, electromagnetic emissions is proposed. The expected maximum peak value is intended to provide a statistical approximation for the worst case emissions scenario that accounts for the variability of the measured interference. The estimates are obtained through Monte Carlo resampling from a non-parametric distribution fitted by means of kernel density estimation applied to the time-frequency representation of the assessed interference. As a key advantage, calculating the expected maximum peak value does not require increasing the dwell time or holding the maximum value over successive sweeps. Results indicate the methodology is better suited than previous approaches for calculating the expected maximum peak value because it does not depend on normality assumptions difficult to guarantee in practice. The proposed technique is an example of how full time-domain EMI measurements can be exploited for obtaining further insights.**

Keywords— Statistical signal processing, Extreme value estimation, Electromagnetic interference, Electromagnetic measurements, Time-domain analysis

I. INTRODUCTION

In emission testing, the electromagnetic disturbance spectrum measured with the receiver's peak detector mode is intended to provide a fast realization of the worst-case scenario with regard the interferences produced by the equipment under test (EUT). In swept receivers, increasing the dwell time enables a better approximation to the actual maximum emissions. Likewise, whenever the EUT generates a highly variable electromagnetic interference (EMI), it is the common practice to increase the number of sweeps and to retain the maximum observation for each frequency step, that is, the "max-hold" feature included in most test receivers.

The aforementioned procedure certainly increases the probability of measuring the worst-case emissions, but still can be heavily time consuming if such worst-case scenario is due to an interference of low repetition frequency. In such cases, the triggering capabilities of Full Time Domain EMI measurement systems (Full TDEMI) can be especially helpful for detecting the highest EMI event (in the time domain) and capturing its whole spectrum in a single acquisition [1], [2].

Despite the advantages provided by the trigger in Full TDEMI measurement systems, it is likely that a significantly long dwell time is still required to measure properly the highest EMI levels at each frequency step. However, increasing indefinitely the dwell time is not feasible. For instance, the memory of the oscilloscope limits the maximum dwell time settable in Full TDEMI measurement systems [3]. Additionally, the blind time between successive deep memory acquisitions and the potentially enormous amount of raw data generated poses constraints to the maximum dwell time, and therefore, to the capability of the measurement system to record EUT's highest emissions.

Nonetheless, time-domain EMI measurements enable the extraction of statistical information about the variability of the disturbance. Such information is useful for calculating the expected maximum emissions levels of the EUT under assessment. In this regard, in a previous paper, the authors investigated the statistical properties of the peak detector in time-domain EMI measurements. Using the extreme value theory, the maximum emission levels were modeled as random variables with Gumbel distribution, and the expressions to evaluate its parameters, expected value, variance and Cramer-Rao bounds were provided [4].

In this regard, the expected value and the variance of the maximum electromagnetic emissions were calculated provided the measured interference is normally distributed at each frequency step. On the other hand, the assumption of normality is not necessarily satisfied, as happens commonly with the impulsive noise [5]. Thus, when the EMI magnitude at each frequency bin is not approximately normally distributed, a robust approach to the extreme value estimation is required in order to provide fair estimations of the expected maximum emissions.

This paper presents a numerical approach for the robust estimation of the expected maximum electromagnetic emissions measured with Full TDEMI measurement systems. The content is organized as follows: Section II introduces Full TDEMI measurement systems; Section III presents the methodology for performing a robust extreme value estimation of the EMI; Section IV focuses on a measurement example employed to compare to the results obtained using the analytical approach and, finally, the conclusions.

II. FULL TDEMI MEASUREMENT SYSTEMS

Full TDEMI measurement systems are oscilloscope based implementations of a CISPR 16-1-1 compliant measuring

978-1-5386-0689-6/17/$31.00 ©2017 IEEE

Proc. of the 2017 International Symposium on Electromagnetic Compatibility - EMC EUROPE 2017, Angers, France, September 4-8, 2017

receiver [6]. According to the CISPR standards, they are a type of FFT-based instruments. Unlike real-time EMI receivers, Full TDEMI measurement systems do not have an intermediate frequency stage and the measured frequency range is not divided into sub-bands. That is the fundamental reason why the whole (full) spectrum is measured in each acquisition, which is a key capability for measuring transient EMI. In general, they require digitizing the EMI using much higher sampling rates than other types of FFT-based receivers causing full-spectrum measurements to be memory intensive when standard dwell times are used.

After deep memory acquisition, the software of the Full TDEMI measurement system performs signal processing tasks including windowing, resolution enhancing, resampling, spectral estimation (using the Short-Time Fourier Transform and the Welch's method) and the detector emulation [2]. Those mathematical transformations are responsible for delivering the measurement results in accordance with CISPR 16-1-1 requirements [7].

In general terms, a Full TDEMI measurement system is described by the block diagram shown in Fig. 1. For the measurement of radiated EMI, a broadband antenna shall be used, while for the measurement of conducted EMI corresponds either a line impedance stabilization network (LISN), a capacitive voltage probe or a current clamp. The measured signal could be amplified and/or filtered if better sensitivity is required [2].

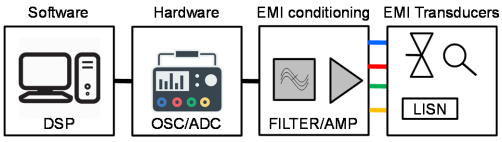

Fig. 1. Block diagram of a Full Time-Domain EMI measurement system [2].

III. ROBUST EXTREME VALUE ESTIMATION FOR EMI MEASUREMENTS

In this section, the fundamental signal processing techniques and the statistical considerations used to estimate robustly the maximum emissions level will be covered in the following subsections.

A. Fundamental signal processing

First, let us consider the continuous-time signal $x(t)$ that represents the EMI under assessment. The measurement process begins when $x(t)$ is digitized and sampled during a time period of length T, at a rate $f_s = N/T_0 = 1/\Delta t$, obtaining the time-discrete signals $x[n]$, where $n = 1, 2, \ldots N$. The digitized EMI signal, $x[n] = x(n\Delta t)$, is assumed to be periodic with the total number of waveform points, which means,

$$x[n+N] = x[n]. \tag{1}$$

Due to the random behavior of EMI, the former assumption of periodicity is not strictly satisfied. However, this is acceptable provided a sufficiently large dwell time with respect to the EMI repetition frequency, that is, $T_0 \gg 1/f_r$. With regard the sampling rate, it must be enough to satisfy the Nyquist criterion and to avoid aliasing [2].

Then, the digitized EMI is transformed to the frequency domain using the Discrete Fourier Transform (DFT) as follows,

$$X[k] = \sum_{n=0}^{N-1} x[n] e^{-i\frac{2\pi nk}{N}}. \tag{2}$$

However, in order to reduce the scalloping loss and the spectral leakage caused by the finite length the time record, $x[n]$ must be multiplied by a window function $w[n]$. It shall be noted that the windowing function is such that its frequency response suits the IF filter requirements of an EMI receiver [8]. If windowing is used, it is necessary to compensate the corresponding energy loss caused by the window using the coherent gain scaling factor [9].

Consequently, to obtain a spectral estimation with the required resolution bandwidth, RBW (that is, 200 Hz, 9 kHz, 120 kHz and 1 MHz for CISPR bands A, B, C/D and, E, respectively), the minimum record length, N_{min}, shall be

$$N_{min} = f_s \frac{w_f}{\mathrm{RBW}}, \tag{3}$$

where w_f is the window factor of the windowing function used, i.e., Gaussian, Hann or Kaiser-Bessel [2].

If $N > N_{min}$, it is possible to define J overlapping windows of N_{min} length in order to determine the frequency and phase content of the j-th local sections of $x[n]$ as it changes over time. This process, called the Short-Time Fourier Transform (STFT), can be expressed as

$$X[k,\tau] = \sum_{n=0}^{N_{min}-1} x[n-\tau] w[n] e^{-i\frac{2\pi nk}{N_{min}}}, \tag{4}$$

where τ describes the dependency on time of each spectral component of the spectrogram [10]. Consequently, the spectrogram time steps of the STFT are given by

$$t_{steps} = \tau \Delta t = j\,(1-o_f)\,N_{min}\,\Delta t, \tag{5}$$

for $j = 1, 2, \ldots J$. Likewise, the spectrogram frequency bins are $f_{bins} = k\Delta f$, where Δf is the frequency resolution. An adequate overlap factor, o_f, must be used to reduce amplitude error caused by the scalloping loss up to an acceptable level [11], [12].

Subsequently, the STFT can be rearranged in a matrix form with the values of each spectral component in the rows and as the time steps in the columns, that is,

$$\mathbf{X}[k,j] = \begin{bmatrix} X[1,1] & X[1,2] & \cdots & X[1,J] \\ X[2,1] & X[2,2] & \cdots & X[2,J] \\ \vdots & \vdots & \ddots & \vdots \\ X[k_{max},1] & X[k_{max},2] & \cdots & X[k_{max},J] \end{bmatrix}. \tag{6}$$

Considering (6) provides the information of the time-frequency distribution of $x(t)$, $\mathbf{X}[k,j]$ can be used for calculating the different detector modes required for standard

978-1-5386-0689-6/17/$31.00 ©2017 IEEE

Proc. of the 2017 International Symposium on Electromagnetic Compatibility - EMC EUROPE 2017, Angers, France, September 4-8, 2017

EMI measurements [4], [12], [13]. In the particular case of the peak detector, $X_{peak}[k]$, it corresponds to,

$$X_{peak}[k] = \max\left\{\left|\mathbf{X}[k,j]\right| \,\middle|\, j \in \{1,2,...J\}\right\}, \quad (7)$$

B. Distribution analysis

Expressions for the expected maximum EMI levels will be presented. The forthcoming analysis assumes the EMI under assessment behaves as a (cyclostationary) random signal and, that the measured time-frame is an independent and representative sample of the interference under assessment.

In this regard, the windowed time frames obtained by the STFT (6) are a group of subsamples from which the EMI spectral content was estimated J times, one spectral estimation from each subsample. The variations of the spectral content at each frequency bin are then analyzed in terms of random variables. This means $X_{peak}[k]$ is an estimator of the extreme value taken by each component of the amplitude spectrum.

If $G_{max}(X[k])$ is the cumulative distribution of $X_{peak}[k]$,

$$G_{\max}\left(X[k]\right) = P\left(X_{peak}[k] \le X[k]\right), \quad (8)$$

and, considering independence between the outcomes of the spectral estimation of each individual subsample, and also, that each individual subsample is identically distributed as $F(X[k])$ since they belong to the same population, then,

$$G_{\max}\left(X[k]\right) = \prod_{j=1}^{J} P\left(X_j[k] \le X[k]\right) = \left[F(X[k])\right]^J. \quad (9)$$

Finally, the probability density function (PDF) of $X_{peak}[k]$ is given by the derivative of $G_{max}(X[k])$, that is,

$$X_{peak}[k] \sim J\left[F(X[k])\right]^{J-1} f\left(X[k]\right), \quad (10)$$

where $f(X[k])$ is the PDF of $X[k]$. This means the PDF of the maximum of each spectral component depends directly on the sample size and on the distribution function of the spectral component.

Unfortunately, the distribution function of each spectral component is generally unknown. However, the generalized extreme value (GEV) distribution allows modeling the largest (and the smallest) value among a large set of independent, identically distributed random values [14], therefore, $X_{peak}[k] \sim f_{GEV}(X[k];\alpha[k],\beta[k],\xi[k])$. In that sense, the GEV distribution is given by,

$$f_{GEV}(X;\alpha,\beta,\xi) = \frac{1}{\beta}\exp\left(-\left(1+\xi\frac{(X-\alpha)}{\beta}\right)^{-\frac{1}{\xi}}\right)\left(1+\xi\frac{(X-\alpha)}{\beta}\right)^{-1-\frac{1}{\xi}} \quad (11)$$

where α, β and, ξ are called the location, scale and, shape parameters respectively. It is important to notice that the dependency with the discrete frequency, k, has been intentionally omitted from (11) for a better readability of the equation.

C. Parameter estimation

In a previous work [4], the above mentioned GEV distribution was simplified to the ξ=0 case, called Gumbel distribution in order to obtain an analytic expression of the location and scale parameters under the assumption that $X[k]$ is normally distributed.

Nonetheless, for the generality of cases, such normality could not be granted and a robust calculation methodology must be applied. However, from each EMI measurement there is a single peak value per frequency step and, consequently, it is not possible to perform parameter estimation based on a sample of maximum values.

In this regard, a numerical approach based on non-parametric distribution fitting and resampling techniques is proposed. In order to proceed, the first step is to create a non-parametrical model for the distribution of $X[k]$ using kernel density estimation (KDE), using (12) [15]. In particular, a Gaussian kernel is used (13) [15], that is,

$$X[k] \sim f\left(X[k]\right) \approx \frac{1}{Jh}\sum_{j=1}^{J} K\left(\frac{X[k]-X[k,j]}{h}\right), \quad (12)$$

where $K(\bullet)$ is the kernel function and $h > 0$ is the smoothing parameter called bandwidth, which are given by,

$$K(u) = \frac{1}{2\pi}e^{-\frac{1}{2}u^2}, \text{ and,} \quad (13)$$

$$h = \left(0.9J^{-1/5}\right)\min\left\{\hat{\sigma}, \text{IQR}/1.34\right\}, \quad (14)$$

where $\hat{\sigma}$ is the standard deviation of the sample and the IQR is the interquartile range. The criteria for choosing h was selected because it provides good performance for both unimodal and bimodal densities in terms of the mean integrated square error[15].

Then, a large number of equally sized samples distributed according to (12) is generated using a Monte Carlo approach. This means, a number $M \ge 1000$ of samples having each J pseudorandom elements approximately distributed as $X[k]$ was computationally generated. Next, (7) is applied to each sample in order to create a set, $S_{peak}[k]$, of maximum values for each frequency step.

$$S_{peak}[k] = \left\{X_{peak,1}[k], X_{peak,2}[k], ...X_{peak,M}[k]\right\}, \quad (15)$$

Finally, α, β and, ξ are estimated using the Maximum Likelihood Estimation (MLE) method for each frequency step.

D. Expected value for the maximum EMI levels

It can be demonstrated that, for $X_{peak}[k] \sim f_{GEV}(X[k];\alpha[k],\beta[k],\xi[k])$, the expected value for the maximum EMI levels is,

$$E\left(X_{peak}\right) = \begin{cases} \alpha + \beta\left(\Gamma(1-\xi)-1\right)/\xi & \text{for } \xi \ne 0,\ \xi < 1 \\ \alpha + \beta\gamma & \text{for } \xi = 0 \\ \infty & \text{for } \xi \ge 1 \end{cases}, \quad (16)$$

978-1-5386-0689-6/17/$31.00 ©2017 IEEE

Proc. of the 2017 International Symposium on Electromagnetic Compatibility - EMC EUROPE 2017, Angers, France, September 4-8, 2017

where γ is the Euler–Mascheroni constant ($\gamma \approx 0.5772$), $\Gamma(\bullet)$ is the gamma function and the dependency with the discrete frequency, k, has been omitted for clarity.

IV. APPLICATION EXAMPLE

This section comprises the measurement methodology and an application example relevant for showing the differences between the estimations performed using the robust and the classical approaches.

A. Test setup

The specific Full TDEMI measurement system that serves as measuring receiver is based on a real-time sampling digital storage oscilloscope Tektronix DPO5104B. A detailed explanation of the features of this Full TDEMI measurement system is found in [3].

In the same manner, an explicit description of the signal processing techniques applied to the measured signal is given in [2]. Measurements were performed using a standard setup for radiated emissions assessment inside a full anechoic chamber.

The sampling frequency was set to 5 GSamples/s. The resolution bandwidth was configured at 120 kHz and the dwell time was set to 10 ms. The measurement distance was 3 m and a Schaffner CBL6143 bilog antenna in horizontal polarization was used. The EMI was generated by a pair of personal computers while transferring a large video file through an Ethernet link.

B. Measurement results

Fig. 2 shows the EMI measurement results obtained by using the standard peak and CISPR average detectors. The weighting caused by the average detector responds to the fluctuation of the EMI levels within the measured time-frame.

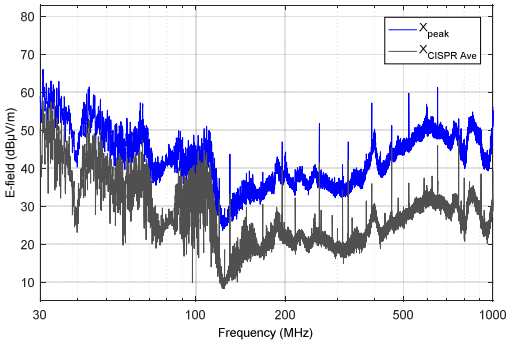

Fig. 2. EMI measurement results with the standard peak and CISPR average detectors.

The time-frequency response of the measured EMI is shown in Fig. 3 spectrogram. On the one hand, it is observed that most components of the lower frequency EMI spectrum are cyclic and stationary. However, above 500 MHz the highest emissions occur during a 3 ms burst-like event.

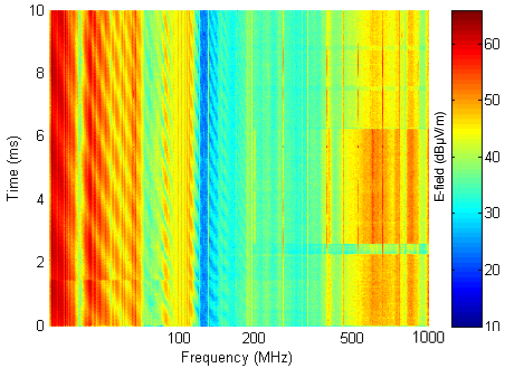

Fig. 3. Spectrogram of the measured EMI.

Likewise, the persistence plot of the measured EMI is useful to realize how the interference varies in amplitude. In that sense, Fig. 4 shows in red tones the most probable amplitude levels and fades to blue tones for the less observed values.

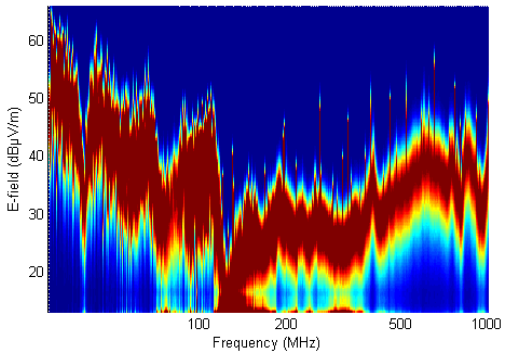

Fig. 4. Persistence plot of the measured EMI.

C. Extreme value analysis

Given the variability observed in the measurement results (Fig. 4), the actual maximum emissions levels could be even higher than the measured peak values. To investigate this, first, a distribution analysis was carried out. In this regard, the amplitude probability distribution of the EMI at three different frequencies is presented, as an example, and their maximum peak values are then estimated using the proposed methodology. Those frequencies are f_1=30.63 MHz, f_2=260.6MHz and, f_3=947.3MHz.

Fig. 5 presents the probability density function fitted for the EMI amplitude at the aforementioned frequencies. It also shows the measured peak value and the expected maximum peak value with the triangle and diamond markers, respectively. It is remarkable how the distribution of the interference changes with frequency. However, at the selected frequencies, the amplitudes have a bell-shaped distribution.

978-1-5386-0689-6/17/$31.00 ©2017 IEEE

Proc. of the 2017 International Symposium on Electromagnetic Compatibility - EMC EUROPE 2017, Angers, France, September 4-8, 2017

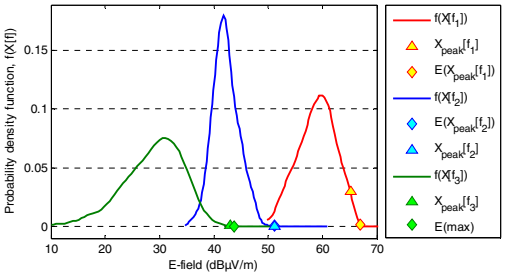

Fig. 5. Estimated probability density functions for the amplitude of the measured EMI at the selected frequencies: f_1 = 30.63 MHz, f_2 = 260.6 MHz and f_3 = 947.3 MHz.

By using the normal probability plot shown in Fig. 6, some remarkable characteristics of the distributions come to light. For instance, the amplitude of some frequency components can be skewed, as happens with $X[f_3]$, or the shape of the distribution tails (fat/short) may depart from the normal distribution which would lead to inaccurate estimations based on the approach that assumes normality [16].

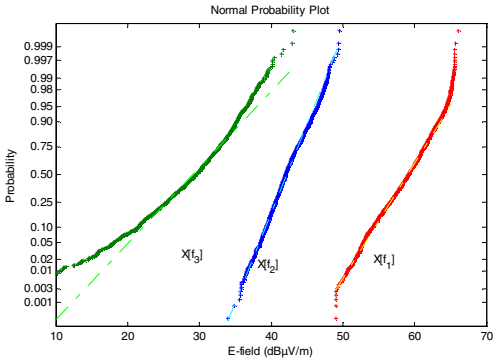

Fig. 6. Normal probability plot for the amplitude of the measured EMI at the selected frequencies.

Consequently, significant differences arises when estimating the maximum peak EMI values depending on the selected approach, as shown in Table I.

TABLE I. COMPARISON OF THE ROBUST AND THE CLASICAL EXPECTED PEAK VALUES AT THE SELECTED FREQUENCIES

Frequency [MHz]		X_{peak} [dBµV/m]	E(X_{peak}) [dBµV/m]	Robust E(X_{peak}) [dBµV/m]
f_1	30.63	65.16	70.72	67.01
f_2	260.6	51.61	51.66	51.61
f_3	974.3	42.46	49.35	43.26

Likewise, the differences in the expected peak values obtained with the classical and with the robust approach are evident when represented in the whole frequency range, as shown in Fig. 7.

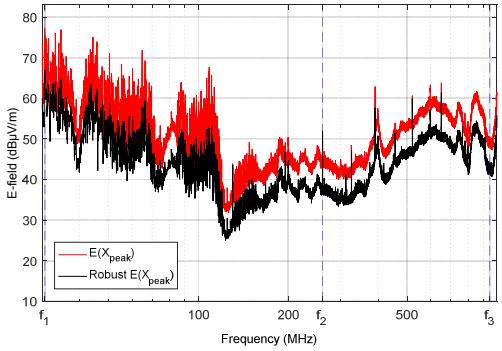

Fig. 7. Comparison of the robust and the clasical expected peak EMI values.

In general, the robust approach delivered more conservative and reasonable estimates. By using the robust estimation, approximately 80% of the frequency components are expected to have a maximum peak value that is less than 1 dB higher than the actual measured value, as shown in Fig 8.

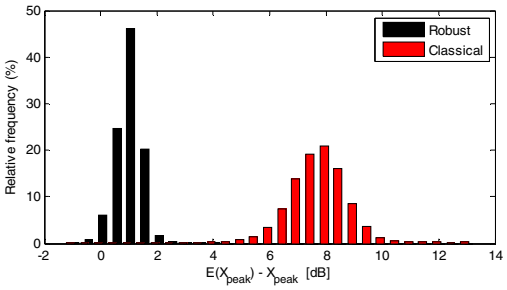

Fig. 8. Histograns of relative frequency for the difference between the measured and the expected peak values.

Likewise, according to the robust estimation, the maximum difference encountered between the expected peak and the measured peak was 3.78 dB at f_4 = 43.17 MHz. Analyzing the distribution of the EMI at that frequency (Fig. 9), it was noticed that the amplitudes were largely variable and that the distribution is bimodal, which explains the higher expected peak value.

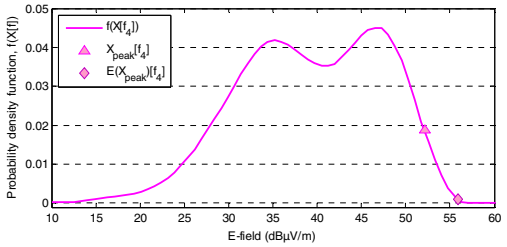

Fig. 9. Estimated probability density functions for the EMI amplitude at f_4 = 43.17 MHz.

978-1-5386-0689-6/17/$31.00 ©2017 IEEE

Proc. of the 2017 International Symposium on Electromagnetic Compatibility - EMC EUROPE 2017, Angers, France, September 4-8, 2017

On the contrary, the estimates obtained by means of the classical Gumbel distribution approximation based on a normality assumption lead to an overestimation of the extreme values, with a mean difference of 7.79 dB between the expected peak and the measured peak.

V. CONCLUSION

A robust statistical estimation of the expected peak EMI value of signal sources which are time varying was achieved following a numerical approach that combines kernel density estimation and Monte Carlo resampling for calculating the parameters of a GEV distribution that model the measured peak emissions as random variables. A key advantage of this approach is that it does not require increasing the dwell time or holding the maximum value over successive frequency sweeps. The experiment confirms this methodology is best suited for calculating the expected maximum peak value of time varying interferences than previous analytical approximations because it does not rely on normality assumptions difficult to ensure in practice.

The proposed technique is an example of how the information provided by full time-domain EMI measurements can be used for obtaining complementary measurement insights helpful in the assessment of the EUT's worst-case emissions that is required for risk and reliability analysis.

In a broader sense, this method could be extended to analyze several factors that influence the EUT's maximum emissions, e.g., the cable layout, turntable rotation, height of the antenna, antenna polarization or even the EUT software configuration Further research is foreseen to allow estimating the distribution function and the maximum EUT's emissions based on larger and more complex data sets comprising the abovementioned sources of variability.

ACKNOWLEDGMENT

This work was supported in part by the EURAMET 15RPT01 research project (the EMPIR is jointly funded by the EMPIR participating countries within EURAMET and the European Union), by the Spanish "Ministerio de Economía, Industria y Competitividad," under projects TEC2013- 48414-C3-3-R and TEC2016-79214-C3-2-R (AEI/FEDER, UE), by the "Secretaria d'Universitats i Recerca del Departament d'Economia i Coneixement de la Generalitat de Catalunya" and the European Social Fund.

REFERENCES

[1] M. Pous, M. Azpúrua, and F. Silva, "Benefits of full time-domain EMI measurements for large fixed installation," *2016 International Symposium on Electromagnetic Compatibility - EMC EUROPE*. pp. 514–519, 2016.

[2] M. A. Azpúrua, M. Pous, S. Çakir, M. Çetintaş, and F. Silva, "Improving Time-Domain EMI measurements through Digital Signal Processing," *Electromagn. Compat. Mag. IEEE*, vol. 4, no. 2, pp. 66–74, 2015.

[3] M. A. Azpúrua, M. Pous, and F. Silva, "A Measurement System for Radiated Transient Electromagnetic Interference Based on General Purpose Instruments," in *Electromagnetic Compatibility (EMC EUROPE), International Symposium on*, 2015.

[4] M. A. Azpurua, M. Pous, and F. Silva, "On the Statistical Properties of the Peak Detection for Time-Domain EMI Measurements," *IEEE Trans. Electromagn. Compat.*, vol. 57, no. 6. IEEE, 2015, pp. 1374–1381.

[5] M. Pous, M. A. Azpúrua, and F. Silva, "Measurement and Evaluation Techniques to Estimate the Degradation Produced by the Radiated Transients Interference to the GSM System," *IEEE Trans. Electromagn. Compat.*, vol. 57, no. 6. 2015, pp. 1382–1390.

[6] M. A. Azpurua, M. Pous, F. Silva, and J. A. Oliva, "Fast and Automated Verification of Multi-channel Full Time-Domain EMI measurement systems," in *2017 IEEE International Instrumentation and Measurement Technology Conference (I2MTC)*, 2017.

[7] IEC CISPR, *16-1-1 ed4.0: Specification for radio disturbance and immunity measuring apparatus and methods - Part 1-1: Radio disturbance and immunity measuring apparatus - Measuring apparatus*. IEC, 2015.

[8] C. Keller and K. Feser, "Fast Emission Measurement in Time Domain," *IEEE Trans. Electromagn. Compat.*, vol. 49, no. 4, 2007.

[9] S. L. Marple, *Digital Spectral Analysis With Applications*. Dover Publications, 2014.

[10] A. Frech, A. Zakaria, S. Braun, and P. Russer, "Ambient noise cancelation with a time-domain EMI measurement system using adaptive filtering," *2008 Asia-Pacific Symposium on Electromagnetic Compatibility and 19th International Zurich Symposium on Electromagnetic Compatibility*. pp. 534–537, 2008.

[11] S. Braun, A. Frech, and P. Russer, "CISPR specification and measurement uncertainty of the time-domain EMI measurement system," *2008 IEEE International Symposium on Electromagnetic Compatibility*. pp. 1–4, 2008.

[12] S. Braun, T. Donauer, and P. Russer, "A real-time time-domain EMI measurement system for full-compliance measurements according to CISPR 16-1-1," *IEEE Trans. Electromagn. Compat.*, vol. 50, no. 2, pp. 259–267, 2008.

[13] F. Krug and P. Russer, "Quasi-peak detector model for a time-domain measurement system," *IEEE Trans. Electromagn. Compat.*, vol. 47, no. 2, pp. 320–326, 2005.

[14] S. Coles, *An Introduction to Statistical Modeling of Extreme Values*. Springer London, 2013.

[15] B. Silverman, "Density estimation for statistics and data analysis," *Chapman Hall*, vol. 37, no. 1, pp. 1–22, 1986.

[16] U. S. Methods, "NIST/SEMATECH, Handbook of Statistical Commerce Department," 2012.

978-1-5386-0689-6/17/$31.00 ©2017 IEEE

6

DECOMPOSITION OF EMI IN THE TIME-DOMAIN

The publications in subsections 6.1, 6.2 and, 6.3 comprise the contributions related to the decomposition of EMI in the time-domain. Considering the Thesis objectives, the most remarkable contributions are outlined below.

Objective 2: The required measurement setup and processing method for ambient noise cancellation using a single antenna was developed and reported. Likewise, the measurement setup and processing method for APD measurements in the presence of broadcasting signals of communications systems was developed and reported.

Objective 3: Algorithms for implementing the empirical mode decomposition for electromagnetic interferences with additional capabilities for detecting and separating, transient-like, impulse noise, were developed. Then, the developed techniques were employed for attenuating, more than 20 dB, broadcasting signals present in EMI measurements performed outside a shielded room. In the same manner, this method was employed for extracting the information about the impulsive noise even in the presence of broadcasting signals during outdoor measurement camping's. APD diagrams of the EMI were measured accurately after the suppression of the communication system signal.

6.1. FUNDAMENTAL JOURNAL ARTICLE 3

M. A. Azpúrua, M. Pous and F. Silva, "Decomposition of Electromagnetic Interferences in the Time-Domain," in *IEEE Transactions on Electromagnetic Compatibility*, vol. 58, no. 2, pp. 385-392, April 2016. doi: 10.1109/TEMC.2016.2518302

Abstract-Electromagnetic interferences are potentially very complex signals formed by the superposition of transient (broadband) and continuous wave (narrowband) components with significant randomness in both amplitude and phase. Decomposing the electromagnetic interference measured in the time domain into a set of intrinsic mode functions is useful to gain insights of the process that generates the interference. Evaluating the intrinsic mode functions contributes to improving the measurement capabilities of the time-domain electromagnetic emissions measurement systems based on the general-purpose oscilloscopes. In this paper, a combination of techniques that includes empirical mode decomposition and transient

mode decomposition is used to separate the main components of complex electromagnetic disturbances. This approach requires no prior information on the spectral content of the measured EMI and it does not perform a domain transformation. Examples of electromagnetic interference decomposition verify the effectiveness and the accuracy of the proposed approach. Finally, a discussion on the advantages, practical applications, limitations, and drawbacks of the described techniques is addressed.

6.2. CONFERENCE PROCEEDING 6

M. A. Azpúrua, M. Pous and F. Silva, "A single antenna ambient noise cancellation method for in-situ radiated EMI measurements in the time-domain," *2016 International Symposium on Electromagnetic Compatibility - EMC EUROPE*, Wroclaw, 2016, pp. 501-506. doi: 10.1109/EMCEurope.2016.7739185

Abstract-This paper presents a single antenna ambient noise cancellation method for in-situ radiated emissions measurements performed using an entirely time-domain approach and the sliding window Empirical Mode Decomposition. The method requires a pair of successive measurements, an initial one for characterizing the ambient noise and a final one for the EMI measurement in the presence of ambient noise. The method assumes the spectral content of the ambient noise is stable between both measurements. The measured time-domain EMI is decomposed into a finite set of intrinsic mode functions. Some modes contain the ambient noise signals while other modes contain the actual components of the EMI. A brute-force search algorithm determines which mode, or combination of modes, maximize the absolute difference between the magnitude of their spectrum and the ambient noise levels for every frequency bin in the measurement bandwidth. Experimental results show the effectiveness of this method for attenuating several ambient noise signals in the 30 MHz-1 GHz band.

6.3. CONFERENCE PROCEEDING 7

M. Pous, **M. A. Azpúrua** and F. Silva, "APD outdoors time-domain measurements for impulsive noise characterization," *2017 International Symposium on Electromagnetic Compatibility - EMC EUROPE,*, Angers, 2017, pp. 1-6. doi: 10.1109/EMCEurope.2017.8094786

Abstract-A novel measurement and post-processing technique for estimating if impulsive noise is capable of degrading the performance of digital communication systems (DCS) is presented. It is based on the well-known capability of the amplitude probability distribution (APD) to estimate the bit-error-rate of digital communication system in the presence of electromagnetic interferences. However, the APD shall be computed from measurements taken in the absence of the useful signal of the communication system, which is a strong handicap for in-situ measurements. The main contribution of the work presented is the combination of time domain EMI measurements and decomposition techniques for separating the impulsive noise from the narrow band signals of the digital communication systems. Therefore, although the communication system signal is present at the test site, the APD diagram is obtained without the influence of the communication system, which is crucial to directly relate the shape of the diagram with the bit-error-rate introduced by the impulsive noise. This is an important step forward compared with the traditional approach as it offers the possibility to study the impact of impulsive interferences although DCS, such as broadcasting services, are present at interference scenarios.

IEEE TRANSACTIONS ON ELECTROMAGNETIC COMPATIBILITY, VOL. 58, NO. 2, APRIL 2016 385

Decomposition of Electromagnetic Interferences in the Time-Domain

Marco A. Azpúrua, *Member, IEEE*, Marc Pous, and Ferran Silva, *Member, IEEE*

***Abstract*—Electromagnetic interferences are potentially very complex signals formed by the superposition of transient (broadband) and continuous wave (narrowband) components with significant randomness in both amplitude and phase. Decomposing the electromagnetic interference measured in the time domain into a set of intrinsic mode functions is useful to gain insights of the process that generates the interference. Evaluating the intrinsic mode functions contributes to improving the measurement capabilities of the time-domain electromagnetic emissions measurement systems based on the general-purpose oscilloscopes. In this paper, a combination of techniques that includes empirical mode decomposition and transient mode decomposition is used to separate the main components of complex electromagnetic disturbances. This approach requires no prior information on the spectral content of the measured EMI and it does not perform a domain transformation. Examples of electromagnetic interference decomposition verify the effectiveness and the accuracy of the proposed approach. Finally, a discussion on the advantages, practical applications, limitations, and drawbacks of the described techniques is addressed.**

***Index Terms*—Digital signal processing, electromagnetic compatibility, electromagnetic interference, electromagnetic measurements, time-domain analysis.**

I. Introduction

ELECTROMAGNETIC interferences are complex signals composed of the superposition of continuous-wave, transient, and random disturbances. In consequence, measuring properly and defining specific features of an electromagnetic interference (EMI) are challenging tasks.

In this regard, the conventional approach for the evaluation of the electromagnetic emissions consists in measuring the amplitude spectrum of the disturbance using a frequency sweep receiver and the CISPR standard detectors [1]. Therefore, the current standard measurement procedures for assessing an EMI neglect important time-domain characteristics of the electromagnetic disturbances, such as the repetition rate, the different emission profiles of an EUT as it changes its operation mode, and the impact of transient events [2]. This is particularly relevant for evaluating and predicting the degradation suffered by digital communication systems due to the influence of a transient EMI [2]. Consequently, in some cases, the standardized methods of EMI measurement and evaluation are not completely suitable, insufficient or might require an enormous amount of time to provide reliable measurement results [3], [4].

Currently, the fast Fourier transform-based EMI test receivers and real-time spectrum analyzers have time-scan measurement capabilities that overcome many of the limitations of the stepped frequency scan in the EMI receivers. However, the bandwidth of their intermediate frequency filter and the tradeoff between the time domain and the frequency-domain resolutions [5] are their main constraints for measuring simultaneously broadband and narrowband interferences on the whole frequency range. Recently, advances in an EMI postprocessing and the enhanced capabilities of digital oscilloscopes allowed to implement entirely time-domain EMI (TDEMI) measurement systems. Those TDEMI systems provide accurate, full spectrum, multichannel, time saving, and cost-effective EMI measurements [6].

Nonetheless, estimating the spectral content of an EMI is only one side of a multifaceted problem. For example, transient, intermittent, or event triggered (i.e., by changing operation modes) disturbances could be unnoticed by conventional frequency sweep EMI measurements because the unsynchronized occurrence of the EMI and its short duration. Previous research has addressed some of those problems using time-domain EMI analysis. In particular, Alban *et al.* [7] used an ad hoc oscilloscope-based TDEMI measurement system for developing a statistical model for the broadband noise in computing platforms. In the field of power electronics, time-domain EMI measurements have also been used for providing time-frequency-energy distributions by means of the wavelet analysis used for emissions mitigation in chaotic converters [8]. More recently, statistical approaches to the evaluation of EMI measured in the time-domain have been used to predict the degradation caused by transient disturbances on digital communication systems [2], [9] and to model the distribution of peak measurements using extreme value theory [10].

In that sense, exploring new processing approaches and techniques is fundamental to enhance the performance of such TDEMI systems. In particular, this paper presents an entirely time-domain method that comprises techniques and algorithms for signal decomposition that offer further possibilities to EMI analysis. This method is based on the empirical mode decomposition (EMD) [11] and includes a preliminary stage of transient EMI separation that improves EMD performance.

The decomposition of an EMI in the time-domain seeks to decompose the main components of the measured signal

Manuscript received June 16, 2015; revised November 20, 2015; accepted January 4, 2016. Date of publication January 25, 2016; date of current version March 8, 2016. This work was supported in part by the EURAMET IND60EMC research project (the EMRP is jointly funded by the EMRP participating countries within EURAMET and the European Union) and by the Spanish "Ministerio de Economía y Competitividad," under project TEC2013-48414-C3-3-R.

The authors are with Group of Electromagnetic Compatibility, Department of Electronic Engineering, Polytechnic University of Catalonia, Barcelona 08034, Spain (e-mail: marco.azpurua@upc.edu; marc.pous@upc.edu; ferran.silva@upc.edu).

Color versions of one or more of the figures in this paper are available online at http://ieeexplore.ieee.org.

Digital Object Identifier 10.1109/TEMC.2016.2518302

0018-9375 © 2016 IEEE. Personal use is permitted, but republication/redistribution requires IEEE permission.
See http://www.ieee.org/publications_standards/publications/rights/index.html for more information.

without applying a domain transformation. Thus, the transient and continuous-wave modes identified usually have a clearer physical meaning and make it possible to apply specific digital processing techniques for improving the overall measurement result in terms of dynamic range and accuracy.

The structure of the paper is as follows: Section II introduces the EMD and discusses its suitability for analyzing EMI. Then, Section III presents an algorithm for separating the transient pulses from the measured EMI. Through the application examples (Section IV), it will be verified how the aforementioned techniques can also be used to effectively improve the measurement results when transformed to the frequency domain.

Finally, it is important to state that the developed algorithms were mostly implemented in MATLAB code. Therefore, the nomenclature used in the algorithms written as pseudocode is influenced by the MATLAB syntax and functions.

II. Empirical Mode Decomposition

The EMD is a method developed for analyzing nonlinear and nonstationary signals. It was introduced by Huang *et al*. in 1998 [12]. EMD has been successfully used to process biological signals [13] and images [14] among other applications. The main capability of the EMD is to decompose complicated datasets into a finite, and often small, number of components called intrinsic mode functions (IMF) that admit well-behaved Hilbert transforms.

Thus far, EMD has not been used to decompose EMI. However, as time-domain techniques gain more acceptance in the EMI assessment, EMD could provide insights to the understanding of the processes generating the disturbance emissions. Next, the EMD algorithm will be explained in terms of its applications for the EMI decomposition.

A. Overview of the EMD algorithm

The foundation of the EMD is to study heuristically the local oscillations of the signal. This is achieved by looking at the evolution of a signal between two consecutive local extrema in order to define a high-frequency function containing its details, features, and shape characteristics. This detailed oscillation is contained between two minima and includes, necessarily, a local maximum peak value. On the other hand, the complementary low-frequency part (local trend) of the signal is called residual $r(t)$. Then, the aforementioned process is iteratively repeated on the successive residuals for all the oscillations composing the entire signal through a process called "shifting," until all IMF have been found [15]. If the residual is monotonic, it means there are no more IMF to be decomposed, then the shifting algorithm stops the iteration and the EMD is complete. Fig. 1 shows a simplified flowchart for the shifting algorithm of the EMD method.

Then, for a given signal in the time domain $x(t)$, the EMD constructs an equivalent representation in terms of the linear combination of the IMF $c_n(t)$, and the residual, as

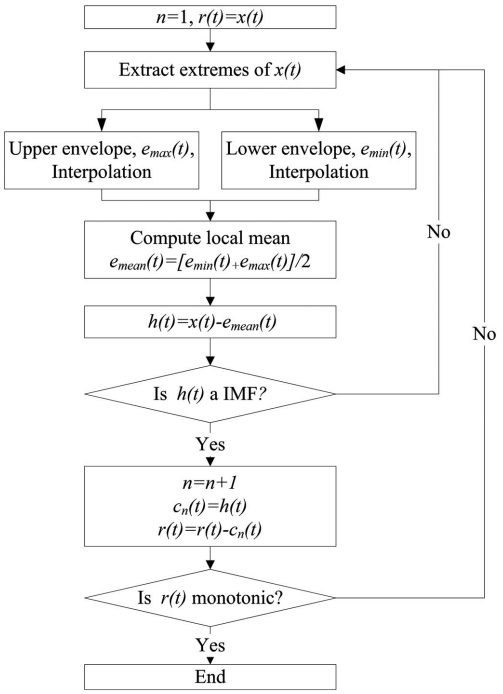

Fig. 1. Flowchart for the "shifting" algorithm of the EMD method. Note: other stopping criteria for the iteration process have also been used [16].

expressed by

$$x(t) = \sum_{n=1}^{N} c_n(t) + r(t) \tag{1}$$

where each mode is constrained to be zero mean and amplitude/frequency modulation waveforms. A complete explanation of the properties of the EMD is provided in [12].

B. EMD of EMIs

Using EMD for analyzing EMI is challenging because of the "mode mixing" phenomena. Mode mixing refers to the presence of oscillations of very disparate amplitude in an IMF or the presence of very similar oscillations in different IMF. Mode mixing often take place when dealing with datasets containing intermittent pulses and noise [17], as usually occurs with EMI.

Additionally, the direct application of the EMD algorithm on measured EMI signals with transient components requires enormous amount of time to reach the stop criteria, because the algorithms attempt to overdecompose the transient pulses, leading to IMF with no clear meaning.

To overcome these drawbacks, it is proposed to separate the transient pulses from the measured EMI in the time domain, as will be explained in the next section. In this case, the transient signal extracted from the EMI is considered to be the first IMF. Then, a variant of the EMD called ensemble empirical mode decomposition (EEMD) is applied on the first residual component of the EMI. EEMD performs the EMD over an ensemble of the signal and additive white Gaussian noise (AWGN). The addition of the AWGN aids solving the mode mixing problem by populating the whole time-frequency space to take advantage of the dyadic filter bank behavior of the EMD [18]. An implementation of the EEMD algorithm has been developed and made available by [19].

III. Transient Mode Decomposition

Before applying EEMD on the measured EMI, the transient pulses shall be separated from the continuous EMI. This is achieved through the automatic recognition of the transients as high amplitude and short-duration signals. By identifying the transient mode within the EMI, it is also possible to estimate its pulse repetition frequency. In order to do so, several processing steps are required due to the potential complexity of the measured EMI. The transient mode decomposition (TMD) algorithm has been implemented in three stages: 1) envelope detection, 2) identification of the transient events and, 3) estimation of the pulse repetition frequency. In the following sections, this algorithm will be explained.

A. Envelope Detection

First, the measured EMI in the time domain $x(t)$ is processed to obtain its analytic signal $x_a(t)$, that is,

$$x_a(t) = A(t)\, e^{j\phi(t)} = x(t) + jH\{x\}(t) \tag{2}$$

where $A(t)$ is the instantaneous amplitude and $H\{x\}(t)$ is the Hilbert Transform of $x(t)$, which is given by [20]

$$H\{x\}(t) = \frac{1}{\pi}\int_{-\infty}^{\infty} \frac{x(\tau)}{t-\tau} d\tau. \tag{3}$$

The instantaneous amplitude allows a better identification of the features of the signal, such as peaks. Next, the algorithm builds a vector with the local maxima found in $A(t)$, x_{peak}, and a vector containing their corresponding time of occurrence t_{peak}. Considering EMI measurements that are intrinsically noisy, the algorithm uses functions for robust peak detection in the presence of random noise that include prominence criteria between adjacent peaks [21].

In general, the elements of x_{peak} are not uniformly distributed in time. Therefore, the robust envelope signal $x_{\text{env}}(t)$ is obtained by interpolating x_{peak} within the measured time interval and then x_{peak} is resampled at the same rate. The specific interpolation method implemented in this part of the algorithm was cubic interpolating splines since it is fast, efficient, and stable [22]. However, other shape preserving interpolation methods can be used. Finally, $x_{\text{env}}(t)$ is scaled to the amplitude of $x(t)$. The simplified algorithm for envelope detection is described as pseudocode.

Algorithm 1-a): Robust envelope detection

$A(t) \leftarrow |x(t) + jH\{x\}(t)|$
$[\,x_{\text{peak}} \quad t_{\text{peak}}\,] \leftarrow \text{peaks}(A(t))$
$x_{\text{env}}(t) \leftarrow spline([\,x_{\text{peak}} \quad t_{\text{peak}}\,], t)$
$x_{\text{env}}(t) \leftarrow scale(x_{\text{env}}(t), x(t))$

B. Identification of Transient Events

TMD second step consists of identifying the start and stop instants of the transient events. For accomplishing this, it is required to define a threshold level δ used as a virtual trigger point for analyzing the transients in $x_{\text{env}}(t)$. However, considering the variability of the peaks, δ must be empirically estimated to provide sufficient sensitivity to the algorithm.

In this regard, δ is calculated considering the ranges of amplitude of the prominent peaks of the envelope signal. Then, an observation window x_w is defined as a subinterval of $x_{\text{env}}(t)$ extracted to evaluate locally the behavior of the envelope signal in order to decide whether and when the transient has finished. The time lapse covered by x_w is Δt and x_w is centered in the observation instant t_{obs}. Δt has been selected as the period of the lowest frequency tone measurable in the band assessed. The basic algorithm written as pseudocode is presented subsequently.

Algorithm 1-b): Automatic identification of the transient events and their durations

```
while t_obs ≤ t_max
    if x_env(t_obs) ≥ δ
        N_events ← N_events + 1
        for t_end = t_obs + Δt/2:t_max − Δt/2
            x_w = x_env(t_end − Δt/2:t_end + Δt/2)
            if x̄_w ≤ α
                start(N_events) ← t_obs
                stop(N_events) ← t_end
                t_obs ← t_end + 1
            end
        break
        end
    t_obs ← t_obs + 1
    end
end
```

In consequence, the algorithm above uses δ to decide if during a certain instant t_{obs} a transient event has been encountered and then examines the mean value of x_w to decide whether or not the transient event has finished in terms of a specified sensitivity factor α. Then, the transient mode is the part of the EMI that occurs between the detected start and stop instants. The continuous EMI is calculated by subtracting the transient mode from the EMI signal.

Afterward, the duration of the N_{events} detected transients are calculated as the difference between the vector containing the start time and the one containing the stop instants. The duration vector is statistically analyzed in order to find significant differences between the transient durations and also to reject outliers,

particularly using the modified Thompson's Tau method [23]. Finally, the average transient event duration $\overline{\Delta t}_{\mathrm{dur}}$ is calculated. The average transient event duration is an important parameter because it can be used to configure the proper record length when performing segmented memory acquisitions in order to optimize the exploitation of the available memory in oscilloscopes [6].

C. Estimation of the Pulse Repetition Frequency

The final step of the TMD algorithm is the estimation of the pulse repetition frequency $\hat{f}_{\mathrm{rep}}$. Estimating $\hat{f}_{\mathrm{rep}}$ is not mandatory for decomposing the EMI in the time domain, but it can be helpful for identifying the source of the inference. In this regard $\hat{f}_{\mathrm{rep}}$ shall be estimated considering the impact of the jitter in successive transient events and the variability in the duration of the detected transient pulses due to the randomness of the measured signal amplitude with respect to the fixed threshold.

Therefore, for estimating the pulse repetition frequency $\hat{f}_{\mathrm{rep}}$, it is required to measure the central tendency of the inverse of the time shift between the start instants and also between the stop instants of successive transient events $\Delta t_{\mathrm{start}}$ and Δt_{stop}. It is important to notice that for estimating the pulse repetition frequency there shall be at least two transient events detected.

The procedure for calculating $\hat{f}_{\mathrm{rep}}$ is described in the following part of the algorithm. $\Delta t_{\mathrm{start}}$ and Δt_{stop} are one-dimensional vector variables and the multiplicative inverse operation done in the third step is performed element-by-element. In the same manner, the $\mathrm{median}()$ function calculates the statistical median of the concatenated vectors $(\Delta t_{\mathrm{start}})^{-1}$ and $(\Delta t_{\mathrm{stop}})^{-1}$.

Algorithm 1-c): Median pulse repetition frequency

1: $\Delta t_{start} \leftarrow start(1 : N_{\mathrm{events}} - 1) - \mathrm{start}(2 : N_{\mathrm{events}})$
2: $\Delta t_{stop} \leftarrow stop(1 : N_{\mathrm{events}} - 1) - \mathrm{stop}(2 : N_{\mathrm{events}})$
3: $\hat{f}_{\mathrm{rep}} \leftarrow median([\,(\Delta t_{\mathrm{start}})^{-1}\ (\Delta t_{\mathrm{stop}})^{-1}\,])$

IV. Application Examples

In this section, examples of EMI decomposition in the time domain will be presented. First, a low-frequency EMI signal was emulated using a controlled test signal synthesized using MATLAB and an Agilent 81160A pulse function arbitrary noise generator. The second scenario corresponds to a radiated emissions test. Measurements were performed with a TDEMI measurement system based on a Tektronix DPO5104B oscilloscope [8]. The assessed bands are in accordance with the CISPR 22 standard for conducted and radiated emissions measurements, respectively.

Despite the specific measurement conditions used for the next application examples, such as frequency range, resolution bandwidth, sampling rate, etc., it is important to remark that the method described previously is neither restricted by them nor by the standard used as a reference.

A. Decomposition of a Synthesized EMI

Fig. 2 shows a 1.6-ms time record of the EMI under consideration. This signal has been synthetically designed to include transient/broadband and continuous wave/narrowband components. In particular, this example provides one quasi-periodic transient pulse with random jitter ($\mathrm{EMI}_{\mathrm{tr}}$) and other three continuous wave signals. The continuous wave interferences are two amplitude modulated (AM) tones with carriers at 250 kHz ($\mathrm{EMI}_{\mathrm{cw1}}$) and 27 MHz ($\mathrm{EMI}_{\mathrm{cw2}}$), respectively, and a very low-frequency Gaussian modulated sinusoid pulse train ($\mathrm{EMI}_{\mathrm{cw3}}$).

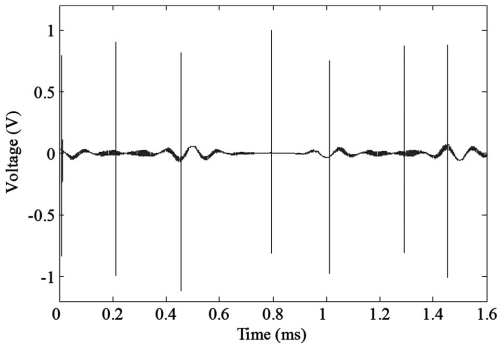

Fig. 2. Test signal for emulating an EMI measured in the time domain.

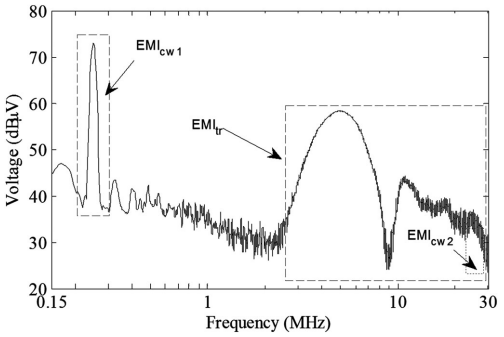

Fig. 3. EMI amplitude spectrum measured between 150 kHz and 30 MHz.

The amplitude spectrum of the EMI under assessment is shown in Fig. 3. The spectral estimation has been calculated using the Welch's periodogram and the processing techniques explained in [4] and [6]. The narrow band signal $\mathrm{EMI}_{\mathrm{cw1}}$ at approximately 250 kHz corresponds to the AM broadcasting. In the upper part of the measured spectrum, the contribution of the broadband interference ($\mathrm{EMI}_{\mathrm{tr}}$) overlaps the narrow band interference at 27 MHz ($\mathrm{EMI}_{\mathrm{cw2}}$) making it impossible to separate them using plain filtering. As expected, $\mathrm{EMI}_{\mathrm{cw3}}$ is completely unnoticed in the amplitude spectrum shown in Fig. 3 because it is out of the measured frequency range.

In order to decompose the EMI in the time domain, first the transient pulses shall be detected and removed using the algorithms for TMD. The estimated pulse duration is 0.78 μs and $\hat{f}_{\mathrm{rep}} \approx 4.4$ kHz. Fig. 4 shows the superposition of the seven

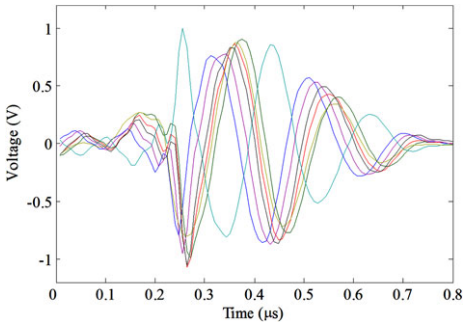

Fig. 4. Transient EMI pulses extracted from the EMI signal in time domain.

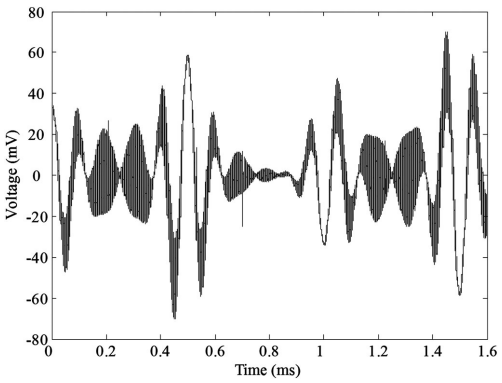

Fig. 5. Continuous wave part of the measured EMI after transient removal.

transient pulses identified in the recorded time frame of the assessed EMI. The amplitude of the transient EMI in the time domain is remarkably high in comparison with the continuous components. Fig. 4 verifies that the algorithm performs robustly even in the presence of jitter.

Once the transient pulses have been identified, they are removed from the EMI in order to perform the EMD on the continuous wave components of the EMI under assessment. Fig. 5 shows the EMI signal in the time domain after transient removal. Notice the amplitudes are under 80 mV, which is approximately two orders of magnitude below the transients.

By means of the EEMD, the continuous part of the EMI was decomposed into three IMF with simple waveforms: IMF_1, IMF_2, and IMF_3. Fig. 6 presents the three IMF that comprise the assessed EMI. The residual is negligible because it is basically random noise introduced by the waveform generator. IMF_1 and IMF_3 are clearly AM signals, EMI_{cw1}, and EMI_{cw2}, respectively. IMF_2 is the very low-frequency Gaussian-modulated sinusoid pulse train, which is EMI_{cw3}. Even if EMI_{cw3} does not have frequency components in the 150 kHz–30 MHz band it is

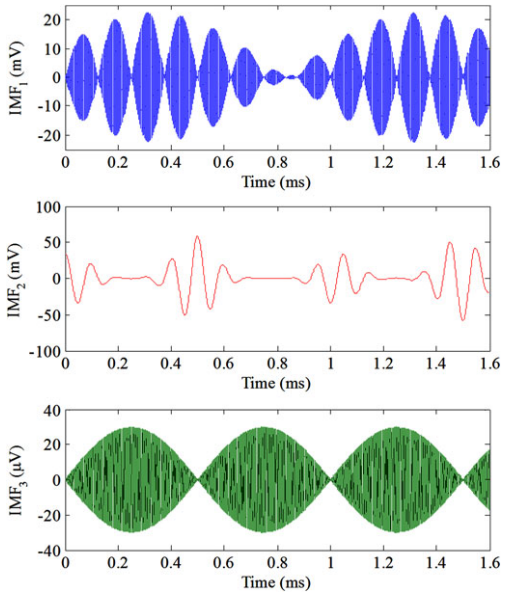

Fig. 6. IMFs of the continuous wave EMI.

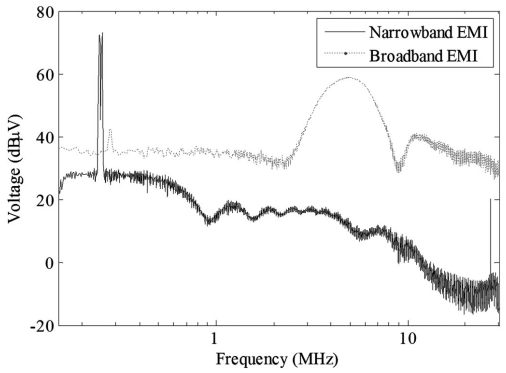

Fig. 7. Spectrum of the narrowband and broadband modes after the decomposition of the EMI measured with a TDEMI system.

a measurable part of the EMI since the time-domain approach provides the complete information of the signal within the instrument bandwidth.

Then, the IMF can be used to improve the results from the spectral estimations in TDEMI measurement systems. The key idea is to obtain the spectral contribution of each IMF using the optimum setting according to the type of signal [6], as shown in Fig. 7. Then, the total amplitude spectrum can be estimated superposing the contribution of each IMF [24].

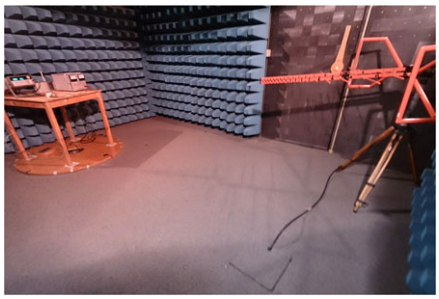

Fig. 8. Measurement setup.

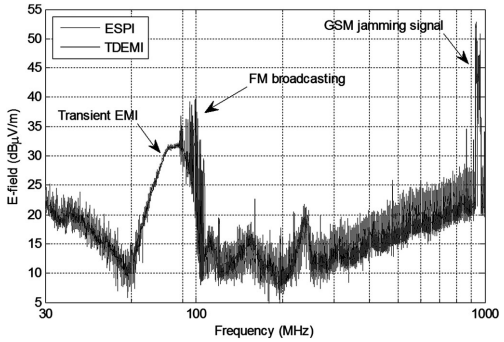

Fig. 9. Radiated EMI spectrum measured between 30 MHz and 1 GHz.

Once the EMI signal is decomposed in the time domain, the frequency-domain results can be presented in terms of the broadband and narrowband IMF as shown in Fig. 8. After decomposition, both narrowband interferences are identified since the citizen band signal is no longer masked by the broadband spectral components of the transient pulse.

The denoising effect provided by the EMI decomposition is remarkable. Also, separating the broadband EMI from the narrowband interferences allow the algorithms to apply specific windowing and filtering; thus, improving the overall results through the reduction of the variability in the amplitude spectrum estimates.

B. Decomposition of Radiated EMI

Inside a fully anechoic chamber (FAC), two sources of radiated disturbances were placed acting as the EUT. The first EMI source is a circuit that generates radiated transients. The other noise source is a GSM jamming device in the 900-MHz band. The door of the FAC was intentionally left open in order to capture noise from radio broadcasting. Radiated emissions measurements were performed in the 30 MHz–1 GHz band. The antenna was positioned for a 3-m EUT-to-test-antenna distance. A Schaffner CBL6143 bilog antenna in horizontal polarization was used. The test setup is shown in Fig. 8.

Emissions measurements were made with a TDEMI measurement system and, for validation purposes, with an EMI test receiver. On the one hand, the TDEMI measurement system used a digital oscilloscope Tektronix DPO5104B, a sampling rate of 5 GS/s and a record length of 1 ms. On the other hand, frequency sweep measurements were done with a R&S ESPI test receiver and the dwell time used was 1 ms. In both cases, the resolution bandwidth was set to 120 kHz in accordance with the CISPR specifications for bands C and D. The overall measurement results are presented in Fig 9.

Fig. 9 indicates there is a broadband disturbance interfering the FM broadcasting band. Likewise, the emissions from the jammer interfere between 900 and 950 MHz with GSM. The results obtained using both measurement systems (TDEMI and EMI test receiver) are in good agreement, that is, they provide the same information in terms of spectral estimation.

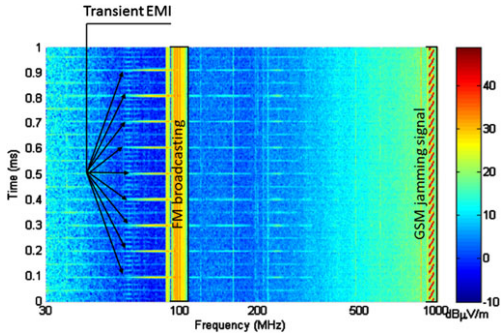

Fig. 10. Spectrogram of the measured EMI.

Fig. 10 shows the spectrogram of the EMI. The time–frequency representation of the measured disturbance verifies the transient behavior of the broadband interference. Fig. 10 also shows the GSM jamming signal is a linear chirp with a 31.25 μs period.

From Fig. 10, it is seen how the transient mode of the measured EMI overlaps the frequency spectrum of FM broadcasting. Furthermore, this spectrogram representation cannot be used for further signal decomposition since the transient duration is shorter than the length of the window required for the selected resolution bandwidth, that is, a resolution constraint in this type of time–frequency representation.

Nonetheless, through the decomposition algorithms presented in Sections II and III, the TDEMI measurement system is able to represent the radiated interferences as IMF. Fig. 11 shows the results of EMI decomposition process. The first IMF correspond to a transient signal with 10-kHz pulse repetition frequency and 0.1-μs duration. IMF_2 is the GSM jamming interference. Finally, IMF_3 is the FM radio broadcasting signal.

The results exhibit some level of mode-mixing between IMF_1 and IMF_2. In the spectrum of IMF_1 there is an attenuated

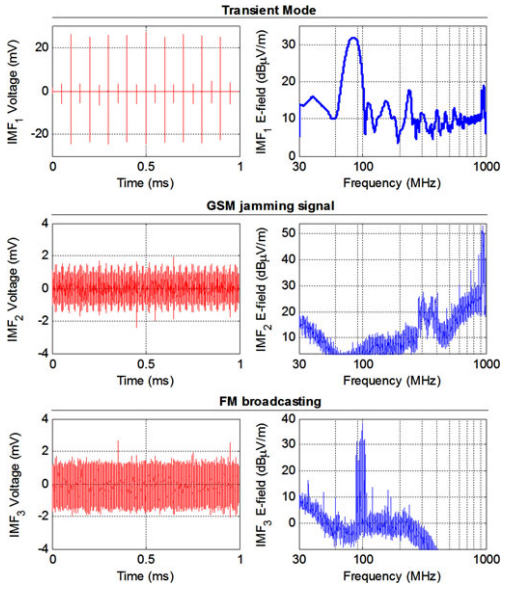

Fig. 11. IMFs in the time domain and in their spectral estimation.

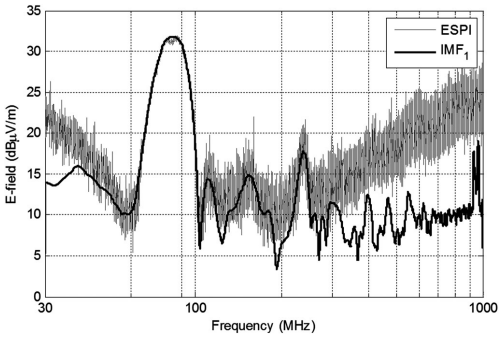

Fig. 12. Comparison between the amplitude spectrum of IMF_1 and the measurement results of the radiated transient disturbances carried out with an EMI test receiver.

component of the GSM jamming signal. Likewise, in the IMF_2 there is a broadband component of noise that corresponds to the transient EMI. Nonetheless, the magnitude of the mode mixed components is near the noise floor, several decibels below the frequencies of maximum emissions. In this example, it would be possible to filter the mode mixed components since they do not overlap in frequency with the predominant interference of each IMF. Conversely, there was no mode-mixing between IMF_3 and the other modes. This means that the transient mode was completely separated of the FM broadcasting signal, as shown in the spectrum of IMF_1.

Aimed at validating the results, frequency sweep measurements were made only for the transient EMI, turning OFF the GSM jammer and closing the door of the anechoic chamber. Fig. 12 shows that the sensitivity of the TDEMI measurement system was improved by the noise reduction in the spectral estimation of the transient IMF.

The results confirm the decomposition algorithms were successful in identifying a finite set of IMF that describes accurately the main components of the EMI. EMI decomposition algorithms required a single time-domain acquisition and no prior assumption was imposed on the frequency content of the measured interference.

V. DISCUSSION

The decomposition of EMIs in the time domain is a methodology useful for analyzing complex disturbances. The combination of EMD and algorithms for transient mode separation provide a heuristic approach to EMI analysis that allows the identification of a finite set of relatively simple IMF that describes the main components of the measured EMI signal.

In comparison with other signal decomposition approaches, the presented techniques have several advantages: it introduces neither distortion nor delay on the IMF, it requires no prior information on the spectral content of the measured EMI, it does not require a domain transformation, it provides IMFs that usually have a clear physical meaning, it is not constrained by time-frequency resolution limits, and it allows a straightforward implementation through software.

Therefore, the decomposition of EMI in the time domain provides several new practical applications to be explored in TDEMI measurement systems, especially for those based on general-purpose oscilloscopes. For example, the EMI decomposition in the time domain could be used for finding, tracking, and identifying sources of an EMI in complex environments, that is, inside large machinery and installations. Also, EMI decomposition in the time domain is potentially applicable for the cancellation of unwanted background ambient noise in emissions measurements performed *in situ,* as required in industrial environments or when assessing interferences of railway systems.

However, EMI decomposition in the time domain has some drawbacks, and its performance is improvable. In particular, with the EMD algorithm, it is not possible to know beforehand how many IMF will be identified. Therefore, the required time to process the signal is not bounded, and this could be impractical for emissions testing measurements purposes. A possibility to reduce the processing time is to establish a fixed number of intrinsic modes obtainable on the basis of the analysis of a preliminary measure.

VI. CONCLUSION

This paper presented the customization of the EMD with transient separation capabilities for the application of EMI decomposition in the time domain. The algorithms are capable of

identifying a finite set of IMFs that describe accurately the main components of the EMI. The presented algorithms required a single time-domain acquisition to perform the EMI decomposition and no prior assumption was made on the frequency content of the measured interferences. The result of the decomposition process provides insights of the measurement results through the use of specific time-domain signal processing techniques.

The main advantage of the applying EMI decomposition in the time domain is the capability of studying the contribution of each IMF to the overall EMI. This allows identifying different narrowband, broadband, and ambient noise components within measurement results. That knowledge would allow TDEMI measurement systems applying specific digital processing techniques for improving measurement results by means of selective denoising.

REFERENCES

[1] *Information Technology Equipment—Radio Disturbance Characteristics —Limits and Methods of Measurement*, CISPR Standard EN 55022, 2008.

[2] M. Pous and F. Silva, "Full-Spectrum APD measurement of transient interferences in time domain," *IEEE Trans. Electromagn. Compat.*, vol. 56, no. 6, pp. 1352–1360, Dec. 2014.

[3] G. Costa, M. Pous, A. Atienza, and F. Silva, "Time-domain electromagnetic interference measurement system for intermittent disturbances," in *Proc. Int. Symp. Electromagn. Compat.*, 2014, pp. 833–837.

[4] M. A. Azpúrua, M. Pous, and F. Silva, "A measurement system for radiated transient electromagnetic interference based on general purpose instruments," in *Proc. Int. Symp. Electromagn. Compat.*, 2015, pp. 1189–1194.

[5] P. M. Oliveira and V. Barroso, "Uncertainty in the time-frequency plane," in *Proc. IEEE 10th Workshop Statist. Signal Array Process.*, 2000, pp. 607–611.

[6] M. A. Azpúrua, M. Pous, S. Çakir, M. Çetintaş, and F. Silva, "Improving time-domain EMI measurements through digital signal processing," *IEEE Electromagn. Compat. Mag.*, vol. 4, no. 2, pp. 82–91, Apr.–Jun. 2015.

[7] E. X. Alban, M. E. Magana, H. G. Skinner, and K. P. Slattery, "Statistical modeling of the interference noise generated by computing platforms," *IEEE Trans. Electromagn. Compat.*, vol. 54, no. 3. pp. 574–584, Jun. 2012.

[8] R. Yang, B. Zhang, D. Qiu, and Z. Liu, "Time-;frequency and wavelet transforms of EMI dynamic spectrum in chaotic converter," *IEEE Trans. Power Electron.*, vol. 24, no. 4. pp. 1083–1092, Apr. 2009.

[9] M. Pous and F. Silva, "Prediction of the impact of transient disturbances in real-time digital wireless communication systems," *IEEE Electromagn. Compat. Mag.*, vol. 3, no. 3. pp. 76–83, Jul./Sep. 2014.

[10] M. A. Azpurua, M. Pous, and F. Silva, "On the statistical properties of the peak detection for time-domain EMI measurements," *IEEE Trans. Electromagn. Compat.*, vol. 57, no. 6, pp. 1374–1381, Dec. 2015.

[11] Y.-Y. Hong and Y.-Q. Bao, "FPGA implementation for real-time empirical mode decomposition," *IEEE Trans. Instrum. Meas.*, vol. 61, no. 12, pp. 1–10, Dec. 2012.

[12] N. E. Huang, Z. Shen, S. R. Long, M. C. Wu, H. H. Shih, Q. Zheng, N.-C. Yen, C. C. Tung, H. H. Liu, N. E. Huang, Z. Shen, S. Long, M. Wu, H. Shih, Q. Zheng, N.-C. Yen, C. Tung, and H. Liu, "The empirical mode decomposition and the Hilbert spectrum for nonlinear and non-stationary time series analysis," *Proc. Roy. Soc. London. Ser. A, Math. Phys. Eng. Sci.*, vol. 454, no. 1971, pp. 903–995, 1998.

[13] M. Blanco-Velasco, B. Weng, and K. E. Barner, "ECG signal denoising and baseline wander correction based on the empirical mode decomposition," *Comput. Biol. Med.*, vol. 38, no. 1, pp. 1–13, 2008.

[14] N. Bi, Q. Sun, D. Huang, Z. Yang, and J. Huang, "Robust image watermarking based on multiband wavelets and empirical mode decomposition.," *IEEE Trans. Image Process.*, vol. 16, no. 8, pp. 1956–1966, Aug. 2007.

[15] T. Tanaka and D. P. Mandic, "Complex empirical mode decomposition," *IEEE Signal Process. Lett.*, vol. 14, no. 2, pp. 101–107, Feb. 2007.

[16] A. Eftekhar, C. Toumazou, and E. Drakakis, "Empirical mode decomposition: Real-time implementation and applications," *J. Signal Process. Syst.*, vol. 73, no. 1, pp. 43–58, 2013.

[17] Y. Gao, G. Ge, Z. Sheng, and E. Sang, "Analysis and solution to the mode mixing phenomenon in EMD," in *Proc. 1st Int. Congr. Image Signal Process.*, 2008, vol. 5, pp. 223–227.

[18] P. Flandrin, G. Rilling, and P. Goncalves, "Empirical mode decomposition as a filter bank," *IEEE Signal Process. Lett.*, vol. 11, no. 2, pp. 112–114, Feb. 2004.

[19] P. J. J. Luukko, J. Helske, and E. Räsänen, "Introducing libeemd: A program package for performing the ensemble empirical mode decomposition," *Comput. Statist.*, pp. 1–13, 2015, early eccess.

[20] K. Dragomiretskiy and D. Zosso, "Variational mode decomposition," *IEEE Trans. Signal Process.*, vol. 62, no. 3, pp. 531–544, Feb. 2014.

[21] T. O'Haver. (2015). "A pragmatic introduction to signal processing with applications in scientific measurement," [Online]. Available: https://terpconnect.umd.edu/~toh/spectrum/TOC.html

[22] C. B. Moler, *Numerical Computing With MATLAB*, 1st ed. Philadelphia, PA, USA: SIAM, 2004.

[23] R. Willink, *Measurement Uncertainty and Probability*. Cambridge, U.K.: Cambridge Univ. Press, 2013.

[24] C. Keller and K. Feser, "Fast emission measurement in time domain," *IEEE Trans. Electromagn. Compat.*, vol. 49, no. 4, pp. 816–824, Nov. 2007.

Marco A. Azpúrua (M'13) received the B.Sc. degree in telecommunications engineering, in 2008, and the M.Sc. degree in electrical engineering from the Universidad Central de Venezuela, Caracas, Venezuela, in 2013. He is currently working toward the Ph.D. degree at the Electromagnetic Compatibility Group, Universitat Politècnica de Catalunya, Barcelona, Spain.

He was a Researcher in the Applied Electromagnetics Laboratory, Instituto de Ingeniería (FII), Caracas. He is a Member of the Venezuelan Standardization Committee for the Telecommunication Sector of CODELECTRA and FODENORCA and has participated in the adoption of the local standards of electromagnetic compatibility. His research interests include electromagnetic compatibility, antenna and microwave measurement technologies, estimation of measurement uncertainty in complex systems, and validation methods.

Marc Pous was born in Barcelona, Spain, in 1983. He received the M.Sc. degree in telecommunications engineering and the Ph.D. degree in radiated transient interferences and digital communication systems evaluation from the Universitat Politècnica de Catalunya, Barcelona, Spain, in 2009 and 2015, respectively.

From 2003 to 2006, he was with the LGAI Technological Centre, Department of Electromagnetic Compatibility. In 2006, he was with the Electromagnetic Compatibility Group, Universitat Politècnica de Catalunya, where he has been participating in international and national research projects related with automotive, aerospace, railway and medical industries. His research interests include development of time domain measurement techniques to capture interferences which are not properly measured following the harmonized EMC standards.

Ferran Silva (S'93–M'98) received the M.Sc. and Ph.D. degrees from the Universitat Politècnica de Catalunya (UPC), Barcelona, Spain, in 1989 and 1997, respectively.

Since 2000, he has been the Director of the Electromagnetic Compatibility Group, Universitat Politècnica de Catalunya (GCEM-UPC) performing technology transfer activities to the industrial sector. He is currently an Associate Professor of Electronics with the Department of Electronic Engineering, UPC. His research interests include electromagnetic compatibility (EMC) in near field and time domain, including transients, with application to automotive, medical systems and installations. He has made more than 90 publications in journals and conferences and contributed to the Wiley Encyclopedia of Biomedical Engineering. He has participated in 14 research projects related to EMC.

Dr. Silva is a Member of the IEEE EMC Society and the Head of the Spanish chapter of the same society; he is also Member of the Spanish Standardization Committees SCTC77-210 and the CTN208 SCCISPR210A. He was the Chairman of the EMC Europe 2006 International Symposium. Since then, he belongs to the Board of Chairmen of EMC Europe.

Proc. of the 2016 International Symposium on Electromagnetic Compatibility - EMC EUROPE 2016, Wroclaw, Poland, September 5-9, 2016

A Single Antenna Ambient Noise Cancellation Method for *In-Situ* Radiated EMI Measurements in the Time-Domain

Marco A. Azpúrua, Marc Pous, Ferran Silva
Grup de Compatibilitat Electromagnètica (GCEM), Departament d'Enginyeria Electrònica (DEE)
Universitat Politècnica de Catalunya (UPC)
Barcelona, Spain
email: marco.azpurua@upc.edu

***Abstract*—This paper presents a single antenna ambient noise cancellation method for in-situ radiated emissions measurements performed using an entirely time-domain approach and the sliding window Empirical Mode Decomposition. The method requires a pair of successive measurements, an initial one for characterizing the ambient noise and a final one for the EMI measurement in the presence of ambient noise. The method assumes the spectral content of the ambient noise is stable between both measurements. The measured time-domain EMI is decomposed into a finite set of intrinsic mode functions. Some modes contain the ambient noise signals while other modes contain the actual components of the EMI. A brute-force search algorithm determines which mode, or combination of modes, maximize the absolute difference between the magnitude of their spectrum and the ambient noise levels for every frequency bin in the measurement bandwidth. Experimental results show the effectiveness of this method for attenuating several ambient noise signals in the 30 MHz – 1 GHz band.**

Keywords— Digital signal processing, electromagnetic compatibility, electromagnetic interference, electromagnetic measurements, time-domain analysis.

I. INTRODUCTION

In-situ electromagnetic interference (EMI) measurements are polluted by noise sources present in the same electromagnetic environment. This unavoidable electromagnetic background noise is a combination of broadcasting signals from telecommunication services and the disturbances radiated by the equipment, machinery and installations that surround the measurement antenna. The electromagnetic ambient noise is a major concern for *in-situ* EMI measurements because it increases the noise floor and reduces the measurement system effective sensitivity and effective dynamic range. Such degradation could make the measurement system unable to detect electromagnetic emissions generated by the EUT under evaluation.

Previously, ambient noise cancellation (ANC) techniques have been developed with the aim of undertaking the challenges imposed by the presence of ambient noise in *in-situ* EMI measurements. Those ANC techniques comprise alternative test methods and specific signal processing. In the following, some of those ANC techniques will be described.

The simplest and more straightforward approximation to handle ambient noise consist in performing a pair of EMI measurements, the first one with the EUT turned off and the later one with the EUT powered and active. With the information provided by the first background ambient noise measurement a few decisions can be made to improve measurement results in presence of ambient noise: 1) tune-out receiver and notch filtering narrow band ambient interferences 2) shortening the measurement distance in order to improve signal-to-noise ratio 3) using the signal substitution method 4) perform a linear subtraction [1]. Those frequency domain approaches to ambient noise reduction are very simple to apply but have many limitations such as: 1) effectiveness restricted to small number of narrow band signals out of the band of the EMI under assessment, 2) induce non-linear near field effects that invalidate the extrapolation of results to the original far-field distance, 3) requires additional signal generator and is again restricted to a single narrow band interference, and 4) is strictly incorrect because both measurements are not simultaneous, even if it provides approximated result in some particular cases.

Some other patented ANC methods for EMI measurement systems rely on adaptive filtering [2], [3]. Those ANC methods use simultaneous measurements performed with two identical antennas on a measurement system with two channels, one channel is expected to detect only the background ambient noise while the other one measures the combination of the EMI with the background ambient noise. Assuming the EMI signal from the EUT is uncorrelated to the ambient electromagnetic noise, and provided that the ambient noise detected by the two separated antennas is highly correlated, adaptive filter methods have been used to suppress the unwanted noise. In this regard, the Least-Mean-Square algorithm [4]–[6] and the frequency domain Overlap-Save method [7] have been used to adjust the coefficients of finite impulse response filters. Attenuation of approximately 30 dB has been reported in simulations and in controlled test scenarios.

978-1-5090-1416-3/16/$31.00 ©2016 IEEE

Proc. of the 2016 International Symposium on Electromagnetic Compatibility - EMC EUROPE 2016, Wroclaw, Poland, September 5-9, 2016

The adaptive filtering based methods of ANC have some shortcomings: 1) require the emissions from EUT to be decoupled from "only ambient noise" reference channel, 2) their effectiveness is difficult to quantify when the ambient noise share the same frequency band as the EUT emissions and 3) would require a synchronous, multiport, real-time EMI receiver.

Finally, another *in-situ* test method for radiated emission assessment that employs spatial spectrum estimation, adaptive beamforming, and spectrogram analysis was presented in [8]. Measurements were performed using a general purpose oscilloscope and a linear array of four omnidirectional antennas. This particular ANC method is restricted by the maximum number of antennas that can be used in the array, which is four, given by the number of channels oscilloscope. This means the algorithm is only capable of suppressing interferences from 3 different directions of arrival. On the other hand, it would be troublesome to obtain a reliable antenna factor for an array whose radiation pattern changes dynamically, thus adding significant uncertainty to the measurement results of electric field strength obtained with such a technique.

In this paper, a single antenna ANC method for *in-situ* radiated EMI measurements is presented. This method uses an entirely time-domain approach and the sliding window Empirical Mode Decomposition (SW-EMD) as the core processing technique. In contrast with previous ANC approaches, this method is entirely applied in the time-domain and is intended as part of a Full Time-Domain EMI (Full-TDEMI) measurement system implemented with general purpose oscilloscopes. In relation with previous work, this method provides full-spectrum ANC capabilities for both continuous and transient ambient noise signals and simplifies the test setup for using a single antenna. Application cases emphasize its suitability for cancelling continuous wave and transient ambient disturbances.

The structure of this paper includes an overview of the SW-EMD (section II), a description the ANC method supported on the Full-TDEMI measurement system (section III) and presents an application example of for *in-situ* EMI assessment (section IV).

II. THE EMPIRICAL MODE DECOMPOSITION

The EMD is a heuristic method developed for analyzing nonlinear and nonstationary signals. It was introduced by Huang et al. in 1998 [9]. The main capability of the EMD is to decompose complex datasets into a finite, and often small, number of components called intrinsic mode functions (IMF) that admit well-behaved Hilbert transforms. EMD is an entirely data-driven algorithm, it does not depend on any predefined basis functions and it does not require a domain transformation.

A. Overview of the EMD algorithm

The initial step of the EMD algorithm [10] is the extraction of the extrema from signal $x(t)$ and creation of the upper envelope, $e_{max}[x(t)]$, and the lower envelope, $e_{min}[x(t)]$ by cubic spline interpolation of the maxima and of the minima, respectively. The mean value of the envelopes, $m[x(t)]$, is then calculated as

$$m[x(t)] = \frac{e_{\max}[x(t)] + e_{\min}[x(t)]}{2}. \quad (1)$$

An iterative process called sifting is used to identify the IMFs. In the first iteration of the sifting process, $m[x(t)]$ is subtracted from original data, that is,

$$imf_1(t) = x(t) - m[x(t)]. \quad (2)$$

Then, the mean value of the envelope of $imf_1(t)$, $m[imf_1(t)]$, is calculated. The sifting process is iterated until $imf_1(t)$ meets the condition of an IMF ($m[imf_1(t)] \approx 0$),

$$imf_1(t) := imf_1(t) - m[imf_1(t)] \quad (3)$$

where ":=" means it becomes.

Once the first sifting process reaches the stopping criteria, the original signal is reduced by the first mode, as given by

$$IMF_1(t) := imf_1(t), \quad (4)$$

$$r_1(t) = x(t) - IMF_1(t). \quad (5)$$

The residue $r_1(t)$ is used as the input data for extracting the second IMF during the next sifting loop. Procedure is repeated until all the IMFs have been decomposed, which means,

$$r_i(t) = r_{i-1}(t) - IMF_i(t) \quad (6)$$

where i is the index of current mode. The EMD algorithm ends when $r_i(t)$ has less than three extrema, because it would be impossible to construct the envelopes, or when all its points are nearly equal to zero. Therefore, the sum of all IMF components and the residue is equal to the original signal, expressed by

$$x(t) = r_n(t) + \sum_{i=1}^{n} IMF_i(t) \quad (7)$$

where n is total number of the decomposed IMF.

B. The Sliding Window EMD

Many variations of the EMD algorithm have been developed. Recently, an improved version of EMD with transient decomposition capabilities was successfully used to decompose EMI complex signals [11]. However, time-domain EMI measurements require long acquisitions at very high sampling rates (several times the Nyquist limit) and analyzing EMI measurements with EMD is a resource and time consuming computational process.

In response to the aforementioned challenge, the SW-EMD was posed as by Stepien [12] as an alternative algorithm to improve computation speeds of the EMD on long datasets. The SW-EMD calculates the EMD in a relatively small window and slides this window along the time axis [12]. The particular implementation of the SW-EMD used in this work differs from original algorithm because it uses partially overlapped time windows with a length that is a function of the desired frequency resolution, according to the criteria used in [13], [14]. The EMD process is repeated for each windowed time frame and the IMFs obtained for each of those windows are then combined to reconstruct the complete set of IMF, as illustrated in Fig. 1.

Proc. of the 2016 International Symposium on Electromagnetic Compatibility - EMC EUROPE 2016, Wroclaw, Poland, September 5-9, 2016

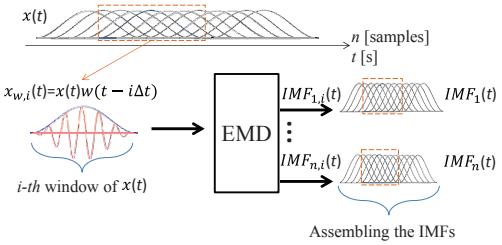

Fig. 1. The sliding window EMD process.

III. A SINGLE ANTENNA ANC METHOD

A. The Full-TDEMI measurement system

In general terms, a Full-TDEMI measurement system is described by the block diagram shown in Fig. 2 [13]. For the measurement of radiated EMI, a broadband antenna shall be used, while for the measurement of conducted EMI corresponds either a current clamp or a line impedance stabilization network (LISN). The measured signal could be amplified or filtered if this provides better sensitivity. In the analog-to-digital converter (ADC), the full spectrum signal is digitized and stored in the time-domain. Finally, the amplitude spectrum is computed via the spectral estimation techniques.

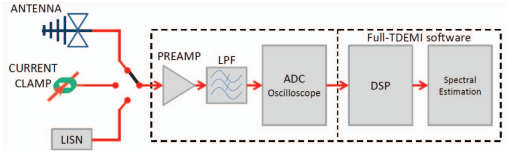

Fig. 2. The Full-TDEMI measurement system block diagram.

B. The measurement setup and procedure

With regard to the measurement setup, the general guidelines for *in-situ* measurements of radiated EMI produced by physically large equipment given in the CISPR TR 16-2-5:2008 technical report [15] shall be followed.

Additionally, the measurement procedure for ANC requires a pair of successive measurements. The first measurement is used for characterizing the ambient noise, $AN(t)$, and shall be performed with the EUT turned off. Then the measurement is repeated with the EUT turned on and without changing any of the elements of the test setup. Finally, both measurements shall be processed by the following ANC algorithm.

C. ANC algorithm

In the current subsection, a description of the ambient noise cancellation algorithm will be given. A simplified flowchart of the ANC algorithm is displayed in Fig. 3. The ANC algorithm has three major processing steps: the IMF combination, the spectral estimation and the linear search stage.

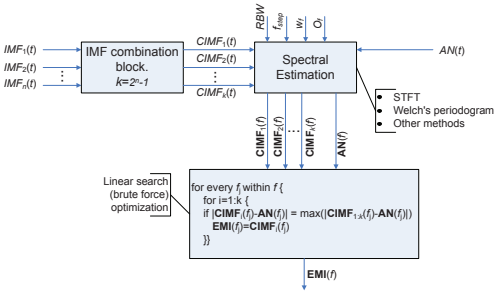

Fig. 3. ANC algorithm flowchart.

The first processing block receives the IMFs as inputs and combines them in the time domain in order to obtain the combined IMFs, CIMF. The combination rule for adding the IMFs follows a Boolean approach in where any single IMF can be (True) or not to be (False) included in a particular CIMF and it can be represented as Table I. From Table I, it is clear that the $CIMF_k$ corresponds approximately to the measured EMI in the presence of ambient noise if the residual is negligible.

TABLE I. CIMFS COMBINATION RULE

$CIMF_m$	IMF_i			
	n	...	2	1
1	F	-	F	T
2	F	-	T	F
...	-	-	-	-
k-1	T	-	T	F
k	T	-	T	T

The second stage of the ANC algorithm corresponds to the spectral estimation. The CIMF and the ambient noise (AN) signals are transformed into the frequency domain using the Short-Time Fourier Transform (STFT) and non-parametric methods, such as Welch's periodogram. The appropriate resolution bandwidth (RBW), frequency step size (f_{step}), window factor (w_f) and overlapping factor (o_f) shall be configured in order to obtain results coherent with EMI receiver specifications.

The last step in the ANC algorithm processing chain is the linear search. Linear search is the simplest form of the brute force search algorithm. The linear search is used to identify, one frequency at the time, which CIMF differs the most form the ambient noise. Therefore, the estimated EMI spectrum is assembled within a "for" loop, cancelling the effect of the CIMFs that are most likely to carry the ambient noise signals.

IV. APPLICATION EXAMPLE

In this section, an application example of the introduced ANC method for *in-situ* radiated EMI measurements in the time domain will be presented. Measurements were performed with a Full-TDEMI measurement system based on a Tektronix DPO5104B oscilloscope, using a sampling rate of 5 GS/s and

Proc. of the 2016 International Symposium on Electromagnetic Compatibility - EMC EUROPE 2016, Wroclaw, Poland, September 5-9, 2016

a record length of 1 ms, in the 30 MHz – 1 GHz frequency band, using a 120 kHz resolution bandwidth and a 30 kHz step size [11], [13], [14], [16]. The test setup was placed inside a Full Anechoic Room (FAR) from which the doors were left intentionally opened in order to capture the ambient noise signals.

The source of the EMI signal was a Comparison Noise Emitter III (CNE-III) from York EMC services. A Schaffner CBL6143 bilog antenna in horizontal polarization was used. The antenna was positioned for a 3-m EUT-to-test-antenna distance. Antenna factors were not applied to the measurements. In consequence, measurement results are given in terms of the voltage measured at the antenna port.

The result of the ambient noise characterization is shown in Fig. 4. The expected signals from radio broadcasting, digital terrestrial television and mobile communication services are clearly identifiable.

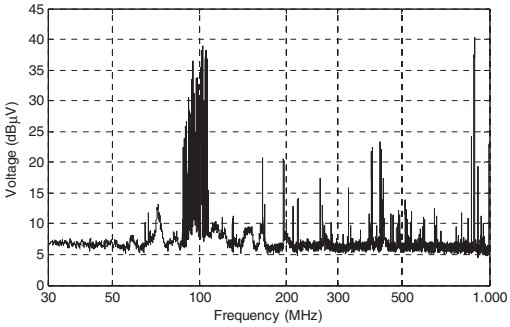

Fig. 4. *In-situ* background ambient noise characterization.

Next, the CNE-III is turned on and the EMI signal is measured in the presence of ambient noise. The results are shown in Fig. 5. The most noticeable aspect of Fig. 5 spectrum is the presence of a broadband noise signal. Inspecting the time domain measurements (Fig 6), a transient event was detected in the EMI measurement. In this particular example, the transient signals were intentionally generated by turning on a set of fluorescent lights in a room next to the FAR.

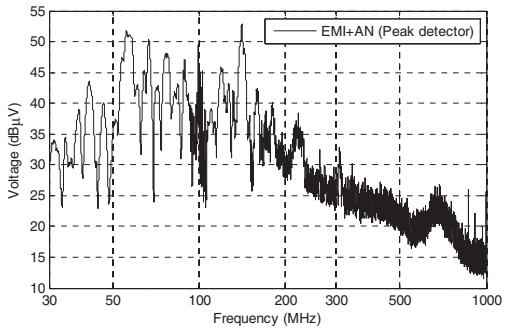

Fig. 5. EMI measurements in the presence of ambient noise.

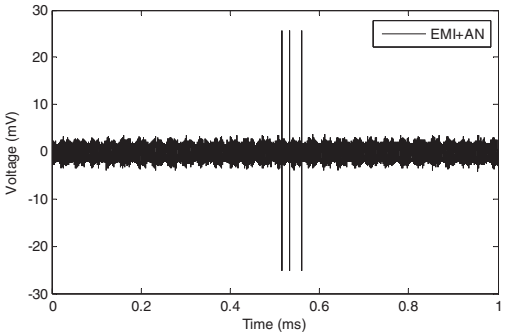

Fig. 6. Time domain EMI measurements in the presence of ambient noise.

The aforementioned transient event is part of the ambient noise signals. In order to remove the transient pulses from the EMI, techniques presented in [11] were applied.

The SW-EMD is used to decompose the measured EMI signal in the presence of ambient noise. Four IMFs were identified, as shown in Fig. 7. IMF_1 corresponds to the transient event. IMF_2 includes the ambient noise signals of higher frequency. IMF_3 contains most of the energy of the EMI. IMF_4 contains the ambient noise signal corresponding with FM broadcasting. Since the EUT has broadband emissions in the whole frequency range, part of the energy of the EMI signal is distributed along the $IMF_{2,3,4}$.

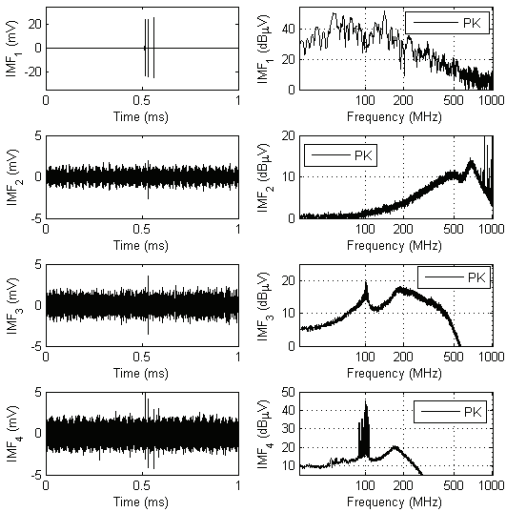

Fig. 7. IMF of the measured EMI in the presence of ambeint noise.

Finally, the EMI signal is estimated using the ANC algorithm explained in the previous section. The results are shown in Fig. 8. Several ambient noise signals have been cancelled achieving up to 25 dB attenuation.

For validation purposes, the EMI measurement was repeated with the FAR doors closed. The results of EMI estimated after applying the ANC method are in excellent agreement with the EMI measurements in the absence of ambient noise. A minor level of mode mixing is evidenced in the FM broadcasting band.

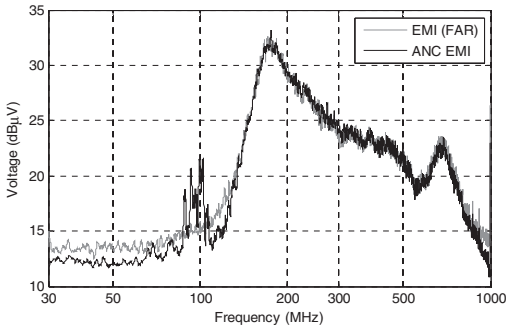

Fig. 8. Estimated EMI amplitud spectrum after ANC.

V. DISCUSION

The presented ANC method relies on the assumption that ambient noise remains stable (in terms of its spectral content) between the EUT being switched off, and the EUT having booted up to normal operation. This rise the concern about changes in the ambient noise caused by sporadic "pop up" signals that may appear during only one of the two required measurements, i.e. mobile radio communication signals from moving sources like police vehicles and similar.

In such situations, this method would be unable to cancel properly such irruptive "pop up" signals. As an alternative, time/frequency representations (spectrograms) of the EMI signal can be used to identify such sporadic signals. Then it would be possible to preprocess the time-domain EMI measurement (time-gating) for excluding the specific sub time-frame in which the intermittent signal occurred. Moreover, this ANC approach could also be extended for using a pair of antennas for performing ambient noise and EMI measurements simultaneously and synchronously, thus improving its capabilities for cancelling sporadic ambient noise signals.

VI. CONCLUSION

A single antenna ANC method for *in-situ* EMI measurements has been introduced. The method requires a pair of measurements, one for characterizing the ambient noise and another for the EMI measurement in the presence of ambient noise. It is based on time-domain EMI decomposition performed using the SW-EMD and a brute-force search algorithm that determines which mode, or combination of modes, maximize the absolute difference between the magnitude of their spectrum and the ambient noise levels for every frequency bin within the measurement bandwidth. In comparison with other previously reported ANC methods for EMI measurements, this ANC method simplifies the measurement setups because it uses only one antenna. Another advantage of the ANC method, in comparison with the previously published techniques, is that it allows cancelling the effect of transient ambient noise. This ANC method is performed through off-line post-processing. Experimental results show the effectiveness of this method for attenuating several ambient noise signals in the 30 MHz - 1 GHz band.

As a final remark, it is important to realize ANC methods are not intended to replace expert judgement in complex *in-situ* radiated EMI measurements. Aspects such as the selection of an adequate antenna location and orientation, the evaluation of multipath induced errors, the identification of sporadic "pop up" signals, among many other factors still require to be analyzed on an individual basis in order to decide the best possible course of action for the radiated emissions assessment.

ACKNOWLEDGMENT

This work was supported in part by the EURAMET IND60EMC research project (the EMRP is jointly funded by the EMRP participating countries within EURAMET and the European Union) and by the Spanish "Ministerio de Economía y Competitividad," under project TEC2013- 48414-C3-3-R.

REFERENCES

[1] J. Svačina, J. Dřínovský, and R. Vídenka, "Virtual anechoic room - An useful tool for EMI pre-compliance testing," in 2007 17th International Conference Radioelektronika, 2007.

[2] M. Marino, "System and method for measuring rf radiated emissions in the presence of strong ambient signals," 2005.

[3] S. Braun, A. Frech, and P. Russer, "Method for rejection of ambient interference signal during measurement of interference emissions of electric and electronic devices, involves digitalizing signal of antenna through analog to digital converter," 2009.

[4] A. Frech, S. Limmer, and P. Russer, "Noise cancelling algorithms for FPGA-based time-domain EMI measurements in real-time," in IEEE International Symposium on Electromagnetic Compatibility, 2011, pp. 484–488.

[5] A. Frech, M. Klugel, and P. Russer, "Adaptive filtering for noise cancellation and signal analysis in real-time," Microwave Conference (EuMC), 2013 European. pp. 1123–1126, 2013.

[6] C. Osterwise, S. L. Grant, and D. Beetner, "Reduction of noise in near-field measurements," in IEEE International Symposium on Electromagnetic Compatibility, 2010, pp. 171–176.

[7] A. Frech, S. Braun, and P. Russer, "Time-domain EMI measurements in the presence of ambient noise," in IEEE International Symposium on Electromagnetic Compatibility, 2009, pp. 139–142.

[8] Z.-H. Lu, J.-B. Liu, and P.-G. Liu, "A Novel Method of Ambient Interferences Suppressing for In Situ Electromagnetic Radiated Emission Test," Electromagnetic Compatibility, IEEE Transactions on, vol. 54, no. 6. pp. 1205–1215, 2012.

[9] N. E. Huang, Z. Shen, S. R. Long, M. C. Wu, H. H. Shih, Q. Zheng, N.-C. Yen, C. C. Tung, H. H. Liu, N. E. Huang, Z. Shen, S. Long, M. Wu, H. Shih, Q. Zheng, N.-C. Yen, C. Tung, and H. Liu, "The empirical mode decomposition and the Hilbert spectrum for nonlinear and non-stationary time series analysis," Proc. R. Soc. London. Ser. A Math. Phys. Eng. Sci., vol. 454, no. 1971, pp. 903–995, 1998.

[10] G. Rilling, P. Flandrin, P. Gon, and D. Lyon, "on Empirical Mode Decomposition and Its Algorithms," IEEEEURASIP Work. Nonlinear Signal Image Process. NSIP, vol. 3, pp. 8–11, 2003.

[11] M. A. Azpúrua, M. Pous, and F. Silva, "Decomposition of

Electromagnetic Interferences in the Time-Domain," IEEE Trans. Electromagn. Compat., pp. 1–8, 2016.

[12] P. Stepien, "Sliding Window Empirical Mode Decomposition -its performance and quality," EPJ Nonlinear Biomed. Phys., vol. 2, no. 1, p. 14, 2014.

[13] M. A. Azpúrua, M. Pous, and F. Silva, "A Measurement System for Radiated Transient Electromagnetic Interference Based on General Purpose Instruments," in Electromagnetic Compatibility (EMC EUROPE), International Symposium on, 2015.

[14] E. M. I. Time-Domain and I. Magazine, "M. Azpúrua, M. Pous and F.," Silva Improv. Meas. through Digit. Signal Process. Electromagn. Compat., 2015.

[15] IEC CISPR, "CISPR TR 16-2-5:2008 Specification for radio disturbance and immunity measuring apparatus and methods - Part 2-5: In situ measurements for disturbing emissions produced by physically large equipment," 2008.

[16] M. A. Azpurua, M. Pous, and F. Silva, "On the Statistical Properties of the Peak Detection for Time-Domain EMI Measurements," pp. 1–8, 2015.

Proc. of the 2017 International Symposium on Electromagnetic Compatibility - EMC EUROPE 2017, Angers, France, September 4-8, 2017

APD Outdoors Time-Domain Measurements for Impulsive Noise characterization

Marc Pous, Marco A. Azpúrua, Ferran Silva
Grup de Compatibilitat Electromagnètica (GCEM), Departament d'Enginyeria Electrònica (DEE)
Universitat Politècnica de Catalunya (UPC)
Barcelona, Spain
email: marc.pous@upc.edu

***Abstract*—a novel measurement and post-processing technique for estimating if impulsive noise is capable of degrading the performance of digital communication systems (DCS) is presented. It is based on the well-known capability of the amplitude probability distribution (APD) to estimate the bit-error-rate of digital communication system in the presence of electromagnetic interferences. However, the APD shall be computed from measurements taken in the absence of the useful signal of the communication system, which is a strong handicap for in-situ measurements. The main contribution of the work presented is the combination of time domain EMI measurements and decomposition techniques for separating the impulsive noise from the narrow band signals of the digital communication systems. Therefore, although the communication system signal is present at the test site, the APD diagram is obtained without the influence of the communication system, which is crucial to directly relate the shape of the diagram with the bit-error-rate introduced by the impulsive noise. This is an important step forward compared with the traditional approach as it offers the possibility to study the impact of impulsive interferences although DCS, such as broadcasting services, are present at interference scenarios.**

Keywords— Amplitude Probability Distribution, Impulsive noise, In-situ measurements, Electromagnetic interference, Electromagnetic measurements, Time-domain analysis

I. INTRODUCTION

A common type of electromagnetic interference (EMI) that is critical for current digital communication systems (DCS), is the impulsive noise or "type A" interference, defined by D. Middleton [1]. This means the noise is broadband, with bandwidths of hundreds of megahertz, and the pulses of the interferences are of short duration. A studied example of this kind of disturbance is the interference occasioned by the spark produced by the discontinuity between the pantograph and the catenary at railway applications [2], [12]. Those sparks generate impulsive noise that propagates as electromagnetic fields and, ultimately, interfere the GSM-R digital communication system. Another example is the well-known disturbance of the Digital Video Broadcasting Terrestrial (DVB-T) interfered by sources of impulsive noise like LED lamps [3].

In CISPR 16-1-1 standard, the amplitude probability distribution (APD) detector is specified for measuring electromagnetic interferences (EMI). As it has been established in several research works [4], [5], [12], this detector is suitable to crosscheck the APD measurements with the degradation that DCS suffer in terms of bit-error-rate (BER) or packet-error-rate, which are the main merit figures which are used nowadays to evaluate DCS performance. Hence, APD shall be used to characterize impulsive noise to protect communication systems, as it is required by the EMC and RED European Directives.

However, the use of APD measurements is limited due to the inconvenient that appear when traditional superheterodyne architecture instrumentation is employed to obtain the measurements. The statistical measurement shall be done at each frequency band and this causes time-limitation problematic above other limitations like being unable to apply strictly the same bandwidth as the communication system [6], [12]. Nevertheless, the novel methodologies based on time-domain captures that have recently appeared enable us to obtain fast APD results at the full frequency range [6], making feasible to implement EMI time-domain measurements in product/generic standards.

As it has been commented, another key point is to consider that many times outdoor measurements shall be carried out to ensure the compliance of a device or installation and to protect digital communication systems. For instance, to evaluate or guarantee that a fixed installation do not will produce interferences to digital communication systems such as mobile communications or broadcasting systems. These in-situ measurements have the handicap that shall be conducted in presence of the communication system that we want to protect. For instance, when in-situ measurements are done we cannot turn off broadcasting services like DVB-T, DAB or mobile communications like GSM, TETRA etc. Therefore, most of the times it is not possible to properly addressing EMC using classical measurements defined in the standards, as the communication system is masking the measurement of the EMI. In addition, this is critical when any of the detectors is employed: the QP, peak or also the new statistical ones like APD. Therefore, it is necessary to improve the outdoors in-situ measurements, as we need to be able to clearly observe the interference produced only by the impulsive noise, eliminating the contribution to the measurement of the communication system's useful signal.

Fortunately, novel full time domain measurements provide new possibilities as we have the amplitude and the phase of the measurement. Therefore, we are capable to apply post-processing techniques capable to decompose time-domain

978-1-5386-0689-6/17/$31.00 ©2017 IEEE

Proc. of the 2017 International Symposium on Electromagnetic Compatibility - EMC EUROPE 2017, Angers, France, September 4-8, 2017

signals/interferences [14]. In the next sections of the paper it is explained and exemplified with in-situ measurements how it is possible to obtain APD measurements, eliminating the contribution of the digital communication system present in the environment. Making possible to determine the BER that the EMI will cause to the communication system, although the signal of the communication system is present and masking the impulsive noise in the frequency domain.

II. METHODOLOGY

A. Full time domain EMI measurement

The full-time-domain EMI (Full TDEMI) measurement system employed have been developed and broadly used in recent years by GCEM-UPC [9-11]. This measurement system is based on time-domain acquisition followed by a post-processing stage, which allows obtaining equivalent results than conventional EMI test receiver. The time-domain data is acquired by a general-purpose oscilloscope and the post-processing is carried out with a standard laptop. It is important to emphasize that the time-domain capture catches the entire spectrum is measured in each acquisition, only limited by the oscilloscope bandwidth. Afterward, the amplitude spectrum of the EMI is computed applying the Short-Time Fourier Transform, non-parametric spectral estimation methods and detector emulation to deliver the results according to CISPR 16-1-1 standard. More details can be found at [9-11].

Besides computing the spectrum with the results according to the CISPR 16-1-1 standard, the time domain signal of the capture is also available. Hence, it is possible also to calculate statistical detectors likewise APD. At the following section, it is explained how to compute the APD diagram from a time domain capture obtained with the Full TDEMI measurement system.

B. APD measurement from Time domain captures

Full spectrum time-domain captures enable us to compute the APD probabilistic detector at the desired frequency band and employing the same resolution bandwidth than the actual communication channel [6], [7]. This is an advantage of using full time domain measurements instead of traditional EMI receivers according to CISPR 16-1-1. The problem is that in EMI receivers, the resolution bandwidth (RBW) of 200 kHz are not available although many communication systems such as GSM have this frequency bandwidth. The employment of the correct RBW according with the bandwidth of the DCS is particularly important when impulsive noise is evaluated. As impulsive noise is defined as a broadband disturbance, the use of filters different from the channel bandwidth of the DCS will incur in large errors. Previously, in [12] it has been demonstrated that the employment of 100 kHz or 300 kHz instead of the 200 kHz channel bandwidth in GSM receivers is traduced to an error larger than 6 dB at the APD detector output when impulsive noise is measured.

The procedure to calculate the APD from the TD captures is to down-convert the time domain signal of the frequency band that we want to evaluate at baseband and afterwards apply a low-pass filter with the same bandwidth of the communication system that we want to analyse. Upcoming, the envelope of the filtered signal is computed to finally obtain the APD diagram. APD is defined as the amount of time the measured envelope of an interfering signal exceeds a certain level [4]. The relation between the $APD_R(r)$ and the probability density function of the envelope R is

$$APD_R(r)=1-F_R(r) \quad (1)$$

and

$$f_R(r) = \frac{d}{dr}F_R(r) = -\frac{d}{dr}APD_R(r) \quad (2)$$

where $F_R(r)$ is the cumulative distribution function (cdf) and $f_R(r)$ is the probability density function (pdf). To obtain the pdf of the interference a histogram is done. Afterwards, the cdf is computed using the pdf results. Last, the APD is directly obtained from the cdf using the expressions shown above.

As it has been mentioned before, the APD main advantage compared with traditional detectors such as the QP is that it is possible to relate the APD measurement with the bit-error-probability caused by EMI. Being capable of knowing beforehand if a digital communication system will be interfered by the EMI and which is the grade of interference caused in terms of BER. Several studies have pointed a way to define limit points or limit lines at the APD diagram with the objective to clearly understand if the APD diagram of an interference will produce malfunction or not to a certain communication system [3], [4], [5], [12]. The limit points are defined considering the required bit error probability and also the sensitivity of the system. As an example that will be used later at the next section, a limit point at the APD diagram for a system that uses a QPSK modulation scheme can be calculated with the expression defined by equation (3).

$$(u_{limit}\ ,\ P_{limit}) \equiv \left(\frac{\beta_1 A}{\sqrt{m}}\ ,\ P_{req}\right) \quad (3)$$

where for a QPSK modulation scheme $\beta_1 = 1$, $m = 2$, A is the rms amplitude of the communication signal and P_{req} is the probability required by the communication system [5]. Hence, if we are available to measure the APD diagram of an impulsive noise, we can determine if it will produce an interference higher than the required BER or it will not produce a significant interference.

However, this analysis of the APD diagram with the limit line shall be done only with the contribution of the interference. If the APD diagram has also the contribution of a signal of the communication system, we will not be able to establish if the interference is harmful to the communication system. Therefore, if the interference study is done outdoors the signal of the DCS will modify the APD diagram and it will be not possible to determine if the impulsive noise will cause fault to the communication system. For this reason, at the following section, a procedure to split up the impulsive noise from the signal of the communication is explained by post-processing time domain captures.

C. Impulsive noise decomposition

The Empirical Mode Decomposition is a heuristic method developed for analyzing nonlinear and nonstationary signals. It was introduced by Huang et al. in 1998 [13]. The main capability of the EMD is to decompose complex datasets into a finite, and often small, number of components called intrinsic

Proc. of the 2017 International Symposium on Electromagnetic Compatibility - EMC EUROPE 2017, Angers, France, September 4-8, 2017

mode functions (IMF) that admit well-behaved Hilbert transforms. EMD is an entirely data-driven algorithm, it does not depend on any predefined basis functions and it does not require a domain transformation.

Recently, the original empirical mode decomposition algorithm was customized in order to enhance its performance when decomposing datasets obtained from EMI measurements. Sliding window techniques allowed for processing massive acquisitions with reasonable computing resources and transient extraction capabilities enable the impulsive noise decomposition. Those techniques have been used for ambient noise cancellation applications during in-situ EMI assessments [15]. The decomposition of impulsive noise is based on the automatic time gating process that recognises pulsed events in order to separate them from the continuous wave noise. In this regard, it analyses the envelope of the EMI for estimating the instant of occurrence and the duration of the pulses. With this information, the impulsive noise can be appropriately windowed for suppressing the continuous wave components of noise outside the minor interval that comprises the impulses. Due to space constraints, it is not possible to provide a detailed description of the technique. The interested reader is suggested to consult the above-mentioned references.

III. RESULTS / STUDY CASE

A. Measurement Scenario

With the aim to demonstrate the capabilities of the methodology described previously, a measurement test scenario is assembled. A digital communication system signal is synthetized by an arbitrary waveform generator and propagated as an electromagnetic field by an antenna. This communication system will be switched on or off with the objective to validate the decomposition of the narrow band communication system signal and the impulsive noise. Simultaneously, a source of impulsive noise is generating a broadband interference, this interference can also be turned on or off for the validation proposes. The biconical antenna used for measuring the electric field receives at the same time the contribution from the DCS signal and the impulsive noise. In Fig. 1 a schematic of the setup is illustrated.

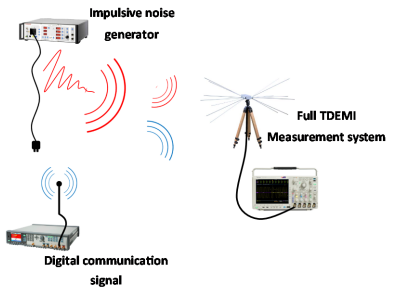

Fig. 1. Illustration of the outdoors test setup where the communication signal and the transient interference are coexisting.

Regarding the communication signal generated, it has been created by using Matlab® Simulink. A 200 kHz bandwidth QPSK signal with a square-root modulation pulse through a roll off factor of 0.2 is generated at baseband. The signal is up-converted to 40.68 MHz which is an industrial, scientific and medical (ISM) radio band and it is worldwide reserved for the use of radio frequency (RF) energy. Therefore, the synthetized signal is emulating a feasible communication system that can be encountered at any outdoor environment. The signal is delivered to the Agilent Technologies arbitrary waveform generator model 81160A, connecting its output to a biconical antenna to propagate the useful signal of the communication system. Concerning the impulsive noise, a Schölder electric fast transient generator model SFT 1400 according to EN 61000-4-4 standard is employed. The interfering pulses are coupled to a main AC wire producing disturbance electromagnetic fields. As it is defined at the standard, the rise time of the pulse is 200 ns, hence spectral components of the interference should appear at 40.68 MHz and reach the receiving measuring system.

The measuring system is composed by a PMM Biconical antenna model BC-01, which is connected to the Full TDEMI measurement system explained in section II.A. The oscilloscope (Tektronix DPO5104B) is used to capture the time domain traces and the computer is employed to control the oscilloscope, compute the frequency domain, the APD diagram and also to perform the decomposition of the signals at it has been described in section II.C.

Following different measurements are shown regarding the interference scenario. Firstly, standard APD full time-domain measurements are conducted to emphasis the necessity of eliminating the contribution of the communication system signal in order to avoid misinterpretation of the APD results.

B. Standard APD measurements results

Three different measurement are performed to highlight the differences that appear at the APD diagram. In the first measurement case only the impulsive noise is active; secondly only the signal of the DCS is present; and thirdly the impulsive interference and the DCS signal are simultaneous present.

The APD diagram is computed at the 200 kHz band centred at 40.68 MHz employing the procedure described in section II.B. In figure Fig. 2, in a blue continuous trace, it can be observed the APD diagram obtained when the DCS signal and the impulsive noise generated are active. Otherwise with a red trace it is shown the result when only the impulsive noise is present and finally, in black the APD result corresponds to the DCS signal without interference.

As it can be clearly observed from the results, the APD diagrams are overlapped when DCS is active, regardless off the impulsive noise is switched on or not. Elsewhere, when the impulsive disturbance is measured with the DCS signal turned off, the shape of the APD diagram changes to a heavy tailed distribution, which is characteristic for impulsive noise interferences. Hence, the problem of obtaining the APD diagram in presence of the DCS signal is that the useful communication signal is masking the impulsive interference.

Proc. of the 2017 International Symposium on Electromagnetic Compatibility - EMC EUROPE 2017, Angers, France, September 4-8, 2017

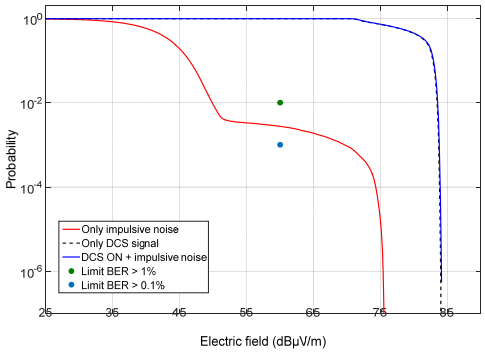

Fig. 2. APD standard measurement when the impulsive noise and the DCS signal are coexistnet, only the interference and only the DCS signal.

In Fig. 2, it can be also observed two limit points, as it has been explained before, with the APD diagram we are capable to relate the measured curve with the BER of the communication system. By means of taken into account the required BEP and the amplitude of the received signal. Related with this amplitude, it is necessary to consider that the signal of the communication system can be received with different levels. For instance, if we are evaluating a mobile DCS, the source of the communication signal is moving and the level of the received signal changes. The amplitude of the signal can be a high level but also it can be reduced according to sensitivity of the communication system. Hence, it is necessary to determine with the limits if the DCS will incur into failure due to an interference given the sensibility of the DCS or at least with an average received level. Practically, it means that even though we are receiving a level of 85 dBµV/m signal when we perform the measurement, we have to consider that the communication system can receive lower levels of useful signal in other situations to compute the limit point. In this study case, the sensibility level of the system working at 40.68 MHz is at 60 dBµV/m. Then the limit points are computed using equation (3). Where A is the rms amplitude of the communication signal and P_{req} is the probability required by the communication system. Hence, if the trace of the APD diagram is above the green point at the APD diagram, the BER will be higher than 1%, otherwise if it is above the blue point the BER will be higher than 0.1%.

If we consider the red trace in Fig. 2, which corresponds to the measurement when the DCS signal was switched off, we can determine that the impulsive interference will cause a BER between 0.1% and 1%. However, if we analyse the APD traces when the DCS signal is switched on (blue and black traces), the APD diagram contains both limit points due to the useful signal of the communication system. Making impossible to use the limit points and conclude if the communication system can be interfered by the impulsive disturbance. Unfortunately, we have to emphasize that in outdoors environments the measurement scenario will always include the signal of the communication system.

To illustrate what it is happening to the APD diagram when the DCS signal is active, the spectrum measurement of the impulsive noise generated by the fast transient generator is shown in Fig. 3. At 40.68 MHz it is observed a narrow band signal which corresponds to the DCS that has been synthetized. As the measurement has been performed outdoor other communication systems like frequency modulation (FM) broadcasting are present from 87.5 MHz to 108 MHz. Additionally, it can be also observed the broadband interference generated by the impulsive noise. The fast transient generator is causing the wide spectrum interference that can be seen from 30 MHz till above 100 MHz. Consequently, the impulsive noise is partially sharing the spectrum with the communication system at 40.68 MHz.

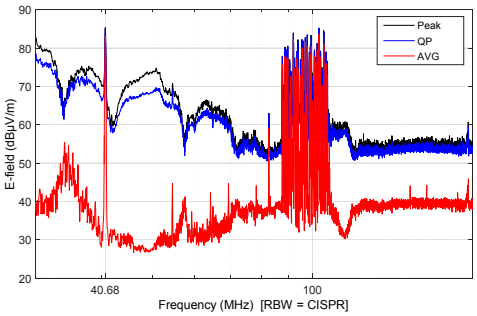

Fig. 3. Frequency domain standard measurement of the outdoor test scenario, where it can be seen the DCS signal at 40.68 MHz and the broadband impulsive noise.

Although it is clearly observed that the impulsive noise and the communication systems are sharing the spectrum, it is not feasible to unequivocally indicate if the impulsive interference will cause malfunction to the communication system from the peak, QP or average measurement.

Therefore, calculating the APD in presence of the communication signal is non-sense as the APD diagram is mostly influenced by the useful signal of the communication system. Especially as we have seen when the signal of the communication system is higher than the interference. For this reason, it is necessary to apply the decomposition method in time domain to split the impulsive noise from the communication signal.

C. Time Domain decomposition methodology to obtain APD in presence of the DCS signal

The solution proposed in this paper is to employ time domain decomposition of the measurement in order to separate the impulsive noise and calculate its APD diagram. In time domain the impulsive noise can be clearly observed and by means of decomposition time-domain techniques it can be split up from the other measured signals, which are narrow band and continuous. This opportunity of post-processing is available because in comparison with the traditional frequency sweep measurements, where we are looking only at the frequency band where we are centred, in Full time domain methodology we are observing the entire spectrum with the amplitude and

phase information. In Fig. 4, the time domain results of applying the decomposition of the interference plus the communication system obtained is observed.

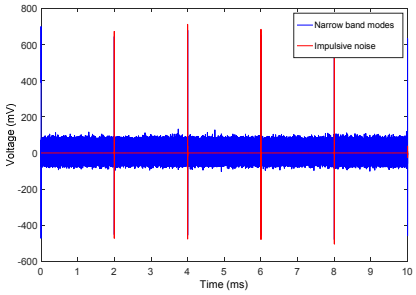

Fig. 4. Time domain decomposition applied splitting up the impulsive noise and the narrow band components.

As a characteristic of the impulsive noise, when we are observing the full spectrum, as it is done in the time-domain measurement, we can clearly identify the pulses of the broadband short duration disturbance. Therefore, it is feasible to apply the post-processing techniques and achieve the red line in Fig. 4, which is the result of splitting the impulsive noise from the narrow band signals of the communication systems.

With the aim to illustrate the accurately splitting of the impulsive noise from the narrow band signals, the frequency domain has been computed in Fig. 5. From these results, it can be verified that the decomposition of the time domain signal has been properly done.

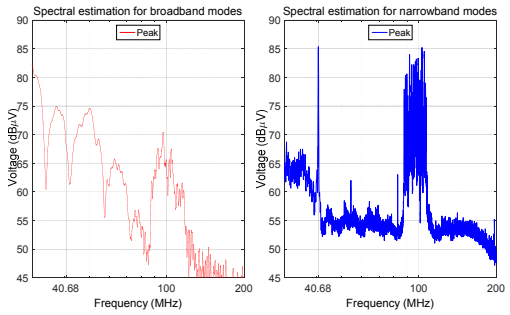

Fig. 5. Frequency domain results of the impulive noise and the narrow band DCS signals.

In Fig. 5, the impulsive noise spectrum only contains the broadband interference from 30 MHz till 120 MHz. Otherwise the spectrum produced by the narrow band modes does not include the broadband interference. Instead of, the narrow band signal from the DCS synthetized at 40.68 MHz and the FM broadcasting signal at 100 MHz is evidently identified. Therefore, it is shown that the impulsive noise has been separated properly and now we are available to compute the APD diagram considering only EMI impulsive noise.

In Fig. 6, the APD diagram of the impulsive noise obtained from the full time domain decomposition is plotted with the solid green line. For validation proposes and since it has been a scenario to demonstrate the applicability of the methodology, we have switched off the signal of the communication system working at 40.68 MHz and computed the APD diagram, which is displayed with the dashed red line in Fig. 6. Finally, the blue line is the APD diagram obtained before applying the decomposition and the influence of the useful signal is masking the entire APD result.

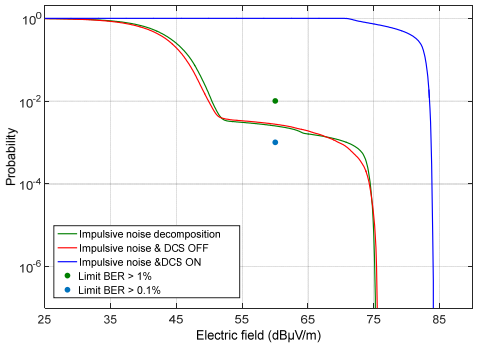

Fig. 6. APD result of the impulsive interference when the time-domain decomposition methodology is applied.

Firstly, it is important to highlight that the shape of the APD diagram is crucially changed when the signal of the communication system is eliminated. The shape is transformed from typically Gaussian noise distribution to a heavy tailed distribution, which is characteristic for impulsive noise disturbances [5], [6]. Elsewhere, the extremely good fitting between the results obtained when the decomposition method is applied with the case when the signal of the communication system is switched off demonstrate the capabilities and the benefits of the methodology developed.

Moreover, with the signal of the DCS eliminated from the APD diagram, it is possible to consider the limit points which relate the APD diagram of the EMI with its associated BER. From Fig. 6, it can be easily concluded that the BER produced by the impulsive noise will be between 0.1% and 1%. Hence, if the 40.68 MHz QPSK communication system only tolerates a BER of 0.1 % the interference will cause a failure. Otherwise we can say unequivocally that if the tolerance of the DCS is up to a BER equal to 1% the impulsive noise will not be harmful.

IV. DISCUSSION AND CONCLUSIONS

A first point of discussion is to highlight the great advantage that introduces the APD diagram, when it is combined with limit points, compared with the traditional detectors like QP which are employed at EMC harmonised standards. With the study case measurements, we have demonstrated that with the APD diagram it is possible to determine the exact BER of a

DCS when impulsive interference is disturbing the system. Once the contribution of the DCS has been removed from the APD diagram. Hence, it is essential to obtain the APD diagram without the contribution of the useful signal of the communication system, which is disgracefully always present when outdoor in-situ measurements are conducted to evaluate real interference scenarios.

In this paper, it has been demonstrated that the novel methodology combining the Full TDEMI with time-domain decomposition of impulsive noise and narrow band signals offers us the possibility to split up the impulsive noise interference from the useful DCS signal. Hence, this is the key point to be able to evaluate the possible degradation caused at the communication systems. Holding the advantage to unequivocally determine if the impulsive noise measured in presence of the communication system will cause a degradation. The methodology will conclude if the transient interference is harmful enough to cause malfunction, according to the maximum bit error probabilities tolerable and its DCS sensibility. Therefore, the novel measurement and post-processing strategy is an overwhelming opportunity for real interference scenarios where it is not available to switch off the communication system to measure and evaluate the interference. Being able to apply this methodology outdoors, especially for mobile communications where the level of the received signal is constantly changed.

ACKNOWLEDGMENT

This work was supported in part by the EURAMET 15RPT01 research project (the EMPIR is jointly funded by the EMPIR participating countries within EURAMET and the European Union) and by the Spanish “Ministerio de Economía, industria y Competitividad,” under projects TEC2013- 48414-C3-3-R and TEC2016-79214-C3-2-R (AEI/FEDER, UE).

REFERENCES

[1] D. Middleton, “Canonical and quasi-canonical probability models of Class A interference,"IEEE Trans. Electromagn. Compat., vol. EMC-25, no. 2, pp. 76 103, May 1983

[2] Dudoyer, S.; Deniau, V.; Ambellouis, S.; Heddebaut, M.; Mariscotti, A., "Classification of Transient EM Noises Depending on their Effect on the Quality of GSM-R Reception," Electromagnetic Compatibility, IEEE Transactions on, vol.55, no.5, pp.867,874, Oct. 2013

[3] Wu, I.; Ohta, H.; Gotoh, K.; Ishigami, S.; Matsumoto, Y., "Characteristics of Radiation Noise from an LED Lamp and Its Effect on the BER Performance of an OFDM System for DTTB," *Electromagnetic Compatibility, IEEE Transactions on* , vol.56, no.1, pp.132-142, Feb 2014

[4] K. Wiklundh, “Relation between the amplitude probability distribution of an interfering signal and its impact on digital radio receivers,” *IEEE Trans. on EMC*, Aug. 2006, pp. 537-544.

[5] Matsumoto, Y., "On the Relation Between the Amplitude Probability Distribution of Noise and Bit Error Probability," *Electromagnetic Compatibility, IEEE Transactions on* , vol.49, no.4, pp.940,941, Nov. 2007

[6] M. Pous and F. Silva, "Full-Spectrum APD Measurement of Transient Interferences in Time Domain," in *IEEE Transactions on Electromagnetic Compatibility*, vol. 56, no. 6, pp. 1352-1360, Dec. 2014.

[7] M. Pous and F. Silva, "APD radiated transient measurements produced by electric sparks employing time-domain captures," *2014 International Symposium on Electromagnetic Compatibility, Gothenburg*, 2014, pp. 813-817.

[8] M. Pous and F. Silva, "Prediction of the impact of transient disturbances in real-time digital wireless communication systems," in *IEEE Electromagnetic Compatibility Magazine*, vol. 3, no. 3, pp. 76-83, 3rd Quarter 2014.

[9] M. A. Azpúrua, M. Pous, S. Çakir, M. Çetintaş, and F. Silva, “Improving Time-Domain EMI measurements through Digital Signal Processing,” *Electromagn. Compat. Mag. IEEE*, vol. 4, no. 2, pp. 66–74, 2015.

[10] M. A. Azpúrua, M. Pous, and F. Silva, “A Measurement System for Radiated Transient Electromagnetic Interference Based on General Purpose Instruments,” in *Electromagnetic Compatibility (EMC EUROPE), International Symposium on*, 2015.

[11] M. A. Azpúrua, M. Pous, and F. Silva, *On the Statistical Properties of the Peak Detection for Time-Domain EMI Measurements*, vol. 57, no. 6. IEEE, 2015, pp. 1374–1381.

[12] M. Pous, M. A. Azpúrua, and F. Silva, *Measurement and Evaluation Techniques to Estimate the Degradation Produced by the Radiated Transients Interference to the GSM System*, vol. 57, no. 6. 2015, pp. 1382–1390.

[13] N. E. Huang, Z. Shen, S. R. Long, M. C. Wu, H. H. Shih, Q. Zheng, N.-C. Yen, C. C. Tung, H. H. Liu, N. E. Huang, Z. Shen, S. Long, M. Wu, H. Shih, Q. Zheng, N.-C. Yen, C. Tung, and H. Liu, “The empirical mode decomposition and the Hilbert spectrum for nonlinear and non-stationary time series analysis,” Proc. R. Soc. London. Ser. A Math. Phys. Eng. Sci., vol. 454, no. 1971, pp. 903–995, 1998.

[14] M. A. Azpúrua, M. Pous and F. Silva, "Decomposition of Electromagnetic Interferences in the Time-Domain," *in IEEE Transactions on Electromagnetic Compatibility*, vol. 58, no. 2, pp. 385-392, April 2016.

[15] M. A. Azpúrua, M. Pous and F. Silva, "A single antenna ambient noise cancellation method for in-situ radiated EMI measurements in the time-domain," *2016 International Symposium on Electromagnetic Compatibility - EMC EUROPE,* Wroclaw, 2016, pp. 501-506.

7

PERFORMANCE OF FULL TIME-DOMAIN EMI MEASUREMENT SYSTEMS

The publications in subsections 7.1, 7.2 and, 7.3 comprise the contributions related to the decomposition of EMI in the time-domain. In concordance with the fourth objective of this Thesis, the highlights of those articles are summarized below.

Objective 4: The baseline requirements of the CISPR 16-1-1 were extensively evaluated using an automated iterative procedure. In this regard, each iteration involved configuring the reference instrument or generator, acquiring, processing, calculating the error and comparing against the standard tolerances. Full TDEMI measurement systems were assessed in CISPR bands A to D for two different models of oscilloscopes. The proposed method exploits arbitrary waveform generators for replacing the CISPR nanosecond baseband pulse generator. The uncertainty of the assessment process is estimated. There is sufficient evidence to attest the evaluated Full TDEMI measurement systems are in conformity with CISPR 16-1-1. Moreover, additional characterization of oscilloscopes for determining its noise figure, sensitivity and effective number of bits was performed under the exact same conditions required for Full TDEMI measurement systems to be CISPR16-1-1 compliant.

7.1. FUNDAMENTAL JOURNAL ARTICLE 4

M. A. Azpúrua, M. Pous, J. A. Oliva, B. Pinter, M. Hudlička and F. Silva, "Waveform Approach for Assessing Conformity of CISPR 16-1-1 Measuring Receivers," in *IEEE Transactions on Instrumentation and Measurement*, vol. PP, no. 99, pp. 1-12, 2018. doi: 10.1109/TIM.2018.2794941

Abstract-An alternative approach for assessing the conformity of electromagnetic interference measuring receivers with respect to the baseline CISPR 16-1-1 requirements is proposed. The method's core is based on the generation of digitally synthesized complex waveforms comprising multisine excitation signals and modulated pulses. The superposition of multiple narrowband reference signals populating the standard frequency bands allows for a single-stage evaluation of the receiver's voltage accuracy and frequency selectivity. Moreover, characterizing the response of the weighting detectors using modulated pulses is more repeatable and less restrictive than the conventional approach. This methodology significantly reduces the amount of time

required to complete the verification of the receiver's baseline magnitudes, because time-domain measurements enable a broadband assessment while the typical calibration methodology follows the time-consuming narrow band frequency sweep scheme. Since the reference signals are generated using arbitrary waveform generators, they can be easily reproduced from a standard numerical vector. For different test receivers, the results of such assessment are presented in the 9 kHz-1 GHz frequency range. Finally, a discussion on the measurement uncertainty of this methodology for assessing measuring receivers is given.

7.2. CONFERENCE PROCEEDING 8

M. A. Azpúrua, J. A. Oliva, M. Pous and F. Silva, "Fast and automated verification of multi-channel full time-domain EMI measurement systems," *2016 2017 IEEE International Instrumentation and Measurement Technology Conference (I2MTC)*, Turin, 2017, pp. 1-6. doi: 10.1109/I2MTC.2017.7969789

Abstract-Recently, concern has been raised with regard to the adequacy of current verification practices carried out in electromagnetic compatibility (EMC) testing laboratories. Bridging the gap in the scope and reliability of the verifications performed in EMC laboratories requires faster and simpler verification methods to be performed prior testing. This paper presents a verification method for Full Time Domain Electromagnetic Interference measurement systems (Full TDEMI) that is intended to be quick and automated in order to become practical under the "just-before-test" approach. The method comprises a four stage process for assessing: sine-wave voltage accuracy, response to pulses, selectivity and input impedance. The verification method has been implemented and executed on an oscilloscope-based Full TDEMI achieving a reduction of time and effort involved while ensuring the compliance with CISPR 16-1-1 applicable requirements. Finally, this verification method improves the statistical significance because of the large number of points and conditions checked by the measurement automation software.

7.3. CONFERENCE PROCEEDING 9

M. A. Azpúrua, M. Pous, M. Fernández Chimeno and F. Silva, "Dynamic Performance Evaluation of Full Time Domain EMI Measurement Systems," *2018 International Symposium on Electromagnetic Compatibility - EMC EUROPE*, Amsterdam, 2018, pp. 1-6. (Accepted paper)

Abstract-This paper presents the evaluation of the performance of Full Time Domain Electromagnetic Interference measurement systems in terms of the noise figure, the linearity, the dynamic range, the voltage standing wave ratio and the crosstalk. The above-mentioned parameters allow a broader characterization of the oscilloscope-based implementations of CISPR 16-1-1 measuring receivers, providing relevant specifications that are beyond the standardized baseline requirements. Such metrics are assessed using the actual settings and operating conditions required for compliant time-domain EMI measurements. For the specific oscilloscope used in the experiments, the noise figure is measured for all the different vertical ranges between 5 mV/div and 1 V/div. Likewise, the linearity and the dynamic range, in terms of the effective number of bits, was measured for sine wave input signals with an rms voltage swept between 20 mV and 1 V. This experiment was repeated for CISPR bands A, B and C/D using 10 kHz, 1 MHz, and 100 MHz sinusoids, respectively. The results allow a more comprehensive comparison between Full TDEMI measurement systems and the more conventional superheterodyne architecture receivers that are completely specified in the frequency domain.

IEEE TRANSACTIONS ON INSTRUMENTATION AND MEASUREMENT, VOL. 67, NO. 5, MAY 2018 1187

Waveform Approach for Assessing Conformity of CISPR 16-1-1 Measuring Receivers

Marco A. Azpúrua, *Member, IEEE*, Marc Pous, José A. Oliva, Borut Pinter, Martin Hudlička, *Senior Member, IEEE*, and Ferran Silva, *Fellow, IEEE*

***Abstract*— An alternative approach for assessing the conformity of electromagnetic interference measuring receivers with respect to the baseline CISPR 16-1-1 requirements is proposed. The method's core is based on the generation of digitally synthesized complex waveforms comprising multisine excitation signals and modulated pulses. The superposition of multiple narrowband reference signals populating the standard frequency bands allows for a single-stage evaluation of the receiver's voltage accuracy and frequency selectivity. Moreover, characterizing the response of the weighting detectors using modulated pulses is more repeatable and less restrictive than the conventional approach. This methodology significantly reduces the amount of time required to complete the verification of the receiver's baseline magnitudes, because time-domain measurements enable a broadband assessment while the typical calibration methodology follows the time-consuming narrow band frequency sweep scheme. Since the reference signals are generated using arbitrary waveform generators, they can be easily reproduced from a standard numerical vector. For different test receivers, the results of such assessment are presented in the 9 kHz–1 GHz frequency range. Finally, a discussion on the measurement uncertainty of this methodology for assessing measuring receivers is given.**

***Index Terms*— Calibration, electromagnetic interference, quality management, standards, time-domain measurements.**

I. Introduction

THE measuring receiver is the fundamental instrument for conducted and radiated electromagnetic emissions testing. According to the standard definition given by the CISPR 16-1-1:2015, it is an "instrument such as a tunable voltmeter, an electromagnetic interference receiver, a spectrum analyzer or a fast Fourier transform (FFT)-based measuring instrument, with or without preselection, that meets the relevant parts of this standard" [1]. In this regard, the standard CISPR 16-1-1 does not provide a particular implementation of a measuring receiver but a number of requirements that manufacturers have to fulfill under a "black-box" approach.

Therefore, assessing of the quantities and ranges that allow certifying the conformity of measuring receivers is mandatory. Such assessment employs calibration and verification results for determining if the measuring receiver performance is within the tolerance margins. However, the variety of implementations of EMI test receivers and the particularity of their requirements have led to a common situation in which the instrument manufacturer can be the only capable entity of performing a complete calibration of their own measuring receivers.

On the one hand, this is because the established method for calibrating the response to pulses of the standard weighing detectors, e.g., the quasi-peak (QP) detector, uses a baseband (nanosecond) pulse generator for providing a set of rectangular pulses with a fixed impulse area and repetition frequency [2]. Such a signal generator is an expensive piece of hardware that can hardly be used for other calibration setups. On the other hand, the vast number of magnitudes, functions, and ranges subject to calibration in modern EMI measuring receivers urges for automated calibration processes programmed for every different manufacturer and model in order to deliver calibration results in a reasonable time frame. Thus, the remarkable amount of resources and effort needed for implementing a specific calibration bench suitable for EMI measuring receiver undermines its widespread adoption by the third-party calibration providers.

At European level, National Metrology Institutes (NMIs) are concerned by the actual metrological capability (beyond the calibration services provided by the first parties) to provide complete calibration and traceability for EMI measuring receivers. In such conditions, it is likely that even accredited test houses are performing electromagnetic emissions testing without an adequate traceability required by the ISO/IEC 17025 standard. Actually, experience indicates that EMI test receivers are often calibrated as spectrum analyzers, which is insufficient. In fact, the critical functions of an EMI measuring receiver that are involved in the determination of compliance must be calibrated, including not only the reading of the spectrum level but also its frequency selectivity and response to pulses of the weighting detectors. Moreover, this situation could happen unnoticed if the procedures involved

Manuscript received July 1, 2017; revised December 13, 2017; accepted December 15, 2017. Date of publication February 1, 2018; date of current version April 5, 2018. This work was supported in part by the EURAMET 15RPT01 Research Project (the EMPIR is jointly funded by the EMPIR participating countries within EURAMET and the European Union), in part by the Spanish Ministerio de Economía, Industria y Competitividad, under Project TEC2016-79214-C3-2-R (AEI/FEDER, UE), in part by the Secretaria d'Universitats i Recerca del Departament d'Economia i Coneixement de la Generalitat de Catalunya, and in part by the European Social Fund. The Associate Editor coordinating the review process was Dr. Mohamed Abou-Khousa. *(Corresponding author: Marco A. Azpúrua.)*

M. A. Azpúrua, M. Pous, J. A. Oliva, and F. Silva are with the Group of Electromagnetic Compatibility, Department of Electronic Engineering, Universitat Politècnica de Catalunya, 08034 Barcelona, Spain (e-mail: marco.azpurua@upc.edu).

B. Pinter is with the Slovenian Institute of Quality and Metrology, 1000 Ljubljana, Slovenia (e-mail: borut.pinter@siq.si).

M. Hudlička is with the Czech Metrology Institute, 638 00 Brno, Czech Republic (e-mail: mhudlicka@cmi.cz).

Color versions of one or more of the figures in this paper are available online at http://ieeexplore.ieee.org.

Digital Object Identifier 10.1109/TIM.2018.2794941

0018-9456 © 2018 IEEE. Personal use is permitted, but republication/redistribution requires IEEE permission.
See http://www.ieee.org/publications_standards/publications/rights/index.html for more information.

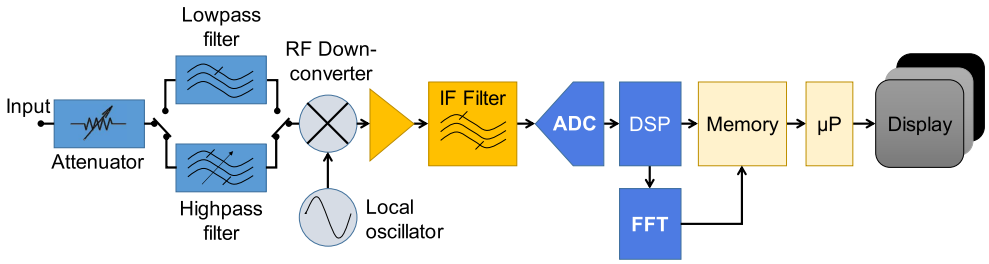

Fig. 1. Block diagram of a real-time EMI analyzer.

in testing and auditing the performance of EMI test receiver do not include specific CISPR 16-1-1 requirements. Hence, many EMI measuring receivers are being calibrated only according to the widespread guidelines used for spectrum analyzers [3], [4].

The abovementioned situation was acknowledged in a previous call from the European Metrology Programme for Innovation and Research (EMPIR), the ongoing Joint Research Project "Development of RF and Microwave Metrology Capability," also known as RFMicrowave (15RPT01), pointed out that "... current knowledge between EMC and RF&MW laboratories is very weak, which reduces awareness in measurements/calibrations and, therefore the overall quality of both EMC and RF&MW measurements" [5].

Particularly, the calibration of CISPR 16-1-1 pulse generators can be challenging in terms of the required accuracy in the determination of its spectral density, which is ±0.5 dB [1], [6]. In a report from EURAMET, the results from an interlaboratory measurement comparison of a pulse generator in accordance with CISPR 16-1-1 were presented. From the six laboratories that participated, METAS, PTB, and Schwarzbeck successfully used a time-domain approach with ultrawideband oscilloscopes, while the other participants preferred to keep undisclosed their calibration method. However, the spread of the results cannot be explained by the uncertainties quoted by the participants [7].

In that sense, a strategy posed by the metrology community for bridging this gap is to introduce a whole new set of more repeatable, reproducible, and less hardware stringent calibration and verification methods suitable for EMI measuring receivers. Previously, the authors presented an automated method for verifying the compliance of full time-domain EMI (TDEMI) measurement systems. The verification method has five stages that cover the baseline parameters that allow an EMI measuring receiver to be compliant with CISPR 16-1-1 requirements, that is, sine-wave voltage accuracy, absolute and relative response to pulses, frequency selectivity, and voltage standing wave ratio (VSWR). Some satisfactory results were presented for the 9 kHz–30 MHz frequency range, which covers the CISPR bands A and B typically related to conducted EMI measurements. The setup employed for the verifications is very compact and uses an arbitrary waveform generator (AWG) and a vector network analyzer (VNA) as standard reference equipment [8].

The continuation of that work is presented here as a time-domain waveform approach for assessing conformity of EMI measuring receivers. By using synthesized multisine excitation signals and modulated pulses, the proposed methodology is aimed to characterize the accuracy, response to pulses, and selectivity of the test receiver using a more accessible and agile strategy, and is addressed to match specific requirements of the FFT-based measuring receivers, including the new generation of real-time EMI measuring systems and also oscilloscope-based implementations of the test receivers, since they can benefit the most from the time-domain measurements.

The structure of this paper is as follows. In Section II, an explanation of two remarkable types of FFT-based EMI measurement system is given. Then, Section III summarizes the key CISPR 16-1-1 requirements that EMI measuring receivers must comply with. Next, Section IV proceeds with the description of the proposed approach for conformity assessment in terms of the standard waveforms and their time- and frequency-domain behaviors. Finally, Section V presents some relevant measurement results of the baseline magnitudes of an oscilloscope-based TDEMI measurement system, and a comparison with the measurement results obtained with a swept receiver is used for cross validation. At the end of this paper, a discussion of scalability of this verification method for calibrating test receivers is presented along with the conclusions of this paper.

II. Overview of FFT-Based EMI Measuring Receivers Architectures

The modern generation of measuring receivers has embraced FFT-based capabilities not only for speeding up emissions' testing but also to provide time-domain and time–frequency analysis features useful for evaluating and mitigating the impact of transient and stochastic disturbances [9]. Currently, real-time analyzers and oscilloscope-based implementations are two differentiated approaches for implementing FFT-based measuring receivers. In this section, both of them are briefly explained in the light of CISPR 16-1-1 compliance feasibility.

A. Real-Time Analyzers

A block diagram of the real-time EMI analyzer's architecture is shown in Fig. 1. This type of measuring receiver

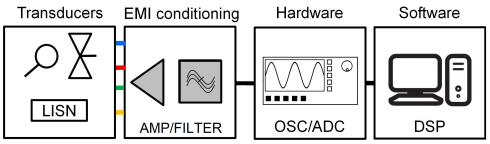

Fig. 2. Block diagram of a full TDEMI measurement system.

uses the mixer and the local oscillator to convert the input signal to a constant intermediate frequency (IF), similarly as with the heterodyne architecture. At IF, the signal is sampled fulfilling the Nyquist criterion using analog-to-digital converters (ADCs) and filtered to avoid aliasing. The time- and value-discrete IF signals are digitally downconverted to baseband and then processed for obtaining the signal spectrum. There are two possibilities for preparing a frequency-domain display. The first one is using digital filters of certain resolution bandwidth (RBW) for emulating the functioning of an analog spectrum analyzer. The second option is to calculate the spectrum of that portion of the spectrum using the FFT with the corresponding windowing for achieving the exact RBW setting. In both cases, it is still necessary to run through the frequency range that has been set on, which means that for spans larger than the IF bandwidth, several iterations of the acquisition are required [10], [11].

B. Full Time-Domain EMI Measurement Systems

Full TDEMI measurement systems are oscilloscope-based implementations of an EMI measuring receiver. In general terms, a full TDEMI measurement system is described by the block diagram shown in Fig. 2 [12], [13]. For the measurement of radiated EMI, a broadband antenna shall be used, while for the measurement of conducted EMI corresponds either a current clamp or a line impedance stabilization network. The measured signal could be amplified or filtered if this provides better sensitivity. In the ADC, the full spectrum signal is digitized in real time and stored in as a time-discrete value-discrete signal.

The final measurement results are computed via the processing techniques implemented in a software layer that provides compliance with the relevant CISPR 16-1-1 requirements.

A screenshot of an actual implementation of the full TDEMI by the Electromagnetic Compatibility Group (GCEM) of the Universitat Politècnica de Catalunya (UPC) is shown in Fig. 3. After deep memory acquisitions, the software of the full TDEMI measurement system performs signal processing tasks, including windowing, resolution enhancing, resampling, spectral estimation (using the short-time FFT and Welch's method), and the detector emulation. Those mathematical transformations are responsible for delivering the measurement results in accordance with CISPR 16-1-1 requirements [13].

Full TDEMI measurement systems capture the whole spectrum of the EMI with every acquisition enabling multidomain analysis. Besides, the triggering and multichannel capabilities found in most oscilloscopes provide additional tools for testing multifunctional mode equipment and for emissions testing parallelization. On the other hand, much higher sampling rates and a deeper memory are required than with real-time analyzers. This imposes bandwidth and dwell-time constraints based on the current oscilloscope technology.

C. Conformity Assessment Needs

Even though real-time analyzers are the intrinsically suitable approach for reaching the higher frequencies with sufficient dynamic range and sensitivity, both architectures are converging in some aspects. For instance, commercial real-time analyzers are offering a larger IF bandwidth. That is the case of the TDEMI X from GAUSS Instruments, the FSW-B512R from Rohde & Schwarz, or the N9030B-RT1 from Keysight Technologies having 645, 512, and 510 MHz of IF bandwidth, respectively. Conversely, oscilloscopes with an effective number of bits [14] suitable for general EMI measurements below 1 GHz are common nowadays. Moreover, PC-based oscilloscopes are more popular as the processing power and the speed of the communication interfaces allow for faster data transfer and software-based processing.

As both the described architectures for FFT-based measuring receivers play an important role in EMI compliance testing, they need a specific approach for assessing their conformity with regard the relevant CISPR 16-1-1 requirements [15], [16]. Research on such aspects has been partially undergone previously, mainly in charge of the first party developers and manufacturers [17]–[19]. Furthermore, a standardized method for performing calibrations and verification of the FFT-based measuring receivers in terms of the CISPR 16-1-1 requirements is not currently available. Sections IV and V will deepen in such matters after the following enumeration of the baseline requirements for EMI measuring receivers.

III. Standard Baseline Requirements for Electromagnetic Interference Measuring Receivers

The normative Annex K "Calibration requirements for measuring receivers" of the CISPR 16-1-1 provides two alternatives with regard to the demonstration of compliance of measuring receivers. The first possibility is using the manufacturer's calibration method for assessing compliance. As stated before, in many cases, this is neither feasible for manufacturer-independent nor for in-house calibration laboratories, because manufacturer's calibration method can hardly be reproduced due to the lack of procedural information and/or hardware resources, e.g., the CISPR pulse generator. The alternative is using a calibration or a traceable verification process that includes at least the following parameters: VSWR, sine-wave voltage accuracy, response to pulses, and selectivity.

Tables I and II summarize the standard baseline requirements applicable to EMI measurement systems in CISPR bands A–D. Those items constitute the baseline (minimum) set of requirements that shall be covered by any calibration or verification method.

Please note that a typical calibration certificate of an EMI measuring receiver may include other additional performance

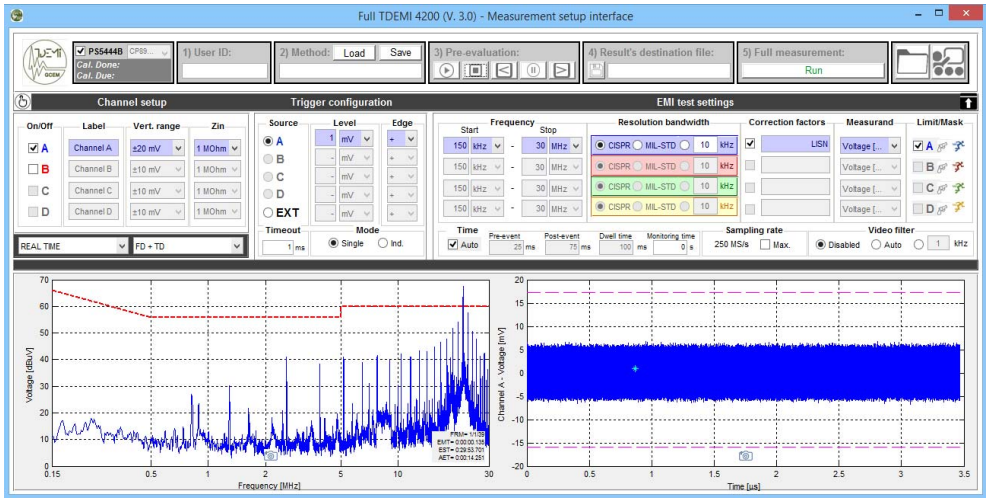

Fig. 3. Graphical user interface of the full TDEMI measurement setup panel.

TABLE I
BASELINE CISPR 16-1-1 REQUIREMENTS FOR ELECTROMAGNETIC INTERFERENCE MEASURING RECEIVERS

Parameter	Subclause	Baseline standard requirements	Freq. ranges
VSWR	4.2, 5.2, 6.2, 7.2	2.0 to 1 (0 dB RF attenuation)	9 kHz - 1 GHz
Sine wave voltage accuracy	4.3, 5.4, 6.4, 7.4	Better than ± 2 dB (50 Ω resistive source impedance)	9 kHz - 1 GHz
Response to pulses[a] (Absolute)	4.4, 5.5, 6.5, 7.5	66 dB(μV) ± 1.5 dB (Flat spectrum within the measured bandwidth)	CISPR Bands A, B, C and D
Response to pulses[a] (Relative)	4.4, 5.5, 6.5, 7.5	Table II.	CISPR Band A, B, C and D
Selectivity[b]	4.5, 5.6, 6.6, 7.6	90 Hz ≤ $B_{1.5}$ ≤ 220 Hz 180 Hz ≤ B_6 ≤ 220 Hz 180 Hz ≤ B_{20} ≤ 440 Hz	CISPR Band A
		4 kHz ≤ $B_{1.5}$ ≤ 10 kHz 8 kHz ≤ B_6 ≤ 10 kHz 10 Hz ≤ B_{20} ≤ 20 kHz	CISPR Band B
		40 kHz ≤ $B_{1.5}$ ≤ 140 kHz 100 kHz ≤ B_6 ≤ 140 kHz 100 kHz ≤ B_{20} ≤280 kHz	CISPR Bands C and D

[a] CISPR 16-1-1 Annexes B and C describe methods for determining the output characteristics of a pulse generator used in verifications and calibrations of the absolute and the relative pulse response.
[b] B_x means the reference bandwidth at the x dB decay level.

tests. However, since partial calibration is allowed by CISPR 16-1-1, the forthcoming description focuses on those that are mandatory, critical, and/or different from the typical tests calibrated in spectrum analyzers. Moreover, given that the superheterodyne type of receivers has been excluded from the scope of this paper, all the specifications that are not relevant for the generality of FFT-based EMI measurement systems have been omitted.

With regard to the requirements highlighted above, some clarifications shall be made: 1) VSWR requirements are only applicable to the 0-dB RF attenuation condition, conversely if RF attenuation is used, the VSWR must be lower than 1.2; 2) narrowband verifications at discrete suggested frequencies (the start, stop, and center frequencies) are replaced by broadband measurements; 3) the pulse repetition frequencies considered are above 10 Hz, because this is the lowest mandatory pulse repetition frequency that is common to all CISPR frequency bands; and 4) for multichannel EMI measurement system, each channel shall be individually and independently verified.

IV. WAVEFORM APPROACH FOR ASSESSING CONFORMITY OF CISPR 16-1-1 MEASURING RECEIVERS

As mentioned in Section I, the proposed methodology is based on the exploitation of the AWG for the generation of reference excitation signals employed for assessing the compliance with CISPR16-1-1 baseline requirements. The VSWR verification is excluded from the scope of the method, since VNA-based measurements are easier and more suitable for this purpose. The explanation of this approach is subdivided into sine-wave and pulse response measures, as follows.

A. Sine-Wave Measures

Conventionally, the method for calibrating the sine-wave accuracy in EMI measuring receivers consists in applying a single tone with a well-known level and frequency and amplitude. The reading of all the standard detectors must be identical. The voltage of the excitation signal is indirectly measured with a reference power meter.

Instead, the proposed approach uses an AWG for synthesizing a multisine-wave signal as the excitation. In that sense,

TABLE II
REQUIREMENTS FOR THE RELATIVE PULSE RESPONSE OF THE STANDARD WEIGHTING DETECTORS

Band	f_{rep} (Hz)	PK/QP (dB)	QP/QP$_{(ref)}$ (dB)	AV/QP (dB)	RMS/QP (dB)
A 9 kHz -150 kHz	10	10.1±1.5	4.0±1.0		8.2±1.5
	25 (ref)	6.1±1.5	0	12.4±1.5	4.2±1.5
	60	3.1±1.5	-3.0±1.0		
	100	2.1±1.5	-4.0±1.0		-1.8±1.5
B 150 kHz – 30 MHz	10	16.6±1.5	10.0±1.5		24.3±2.0
	20	13.1±1.5	6.5±1.0		
	100 (ref)	6.6±1.5	0	32.9±1.5	14.3±1.5
	500			22.9±1.5	
	1000	2.1±1.5	-4.5±1.0	17.4±1.5	4.3±1.5
C, D 30 MHz – 1 GHz	10		14.0±1.5		
	20		9.0±1.0		
	100 (ref)	12.0±1.5	0		20.1±1.5
	1000		-8.0±1.0	38.1±1.5	10.1±1.0
	5000			26.3±1.5	

let us define a standard periodic signal $x(t)$ formed by a well-known combination of tones with controlled amplitude, frequencies, and phases as

$$x(t) = \sum_{i=1}^{N_{\text{tones}}} A_i(f_i)\sin((2\pi f_i)t + \phi_i(f_i)) \quad (1)$$

where A_i, f_i, and ϕ_i are, respectively, the amplitude, frequency, and phase of the ith tone and N_{tones} is the number of tones conforming $x(t)$.

Such signal is designed for providing independent control for the amplitude and phase of each tone, which allows adjusting the crest factor in the time domain [20]. Then, $x(t)$ is numerically sampled at a rate $f_s \geq 2f_{\max}$, where $f_{\max}$ is the upper bound of the frequency range to be evaluated. A sampling rate greater than or equal to the sampling rate of the measuring receiver is recommended.

A time-discrete signal $x[n]$ is then obtained, where $n = 0, 1, 2\ldots$ is the integer variable used as the time step index. At that point, a time period of $x[n]$ is normalized and transformed into a discrete-valued signal with the same resolution of the AWG's digital-to-analog converter (DAC). Such time- and value-discrete vector is configured in the AWG and its DAC's output is smoothed by the interpolation filter and then scaled for approximating the voltage waveform as faithfully as possible, obtaining $\hat{x}[n]$. Fig. 4 shows, as an example, a period of a normalized multisine-wave excitation signal.

Considering the theoretical value of $\hat{x}[n]$ is exactly known, it can be used for calculating the reference spectrum, $\hat{X}[f]$, of the excitation signal. Welch's method for spectral estimation is used as explained in [12] and [21]. An appropriate windowing function for providing a suitable RBW must be selected, e.g., the Gaussian or the Kaiser–Bessel functions [13]. Window overlapping of more than 90% is recommended for reducing scalloping errors.

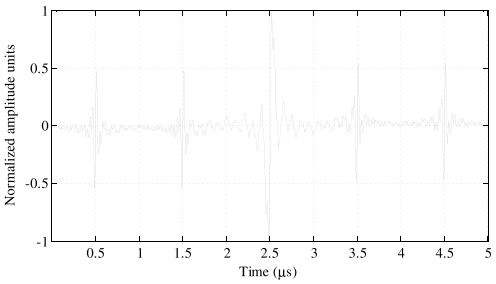

Fig. 4. Example of a multisine-wave excitation signal for assessing CISPR band B.

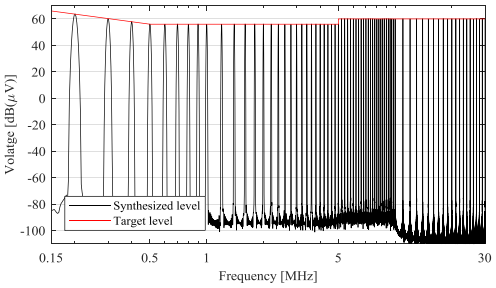

Fig. 5. Reference spectrum of a multisine-wave excitation signal that follows the CISPR 32 class B QP emissions' limit.

Fig. 5 shows the amplitude spectrum calculated from the theoretical excitation signal used in the previous example. Please note that the time-domain waveform was designed for providing tones with frequency-dependent amplitudes that follow the CISPR 32 limit line defined for class B equipment when using the QP detector. Beware, CISPR 16-1-1 does not specify the particular signal level at which the sine-wave level error calibration must be performed. However, authors recommend using the emissions' limit lines as the target for adjusting the excitation signal level, since this is the condition in which measurement accuracy is critical for determining compliance with EMC standards.

Nonetheless, other criteria can be used for designing the waveform of the excitation signal. For instance, pseudorandom and independent amplitudes, frequency, and phases can provide a noise-like multisine wave that allows obtaining statistical information about the variability of the assessed quantities.

In any case, the multisine-wave excitation signal must be fed to the measuring receiver for measuring its spectrum. The sine-wave accuracy is assessed by calculating the error in the voltage measured with respect to the reference value (previously calculated) at the exact frequencies for which the tones were generated.

On the other hand, selectivity requirements are assessed by iteratively measuring the 1.5-, 6-, and 20-dB decay bandwidths for each tone generated. Finally, please note that the frequency

TABLE III
STANDARD IMPULSE AREA SPECIFICATION

Frequency Band	Impulse area (μVs)
A	13.5
B	0.316
C	0.044
D	0.044

spacing of the multisine waveforms should respect RBW requirements for avoiding the component's overlapping.

B. Absolute and Relative Pulse Response

According to CISPR-16-1-1, the absolute and relative pulse response for the peak, QP, average (AV), and rms detectors shall be evaluated. The aim of these pulse measures is to emulate the broadband-impulsive interferences, which are common in EMC tests. The requirements of these pulses are described in CISPR 16-1-1, defining they must be flat in the frequency band under assessment with a level equivalent to a tone having an rms voltage of 2 mV, which means 66 dB (μV). These flat pulses are applied for different repetition rates in order to obtain a certain ratio between peak, QP, AV, and rms detectors, weighting the repetitiveness of the measured interferences [1].

In the CISPR 16-1-1, the waveform of the pulses is defined in open-circuit conditions according to their impulse area, and those specifications are reproduced in Table III.

Therefore, if we consider the pulses are perfectly rectangular, the amplitude of the required impulse is given by

$$A_{\text{imp}} = U_{\text{peak}} \times T_d \tag{2}$$

where U_{peak} is the peak voltage of the RF-modulated signal during ON state and T_d is the duration time of RF impulse in the course of the ON condition.

With the standard approach, it is technically possible to generate such flat pulse at all the frequency range for CISPR bands A–D. However, this is no longer feasible for higher frequencies, because there are no pulse generators capable of producing such extremely high voltage in fractions of picoseconds. That is why CISPR 16-1-1 indicates that "above 1 GHz, the required impulse area is defined using a pulse-modulated carrier at the frequency of test..." Therefore, in CISPR 16-1-1 Annex E, an alternative method is mentioned for the impulse evaluation above 1 GHz.

Nonetheless, in the proposed approach the AWG was only used for synthetizing the standard pulses for bands A and B while and for bands C and D the pulse-modulated RF technique mentioned in CISPR 16-1-1 Annex E was adapted. Therefore, we propose employing this technique for frequencies below 1 GHz as this procedure is easy to implement and it is already widely accepted for larger frequencies, as demonstrated by the accreditation of such procedure held by recognized NMIs.

Hence, the test setup for assessing the absolute and relative pulse response of the measuring receivers is according to Fig. 6.

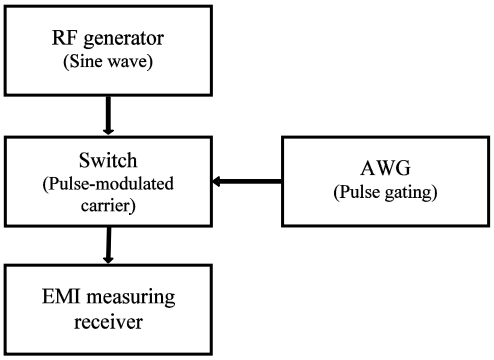

Fig. 6. Simplified block diagram of the test setup for assessing the absolute and relative pulse response of the measuring receivers.

TABLE IV
REFERENCE PULSE DURATION AND AMPLITUDE SPECIFICATION

Frequency Band	T_d (μs)	U_{rms} (mV)
A	100	95.5
B	2.2	101.6
C	0.167	186.3
D	0.167	186.3

The RF generator provides a continuous wave signal at the different frequencies selected for bands C and D. Then, the AWG produces the gating signal that modulates the carrier by switching ON and OFF the CW signal, creating a pulse according to CISPR16-1-1 requirements. Finally, the modulated pulse is fed directly to the EMI measuring receiver. The amplitude of the CW signal and the gating duration are defined in Table IV for bands A–D.

The specific carrier frequency and pulse repetition frequency of the modulating pulse must be iteratively configured to provide the excitation waveform suitable to evaluate the pulse response of the EMI measuring receiver in the conditions specified in Table I. As an example, Fig. 7 shows a 1-GHz pulse-modulated signal with a 1-kHz repetition frequency generated for assessing the response to pulses of a measuring receiver in CISPR bands C and D.

V. RESULTS

The following results are referred to the assessment of conformity performed on two different versions of full TDEMI measurement systems. The oscilloscopes involved are the PicoScope 5444B from Pico Technologies (OSC1) and the DPO5104B from Tektronix (OSC2).

The PicoScope 5444B has a 200-MHz bandwidth, a maximum sampling rate of 1 GSamples/s, 512 MSamples of memory depth, and its nominal input impedance is 1 MΩ. Therefore, an external 50-Ω matching load was connected in parallel to each oscilloscope's input channel. This measurement system is typically used for conducted EMI measurement, and thus it was assessed in CISPR bands A and B.

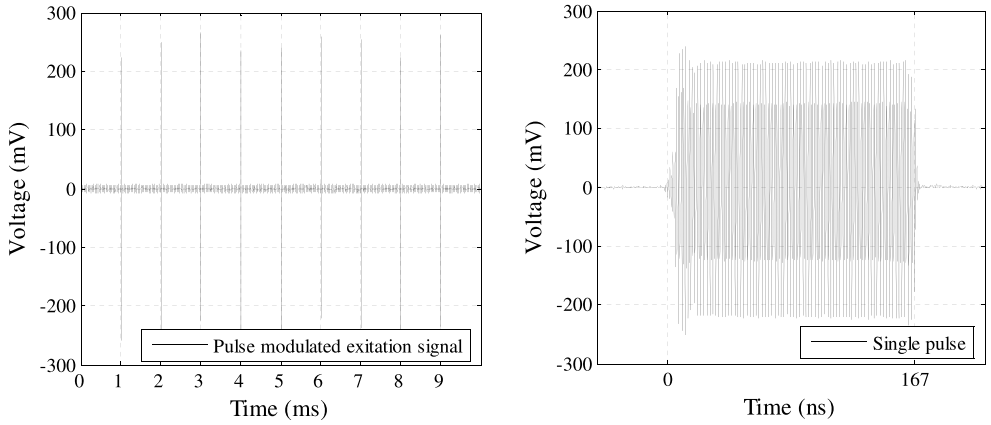

Fig. 7. Example of a 1-GHz pulse-modulated signal with a 1-kHz repetition frequency generated for assessing the response to pulses of a measuring receiver in CISPR bands C and D.

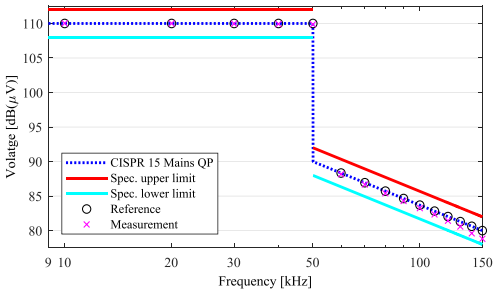

Fig. 8. Band A sine-wave accuracy assessment with respect to CISPR 15 QP emissions' limits for a full TDEMI measurement system.

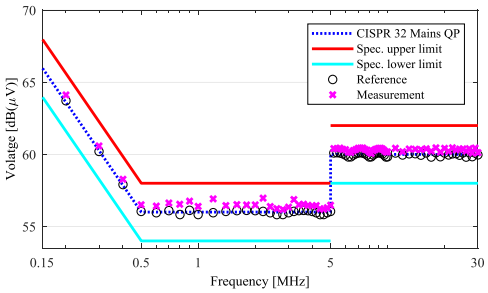

Fig. 9. Band B sine-wave accuracy assessment with respect to CISPR 32 QP class B emissions' limits for a full TDEMI measurement system.

The DPO5104B has a 1-GHz bandwidth, a maximum sampling rate of 10 GSamples/s, 50 MSamples of memory depth, and its nominal input impedance can be set to 50 Ω. This measurement system is more suited for radiated EMI measurement, and thus it was assessed in CISPR bands C and D. In practice, it may require additional external preamplification for increasing the sensitivity of the measurement system [12].

For generating the multisine-wave excitation signals, a pulse function arbitrary generator model 81160A from Keysight Technologies was used. It has a DAC with 14 bit of vertical resolution at 2.5 GSamples/s and a 330-MHz bandwidth for pulses extendable to 500 MHz for single tones.

An additional signal generator from Rohde & Schwarz model SML was employed for providing the sine wave in the assessment bands C and D. The switch Mini-circuits ZSWA-4-30DR was used in the pulse response test setup for modulating the sine waves according to the general procedure previously explained.

Cable attenuation was corrected in measurements. In all cases, low loss 50-Ω coaxial cables were used and their attenuation was measured for each frequency band.

A. Multisine-Wave Measurements

Previously, it was mentioned that different criteria could be used in the definition of the waveform of the test signal. In this regard, the multisine-wave signal employed for assessing OSC1 was designed using a couple of standard limit lines as reference. Conversely, OSC2 was evaluated using a pseudorandom selection of the amplitude of the individual tones. It is important to state that, even if neither criterion is preferred in terms of assessing compliance with CISPR 16-1-1 baseline requirements, however, they can deliver different insights, as it will be shown in what follows.

Figs. 8 and 9 show the measurement results of the sine-wave accuracy assessment performed for the abovementioned measuring receiver in CISPR bands A and B, respectively. In both figures, the blue dashed line represents the target level and the red and cyan lines provide an indication of the tolerance defined in Table I. Likewise, the black circles correspond to the achieved reference level, while the magenta markers symbolize the measurement result.

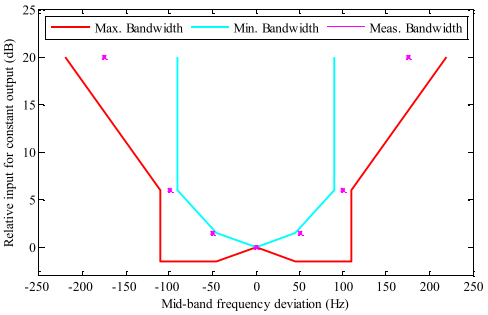

Fig. 10. Band A frequency selectivity assessment with respect to the equivalent IF filter mask.

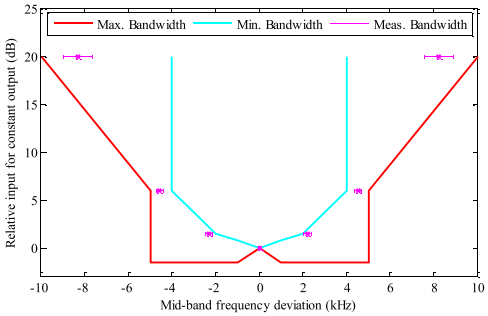

Fig. 11. Band B frequency selectivity assessment with respect to the equivalent IF filter mask.

On the one hand, band A target level was selected based on the QP limits for radio disturbances applicable to electrical lighting equipment according to the CISPR 15 standard [23]. On the other hand, band B target level was chosen based on the QP emissions limits for class B (domestic) equipment according to the CISPR 32 standard [24].

In both cases, just a single measurement was required for assessing the compliance of each CISPR band in terms of the accuracy of sine-wave measures, which, in this case, is favorable because worst case errors are lower than ± 1 dB.

Moreover, the same measurement results were used for calculating the 1.5-, 6-, and 20-dB decay bandwidth at each frequency component of the spectrum. Figs. 10 and 11 present the midband frequency deviation obtained from previous measurements. Mean values are marked with an "x" along with an error bar symbolizing the range of the variations of each measure. Again, results demonstrate compliance with CISPR 16-1-1 standard requirements.

Fig. 12 shows the summary of the measurement results from the sine-wave accuracy, frequency error, and selectivity assessment performed using pseudorandomly generated sine-wave excitations signals in bands C and D; 200 sine waves with random amplitude, frequency, and phase were generated at

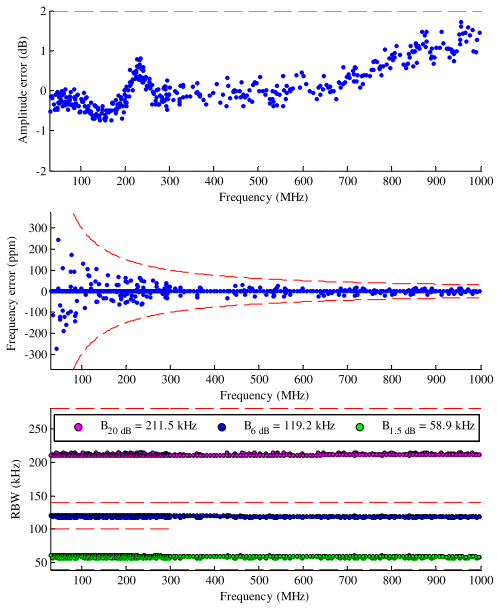

Fig. 12. Bands C and D sine-wave level error, frequency error, and selectivity assessment using pseudorandom multisine excitations for a full TDEMI measurement system.

each band. The amplitudes were uniformly distributed between 80 and 120 dB(μV), the phases were uniformly distributed in the [0, 2π] range, and the frequencies where equidistantly chosen between the upper and the lower frequency of the band plus a random frequency shift uniformly distributed between $\pm$RBW/2.

In this regard, the three subplots in Fig. 12 show that the performance of the full TDEMI measurement system is compliant with standard requirements, since all the measured points are included in the tolerance margins declared in Table I. Interestingly, this methodology can be interpreted as an empirical Monte Carlo evaluation of the baseline parameters variability in measuring receivers.

Consequently, the statistical information obtained from previous measurements enabled additional exploitation of the result, comprising the analysis of the approximated distribution of the parameters under assessment.

Fig. 13 shows the histograms of relative frequency for the error in the amplitude of the measured tones. This information can be used in more realistic uncertainty estimations in EMI measurements.

B. Absolute and Relative Pulse Response

The pulse response assessment is shown in Fig. 14 for bands A and B (OSC 1) at the reference repetition frequency. The most relevant aspects to notice are the flatness of the frequency response and the ratios between peak/QP and QP

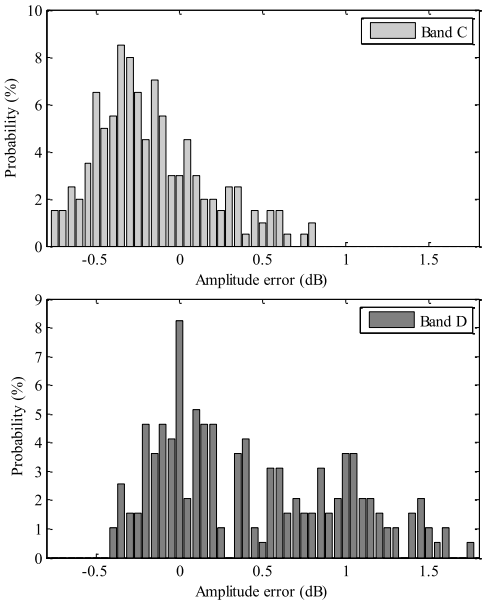

Fig. 13. Approximated empirical probability distribution for the amplitude error in sine-wave measurements for a measuring receiver in bands C and D.

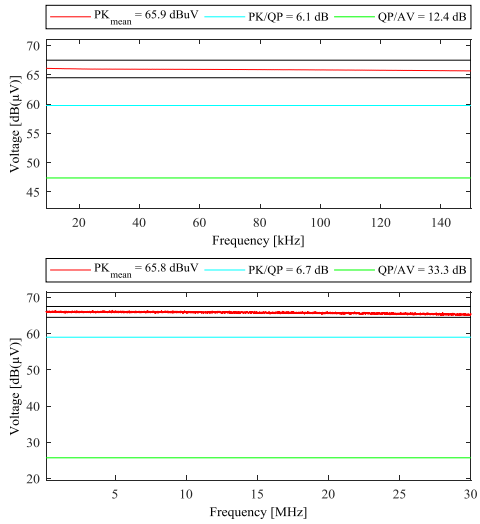

Fig. 14. Bands A (above) and B (below) assessment results of the absolute response to pulses for a full TDEMI measurement system (OSC1).

average, which fulfill standard requirements. It is important to highlight that this is a full-spectrum and multidetector characterization of the pulse response. For band A, the maximum errors registered were 0.7, 0.17, and 0.19 dB for the absolute

TABLE V
RESULTS FROM THE RELATIVE PULSE RESPONSE VERIFICATION

	Band	f_{rep} [Hz]	PK/QP [dB]	QP/QP$_{(ref)}$ [dB]	AV/QP [dB]	RMS/QP [dB]
OSC1	A	10	9.1	3.0		7.6
	A	25 (ref)	6.1	0	12.4	4.5
	A	60	3.1	-2.9		
	A	100	2.1	-4.0		-1.4
	B	10	17.5	11.5		25.1
	B	20	13.2	6.6		
	B	100 (ref)	6.7	0.0	33.1	14.9
	B	500			23.2	
	B	1000	2.1	-4.5	17.8	4.8
OSC2	C&D	100 (ref)	11.9	0		19.9
	C&D	1000		-8.0	38.4	10.4
	C&D	5000			26.4	

PK, the QP/PK, and the QP/AV responses, respectively. For band B, the maximum errors registered were 0.8, −0.13, and −0.4 dB for the absolute PK, the QP/PK, and the QP/AV, respectively.

With regard the assessment of the relative pulse response, the results were satisfactory for both versions of full TDEMI measurement systems, that is, bands A and B for OSC1 and bands C and D for OSC2. Table V shows the mean value of the measurements performed in each frequency band. For bands C and D, only pulse repetition frequencies above 100 Hz were validated due to the oscilloscope memory constraints that did not allow measuring sufficiently large time record. Additionally, for bands C and D, pulse response measurements were performed at 30 MHz, 300 MHz, and 1 GHz.

Table V results must be compared with Table II requirements in order to determine if the measured relative pulse response is within the tolerances defined in the CISPR 16-1-1 standard. For example, the specified relative response of the peak detector with respect to the QP detector at a repetition frequency of 20 Hz is 13.1 ± 1.5 dB and the result from the assessment was 13.2 dB, which is satisfactory. A similar analysis is applied to every band, detector and pulse repetition frequency.

VI. MEASUREMENT UNCERTAINTY

The accuracy of the measurement system is the foundation for a method to become accepted as relevant for the application it is intended to address. On the one hand, the waveform approach for assessing conformity of CISPR 16-1-1 measuring receivers would only be conclusive if the pulse generators provide excitation signals that are precise and well fitted to their expected mathematical representation (golden reference). On the other hand, it is also important to estimate the uncertainty of the measurements made with a full TDEMI measurement system following the CISPR 16-4-2 approach [24]. Therefore, this section discusses the appropriateness of the proposed assessment method in terms of the characterization of the pulse generators, the adequacy of the oscilloscopes' specifications (ADC dynamic figures) for

EMI measurements, and the overall uncertainty analysis of the assessment performed to the full TDEMI measurement systems.

A. Characterization of the Pulse Generators

The 81160A pulse function arbitrary noise generator, which was used for obtaining most of the presented results, has 14 bits of vertical resolution in the DAC, can deliver up to 2.5 GSamples/s, has a time resolution of 300 ps $\pm$ 50 ppm, and has a 330-MHz bandwidth for pulses extendable to 500 MHz for single tones. Similarly, the SML signal generators provide an accuracy in the sine-wave level that is better than 0.5 dB for frequencies below 2 GHz.

In practice, the spectrum of the abovementioned pulse generators can be calibrated using the black box approach focusing on the parameters that are relevant for assessing the EMI measuring receivers. Even if a comprehensive description of the calibration methods for pulse generators is beyond the scope of this paper, it is important to consider the following aspects.

First, the calibration of a CISPR pulse generator can be performed by several methods, such as the measurement of one spectrum line amplitude [25], the Fourier transform of time-domain pulse waveform [26], and the IF measurement method. From the metrology point of view, the most accurate is the Fourier transform from samples of a well-characterized oscilloscope (broadband sampling oscilloscope with characterized attenuators at the input). However, such a characterization is likely to be beyond the actual capabilities of secondary-level calibration laboratories or in EMC test laboratories. Still, CISPR 16-1-1 Annex B states that "The impulse area should be known within $\pm$0.5 dB and the repetition frequency to within about 1%" [1] can be shown to be achievable even by using low-grade oscilloscopes.

Conversely, calibrating the spectrum of complex multisine-wave signals used in the assessment of the level accuracy is a more challenging task, because it is not possible to measure with a calibrated thermal or diode power detector. For this purpose, a calibrated spectrum analyzer could be used to tune the desired tone with proper RBW. Experience indicates that the typical uncertainty of this kind of measurement is below 0.2 dB. Lower uncertainties could be achieved by using the FFT-method and metrology-level digitizers of appropriate resolution (16 bit or higher).

Finally, it is important to remark that metrological traceability is fundamental for the reliability of the proposed assessment method. The reference waveform generators must be characterized and calibrated independently before being used for assessing a measuring receiver. Moreover, any conformance testing report resulting from applying the proposed assessment method must include a statement of the uncertainty of the reference waveforms used for evaluating the measuring receiver.

B. Oscilloscopes' Specifications and EMI Measurements

Table VI presents the relevant specifications of OSC1 and OSC2 when they are configured at the actual operating settings of full TDEMI systems. In both cases, the specified accuracy of the signal level at the output of the generator is significantly better than the measurement accuracy of the oscilloscopes and satisfy the baseline requirements of CISPR 16-1-1 shown in Tables I and II. For those reasons, the suitability of the proposed assessment method is, in principle, granted for the application which it is intended.

TABLE VI
OSCILLOSCOPES SPECIFICATIONS AT THE OPERATING CONDITIONS CONFIGURED IN THE FULL TDEMI MEASUREMENT SYSTEM

		CISPR frequency band		
		A	B	C&D
OSC1	Resolution (flexible) [bits]	12 to 16	8 to 14	-
	ENOB [bits]	8.1 to 8.7	7.9 to 8.2	-
	Enhanced resolution [bits]	2	1.5	-
	Sampling frequency [MS/s]	62.5	125	-
	Time resolution [ns]	16	8	-
	Bandwidth (Limited) [MHz]	60	60	-
OSC2	Resolution (flexible) [bits]	-	-	8
	ENOB [bits]	-	-	6
	Enhanced resolution [bits]	-	-	0.5 to 1.5
	Sampling frequency [GS/s]	-	-	1, 2.5, 5
	Time resolution [ns]	-	-	1, 0.4, 0.2
	Bandwidth (Limited) [MHz]	-	-	500/1000

Considering the criteria above, it is reasonable to assume that the errors observed in the sine-wave level characterization are primarily due to the receiver implementation under assessment. Henceforth, one could argue that even if the observed sine-wave level error is compliant with CISPR 16-1-1, the accuracy of the assessed full TDEMI measurement systems is rather low from a metrological perspective, in comparison to what could be expected entirely from frequency-domain receivers.

Nonetheless, it is important to remind that in practice, when it comes to real-life EMI measurements, the most important feature of a test receiver is its capability for detecting noncompliant electromagnetic emissions and worst case disturbance events. That is the key reason why FFT-based systems offer advantages to practitioners, even if this means compromising the dynamic range, the sensitivity, and the accuracy in comparison to measuring receivers based on the superheterodyne architecture. In fact, this is possible thanks to the not-so-restrictive baseline requirements of CISPR 16-1-1.

C. Uncertainty on the Assessment of Full TDEMI Receivers

The main contributions to the uncertainty in the measurement performed during the assessment are associated with the signal acquisition (cable attenuation, mismatch, ADC resolution, thermal noise, linearity, and so on) and to the signal processing.

In that sense, the uncertainty contribution due to impedance mismatch, u_M, between the cable from the signal generator and the oscilloscope channel is given by

$$u_M = \frac{1}{\sqrt{2}} 20 \log(1 + |\Gamma_1||\Gamma_2|) \tag{3}$$

TABLE VII
GENERAL UNCERTAINTY BUDGET FOR THE ASSESSMENT OF A FULL TDEMI MEASURING RECEIVER

Quantity	Estimate	Standard uncert.	Prob. Distrib.
Cable transfer function	0.1 dB	0.05 dB	Rectangular
Impedance mismatch	0.1 dB	0.07 dB	U-shaped
Oscilloscope freq. response	±0.2 dB	0.1 dB	Rectangular
Oscilloscope DC accuracy	0.1 dB	0.05 dB	Rectangular
Oscilloscope linearity error	0.1 dB	0.05 dB	Rectangular
Oscilloscope timebase	0 dB	0.06 dB	Normal
Osc. Vert. resolution	0 dB	0.02 dB	Triangular
Sig. generator error	0 dB	0.2 dB	Regtangular
Processing error	0 dB	0.05 dB	Normal
Repetitivity (Type A)	0.1 dB	0.05 dB	Normal
Combined uncertainty (u_c)		0.27 dB	
Expanded uncertainty ($2u_c$)		**0.54 dB**	

where Γ_1 is the reflection coefficient of the cable and Γ_2 is the reflection coefficient of the oscilloscope.

Moreover, the uncertainty of the limited oscilloscope vertical resolution, u_{res}, is given by

$$u_{\text{res}} = \frac{2}{\sqrt{6}} \frac{U_{\max}}{U_{\text{meas}}(2^{\text{ENOB}})} * 100[\%] \tag{4}$$

where $U_{\max}$ is the full vertical scale, U_{meas} is the measured amplitude, and $1/\sqrt{6}$ is due to the triangular distribution. Moreover, there is also the uncertainty contribution of the oscilloscope gain at dc, which is calibrated with a precision dc source and digital voltmeter.

Likewise, the uncertainty due to the oscilloscope noise can be calculated using

$$u_{\text{noise}} = \sqrt{4kTBR} \tag{5}$$

were k is the Boltzmann constant, T is the temperature in Kelvin, B is the oscilloscope bandwidth, and R is the oscilloscope input impedance.

Finally, the uncertainty contribution of the oscilloscope's linearity and time base errors is evaluated using precise and well-known sinusoidal test signals of different amplitudes and frequencies.

Regarding the uncertainty contribution of the signal processing performed by the full TDEMI software, u_{DSP}, it is due to the mathematical operations of windowing, resampling, flatness correction, padding, and rounding, among others, that are performed before providing the EMI measurement results to the end user. This uncertainty contribution has been bounded to less than 0.05 dB in 99% of cases. This estimation has been made by means of testing the algorithms with ideal mathematical representations of the input signal. Monte Carlo simulations have been used to exercise the algorithms with millions of possible combinations of the actual measurement parameters in order to obtain a realistic quantification.

Table VII shows an example of the measurement uncertainty estimated for the assessment of the full TDEMI measurement system based on OSC1 for CISPR band B. This general budget can be filled with the values of other bands or oscilloscope models.

VII. CONCLUSION

In this paper, a time-domain-based waveform approach was used for assessing the conformity of measuring receivers with respect to CISPR 16-1-1 requirements. The frequency range covered was 9 kHz–1 GHz, comprising CISPR bands A–D. The proposed test setups are more affordable, versatile, and flexible than conventional implementations based on manufacturer's calibration methods. Moreover, it was demonstrated that the usage of the CISPR baseband pulse generator can be avoided by taking alternative approaches such as employing AWG. In fact, results could encourage test houses and manufacturer-independent industrial calibration laboratories to implement their own assessment bench for the internal verification of the receiver's baseline requirements. A key advantage of this approach is that waveforms can be represented as numerical vectors and they could be easily reproduced or shared by any laboratory having an adequate AWG. On the other hand, the scalability of our approach is granted with the usage of AWG of broader capacity.

REFERENCES

[1] *Specification for Radio Disturbance and Immunity Measuring Apparatus and Methods—Part 1-1: Radio Disturbance and Immunity Measuring Apparatus—Measuring Apparatus*, IEC Standard CISPR 16-1-1 ed4.0, 2015.

[2] R. D. Drosd, "Transmission line pulse generator," U.S. Patent 2 769 101, Jul. 29, 1955.

[3] *A Guide to Calibrating Your Spectrum Analyzer*, Fluke Corp., Everett, WA, USA, 2006.

[4] C. Rauscher, *Fundamentals of Spectrum Analysis*, 5th ed. Munich, Germany: Rohde & Schwarz, 2011.

[5] (2015). *Publishable Summary for 15RPT01 Microwave Development of RF and Microwave Metrology Capability*. Accessed: Oct. 9, 2017. [Online]. Available: http://rfmw.cmi.cz/documents/misc/15RPT01_Publishable_Summary.pdf

[6] R. B. Andrews, "An impulse spectral intensity measurement system," *IEEE Trans. Instrum. Meas.*, vol. 15, no. 4, pp. 299–303, Dec. 1966.

[7] M. Zeier. (Aug. 3, 2009). *EURAMET Project 1064: Spectrum of Pulse Generators in Accordance With CISPR-16-1-1*, Bern-Wabern, Switzerland, Accessed: Oct. 9, 2017. [Online]. Available: https://www.euramet.org/get/?tx_stag_base%5Bfile%5D=3404&tx_stag_base%5Baction%5D=downloadRaw&tx_stag_base%5Bcontroller%5D=Base

[8] M. A. Azpúrua, M. Pous, F. Silva, and J. A. Oliva, "Fast and automated verification of multi-channel full time-domain EMI measurement systems," in *Proc. IEEE Int. Instrum. Meas. Technol. Conf. (I2MTC)*, Turin, Italy, May 2017, pp. 785–790.

[9] P. Russer, "EMC measurements in the time-domain," in *Proc. 30th URSI Gen. Assembly Sci. Symp.*, Istanbul, Turkey, Aug. 2011, pp. 1–35.

[10] V. Iglesias, J. Grajal, M. A. Sánchez, and M. López-Vallejo, "Implementation of a real-time spectrum analyzer on FPGA platforms," *IEEE Trans. Instrum. Meas.*, vol. 64, no. 2, pp. 338–355, Feb. 2015.

[11] D. Liebl, *Measuring With Modern Spectrum Analyzers*. Munich, Germany: Rohde & Schwarz, Mar. 2013.

[12] M. A. Azpúrua, M. Pous, and F. Silva, "A measurement system for radiated transient electromagnetic interference based on general purpose instruments," in *Proc. IEEE Int. Symp. Electromagn. Compat. (EMC)*, Dresden, Germany, Aug. 2015, pp. 1189–1194.

[13] M. A. Azpúrua, M. Pous, S. Çakir, M. Çetintaş, and F. Silva, "Improving time-domain EMI measurements through digital signal processing," *IEEE Electrmagn. Compat. Mag.*, vol. 4, no. 2, pp. 82–91, 2nd Quart., 2015.

[14] R. Lapuh, B. Pinter, B. Voljc, Z. Svetik, and M. Lindic, "Digital oscilloscope calibration using asynchronously sampled signal estimation," *IEEE Trans. Instrum. Meas.*, vol. 60, no. 7, pp. 2570–2577, Jul. 2011.

[15] M. Monti, E. Puri, and M. Monti, "Hidden aspects in CISPR 16-1-1 full compliant fast Fourier transform EMI receivers," in *Proc. Int. Symp. Electromagn. Compat. (EMC EUROPE)*, Wroclaw, Poland, Sep. 2016, pp. 34–39.

[16] A. Mariscotti, "On time- and frequency-domain equivalence for compliant EMI measurements," in *Proc. IEEE Instrum. Meas. Technol. Conf. (IMTC)*, Warsaw, Poland, May 2007, pp. 1–5.

[17] S. Braun, T. Donauer, and P. Russer, "A real-time time-domain EMI measurement system for full-compliance measurements according to CISPR 16-1-1," *IEEE Trans. Electromagn. Compat.*, vol. 50, no. 2, pp. 259–267, May 2008.

[18] H. H. Slim, C. Hoffmann, S. Braun, and P. Russer, "A novel multichannel amplitude probability distribution for a time-domain EMI measurement system according to CISPR 16-1-1," in *Proc. 10th Int. Symp. Electromagn. Compat.*, York, U.K., Sep. 2011, pp. 22–25.

[19] J. Medler, "Use of FFT-based measuring instruments for EMI compliance measurements," in *Proc. Int. Symp. Electromagn. Compat.*, Tokyo, Japan, May 2014, pp. 89–92.

[20] M. Friese, "Multitone signals with low crest factor," *IEEE Trans. Commun.*, vol. 45, no. 10, pp. 1338–1344, Oct. 1997.

[21] C. Keller and K. Feser, "Fast emission measurement in time domain," *IEEE Trans. Electromagn. Compat.*, vol. 49, no. 4, pp. 816–824, Nov. 2007.

[22] *Limits and Methods of Measurement of Radio Disturbance Characteristics of Electrical Lighting and Similar Equipment*, IEC Standard CISPR 15 ed8.1, 2015.

[23] *Electromagnetic Compatibility of Multimedia Equipment—Emission Requirements*, IEC Standard CISPR 32 ed2.0, 2015.

[24] *Specification for Radio Disturbance and Immunity Measuring Apparatus and Methods—Part 4-2: Uncertainties, Statistics and Limit Modelling—Measurement Instrumentation Uncertainty*, IEC Standard CISPR 16-4-2 ed2.1, 2014.

[25] P. G. A. Jespers and G. A. Jackson, "Calibration of nanosecond pulse generators," *IEEE Trans. Electromagn. Compat.*, vol. EMC-14, no. 2, pp. 68–72, May 1972.

[26] S. Pasakawee and V. Sittakul, "Calibration and uncertainty evaluation of pulse generator for EMC testing using FFT technique," in *Proc. 13th Int. Conf. Elect. Eng./Electron., Comput., Telecommun. Inf. Technol. (ECTI-CON)*, Chiang Mai, Thailand, Jun./Jul. 2016, pp. 1–5.

Marco A. Azpúrua (S'07–M'13) received the B.Sc. degree in telecommunications engineering and the M.Sc. degree in electrical engineering from the Universidad Central de Venezuela, Caracas, Venezuela, in 2008 and 2013, respectively. He is currently pursuing the Ph.D. degree with the Electromagnetic Compatibility Group, Universitat Politècnica de Catalunya, Barcelona, Spain.

He was a Researcher with the Applied Electromagnetics Laboratory, Foundation Engineering Institute, Caracas. His current research interests include electromagnetic compatibility, antenna and microwave measurement technologies, and the estimation of measurement uncertainty in complex systems and validation methods.

Marc Pous was born in Barcelona, Spain, in 1983. He received the M.Sc. degree in telecommunications engineering and the Ph.D. degree in radiated transient interferences and digital communication systems evaluation from the Universitat Politècnica de Catalunya, Barcelona, in 2009 and 2015, respectively.

From 2003 to 2006, he was with the Department of Electromagnetic Compatibility, LGAI Technological Centre S.A., Barcelona. Since 2006, he has been with the Electromagnetic Compatibility Group, Universitat Politècnica de Catalunya, where he has been participating in international and national research projects related with automotive, aerospace, railway, and medical industries. His current research interests include the development of time-domain measurement techniques to capture interferences, which are not properly measured following the harmonized electromagnetic compatibility standards.

José A. Oliva was born in Barcelona, Spain, in 1991. He received the M.Sc. degree in telecommunications engineering from the Universitat Politècnica de Catalunya (UPC), Barcelona, in 2016.

Since 2016, he has been with the Electromagnetic Compatibility Group, UPC, where he has been involved in the development of a measuring system in the time domain for the electromagnetic interference. His current research interests include electromagnetic compatibility.

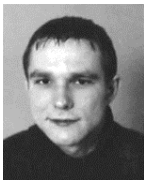

Borut Pinter was born in Murska Sobota, Slovenia, in 1975. He received the B.Sc. degree in physics from the Faculty for Mathematics and Physics, University of Ljubljana, Ljubljana, Slovenia, in 2005.

He joined the Slovenian Institute of Quality and Metrology, Ljubljana, in 2003, where he is currently a Research and Development Scientist. He is currently involved in local and international research projects. His current research interests include the field of high frequency (RF and microwave) electrical metrology, time and frequency, acoustics and vibration, dc and low-frequency impedance (capacitance, resistance, and inductance), and optical fiber metrology.

Martin Hudlička (S'04–M'08–SM'15) received the M.Sc. degree in engineering and the Ph.D. degree in electrical engineering from Czech Technical University in Prague, Prague, Czech Republic, in 2004 and 2007, respectively. His Ph.D. thesis was related to the propagation of electromagnetic waves in periodic structures.

He joined the Department of Primary Metrology of RF Electrical Quantities, Czech Metrology Institute, Prague, in 2007, where he is currently a Metrologist and a Researcher. His current research interests include microwave and millimeter-wave measurements and modern communication technologies.

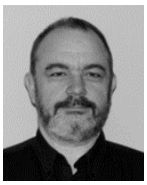

Ferran Silva (M'76–SM'81–F'87) received the M.Sc. and Ph.D. degrees from the Universitat Politècnica de Catalunya (UPC), Barcelona, Spain, in 1989 and 1997, respectively.

Since 2000, he has been the Director of the Electromagnetic Compatibility Group, UPC, performing technology transfer activities to the industrial sector, where he is currently an Associate Professor of electronics with the Department of Electronic Engineering. He has published over 90 papers in journals and conferences, and contributed to the *Wiley Encyclopedia of Biomedical Engineering*. He has participated in 14 research projects related to electromagnetic compatibility (EMC). His current research interests include EMC in near field and time domain, including transients, with application to automotive, medical systems, and installations.

Dr. Silva is a member of the IEEE EMC Society and the Spanish Standardization Committees SCTC77-210 and the CTN208 SCCISPR210A. He is the Head of the Spanish Chapter of the IEEE. He was the Chairman of the EMC Europe 2006 International Symposium. Since2006, he belongs to the Board of Chairman of EMC Europe.

This full text paper was peer-reviewed at the direction of IEEE Instrumentation and Measurement Society prior to the acceptance and publication.

Fast and Automated Verification of Multi-channel Full Time-Domain EMI measurement systems

Marco A. Azpúrua, José A. Oliva, Marc Pous, Ferran Silva
Grup de Compatibilitat Electromagnètica (GCEM), Departament d'Enginyeria Electrònica (DEE)
Universitat Politècnica de Catalunya (UPC)
Barcelona, Spain
email: marco.azpurua@upc.edu

***Abstract*—Recently, concern has been raised with regard to the adequacy of current verification practices carried out in electromagnetic compatibility (EMC) testing laboratories. Bridging the gap in the scope and reliability of the verifications performed in EMC laboratories requires faster and simpler verification methods to be performed prior testing. This paper presents a verification method for Full Time Domain Electromagnetic Interference measurement systems (Full TDEMI) that is intended to be quick and automated in order to become practical under the "just-before-test" approach. The method comprises a four stage process for assessing: sine-wave voltage accuracy, response to pulses, selectivity and input impedance. The verification method has been implemented and executed on an oscilloscope-based Full TDEMI achieving a reduction of time and effort involved while ensuring the compliance with CISPR 16-1-1 applicable requirements. Finally, this verification method improves the statistical significance because of the large number of points and conditions checked by the measurement automation software.**

Keywords—electromagnetic compatibility; electromagnetic interference; just-before-test; quality management; standards.

I. INTRODUCTION

According to the definition given in the International Vocabulary of Metrology, verification is "the provision of objective evidence that a given item fulfills specified requirements" [1]. Incidentally, verifications shall be routinely yet rigorously carried out in accredited electromagnetic compatibility (EMC) testing laboratories. However, this might not be the general case, as explained below.

In a recent call from the European Metrology Programme for Innovation and Research (EMPIR), the ongoing Joint Research Project "RFMicrowave" (15RPT01) pointed out "…current knowledge between EMC and RF&MW laboratories is very weak, which reduces awareness in measurements/calibrations and, therefore the overall quality of both EMC and RF&MW measurements". One of the objectives of this very same project is to introduce a whole new set of verification methods suitable for EMC testing, that allow raising awareness of any problems just before starting tests [2].

The cornerstone of this "just-before-test" approach is that verification methods used in EMC testing must be reliable but also fast and automated for them to become compatible with the testing activities workload of certification laboratories. Depending on the particularities of certain EMC test, Vector Network Analyzer (VNA) and/or time-domain based verification methods are intended to address this "just-before-test" approach.

Specifically, within the scope of the standards that define the radiofrequency emission requirements, verifications must be systematically performed in order to confirm the measuring receivers meets the specifications of CISPR 16-1-1 and the adequacy of the test setup [3]. This is a challenging task for a testing laboratory because most test receivers are not provided with any means for performing such verification.

In the vast majority of cases, testing laboratories only perform intermediate checks such as a manual corroboration of the amplitude/frequency accuracy of the test receiver or by means of the embedded self-test option found on most instruments. Moreover, those partial verifications are performed on a "from-time-to-time" basis and not "just-before-test" mainly due to logistical constraints. Therefore, this current situation is against the best practices for assuring the quality of emissions testing.

In this regard, using a time-domain approach to the verification of electromagnetic interference (EMI) measuring receivers can reduce significantly the efforts required to perform instrument verification. Furthermore, (Full) Time-Domain EMI measurement systems [4]–[9] can benefit the most from time-domain verification methods because of the straightforward relationship between the expected outcome and the results of the verification in both time and frequency domains.

In this paper, a fast and automated verification method for multi-channel Full Time-Domain EMI (Full TDEMI) measurement systems is presented, intended to address the "just-before-test" approach. In that sense, first a summary of the key CISPR 16-1-1 requirement that must be verified in Full-TEDMI measurement systems is given (section II), then the implemented verification setup and algorithms are briefly described (section III) and the results of a verification of a Full TDEMI measurement system performed just before a conducted EMI testing will be presented as an example (section IV).

978-1-5090-3596-0/17/$31.00 ©2017 IEEE

II. STANDARD REQUIREMENTS FOR FULL TDEMI MEASUREMENT SYSTEMS

According to the standard definition measuring receiver, it is an "instrument such as a tunable voltmeter, an EMI receiver, a spectrum analyzer or an FFT-based measuring instrument, with or without preselection, that meets the relevant parts of this standard" [3]. In that sense, the proposed verification method shall provide objective evidence that a Full TDEMI measurement system fulfills the definition of measuring receiver concerning the compliance with requirements specified in the CISPR 16-1-1 standard.

Incidentally, the particularities of Full TDEMI measurement systems oblige to verify them differently in comparison with a frequency sweep or stepped scan receivers. Next, an overview of Full TDEMI measurement systems will be given in order to list a verifiable set of relevant requirements in terms of the CISPR 16-1-1 standard.

A. Overview of Full TDEMI measurement systems

In general terms, a Full-TDEMI measurement system is described by the block diagram shown in Fig. 1 [4], [7]. For the measurement of radiated EMI, a broadband antenna shall be used, while for the measurement of conducted EMI corresponds either a current clamp or a line impedance stabilization network (LISN). The measured signal could be amplified or filtered if this provides better sensitivity. In the analog-to-digital converter (ADC), the full spectrum signal is digitized and stored in the time-domain. Finally, the amplitude spectrum is computed via the spectral estimation techniques.

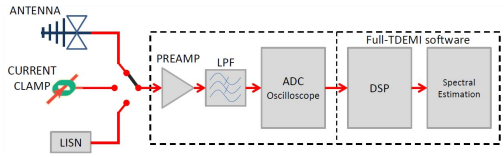

Fig. 1. The Full-TDEMI measurement system block diagram.

After deep memory acquisition, the software of the Full TDEMI measurement system performs signal processing tasks including windowing, resolution enhancing, resampling, spectral estimation (using the Short-Time Fourier Transform and the Welch's method) and the detector emulation. Those mathematical transformations are responsible for delivering the measurement results in accordance with CISPR 16-1-1 requirements [4].

B. Applicable CISPR 16-1-1 requirements

CISPR 16-1-1 (Annex K) gives two alternatives with regard to the demonstration of compliance of measuring receivers. The first possibility is using the manufacturer's calibration process for verifying compliance, but this is not feasible on a "just-before-test" approach primarily because reproducibility constrains. The alternative is using a verification process that includes at least the following parameters: voltage standing wave ratio (VSWR), sine wave voltage accuracy, response to pulses and selectivity.

The tables I and II summarize the standard requirements applicable to Full TDEMI measurement systems, in CISPR bands A to D. Those items constitute the minimum set of requirements that shall be covered by the verification method.

TABLE I. APPLICABLE CISPR 16-1-1 REQUIREMENTS FOR FULL TDEMI MEASUREMENT SYSTEMS

Parameter	Subclause	Requirements	Freq. ranges
VSWR	4.2, 5.2, 6.2, 7.2	2.0 to 1 (0 dB RF attenuation)	9 kHz - 1 GHz
Sine wave voltage accuracy	4.3, 5.4, 6.4, 7.4	Better than ± 2 dB (50 Ω resistive source impedance)	9 kHz - 1 GHz
Response to pulses [a] (Absolute)	4.4, 5.5, 6.5, 7.5	66 dBµV ± 1.5 dB (Flat spectrum within the measured bandwidth)	CISPR Bands A, B, C and D
Response to pulses [a] (Relative)	4.4, 5.5, 6.5, 7.5	Table II.	CISPR Band A, B, C and D
Selectivity[b]	4.5, 5.6, 6.6, 7.6	90 Hz ≤ $B_{1.5}$ ≤ 220 Hz 180 Hz ≤ B_6 ≤ 220 Hz 180 Hz ≤ B_{20} ≤ 440 Hz	CISPR Band A
		4 kHz ≤ $B_{1.5}$ ≤ 10 kHz 8 kHz ≤ B_6 ≤ 10 kHz 10 Hz ≤ B_{20} ≤ 20 kHz	CISPR Band B
		40 kHz ≤ $B_{1.5}$ ≤ 140 kHz 100 kHz ≤ B_6 ≤ 140 kHz 100 kHz ≤ B_{20} ≤ 280 kHz	CISPR Bands C and D

[a] CISPR 16-1-1 Annexes B and C describe methods for determining the output characteristics of a pulse generator used in verifications and calibrations of the absolute and the relative pulse response.

[b] B_x means the reference bandwidth at the x dB decay level.

TABLE II. REQUIREMENTS FOR THE RELATIVE PULSE RESPONSE OF THE STANDARD WEIGHTING DETECTORS

Band	f_{rep} (Hz)	PK/QP (dB)	QP/QP$_{(ref)}$ (dB)	AV/QP (dB)	RMS/QP (dB)
A	10	10,1±1,5	4,0±1,0		8,2±1,5
A	25 (ref)	6,1±1,5	0	12,4±1,5	4,2±1,5
A	60	3,1±1,5	-3,0±1,0		
A	100	2,1±1,5	-4,0±1,0		-1,8±1,5
B	10	16,6±1,5	10,0±1,5		24,3±2,0
B	20	13,1±1,5	6,5±1,0		
B	100 (ref)	6,6±1,5	0	32,9±1,5	14,3±1,5
B	500			22,9±1,5	
B	1000	2,1±1,5	-4,5±1,0	17,4±1,5	4,3±1,5
C,D	10		14,0±1,5		
C,D	20		9,0±1,0		
C,D	100 (ref)	12,0±1,5	0		20,1±1,5
C,D	1000		-8,0±1,0	38,1±1,5	10,1±1,0
C,D	5000			26,3±1,5	

With regards to the requirements highlighted above some clarifications shall be made: a) VSWR requirements are only applicable to the 0 dB RF attenuation condition because Full TDEMI measurement systems have robust oscilloscope-type

inputs and it is often unnecessary to use additional RF attenuation for protecting the instruments' input; b) Narrowband verifications at discrete suggested frequencies (the start, stop and centre frequencies) are replaced by broadband (full-spectrum) measurements; c) the pulse repetition frequencies used are above 10 Hz because this is the lowest mandatory pulse repetition frequency common to all CISPR frequency bands; d) for multi-channel Full TDEMI measurement system each channel shall be individually and independently verified.

III. A JUST-BEFORE-TEST VERIFICATION METHOD

As mentioned previously, the verification method described below is intended to address the requirements identified in section II following both the "just-before-test" and the "black-box" approaches. This means it comprises a procedure (automation algorithm) that verifies the instrument meets a specific response when a defined signal is applied to its input using a reduced set-up of instruments.

A. The setup of the verification method

The test setup is formed by a VNA and an Arbitrary Waveform Generator (AWG). In this particular case, the VNA R&S ZVRE and the Pulse Function Arbitrary Generator Keysight 81160A (14-bit resolution) are employed.

On the one hand, the VNA is used for: a) measuring the VSWR and the impedance at the input of each channel of the Full TDEMI measurement system; b) measuring and correcting the cable attenuation. On the other hand, the AWG is used for synthesizing the reference tones and pulses required to verify the rest of the parameters. If the specific VNA/AWG used in the implementation has as many ports/outputs as inputs has the Full TDEMI measurement system, the procedure can be optimized by assigning an individual port/output for every measurement channel. This is significant because reduces the duration of the verification process through the simultaneous evaluation of all the channels of the Full TDEMI measurement system.

B. Automation of the verification method

The verification is automated by using a 5 stage routine embedded in the Full TDEMI measurement software application. Those stages are attenuation measurement, sine wave measurements (amplitude and frequency accuracy), pulse response measurements (absolute and relative), VSWR and impedance measurements and, finally, report generation. Those stages are executed in sequence, requiring a minimal level of interaction and surveillance from the technician, who is notified whenever it is required to change the connection between instruments if an error has occurred (i.e. communication errors), and when the verification process is completed. In the case it is possible to provide an individual signal source output for every measurement channel, end-user intervention is further reduced.

Cable attenuation measurements are performed in the first stage (Fig. 2). In that sense, VNA is configured to measure the complex S_{21} using the maximum number of points (1601 in this case) in the frequency range required by the verification process. The results are acquired by the software application for calculating the corresponding attenuation correction factors of each channel. The process is repeated iteratively (for i=1,2,3,4), one channel at the time.

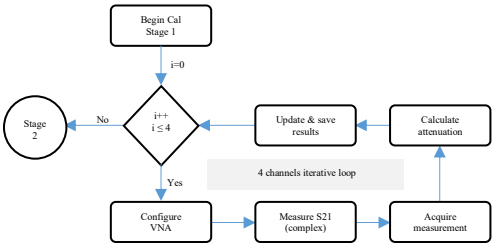

Fig. 2. Attenuation measurements flowchart (Stage 1).

Stage 2 is intended to verify the sine wave amplitude and frequency accuracy. For that reason, a sample of reference continuous wave RF tones that have certain, well-known, characteristics is generated. In this sample, the amplitude and frequency of the tones are selected using a hybrid random-systematic approach without reposition and, in consequence, some restrictions are applied. Half the sample is formed by tones whose frequency are selected systematically to match exactly the frequency steps at which the spectral estimation is performed. The other half of the sample is tones that have a completely random frequency selected between the lower and upper measurement frequency of the CISPR band under verification. The amplitude of the tones is also randomly chosen within a configurable interval defined by a lower and upper bound around 66 dBµV. This hybrid sampling approach is used for collecting significant information about the measurement accuracy in the whole band under different sensitivity conditions (vertical scale). This data could be used to quantify the error contributions of frequency-overlapping and interpolation. Uniformly distributed pseudorandom number generators are used for defining the characteristics of the tones of the sample. The sample size, N, is defined as a percentage of the total number of measurement points.

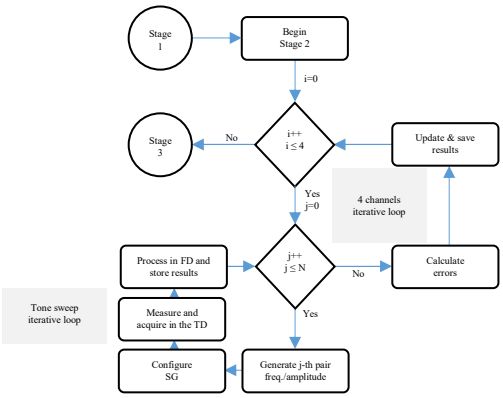

Fig. 3. Sine wave measurements flowchart (Stage 2)

The process represented in the simplified flowchart of Fig. 3 shows the sine wave measurement stage is repeated iteratively for each tone within the selected sample and then for each channel (for i=1,2,3,4), one at the time.

Next, during the third stage, a specific pulsed signal is synthesized for having a flat frequency response (66 dBµV ±1,5 dB) while respecting the spectral density requirements that are summarized in Table III.

TABLE III. TEST PULSE CHARACTERISTICS FOR EMI TEST RECEIVERS [3]

Band	Frequency	Impulse area	f_{rep} (ref.)
A	9 kHz to 150 kHz	13,5 µVs	25 Hz
B	0,15 MHz to 30 MHz	0,316 µVs	100 Hz
C	30 MHz to 300 MHz	0,044 µVs	100 Hz
D	300 MHz to 1 000 MHz	0,044 µVs	100 Hz

The pulse waveform shall be changed for each j-th CISPR bands under assessment because of the different requirements of the reference pulses. The pulse repetition frequency is set at the reference value for recording the absolute calibration. Then this process is looped for every repetition frequency in Table II in order to verify the relative response requirements of the weighing detectors. Once again, this process iterates until every combination of bands, channel, and pulse repetition frequency have been measured (Fig. 4).

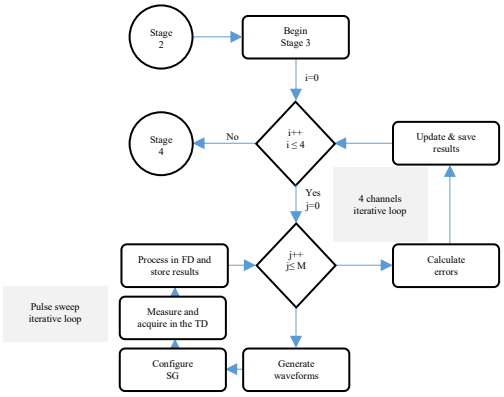

Fig. 4. Pulse response measurements flowchart (Stage 3).

In the fourth stage (Fig. 5), VNA is used to measure the complex voltage reflection coefficient at the input of each channel of the Full TDEMI measurement system. No RF attenuation is used.

Finally, in its last stage, the calibration algorithm generates the result plots and a report on an excel spreadsheet, including summary statistics as the Root Mean Squared Error (RMSE), the maximum error, the mean value, the standard deviation (STD) and the tolerances. This automatically generated summary report provides the user with concise information required to verify the Full TDEMI performance in terms of the standard requirements.

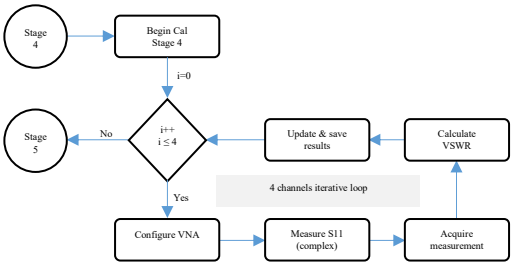

Fig. 5. VSWR measurements flowchart (Stage 4).

IV. VERIFICATION RESULTS

In this section, the results of the verification of a specific Full TDEMI measurement system will be presented. It is the case of the Full TDEMI 4200 which relies on the USB oscilloscope "Picoscope 5444B" from Pico Technology®. The Full TDEMI 4200 has 4 channels and 200 MHz of nominal bandwidth. Thus, the verification will be performed in the CISPR bands A (9 kHz – 150 kHz) and B (150 kHz – 30 MHz).

Concerning the sine wave measurements, Fig. 6 shows the errors in amplitude (voltage) of the reference tones injected to the measuring apparatus for N=200. In both bands, and in every channel, the observed errors are below 1 dB in the worst case, as shown in Table IV.

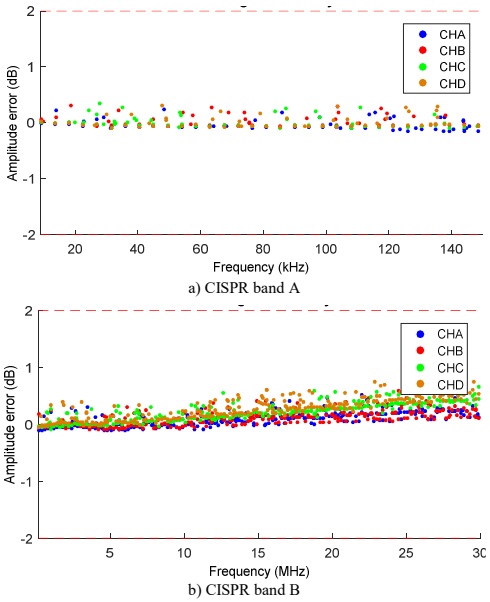

Fig. 6. Sine wave voltage accuracy verification results.

TABLE IV. SUMMARY FROM SINE WAVE VOLTAGE ACCURACY VERIFICATION

CH	Band	RMSE [dB]	Max [dB]	STD [dB]
A	A	0.103	0.242	0.098
	B	0.168	0.599	0.138
B	A	0.108	0.319	0.105
	B	0.175	0.588	0.130
C	A	0.110	0.345	0.110
	B	0.283	0.685	0.167
D	A	0.109	0.307	0.108
	B	0.349	0.922	0.192

Likewise, for the pulse response absolute measurements, Fig. 7 shows the results for each CISPR frequency band. The most relevant aspects to notice are the flatness of the frequency response and the ratios between peak/quasi-peak and quasi-peak average, which fulfill standard requirements. It is important to highlight this is a full-spectrum, multi-channel and multi-detector characterization of the pulse response. In both bands, for every channel and, all detectors the observed errors are below 1 dB in the worst case, as shown in Table V.

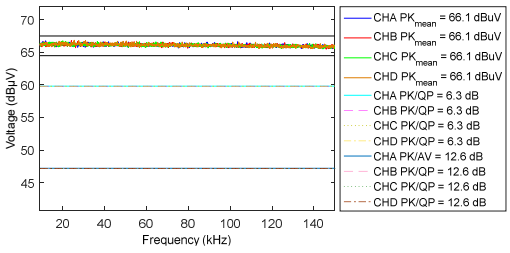

a) CISPR band A

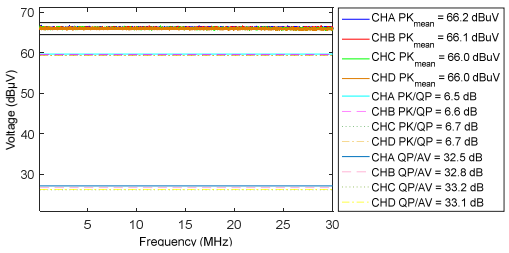

a) CISPR band B

Fig. 7. Response to pulses (absolute) verification results.

TABLE V. SUMMARY FROM THE ABSOLUTE PULSE RESPONSE VERIFICATION

CH	Band	f_{rep} [Hz]	PK	QP/PK	AV/QP
			Max error [dB]	Max error [dB]	Max error [dB]
A	A	25	0.716	0.168	0.189
A	B	100	0.802	-0.132	-0.371
B	A	25	0.764	0.173	0.195
B	B	100	0.7	-0.03	-0.067
C	A	25	0.75	0.173	0.196
C	B	100	0.779	0.09	0.262
D	A	25	0.837	0.182	0.207
D	B	100	0.545	0.062	0.193

With regards the relative pulse response verification, the results were satisfactory for all channels. Table VI shows only the results of the measurements performed on Channel A, because of space constraints. However, the differences in the relative pulse response observed among channels is negligible.

TABLE VI. RESULTS FROM THE RELATIVE PULSE RESPONSE VERIFICATION

Band	f_{rep} [Hz]	PK/QP [dB]	QP/QP$_{(ref)}$ [dB]	AV/QP [dB]	RMS/QP [dB]
A	10	9.11	3.01		7.55
A	25 (ref)	6.106	0	12.36	4.51
A	60	3.16	-2.93		
A	100	2.13	-3.96		-1.38
B	10	17.48	11.46		25.13
B	20	13.18	6.58		
B	100 (ref)	6.66	0.06	33.09	14.91
B	500			23.18	
B	1000	2.13	-4.47	17.85	4.83

Finally, the Voltage Standing Wave Ratio (VSWR) is measured at the input of every channel of the PicoScope 5444B using a 50 Ω termination in parallel to the high impedance provided by the instrument. VSWR measurement is displayed in Fig. 8. The measured VSWR remains below the 1.2 threshold even if the maximum allowed VSWR is 2 without an attenuator.

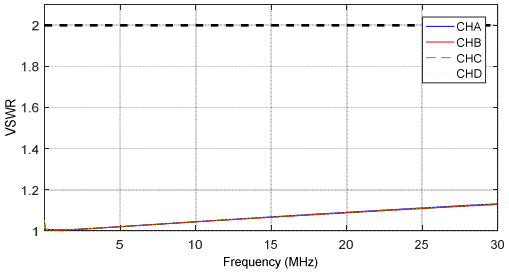

Fig. 8. VSWR verification results.

V. CONCLUSIONS

Throughout the examination of the results of the verification process, it was concluded this specific Full TDEMI measurement system performed in compliance with the CISPR 16-1-1 applicable requirements. The whole verification process (five stages) takes approximately 1 hour to be completed, using a standard desktop computer. This means, approximately 15 min per measurement channel, which is fast enough to be used under the "just-before-test" approach, whenever necessary. In fact, this activity could be executed during the warm-up time recommended for some measuring instruments, which means the verifications would not cause further delays in the typically busy schedule of an EMC testing laboratory.

Moreover, this verification procedure could be used as the core of a calibration procedure of Full TDEMI measurement systems. In order to achieve this, further work shall be done in terms of the measurement uncertainty analysis and also with regards a well-defined measurement traceability chain.

Acknowledgment

This work was supported in part by the EURAMET 15RPT01 research project (the EMPIR is jointly funded by the EMPIR participating countries within EURAMET and the European Union) and by the Spanish "Ministerio de Economía y Competitividad," under project TEC2013- 48414-C3-3-R.

References

[1] Joint Committee For Guides In Metrology (JCGM), "International vocabulary of metrology — Basic and general concepts and associated terms (VIM)," VIM3 Int. Vocab. Metrol., vol. 3, no. Vim, p. 104, 2012.

[2] "Publishable Summary for 15RPT01 RFMicrowave Development of RF and microwave metrology capability," 2015.

[3] IEC CISPR, 16-1-1 ed4.0: Specification for radio disturbance and immunity measuring apparatus and methods - Part 1-1: Radio disturbance and immunity measuring apparatus - Measuring apparatus. IEC, 2015.

[4] M. A. Azpúrua, M. Pous, S. Çakir, M. Çetintaş, and F. Silva, "Improving Time-Domain EMI measurements through Digital Signal Processing," Electromagn. Compat. Mag. IEEE, vol. 4, no. 2, pp. 66–74, 2015.

[5] M. A. Azpúrua, M. Pous, and F. Silva, "Decomposition of Electromagnetic Interferences in the Time-Domain," IEEE Trans. Electromagn. Compat., pp. 1–8, 2016.

[6] M. A. Azpurua, M. Pous, and F. Silva, On the Statistical Properties of the Peak Detection for Time-Domain EMI Measurements, vol. 57, no. 6. IEEE, 2015, pp. 1374–1381.

[7] M. A. Azpúrua, M. Pous, and F. Silva, "A Measurement System for Radiated Transient Electromagnetic Interference Based on General Purpose Instruments," in Electromagnetic Compatibility (EMC EUROPE), International Symposium on, 2015.

[8] M. A. Azpúrua, M. Pous, and F. Silva, "On-board compact system for full time-domain electromagnetic interference measurements," 2016 ESA Workshop on Aerospace EMC (Aerospace EMC). pp. 1–4, 2016.

[9] M. Pous, M. A. Azpúrua, and F. Silva, Measurement and Evaluation Techniques to Estimate the Degradation Produced by the Radiated Transients Interference to the GSM System, vol. 57, no. 6. 2015, pp. 1382–1390.

Dynamic Performance Evaluation of Full Time Domain EMI Measurement Systems

Marco A. Azpúrua, Marc Pous, Mireya Fernandez and, Ferran Silva
Grup de Compatibilitat Electromagnètica
Universitat Politècnica de Catalunya
Barcelona, Spain
email: marco.azpurua@upc.edu

***Abstract*— This paper presents the evaluation of the performance of Full Time Domain Electromagnetic Interference measurement systems in terms of the noise figure, the linearity, the dynamic range, the voltage standing wave ratio and the crosstalk. The abovementioned parameters allow a broader characterization of the oscilloscope-based implementations of CISPR 16-1-1 measuring receivers, providing relevant specifications that are beyond the standardized baseline requirements. Such metrics are assessed using the actual settings and operating conditions required for compliant time-domain EMI measurements. For the specific oscilloscope used in the experiments, the noise figure is measured for all the different vertical ranges between 5 mV/div and 1 V/div. Likewise, the linearity and the dynamic range, in terms of the effective number of bits, was measured for sine wave input signals with an rms voltage swept between 20 mV and 1 V. This experiment was repeated for CISPR bands A, B and C/D using 10 kHz, 1 MHz, and 100 MHz sinusoids, respectively. The results allow a more comprehensive comparison between Full TDEMI measurement systems and the more conventional superheterodyne architecture receivers that are completely specified in the frequency domain.**

Keywords*— *Dynamic range, electromagnetic interference, measuring receiver, noise figure, time-domain measurements

I. INTRODUCTION

The measuring receiver is the fundamental instrument for conducted and radiated electromagnetic emissions testing. According to the standard definition given by the CISPR 16-1-1:2015, it is an "instrument such as a tunable voltmeter, an electromagnetic interference receiver, a spectrum analyzer or a Fast Fourier Transform (FFT) based measuring instrument, with or without preselection, that meets the relevant parts of this standard" [1]. In this regard, the standard CISPR 16-1-1 does not provide a particular implementation of a measuring receiver but a number of requirements that manufacturers have to fulfill under a "black-box" approach.

However, in practice, there are two broad categories for classifying the measuring receivers. On the one hand, there are conventional swept receivers with super-heterodyne architecture that, fundamentally, measure the amplitude of the spectrum in the frequency domain [2]. On the other hand, there are the FFT-based measuring receivers that take advantage of time-domain measurements for speeding up emissions testing and for providing time-frequency analysis features which are useful for evaluating and mitigating the impact of transient and stochastic disturbances [3]–[5]. Currently, real-time analyzers [6], [7] and oscilloscope-based implementations are the two approaches for realizing FFT-based measuring receivers.

In recent years, the idea of using oscilloscopes for EMI measurements [8], beyond pre-certification purposes, has been brought back for discussion in academia [9], [10]. What has been called "Full TDEMI measurement systems" is a software-defined implementation of a measuring receiver that allows for EMI testing using oscilloscopes while meeting all baseline requirements of CISPR 16-1-1 [10], [11]. In that sense, previous studies by the authors have reported that, provided a general-purpose oscilloscope with the appropriated technical specifications, Full TDEMI measurement systems fulfill CISPR 16-1-1 baseline requirements for CISPR bands A to D. In particular, two different implementations of the Full TDEMI measurement system were characterized with regards the sine-wave voltage accuracy (level error), the frequency selectivity, the pulse response (absolute and relative) and, the voltage standing wave ratio (VSWR) at the receiver's RF input port. The results of such characterization provided sufficient evidence to conclude CISPR 16-1-1 requirements were satisfied [10], [11].

Nonetheless, CISPR 16-1-1 requirements might be insufficient for providing a complete description of Full TDEMI measuring systems. In fact, other parameters such as the noise figure, the displayed average noise level, the dynamic range, among others, are commonly used to benchmark spectrum analyzers and measuring receivers. Translating the dynamic performance metrics of oscilloscopes for delivering such complementary specifications regarding Full TDEMI measurement systems is the objective of this paper. The paper is organized as follows. First, an outline of Full TDEMI measurement systems is provided along with some summarized results that support their compliance with CISPR 16-1-1 requirements in CISPR bands A to D (9 kHz – 1 GHz). Then, section III defines the dynamic performance measures included in the scope of this paper and presents the mathematical relationship between them. Subsequently, the actual results of the evaluation of the noise figure, the linearity, the dynamic range, the VSWR and the crosstalk are given in section IV. Finally, the paper closes with the conclusions and a couple of remarks concerning the adequacy of the test setup used in the experiments.

978-1-4673-9698-1/18/$31.00©2018 IEEE

II. FULL TIME DOMAIN EMI MEASUREMENT SYSTEMS

A. Overview of Full TDEMI measurement systems

Full TDEMI measurement systems are oscilloscope-based implementations of an EMI measuring receiver. In general terms, a Full TDEMI measurement system is described by the block diagram shown in Fig. 1 [9], [11]. For the measurement of radiated EMI, a broadband antenna shall be used, while for the measurement of conducted EMI corresponds either a current clamp or a Line Impedance Stabilization Network (LISN). The measured signal could be amplified or filtered if this provides better sensitivity. In the analog-to-digital converter (ADC), the full spectrum signal is digitized in real-time and stored in as a time-discrete value-discrete signal.

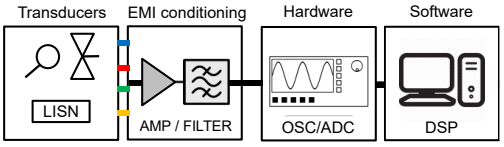

Fig. 1. Block diagram of a Full Time-Domain EMI measurement system.

The final measurement results are computed via the processing techniques implemented in a software layer that provides compliance with the relevant CISPR 16-1-1 requirements. After deep memory acquisitions, the software of the Full TDEMI measurement system performs signal processing tasks including windowing, resolution enhancing, resampling, spectral estimation (using the Short-Time FFT and the Welch's method) and the detector emulation. Those mathematical transformations are responsible for delivering the measurement results in accordance with CISPR 16-1-1 requirements [11].

Full TDEMI measurement systems capture the whole spectrum of the EMI with every acquisition enabling multi-domain analysis. Besides, the triggering and multichannel capabilities found in most oscilloscopes provide additional tools for testing multi-functional mode equipment and for emissions testing parallelization. On the other hand, much higher sampling rates and a deeper memory are required than with real-time analyzers. This imposes bandwidth and dwell time constraints based on the current oscilloscope technology.

B. Summary of the oscilloscope's specifications

The capability of a Full TDEMI measurement system to comply with CISPR 16-1-1 baseline requirements depends not only on the application of the adequate processing techniques (software) but also on the adequacy of the oscilloscope in terms of resolution, an effective number of bits, sampling frequency, and bandwidth. That being said, Table I gives a summary of the key specifications of DPO5104B from Tektronix®.

Regarding the specifications shown in Table I, the oscilloscope has a 1 GHz bandwidth, a maximum sampling rate of 10 GS/s, 50 MS of memory depth, and its nominal input impedance can be set to 50 Ω. The preselection is not used by default and overload is prevented by adjusting dynamically the vertical scale while attempting to maximize the sensitivity.

TABLE I. OSCILLOSCOPES SPECIFICATIONS AT THE OPERATING CONDITIONS CONFIGURED IN THE FULL TDEMI MEASUREMENT SYSTEM

Resolution [bits]	8
ENOB [bits]	6
Enhanced resolution [bits]	0.5 to 4
Max sampling frequency [GS/s]	10
Sampling freq. for Band A (typical) [MS/s]	50
Sampling freq. for Band B (typical) [MS/s]	500
Sampling freq. for Band C/D (typical) [GS/s]	5
Bandwidth (Bands A/B/C&D) [MHz]	20/500/1000
Input impedance	50Ω / 1 MΩ

C. Compliance with CISPR 16-1-1 baseline requirements

As has been extensively explained in [11], Full TDEMI measurement systems based on the selected oscilloscope have demonstrated to be compliant with CISPR 16-1-1 requirements. Table II shows the summary results from the corresponding assessment of conformity.

TABLE II. RESULTS FROM THE ASSEMENT OF CONFORMITY PERFORMED ON FULL TDEMI MEASUREMENT SYSTEMS.

			Band C/D	
			Cal.	**Req.**
Level error [dB]			±1.5	± 2 dB
Selectivity [kHz]	1.5 dB		59±2	[40, 140]
	6 dB		119±2	120±20
	20 dB		210±2	[100, 280]
Response to pulses (absolute) error	PK [dB]		±0.1	± 1.5
	QP [dB]		±0.1	± 1.5
	AV [dB]		±0.1	± 1.5
Response to pulses (relative) error	PK/QP [dB]	100 Hz	11.9	12.0 ± 1.5
		1 kHz	-	-
		5 kHz	-	-
	QP/QP(ref) [dB]	100 Hz	0	0
		1 kHz	-8.0	-8.0±1.0
		5 kHz	-	-
	AV/QP [dB]	100 Hz	-	-
		1 kHz	38.4	38.1±1.5
		5 kHz	26.4	26.3±1.5
VSWR (0 dB att)			<1.4	2.0 to 1

Typical values for every channel of the corresponding Full TDEMI measurement system.
*Reference pulse repetition frequency.

With this oscilloscope, it is possible to declare compliance with sine wave accuracy (amplitude level error), absolute and relative response to pulses, frequency selectivity, and VSWR requirements.

978-1-4673-9698-1/18/$31.00©2018 IEEE

Even if compliance with the CISPR 16-1-1 baseline requirements has been achieved using the previously specified oscilloscope, the reported results provide scarce information regarding the actual dynamic performance of the Full TDEMI measurement system.

III. Dynamic Performance Measures

Considering oscilloscopes are used by the Full TDEMI measuring receivers, their dynamic characterization should be performed at the operating conditions required for compliance with CISPR 16-1-1. In summary, from the oscilloscope's calibration methods it is well known the importance of quantifying the ADC noise, the gain and the linearity of the channels, and the input mismatch and crosstalk [12]–[14]. In the following subsections, such aspects will be investigated.

A. Noise Figure

The noise contribution from circuit elements is usually defined in terms of noise figure, and it accounts for the amount of noise that a circuit adds to the signal. In this regard, the noise figure of a circuit, *NF*, is defined as the signal-to-noise ratio (*SNR*) at the input divided by the *SNR* at the output expressed in decibels, that is,

$$NF = 10\log\left(\frac{SNR_{input}}{SNR_{output}}\right)\Bigg|_{B_{input}=B_{output}} > 1 \quad (1)$$

where *B* is the bandwidth. Equation (1) can be simplified for the case of a test receiver because the level of the signal is the same at the input and at the output (displayed measurement result). Assuming true noise at the input of the receiver when terminated in a 50 Ω, the former equation can be written as,

$$NF = N_{output}[\text{dB}] - 10\log(kTB) \quad (2)$$

where *k* is the Boltzmann constant and *T* is the temperature in Kelvins.

Typically, *NF* is specified for a 1 Hz bandwidth and a room temperature of 21 ºC. Therefore, *NF* is given by

$$NF\big|_{B=1\,\text{Hz}} = N_{output}[\text{dBm}] - 10\log(\text{RBW}) + 174\,\text{dBm} \quad (3)$$

where RBW is the resolution bandwidth used for measuring the displayed noise level noise, N_{output}.

For oscilloscopes, the N_{output} depends on the vertical noise at the different volts-per-div sensitivities. Therefore, vertical noise must be measured for each vertical range setting with every oscilloscope channel terminated into 50 Ω and using the same sample rate and acquisition mode specified for EMI measurements [9]. Then, the recorded base-line noise floor waveform is transformed into the frequency domain according to the method described in [4], [15]. Finally, N_{output} is the average noise level measured with the rms detector for each CISPR band.

B. Linearity and Dynamic Range

A perfect linear oscilloscope would be able of registering the waveforms without distortion. However, the effect of quantization noise and other nonlinearities limit the dynamic performance of the ADC and, in consequence, the actual specifications of Full TDEMI measurement systems.

The effective number of bits (*ENOB*) is a measure that summarizes information about the linearity and the dynamic range of the ADC. The equation of the *ENOB* is derived from the theoretical *SNR* of an ideal N-bit ADC, by replacing the *SNR* by the Signal-to-Noise-and-Distortion (SINAD), that is,

$$ENOB = \frac{SINAD - 1.76\,\text{dB}}{6.02}. \quad (4)$$

Equation (4) assumes a full-scale input signal, but this is not recommended in order to avoid distortion due to signal clipping. If the signal level is reduced, the value of SINAD decreases and the *ENOB* decreases. Thus, a correction factor, that normalizes the *ENOB* value to a full-scale, $V_{\text{full scale}}$, must be added for calculating it at reduced signal amplitudes, V_{input}, as shown in (5),

$$ENOB = \frac{SINAD[dB] - 1.76\,\text{dB} + 20\log\left(\frac{V_{\text{full scale}}}{V_{\text{input}}}\right)}{6.02} \quad (5)$$

On the other hand, SINAD expressed in decibels, is given by (6),

$$SINAD = 20\log\left(\frac{S}{N+D}\right) = -10\log\left[10^{-\frac{SNR}{10}} + 10^{-\frac{THD}{10}}\right] \quad (6)$$

where *SNR* and *THD* are the signal-to-noise ratio and the total harmonic distortion, respectively. Then, the *SNR* and the *THD* must be measured for the all vertical ranges of the oscilloscope and for every measurable CISPR band.

The *SNR* is measured using a well-known sinusoidal input signal. The level of the reference signal is taken directly form the final measurements displayed in the frequency domain using the standard detectors and resolution bandwidths. It is important to notice that cable attenuation must be corrected in the signal level measurement. The (output) noise level, for each vertical scale and corresponding RBW, is obtained from the previously characterized noise figure (3).

Moreover, *SNR* could be theoretically estimated using the following expression,

$$SNR = 6.02(N + N_E) + 1.76\,\text{dB} + G_P + G_{Window} + G_{Welch} \quad (7)$$

where *N* is the number of physical bits of the ADC, N_E is the increase in the number of bits due to the smoothing filter applied by the oscilloscope in high resolution algorithm, G_P is the FFT processing gain, G_{Window} is the processing gain from using a non-rectangular windowing function, G_{Welch} is the reduction of the white noise variance when estimating the spectrum using the Welch's method.

For instance, Tektronix oscilloscopes can reduce the waveform noise HiRes by applying a smoothing digital boxcar filter on the decimated acquisition. The filter 3 dB bandwidth is approximately 0.44 of the sample rate. In the same vein, N_E is given by

978-1-4673-9698-1/18/$31.00©2018 IEEE

$$N_E = \frac{1}{2}\log_2(D) = \frac{1}{2}\log_2\left(\frac{F_{\max}}{F_s}\right), \quad (8)$$

where D is the decimation factor that is calculated as the ratio between the maximum non-interleaved sampling frequency of the scope, F_{max}, and the actual sampling frequency set for the output waveform [9].

The FFT processing gain, G_P, is obtained by means of oversampling the time-domain waveforms. Such reduction in the noise floor is explained by the spectral spreading of the quantization noise power as the sampling frequency increases [8]. G_P is given by (9),

$$G_P = 10\log\left(\frac{F_s}{2B}\right), \quad (9)$$

Likewise, the G_{Window} is the reduction of the noise due to the filtering effect of the bell-shaped windowing function applied to the time-domain signal. It is measured as the ratio between the RBW and the Equivalent Noise Bandwidth, ENBW, expressed in decibels, that is,

$$G_{Window} = 10\log\left(\frac{\mathrm{RBW}}{\mathrm{ENBW}}\right). \quad (10)$$

Additionally, time-domain EMI measurements typically use the Welch's method for estimating the spectrum of the measured signals over the set of highly overlapped windows that segments the whole waveform acquisition. Consequently, when estimating the noise spectrum, there is a reduction of its amplitude variance due to the combination of spectrum calculated for all the overlapped windows according to the standard weighting detectors, in comparison with the spectrum that would have been obtained using the regular periodogram, that is, with neither windowing nor overlapping applied.

In that sense, such reduction is given by

$$G_{Welch} = 10\log\left(\frac{\mathrm{Var}\{\mathrm{P_X}\}}{\mathrm{Var}\{\mathrm{P_W}\}}\right), \quad (11)$$

where $\mathrm{Var}\{\mathrm{P_X}\}$ is the variance of noise spectrum estimated using a regular periodogram while the $\mathrm{Var}\{\mathrm{P_W}\}$ is the variance of noise spectrum estimated using the Welch's periodogram for a given window function, resolution bandwidth, and overlapping factor. Both variances can be numerically calculated using the Monte Carlo approach.

Consequently, the theoretical model for the SNR of Full TDEMI measurement systems can be used for calculating a maximum *SNR* under the assumption the ADC is ideal. The results are shown in Table III.

Conversely, total harmonic distortion is defined as the ratio of the total rms voltage of the harmonics to that of the fundamental component. In decibels, it is calculated as,

$$THD = 10\log\left(\sum_{i=2}^{N_h} V_i^2\right) - 20\log(V_1), \quad (12)$$

where V_1 is the rms voltage of the fundamental frequency, V_i is the rms voltage of the i-th harmonic and N_h is the highest order of the harmonic that is measured above the instrument noise floor.

TABLE III. THEORETICAL SIGNAL OT NOISE RATIO FOR FULL TDEMI MEASUREMENT SYSTEMS FOR CISPR BANDS A TO D

Oscilloscope Specs	**CISPR Bands**		
	A	B	C/D
N [bits]	8		
$F_{\max}$ [GS/s]	10		
F_s [MS/s]	50	500	5000
N_E [bits]	3.8	2.2	0.5
B [Hz]	150×10^3	30×10^6	1×10^9
G_P [dB]	22.2	9.2	4.0
RBW [kHz]	0.2	9	120
ENBW	0.15	6.78	90.42
G_{Window} [dB]	1,23		
Dwell time *(ms)*	100	10	10
Window type	Kaiser-Bessel (β=16.7)		
Overlapping	80%		
G_{Welch}	12,7	19,6	31,0
***SNR* [dB]**	**109**	**93**	**89**

C. VSWR and Crosstalk

The evaluation of the *VSWR* is intended to measure the impedance matching of the oscilloscope to the 50 Ω characteristic impedance required for the entire EMI measurement system. It is measured directly using a Vector Network Analyzer, for all the possible vertical range settings of the oscilloscope and covering the complete bandwidth.

On the other hand, the crosstalk evaluation is intended to quantify the coupling between the oscilloscopes channels by means of two-port S-parameters measurements. Crosstalk must be taken into account when performing multichannel EMI measurements according to the test setups suggested in [12].

IV. RESULTS

This section comprises the measurement results for the dynamic performance evaluation carried out to a Full TDEMI measurement system implemented with the oscilloscope. Whenever applicable, the reference signal generator used was the 81160A Pulse Function Arbitrary Generator from Keysight technologies.

A. Noise Figure

Fig. 2 shows the measured noise figure referenced to a resolution bandwidth of 1 Hz for the Full TDEMI measurement system under evaluation. There is a clear linear increase in the noise figure as the vertical range of the oscilloscope is set for measuring signals with a larger peak-to-peak voltage. This means a loss in sensitivity of the measurement system that should be considered when measuring simultaneously broadband impulsive noise and narrowband interferences.

978-1-4673-9698-1/18/$31.00©2018 IEEE

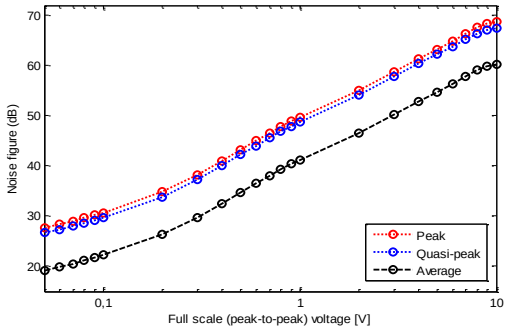

Fig. 2. Noise figure referenced to a RBW of 1 Hz for a Full TDEMI measurement system based on OSC 2 configured for having 1 GHz of bandwidth and a sampling rate of 5 GS/s.

Fig. 2 can also be used for determining if, for a given signal amplitude, there will be enough margin with respect a certain emission limit. For example, for a noise figure of 30 dB and a resolution bandwidth 120 kHz, the displayed average noise level would be -94 dBm or 14 dBμV, approximate. Likewise, it is important to notice that for the maximum sensitivity and with the average detector, the results suggest the Full TDEMI measurement system have a displayed average noise level (*RBW*=1 Hz) of approximately -155 dBm, which is in line with many commercial test receivers.

B. Linearity and Dynamic Range

Fig. 3 shows the correspondence of the voltage level measurements performed with Full TDEMI system and the input voltage applied to the reference signal generator. The measurement was repeated at three different frequencies using the specific settings required for CISPR bands A to D. Results show that for sine wave having amplitudes swept over the oscilloscope vertical ranges, the level error is linear and remains below ±0.15 dB which is significantly less than the CISPR 16-1-1 requirement of ±2 dB.

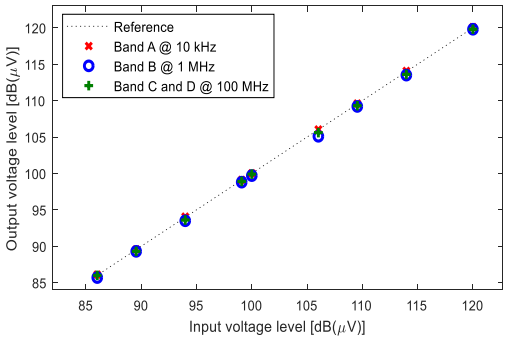

Fig. 3. Linear amplitude voltage swept and error level measurements.

Fig. 4 shows the measured *SNR*. The measured *SNR* ratio is closer to the theoretical value provided in Table IV as the full scale voltage level increases. As expected, the *SNR* is higher the lower the frequency of the CISPR band under assessment is. This is because the usage of a narrower *RBW* and also due to the noise reduction achieved by the combination of signal oversampling and high resolution waveform smoothing.

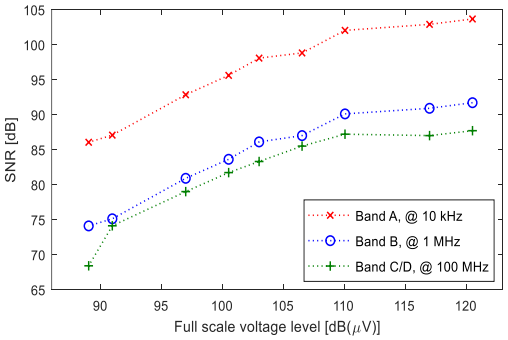

Fig. 4. Signal to noise ratio of a Full TDEMI measurement system.

Regarding the *ENOB*, Fig. 5 shows a linear tendency in the increase of the *ENOB* as the full scale voltage level growths. Moreover, *ENOB* is less sensitive to the vertical range setting when performing measurements in CISPR bands A and B in comparison with the measurements in bands C and D. This is explained by the combination of a lower *SNR* and higher *THD* that characterizes the oscilloscope dynamic performance at frequencies in the range of bands C/D versus the higher *SNR* and lower *THD* observed in bands A/B.

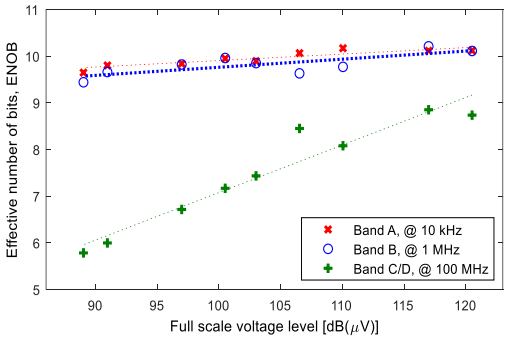

Fig. 5. An effective number of bits of a Full TDEMI measurement system.

C. VSWR and Crosstalk

Fig. 6 presents the measurement results for the maximum *VSWR* (red axis on the left hand side) taken from all oscilloscope channels and among all the different vertical ranges. Likewise, Fig. 6 shows the mean and the min-max range of the oscilloscope input impedance. The evidence supports that the oscilloscope fulfills the requirements of CISPR 16-1-1 in terms of the maximum *VSWR* without an attenuator.

978-1-4673-9698-1/18/$31.00©2018 IEEE

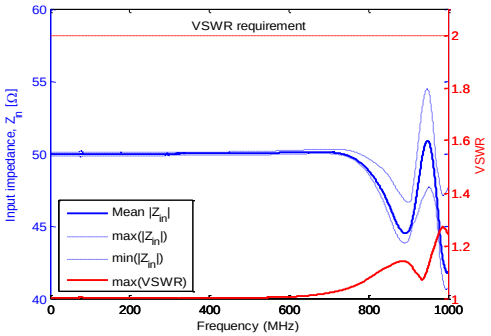

Fig. 6. VSWR evaluation of a Full Time-Domain EMI measurement system.

Furthermore, crosstalk was found to be higher between pairs of adjacent channels. In the worst case, approximately 60 dB of isolation was exhibited between pairs of adjacent channels, while for rest of pairs more than 75 dB of isolation is guaranteed. For frequencies below 600 MHz, all the pairs of channels experience similar crosstalk, however, above 600 MHz crosstalk is significantly larger among pairs of adjacent channels (S_{21}, S_{32}, S_{43}) than with the rest of pairs.

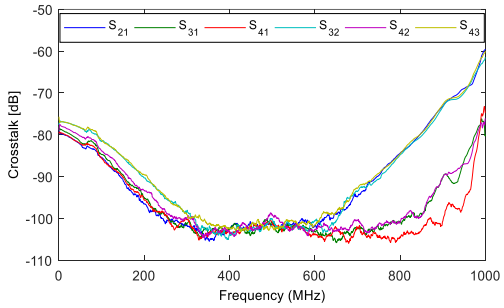

Fig. 7. Crosstalk evaluation of a Full Time-Domain EMI measurement system.

V. CONCLUSION

The dynamic performance of a Full TDEMI measurement system based on the general-purpose oscilloscope Tektronix DPO 5104B has been presented. The influence of the configured vertical scale, sampling rate and acquisition modes were observed in the noise figure, the signal-to-noise ratio and in the effective number of bits. Using oscilloscopes for EMI measurements involves making compromises between the dynamic range and the sensitivity that are relevant, therefore, they must be characterized. However, currently such evaluation is beyond the scope of CISPR 16-1-1 baseline requirements.

ACKNOWLEDGMENT

This work was supported in part by the EURAMET 15RPT01 research project (the EMPIR is jointly funded by the EMPIR participating countries within EURAMET and the European Union), by the Spanish "Ministerio de Economía, Industria y Competitividad," under project TEC2016-79214-C3-2-R (AEI/FEDER, UE), by the "Secretaria d'Universitats i Recerca del Departament d'Economia i Coneixement de la Generalitat de Catalunya" and the European Social Fund and COST ACTION IC1407.

REFERENCES

[1] IEC CISPR, *16-1-1 ed4.0: Specification for radio disturbance and immunity measuring apparatus and methods - Part 1-1: Radio disturbance and immunity measuring apparatus - Measuring apparatus*. IEC, 2015.

[2] G. A. Jackson, "The early history of radio interference," *Electron. Radio Eng. J. Inst.*, vol. 57, no. 6, pp. 244–250, 1987.

[3] C. Hoffmann, H. H. Slim, and P. Russer, "A time-domain system for the measurement of non-stationary EMI up to 40 GHz," *Electromagnetic Compatibility (APEMC), 2012 Asia-Pacific Symposium on*. pp. 205–208, 2012.

[4] M. A. Azpúrua, M. Pous, and F. Silva, "A measurement system for radiated transient electromagnetic interference based on general purpose instruments," in *IEEE International Symposium on Electromagnetic Compatibility (EMC)*, 2015, vol. 2015–*Septm*.

[5] M. Pous, M. A. Azpúrua, and F. Silva, "Radiated transient interferences measurement procedure to evaluate digital communication systems," in *2015 IEEE International Symposium on Electromagnetic Compatibility (EMC)*, 2015, pp. 456–461.

[6] S. Braun, T. Donauer, and P. Russer, "A real-time time-domain EMI measurement system for full-compliance measurements according to CISPR 16-1-1," *IEEE Trans. Electromagn. Compat.*, vol. 50, no. 2, pp. 259–267, 2008.

[7] C. Hoffmann and P. Russer, "A real-time low-noise ultrabroadband time-domain EMI measurement system up to 18 GHz," *IEEE Trans. Electromagn. Compat.*, vol. 53, no. 4, pp. 882–890, 2011.

[8] F. Krug and P. Russer, "The time-domain electromagnetic interference measurement system," *IEEE Trans. Electromagn. Compat.*, vol. 45, no. 2, pp. 330–338, 2003.

[9] M. A. Azpúrua, M. Pous, S. Çakir, M. Çetinta, and F. Silva, "Improving time-domain EMI measurements through digital signal processing," *IEEE Electromagn. Compat. Mag.*, vol. 4, no. 2, pp. 82–90, 2015.

[10] M. A. Azpúrua, M. Pous, J. A. Oliva, and F. Silva, "Fast and automated verification of multi-channel full time-domain EMI measurement system," in *2017 IEEE International Instrumentation and Measurement Technology Conference (I2MTC)*, 2017, pp. 1–6.

[11] M. A. Azpúrua, M. Pous, J. A. Oliva, M. Hudlička, B. Pinter, and F. Silva, "Waveform Approach for Assessing Conformity of CISPR 16-1-1 Measuring Receivers," *IEEE Trans. Instrum. Meas.*, vol. PP, no. 99, pp. 1–14, 2018.

[12] R. A. Belcher, "ADC Standard IEC 60748-4-3: Precision Measurement of Alternative ENOB Without a Sine Wave," *IEEE Trans. Instrum. Meas.*, vol. 64, no. 12, pp. 3183–3200, 2015.

[13] D. A. Humphreys, M. Hudlička, and I. Fatadin, "Calibration of Wideband Digital Real-Time Oscilloscopes," *IEEE Trans. Instrum. Meas.*, vol. 64, no. 6, pp. 1716–1725, 2015.

[14] C. F. M. Carobbi, "An investigation on oscilloscope input mismatch," in *IEEE International Symposium on Electromagnetic Compatibility*, 2017, pp. 333–338.

[15] C. Keller and K. Feser, "Fast Emission Measurement in Time Domain," *IEEE Trans. Electromagn. Compat.*, vol. 49, no. 4, 2007.

978-1-4673-9698-1/18/$31.00©2018 IEEE

8

CONCLUSIONS AND FURTHER WORK

8.1. CONCLUSIONS

Full TDEMI technology for radiofrequency emission measurements is a reliable and complementary alternative for the traditional EMI measurements. It enables the use of general-purpose real-time sampling oscilloscopes for electromagnetic interference measurements, thus it is entirely based on time-domain instrumentation. It replaces the super-heterodyne architecture of conventional swept frequency receiver with the signal processing required to perform spectral estimation.

Regarding the series of processing steps undergone by the measured time-domain signal, it is important to highlight those who are essential for delivering results that are directly comparable to an actual swept frequency receiver. In that sense, the following elements of the processing chain were primordial for the fulfillment of the first objective of this objective.

- Optimizing the acquisition. This means determining the best possible oscilloscope configuration in terms of the sampling rate, record length, number of acquisitions, acquisition mode and vertical range. For instance, using a combination of oversampling and resolution enhancing smoothing allow for an effective reduction of the noise in the waveforms, thus achieving a better dynamic range in the spectral measurements. Likewise, it is necessary to manage the oscilloscope memory in order to record events of sufficient duration with respect the interference repetition frequency. This is fundamental for properly emulating the response of the standard weighting detectors.
- Short-Time Fourier Transform (STFT) for non-parametric spectral estimation and detector emulation. Typically, EMI measurement (dwell) time is larger than the minimum interval required to calculate the spectrum for a given resolution bandwidth. Thus, the STFT is used to calculate the frequency content of local sections of the interference as it changes over time. Those shorter sections have the same time length and are selected using a windowing function that slides along the recorded time-domain signal. Therefore, the STFT becomes a parallel implementation of a filter bank whose frequency response is dependent on the selected windowing function. With such information, it is possible to deliver, simultaneously, a spectral estimation for all the standard weighting detectors and, also, any other kind of statistical detector.

- Selecting a suitable windowing function and overlapping factor. On the one hand, the equivalent frequency selectivity of STFT filter bank, and thus the resolution bandwidth, depends on the length (duration) of the local sections of the signal which is in turn determined from the frequency response of the windowing function. Therefore, the frequency response of the windowing function must be compliant with the selectivity requirements set for the different frequency bands in accordance with the CISPR 16-1-1 standard. On the other hand, windowing causes processing losses, scalloping errors and spectral leakage. In consequence, processing losses must be compensated, scalloping errors must be reduced through an optimum overlapping and sidelobe levels must be considered in order to guarantee sufficient dynamic margin. After multiple tests, the Kaiser–Bessel windowing function with a parameter $\beta = 16.7$ and a minimum of 80 % of overlapping have proven to be a suitable selection for Full TDEMI measurements.

With respect their performance, the Full TDEMI measurement system have been evaluated following two complementary approaches, one for verifying conformity with the applicable standard requirements and another one for characterizing their dynamic performance. The main conclusions of both assessments are:

- CISPR 16-1-1 baseline requirements were assessed using a time-domain based waveform approach. In accordance with the bandwidth of the Full TDEMI measurement systems under evaluation, the frequency range covered was 9 kHz – 1 GHz, comprising CISPR bands A–D. Results showed that Full TDEMI measurement systems based in the oscilloscopes models Tektronix DPO5104B (for CISPR bands A, B and C/D) and PicoScope 5444B (for CISPR bands A and B) satisfactorily meet the requirements of sine wave level error, frequency selectivity, absolute and relative frequency response and voltage standing wave ratio. Moreover, the proposed test setup, based on arbitrary pulse generators, was found to be more affordable, versatile, and flexible than other calibration methods used for EMI measuring receivers. In fact, it was demonstrated that the usage of the CISPR baseband pulse generator can be avoided. A collateral advantage of this approach is that waveforms can be represented as exact numerical vectors and they could be easily reproduced by, or shared between, any laboratory having an adequate arbitrary pulse generator.

- The dynamic performance evaluation of Full TDEMI measurement systems is aimed to determine the influence of the configured vertical scale, sampling rate and acquisition modes in the noise figure, the signal-to-noise ratio and in the effective number of bits. In other words, it characterized the trade-off between the dynamic range and the sensitivity that is intrinsic to the usage of oscilloscopes for EMI measurements. In this regard, the measured signal to noise ratio in the Full TDEMI measurement system implemented with the oscilloscope Tektronix DPO5104B was found to be between 70 dB and 100 dB, while the effective number of bits ranged from 6 to 10. In general, a better dynamic performance was exhibited when the amplitude of the input signal was larger with respect the instrument noise. This suggests that Full TDEMI measurement system can benefit significantly from pre-amplification. As expected, better dynamic performance was also evidenced as the amplitude of the input signal approached the maximum input voltage. Comparatively, in the best scenario, Full TDEMI measurement systems can provide a similar displayed average noise level than many commercial spectrum analyzers, however, in general, the sensitivity of Full TDEMI measurement systems is lower than the specified by superheterodyne architecture receivers. This is to be expected because of the larger bandwidth.

Beyond the actual advantages and drawbacks raised by the specified performance of Full TDEMI measurement systems, a set of alternative test methods were proposed for improving emissions testing

through the exploitation of the multichannel and the triggering capabilities of oscilloscopes. Hereof, it can be concluded that,

- Multichannel capabilities of oscilloscopes enable single stage evaluation of the conducted EMI of all the mains lines of the equipment under test. For this purpose, individual RF outputs are required for each line of the LISN or, alternatively, a multiline voltage probe. Consequently, there is a reduction in the number of iterations required to complete the conducted emissions test. Furthermore, the common mode and the differential mode voltage noise can be directly calculated from the time-domain measurements, which is very useful for defining EMI mitigation strategies in the case of non-compliant products. Additionally, transient disturbances related to a single event can be measured simultaneously in all the EUT's mains lines. A successful measurement campaign in which an automated storage and retrieval system, namely a large fixed installation, was evaluated on site regarding its conducted and radiated radiofrequency emissions provides a clear example of the benefits from the usage of the multichannel Full TDEMI approach [23].

- The concurrent conducted and radiated EMI measurements allow correlating, in both time and frequency domains, the measured voltages/currents and the electric/magnetic fields. An example of such application was the proposed on-board measurement system for the evaluation of the indirect effects of lightning strikes in Unmanned Aerial Vehicles. In this particular case, EMI monitoring can be triggered by the transient disturbances coupled into cables and antennas inside the fuselage [22].

- The parallelization of multi-antenna radiated emissions testing is useful in test setups that requires measuring low-frequency magnetic fields below 30 MHz and also the electric field above 30 MHz. For instance, the EMC standards for railway applications (IEC 62236 and EN 50121-3-1) requires the rolling stock to be evaluated in static conditions and in dynamic mode, circulating at low speed and accelerating and/or braking at the measurement point. In such scenario, up to three antennas could be used to measure simultaneously the radiated emissions, that is, a magnetic field loop antenna (9 kHz – 30 MHz), a biconical antenna (30 MHz – 200 MHz) and a log-periodic antenna (200 MHz – 1 GHz). Being able of measuring with multiple channels simultaneously reduces the number of test iterations. This is particularly relevant in this kind of *in-situ* measurements that are typically very expensive and time-consuming. At the same time, the test reliability improves as the equivalent measurement time increases up to 2500 times in comparison with the frequency sweep measurement approach. A conference proceeding reporting the experience on the usage of Full TDEMI measurement systems in the *in-situ* assessment of the emissions of a rolling stock can be found in [24].

As has been shown, the proposed alternative test methods have improved significantly the EMC testing process in a variety of industries by reducing the amount of time and the efforts required for performing a complete system evaluation due to the following reasons.

- Time-domain EMI measurements deliver faster results because the interference's spectrum is simultaneously estimated for all the standard weighting detectors required to determine compliance with respect to the maximum emissions limits defined in the corresponding generic or product standard.

- The number of measurement iterations is reduced because of the multichannel capabilities of oscilloscopes and also because of an agile identification of the worst case emissions in EUT having several different operating modes.

- Full TDEMI measurement system is a cost-effective, versatile and robust alternative to real-time spectrum analyzers for EMI measurements in the range of few gigahertz. This means Full TDEMI measurement systems offer an affordable solution for *in-situ* emissions testing, for in-house laboratories of SME's and also for university EMC laboratories.

The above-mentioned conclusions primarily relate the contributions of Full TDEMI measurement systems regarding its technical implementation and its application for standard EMI measurements. Moreover, as has been defined in the objectives, the Thesis comprised the following of contributions focused on theoretical aspects of the signal and statistical processing of EMI measurements.

On the topic of the statistical modeling of the worst-case disturbance emissions levels (extreme values), an analytic model for the probability distribution function of peak detector measurements was proposed. Assuming the peak detector measurements of random interferences have a normal distribution, the mathematical expressions for its expected value and for its variance were obtained. Computational validations were performed using the Monte Carlo method and experimental validations were carried out by measuring predefined stochastic and cyclostationary signals generated using arbitrary waveform generators. However, it was later found that if the measured signal does not satisfy the model assumptions, the model overestimated the expected maximum value.

A continuation of the aforementioned work, employed a robust approach for calculating, numerically, such expected maximum. It involved using non-parametric kernel-fitting and bootstrapping for delivering the estimates of the expected maximum and the variance. The practical interpretations of this contributions are several. First, it can be used to predict a likely "long-term" max-hold value based on the statistical information contained in a single short-duration acquisition. This is important for overcoming the memory limited duration of a single "gapless" time-domain EMI measurement. Secondly, the expected maximum value is robust against outliers (very rare events) while max-hold value measurement is very sensible to them. This is because calculating the expected maximum detector requires using time-frequency information for calculating the most likely value for the peak emissions at each frequency step. Thirdly, the variance of the expected value of the peak emissions has lower variance than the actual peak value, consequently, the uncertainty of the expected maximum detector is lower in comparison to the uncertainty of the peak detector.

Beyond its theoretical interest, the author believes the expected maximum detector has two drawbacks in practice. The first one is that it is not yet correlated to EMI observable problems and, thus, emissions requirements are not defined in its terms. The second one is that the expected maximum peak value is not intuitive by itself. It can, in theory, take values that are above or below the measured peak value depending on the distribution function of the measured interference.

Likewise, other contributions are related to the transient and continuous wave noise decomposition. In the first place, custom algorithms for implementing the empirical mode decomposition for electromagnetic interferences with additional capabilities for detecting and separating, transient-like, impulse noise, were developed. In comparison with other signal decomposition approaches, the presented techniques have several advantages: it introduces neither distortion nor delay on the IMF, it requires no prior information on the spectral content of the measured EMI, it does not require a domain transformation, it provides IMFs that usually have a clear physical meaning, it is not constrained by time-frequency resolution limits, and it allows a straightforward implementation through software. Therefore, the decomposition of EMI in the time domain provides several new practical applications to be explored in Full TDEMI measurement systems,

especially for those based on general-purpose oscilloscopes. For example, the heuristic capability for isolating impulsive interference from continuous wave signals through time-gating is useful for the outdoors evaluation of the APD detector even in the presence of the broadcasting signals of the corresponding the communication system.

In the same vein, EMI decomposition in the time domain is potentially applicable for the cancellation of unwanted background ambient noise in emissions measurements performed *in situ*, as required in industrial environments or when assessing interferences of railway systems. This application was conducted with successful results in proof-of-concept experiment was a single antenna test setup was used to apply selective denoising on the emissions measurements. Such ambient noise cancellation method relies on the classification of the decomposed intrinsic mode functions based on a preliminary characterization of the ambient noise. Therefore, this ambient noise cancellation method assumes the ambient noise is stationary and it is limited in terms of its capability of recognizing sporadic signals. Nonetheless, the short time acquisitions used during radiated EMI measurements are less likely to suffer from variations in the signature spectrum of the ambient noise.

However, EMI decomposition in the time domain has some drawbacks, and its performance is improvable. In particular, the EMD algorithm, it is not possible to know beforehand how many IMF will be identified. Therefore, the required time to process the signal is not bounded, and this could be impractical for emissions testing measurements purposes. A possibility to reduce the processing time is to establish a fixed number of intrinsic modes obtainable on the basis of the analysis of a preliminary measure.

As has been exposed throughout the different objectives of this Thesis, full time-domain EMI measurements are not only feasible for compliant emissions testing but also an extremely valuable resource when they are properly taken advantage for visualizing, analyzing and troubleshooting EMI phenomena. The compendium of contributions grouped in this thesis advanced the prior state-of-the-art on time-domain EMI measurements, that was focused in the hardware implementation of real-time analyzers of high bandwidth, and have helped to expand the knowledge on time-domain measurement technology and its usage for setting alternative emissions testing methods. Yet, the research on time-domain based EMI measurements and applications is not finalized. In the near future, further work is expected to take place in terms of research, technology development, and standardization activities as consequence of this study.

8.2. FURTHER WORK

Research on full time domain EMI measurements will continue in the future. According to the author's criterion and the cumulative experiences of these last years of investigation in the field, some remarkable potential research topics can be listed, as follow:

- Full TDEMI measurement systems shall be further developed to embrace EMI measurements at frequencies below 9 kHz. In fact, EMI problems from disturbances in the 2 kHz – 150 kHz have been reported in modern sampling-based smart energy meters [69]. In that sense, time-domain EMI measurements can be used to study the waveforms of the problematic conducted disturbances in order to characterize them and also to define suitable test bench and procedures to ensure metering devices such as the static energy meter. In that sense, efforts are also needed in terms of specifying the instrumentation, the detectors and the emissions limits below 9 kHz because, nowadays, standards

provide little to none information in this regard. Likewise, the automation of low-frequency harmonics emissions, flickers, and discontinuous disturbances (clicks test) measurements can be embraced under the same approach as the Full TDEMI measurement system.

- Evaluating the performance and the feasibility of Full TDEMI measurement systems for emissions measurements above 1 GHz. Real-time sampling oscilloscopes with a bandwidth larger than 1 GHz are commercially available, however, other challenges may arise. For instance, the increase in the volume of data due to even higher sampling rates or the bottleneck in processing caused by the limited velocity of the PC interfaces – oscilloscope interface is a couple of aspects to take into account in practice. Similarly, the noise figure, the sensitivity and dynamic range of such high bandwidth oscilloscopes must also be considered in order to determine if the achievable performance is enough for EMI measurements. From the economical point-of-view, it becomes unclear whether implementing Full TDEMI systems beyond a few gigahertz remains as cost-effective as it is below or equal to 1 GHz.

- Developing the metrology for full time-domain EMI measurements. This means, bridging the gap between oscilloscope calibrations and measuring receiver specifications. Metrology level reference standards can be used to reduce the uncertainty of the performance verifications carried out in this work. Defining a set of particular requirements and indicators for benchmarking Full TDEMI measurement systems implemented using different models of oscilloscopes is still a pending subject. Moreover, developing time-domain based calibration methods that are specific for statistical detectors, such as the APD, will require research efforts.

- Continue the research on ambient noise cancellation for EMI measurements in open area test sites. Dual-antenna approaches have been previously reported at proof-of-concept or at simulation level, but they were not reproduced with or compared to what is possible to achieve with Full TDEMI measurement systems. More complex test setups, involving three, or more, antennas placed in the at near, far (normative) and outer (outside the EUT's radius of detectable emissions) distances could provide additional information for signal classification during selective denoising.

Full TDEMI measurement technology can become an enabler of multiple interesting applications in the field of the EMC, that properly could not be considered research. For instance, some of them are mentioned below:

- Concurrent voltage and current measurements for dynamic characterization of the mains impedance intended to correct the conducted emissions measurements performed *in-situ* with respect a 50 Ω measurement system. This idea has been previously proposed in order to improve the correlation of on-site conducted EMI measurements in comparison to the ones performed at a standard testing laboratory [70] and it could be further developed using the Full TDEMI platform due to its synchronous multichannel features.

- Time-efficient, broadband, high-resolution, three-dimensional evaluation of the radiated emissions of EUTs in anechoic chambers. Combining the fast and full spectrum measurement results delivered by the Full TDEMI measurement systems with a small step sizes for the turntable angular position and the mast height it is possible to collect enough data to reproduce the radiation pattern of an EUT at any frequency of interest. The potential application of such analysis would be finding the worst case emissions of an EUT with an improved level of confidence in comparison with the common approach that consists of measuring with the antenna axis perpendicular to the "four faces" of an EUT and at four heights each.

- Implementing an EMI toolbox for a live selection and design of appropriate filters and components for suppressing common and differential mode noise. This idea, while certainly not new in itself [71–73], can be very handy and fitted as a tool for Full TDEMI measurement systems.

Another important task that will require further work for Full TDEMI measurements to be widely used in the EMC community is the standardization. It is of general knowledge that standardization activities have a lot of inertia to overcome, and the committees for EMC are no different from the rest. However, some of the alternative testing methods enabled by multichannel Full TDEMI measurements can be of great aid for many industries, especially for those who require testing large-complex systems. Perhaps the clearer example of such situation is the railway sector. Luckily, CISPR 16-1-1 allows any kind of implementation of measuring receivers as long they comply with the standard baseline requirements. Therefore, it is not necessary to further specify the instrumentation in order to provide guidance that specifies how to use oscilloscopes for evaluating radiofrequency emissions. Such guidance can be delivered through informative (at first) or normative annexes to the standards dealing with the emissions requirements for specific products that are incompatible with conventional practices.

In consequence, in the near future there is plenty of work remaining in the field of time domain EMI measurements. Either as a topic of research by itself or as a measurement technology that enables another kind of applications, Full TDEMI measurement systems will be further developed in forthcoming years.

BIBLIOGRAPHY

[1] G. Jackson, "The early history of radio interference," *Journal of the Institution of Electronic and Radio Engineers*, vol. 57, no. 6, p. 244, 1987.

[2] IEC CISPR, "16-1-1 ed4.0: Specification for radio disturbance and immunity measuring apparatus and methods - Part 1-1: Radio disturbance and immunity measuring apparatus - Measuring apparatus," 2015.

[3] P. Russer, "Emc measurements in the time-domain," in *2011 XXXth URSI General Assembly and Scientific Symposium*, pp. 1–35, Aug 2011.

[4] E. L. Bronaugh, "An Advanced Electromagnetic Interference Meter for the Twenty-First Century," in *8th International Zurich Symposium On Electromagnetic Compatibility*, (Zurich, Switzerland), pp. 215–219, 1989.

[5] F. Krug and P. Russer, "The time-domain electromagnetic interference measurement system," *IEEE Transactions on Electromagnetic Compatibility*, vol. 45, no. 2, pp. 330–338, 2003.

[6] F. Krug and P. Russer, "Time-Domain Broad-Band EMI Measurement Techniques," in *2002 32nd European Microwave Conference*, pp. 1–4, 2002.

[7] S. Braun, T. Donauer, and P. Russer, "A real-time time-domain EMI measurement system for full-compliance measurements according to CISPR 16-1-1," *IEEE Transactions on Electromagnetic Compatibility*, vol. 50, pp. 259–267, may 2008.

[8] C. Hoffmann and P. Russer, "A real-time low-noise ultrabroadband time-domain EMI measurement system up to 18 GHz," *IEEE Transactions on Electromagnetic Compatibility*, vol. 53, no. 4, pp. 882–890, 2011.

[9] M. Azpúrua, M. Pous, J. A. Oliva, and F. Silva, "Fast and automated verification of multi-channel full time-domain EMI measurement system," in *2017 IEEE International Instrumentation and Measurement Technology Conference (I2MTC)*, (Turin), pp. 1–6, 2017.

[10] M. A. Azpúrua, M. Pous, J. A. Oliva, M. Hudlička, B. Pinter, and F. Silva, "Waveform Approach for Assessing Conformity of CISPR 16-1-1 Measuring Receivers," *IEEE Transactions on Instrumentation and Measurement*, vol. PP, no. 99, pp. 1–14, 2018.

[11] European Union, "Directive 2014/30/EU of the European Parliament and of the Council of 26 February 2014 on the harmonisation of the laws of the Member States relating to electromagnetic compatibility (recast) Text with EEA relevance."

[12] K. Armstrong, "Emc and functional safety," *IEE Review*, vol. 46, pp. 34–37, Nov 2000.

[13] B. Audone, R. Paviolo, and S. Fazari, "Emc testing of medical devices," in *2013 International Symposium on Electromagnetic Compatibility*, pp. 1039–1044, Sept 2013.

[14] I. EMC, "Publishable JRP Summary Report for JRP IND60 EMC Improved EMC Test Methods in Industrial Environments," tech. rep., EURAMET, 2015.

[15] M. Pous and F. Silva, "Prediction of the impact of transient disturbances in real-time digital wireless communication systems," 2014.

[16] M. Pous and F. Silva, "Full-Spectrum APD Measurement of Transient Interferences in Time Domain," 2014.

[17] M. A. Azpúrua, M. Pous, S. Çakir, M. Çetinta, and F. Silva, "Improving time-domain EMI measurements through digital signal processing," *IEEE Electromagnetic Compatibility Magazine*, vol. 4, no. 2, pp. 82–91, 2015.

[18] M. A. Azpúrua, M. Pous, and F. Silva, "On the Statistical Properties of the Peak Detection for Time-Domain EMI Measurements," *IEEE Transactions on Electromagnetic Compatibility*, vol. 57, no. 6, pp. 1374–1381, 2015.

[19] M. Azpúrua, M. Pous, and F. Silva, "Decomposition of Electromagnetic Interferences in the Time-Domain," *IEEE Transactions on Electromagnetic Compatibility*, vol. 58, no. 2, pp. 385–392, 2016.

[20] M. Azpúrua, M. Pous, and F. Silva, "A measurement system for radiated transient electromagnetic interference based on general purpose instruments," in *IEEE International Symposium on Electromagnetic Compatibility (EMC)*, vol. 2015-Septm, (Dresden), 2015.

[21] M. Pous, M. A. Azpúrua, and F. Silva, "Measurement and Evaluation Techniques to Estimate the Degradation Produced by the Radiated Transients Interference to the GSM System," *IEEE Transactions on Electromagnetic Compatibility*, vol. 57, no. 6, pp. 1382–1390, 2015.

[22] M. A. Azpúrua, M. Pous, and F. Silva, "On-board compact system for full time-domain electromagnetic interference measurements," in *2016 ESA Workshop on Aerospace EMC (Aerospace EMC)*, (Valencia), pp. 1–4, 2016.

[23] M. Pous, M. Azpurua, F. Silva, M. Azpúrua, F. Silva, M. Azpurua, and F. Silva, "Benefits of full time-domain EMI measurements for large fixed installation," in *IEEE International Symposium on Electromagnetic Compatibility*, vol. 2016-Novem, pp. 514–519, 2016.

[24] M. Pous, M. A. Azpúrua, and F. Silva, "Full Time Domain EMI measurement system applied to Railway emissions according to IEC 62236-3-1/EN 50121-3-1 standards," in *2018 International Symposium on Electromagnetic Compatibility - EMC EUROPE*, (Amsterdam), pp. 1–6, 2018.

[25] M. A. Azpúrua, J. A. Oliva, M. Pous, and F. Silva, "Robust extreme value estimation for full time-domain EMI measurements," in *2017 International Symposium on Electromagnetic Compatibility - EMC EUROPE*, (Angers), pp. 1–6, 2017.

[26] M. Azpúrua, M. Pous, and F. Silva, "A single antenna ambient noise cancellation method for in-situ radiated EMI measurements in the time-domain," in *2016 International Symposium on Electromagnetic Compatibility - EMC EUROPE*, vol. 2016-Novem, (Wroclaw), pp. 501–506, IEEE, sep 2016.

[27] M. Pous, M. A. Azpúrua, and F. Silva, "APD oudoors time-domain measurements for impulsive noise characterization," in *2017 International Symposium on Electromagnetic Compatibility - EMC EUROPE*, pp. 1–6, 2017.

[28] M. A. Azpúrua, M. Pous, and F. Silva, "Dynamic Performance Evaluation of Full Time Domain EMI Measurement Systems," in *2018 International Symposium on Electromagnetic Compatibility - EMC EUROPE*, (Amsterdam), pp. 1–6, 2018.

[29] E. L. Bronaugh and J. D. M. Osburn, "New ideas in emc instrumentation and measurement," in *10th International Zurich Symposium On Electromagnetic Compatibility, Zurich, Switzerland*, no. 58J1, p. 323–326, 1993.

[30] A. Schutte and H. C. Karner, "Comparison of time domain and frequency domain electromagnetic susceptibility testing," in *Proceedings of IEEE Symposium on Electromagnetic Compatibility*, pp. 64–67, Aug 1994.

[31] P. A. Sikora, "An emi receiver design using modern digital technique.," in *11th International Zurich Symposium on Electromagnetic Compatibility, Zurich, Switzerland*, no. 86N2, pp. 453–458, Mar. 1995.

[32] F. Krug and P. Russer, "Ultra-fast broadband EMI measurement in time-domain using FFT and periodogram," in *2002 IEEE International Symposium on Electromagnetic Compatibility*, vol. 2, pp. 577–582 vol.2, 2002.

[33] F. Krug and P. Russer, "Signal processing methods for time domain EMI measurements," *2003 IEEE International Symposium on Electromagnetic Compatibility, 2003. EMC '03.*, vol. 2, 2003.

[34] F. Krug and P. Russer, "Quasi-peak detector model for a time-domain measurement system," *IEEE Transactions on Electromagnetic Compatibility*, vol. 47, no. 2, pp. 320–326, 2005.

[35] F. Krug, D. Mueller, and P. Russer, "Signal processing strategies with the TDEMI measurement system," *IEEE Transactions on Instrumentation and Measurement*, vol. 53, no. 5, pp. 1402–1408, 2004.

[36] A. J. Rowell, D. Bozec, S. A. Seller, L. M. McCormack, C. A. Marshman, and A. C. Marvin, "Improved measurement of radiated emissions from moving rail vehicles in the frequency range 9 khz to 1 ghz," in *2004 International Symposium on Electromagnetic Compatibility (IEEE Cat. No.04CH37559)*, vol. 1, pp. 19–24 vol.1, IEEE, Aug 2004.

[37] S. Verdaguer, M. Fernández, A. Vidal, and F. Silva, "Emi receiver plus digitizer rf transient measurements," in *EMC York 2004 International Conference and Exhibition*, pp. 635–640, 2004.

[38] Y. Kuznetsov, A. Baev, M. Bekhtin, S. Braun, and P. Russer, "The time-domain emi measurement system based on a multi-level analog-to-digital converter," in *2005 European Microwave Conference*, vol. 3, pp. 4 pp.–, IEEE, Oct 2005.

[39] S. Braun and P. Russer, "A low-noise multiresolution high-dynamic ultra-broad-band time-domain EMI measurement system," nov 2005.

[40] S. Braun, M. Aidam, and P. Russer, "Development and evaluation of a realtime time-domain emi measurement system for automotive testing," in *2007 IEEE International Symposium on Electromagnetic Compatibility*, pp. 1–4, IEEE, July 2007.

[41] S. Braun and P. Russer, "Uncertainty analysis and novel test procedures performed with a realtime time-domain emi measurement system," in *2007 IEEE International Symposium on Electromagnetic Compatibility*, pp. 1–4, IEEE, July 2007.

[42] S. Braun, A. Frech, and P. Russer, "CISPR specification and measurement uncertainty of the time-domain EMI measurement system," *2008 IEEE International Symposium on Electromagnetic Compatibility*, pp. 1–4, aug 2008.

[43] S. Braun, "An overview of emission measurements in time-domain," in *Proceedings of the 2009 International Symposium on EMC EMC*, vol. 9, pp. 20–24, 2009.

[44] H. Westenberger, "Use of time domain methods for cispr16 compliant emi measurements," in *2009 IEEE International Conference on Microwaves, Communications, Antennas and Electronics Systems*, pp. 1–4, IEEE, Nov 2009.

[45] C. Hoffmann and P. Russer, "A real-time low-noise ultrabroadband time-domain EMI measurement system up to 18 GHz," *IEEE Transactions on Electromagnetic Compatibility*, vol. 53, no. 4, pp. 882–890, 2011.

[46] H. H. Slim, C. Hoffmann, S. Braun, and P. Russer, "A novel multichannel amplitude probability distribution for a time-domain EMI measurement system according to CISPR 16-1-1," in *10th International Symposium on Electromagnetic Compatibility*, pp. 22–25, 2011.

[47] S. Braun, "A novel time-domain EMI measurement system for measurement and evaluation of discontinuous disturbance according to CISPR 14 and CISPR 16," in *2011 IEEE International Symposium on Electromagnetic Compatibility*, pp. 480–483, IEEE, aug 2011.

[48] G. Costa, M. Pous, A. Atienza, and F. Silva, "Time-Domain Electromagnetic Interference Measurement System for intermittent disturbances," in *2014 International Symposium on Electromagnetic Compatibility*, pp. 833–837, IEEE, sep 2014.

[49] M. Mardiguian, *EMI Troubleshooting Techniques*. Electronics Workbench Circuit Solution Series, McGraw-Hill Education, 1999.

[50] S. Alessio, *Digital Signal Processing and Spectral Analysis for Scientists: Concepts and Applications (Signals and Communication Technology)*. Signals and Communication Technology, Springer, 2015.

[51] M. S. Bartlett, "Smoothing periodograms from time-series with continuous spectra," *Nature*, vol. 161, p. 686, May 1948.

[52] P. Welch, "The use of fast fourier transform for the estimation of power spectra: A method based on time averaging over short, modified periodograms," *IEEE Transactions on Audio and Electroacoustics*, vol. 15, pp. 70–73, Jun 1967.

[53] V. Iglesias, J. Grajal, M. A. Sanchez, and M. Lopez-Vallejo, "Implementation of a Real-Time Spectrum Analyzer on FPGA Platforms," *IEEE Transactions on Instrumentation and Measurement*, vol. 64, pp. 338–355, feb 2015.

[54] D. Liebl, *Measuring with Modern Spectrum Analyzers*. Munich: Rohde&Schwarz, 2013.

[55] C. Paul, *Introduction to Electromagnetic Compatibility*. Wiley Series in Microwave and Optical Engineering, Wiley, 2006.

[56] D. Prutchi and M. Norris, "Electromagnetic compatibility and medical devices: Electromagnetic fields," in *Design and Development of Medical Electronic Instrumentation*, John Wiley & Sons, 2005.

[57] M. J. Nave, "A novel differential mode rejection network for conducted emissions diagnostics," in *National Symposium on Electromagnetic Compatibility*, pp. 223–227, May 1989.

[58] J. Stahl, D. Kuebrich, A. Bucher, and T. Duerbaum, "Characterization of a modified lisn for effective separated measurements of common mode and differential mode emi noise," in *2010 IEEE Energy Conversion Congress and Exposition*, pp. 935–941, IEEE, Sept 2010.

[59] CENELEC, "En 50121-3-1 railway applications. electromagnetic compatibility. rolling stock. train and complete vehicle," 2017.

[60] A. Frech and P. Russer, "Real-time ambient noise cancellation for emi measurements on open area test sites," in *2012 Asia-Pacific Symposium on Electromagnetic Compatibility*, pp. 213–216, May 2012.

[61] CISPR 16-2-3, "Specification for radio disturbance and immunity measuring apparatus and methods - Part 2-3: Methods of measurement of disturbances and immunity - Radiated disturbance measurements," *International Electrotechnical Commission*, 2016.

[62] CISPR 16-1-4, "Specification for radio disturbance and immunity measuring apparatus and methods - Part 1-4: Radio disturbance and immunity measuring apparatus - Antennas and test sites for radiated disturbance measurements," *International Electrotechnical Commission*, 2010.

[63] A. Frech, A. Zakaria, S. Braun, and P. Russer, "Ambient noise cancelation with a time-domain EMI measurement system using adaptive filtering," in *2008 Asia-Pacific Symposium on Electromagnetic Compatibility and 19th International Zurich Symposium on Electromagnetic Compatibility*, pp. 534–537, IEEE, may 2008.

[64] A. Frech, S. Limmer, and P. Russer, "Noise cancelling algorithms for FPGA-based time-domain EMI measurements in real-time," in *IEEE International Symposium on Electromagnetic Compatibility*, pp. 484–488, Aug 2011.

[65] A. Frech, S. Braun, and P. Russer, "Time-domain EMI measurements in the presence of ambient noise," in *IEEE International Symposium on Electromagnetic Compatibility*, pp. 139–142, 2009.

[66] A. Frech, M. Klügel, and P. Russer, "Adaptive filtering for noise cancellation and signal analysis in real-time," in *2013 European Microwave Conference*, pp. 1123–1126, Oct 2013.

[67] Z.-H. Lu, J.-B. Liu, and P.-G. Liu, "A novel method of ambient interferences suppressing for in situ electromagnetic radiated emission test," *IEEE Transactions on Electromagnetic Compatibility*, vol. 54, pp. 1205–1215, dec 2012.

[68] Z.-H. Lu, L. Ding, X.-H. Lin, and M.-T. Lin, "An innovative virtual chamber measurement method based on spatial domain cancellation technique for radiation emission in situ test," *IEEE Transactions on Electromagnetic Compatibility*, vol. 59, pp. 342–351, apr 2017.

[69] C. Keyer, F. Buesink, and F. Leferink, "Mains power synchronous conducted noise measurement in the 2 to 150 kHz band," in *2016 International Symposium on Electromagnetic Compatibility - EMC EUROPE*, IEEE, sep 2016.

[70] O. Sen, S. Cakır, M. Cınar, M. Pous, F. Silva, and M. Cetintasş, "Alternative conducted emission measurements on mains without LISNs," *IEEE Electromagnetic Compatibility Magazine*, vol. 4, no. 4, pp. 58–65, 2015.

[71] P.-S. Chen and Y.-S. Lai, "Effective EMI filter design method for three-phase inverter based upon software noise separation," *IEEE Transactions on Power Electronics*, vol. 25, pp. 2797–2806, nov 2010.

[72] B. Narayanasamy, H. Jalanbo, and F. Luo, "Development of software to design passive filters for EMI suppression in SiC DC fed motor drives," in *2015 IEEE 3rd Workshop on Wide Bandgap Power Devices and Applications (WiPDA)*, IEEE, nov 2015.

[73] M. C. D. Piazza, M. Luna, G. Vitale, G. Ala, G. C. Giaconia, G. Giglia, and P. Zanchetta, "ODEF: An interactive tool for optimized design of EMI filters," in *IECON 2016 - 42nd Annual Conference of the IEEE Industrial Electronics Society*, IEEE, oct 2016.